Linear actuator for a submersible water pump for use in boreholes

Martin Cain

Durham University

School of Engineering

Linear Actuator for a Submersible Water Pump for Use in Boreholes

Martin Cain

2007

This thesis is submitted in partial fulfilment of the requirements for the degree of

Master of Philosophy

Declaration

I hereby declare that this thesis is a record of work undertaken by myself, that it has not been the subject of any previous application for a degree, and that all sources of information have been duly acknowledged.

Acknowledgements

For their contributions and support during this research, I would like to thank my supervisor Dr. Tim Short and my former joint supervisor Dr. Marcus Mueller. I would also like to thank Dr. Patrick Brooking for his advice, help, and support during my time at Durham University. The work done by the technicians of the department is very much appreciated. Many thanks.

Part of this work has been carried out under the funding of the EPSRC research grant GR/R51537, the remainder of the work was carried out under the funding of the School of Engineering, University of Durham, by means of a postgraduate grant, without such support this work would not have been possible.

External to the University, I wish to thank Mr D. Clark and Miss B.M. O'Keefe for their contribution when proofreading the thesis.

Abstract

Both the theory and the test results show that the E-core electromagnet linear actuator, which is based on the variable reluctance principle, can generate a normal force in excess of $400kNm^{-2}$ when there is a flux density of 1T within the airgap.

When the actuator is used as a driver in a submersible water pump for use in boreholes the results show that the pump is capable of pumping up to 90% of the expected value. Pressures in excess of 10 Bar have been achieved, whilst the pump was operating at frequencies up to 30Hz. The flow rate was less than $0.2ls^{-1}$, however improvements to the pumping system are given, and the desired $1ls^{-1}$ flow rate is achievable at a delivery head of 100m.

The use of linear actuators for use in submersible water pumps is a relatively new technology, and as the demand for safe clean water increases, it provides for sustainable development. The actuator utilises a D.C. supply with solar panels as the source, giving the potential for global use, particularly in developing countries (the South).

The design of the driver can be optimised for selected parameters. However, the development of such drivers does have limitations, the overall diameter of the pump is restricted to that of the bore-hole size, 4 or 6 inches; further the length of the pump is dictated by the straightness of the bore-hole. Consequently, design tools, for the design of E-core Variable Reluctance Linear Actuators, (VRLA), are given.

Contents

CHAPTER 1

Chapter 1
Introduction

1 Introduction

This chapter first states the aim of the thesis and then gives the background to the thesis, which gives an insight to the reason why the work was initiated. The chapter then goes through the thesis explaining what is in each chapter.

1.1 The Aim of the Thesis

The aim of the research is to design and develop a linear actuator pumping mechanism for a submersible water pump for use in boreholes. The pump capacity is to be able to achieve a delivery head pressure in excess of 10Bar with a minimum flow rate of $1.0ls^{-1}$.

1.2 Background

Many people in rural areas of developing countries (hereafter termed as 'the South') have a shortage of a clean water supply, which leads to terminal health and extreme living conditions, leaving little option, to either migrate to urban areas intensifying existing problems or die in the rural districts.

It is not financially viable to provide distribution girds for the geographically vast rural areas of the South, therefore sustainable stand alone water systems are vital for the survival of the billions of people living in such areas. Encompassed in nearly all water systems is the use of some type of pump.

The provision of clean safe water is paramount to the survival of the South; many

methods of extraction currently exist, each having their own capabilities and problems, with some supplies being tapped from boreholes. The use of a borehole in order to provide a safe water supply, is not a new concept, neither is the use of photovoltaic (PV) water pumps, however the use of a submersible solar powered water pump (PVP) driven by a linear actuator in conjunction with an induced flow system is.

The problems of other water pumping systems and types of pump have been investigated and in an effort to resolve the problems of past system failures, in particular those of PV systems possible solutions have been explored. This includes the problems and choice of solar panels, whether or not controllers are required, and the design of a linear actuator as a driver for the pump.

Consideration of sustainable development and the consequence of pump failure has been the drive throughout the design and development of the linear actuator, the urgency of finding an 'off the shelf' pump for universal use rather having to design for each geographical site and the differing social and economic circumstances can not be overstated. However, the proposed linear actuator and water pumping system is not the solution to the worlds rural water supply shortage problems, but it will, providing there is adequate empathy of the problems of the South, go a long way to abating the problem.

Unlike many of the world's natural resources, water can be replenished. However, it is vitally important that humans conserve water and help to maintain the quality of water by discontinuing practices that contaminate and pollute the supply faster than it can replenish itself. Humanity requires a supply of fresh water to sustain life. Water supply systems provide water for irrigation, homes, businesses, industry, and waste removal.

Hand-carried water is still common practice in the South, where water is carried from rivers/streams/ponds to small villages/communities, in much the same way as they did in antediluvian times. When surface water becomes scarce, people use the stored rainwater, which is caught by and stored in open tanks. In deserts such as the

Sahara, the only dependable water sources are the oases. Elsewhere, water supplies are often inadequate because supplies are limited and the water is often contaminated. Such water was often responsible for typhoid, dysentery, and cholera. Along with malaria, these diseases are still a major problem today, particularly in the South.

From information gathered, globally the total amount of fresh water is 2.53% of the total water on the planet, some 35,029,000km^3 or 3.223 x 10^{16} litres, [1-4]. The majority of freshwater is groundwater; although plentiful as a resource, its needs to be tapped. It follows that one appropriate method of doing so is by the use of boreholes, where the water is withdrawn by means of a pumping mechanism.

The problem of 'clean' water is an international problem with no easy solution. The South bears the brunt of the problem, which is exacerbated by global warming, population displacement, and migration, to name but a few. However, development of new techniques may well go a long way to abating the problem. People must work together as change is difficult to implement; for any scheme to work the social aspects and consequences must be taken into full consideration.

Water is the fundamental requirement for life, and because individual circumstances, which dictate the amount of water individuals require, vary throughout the world, no exact figure can be placed on consumption. However, a guide to the minimum requirements to sustain life is available from the WHO[5], (Re: Table 1).

Table 1 shows the minimum requirements' of water intake per day with respect to individuals', animals, and crops per cultivated hectare, for tropical areas. It should be noted that these figures were published in 2003, and are read as a true account at the time of publication. Undoubtedly these figures will change in the future. It is suspected that the figures will increase due to such aspects as health issues and climate change. As climate change develops, the problem will be exacerbated.

Per Person		Litres/day
To Survive		5
Minimum		10
Normal conditions of life in village.		30
Per Animal		**Litres/day**
Cattle		40
Sheep and Goat		5
Horse		40
Donkey		20
Camel		20
Per Cultivated Hectare	**m^3/day**	**Litres/day**
Village farming	60	60 000
Rice	100	100 000
Other cereals	45	45 000
Sugar canes	66	66 000
Cotton	55	55 000

Table 1 - The basic requirements for water in tropical areas.

Apart from the immediate needs of people, social issues, economic issues and environmental issues, (i.e. sustainable development) need to be considered, and most importantly the health issues of the South.

Factors Affecting Sustainable Development

- **General** - Population [6, 7], Population Movement [7, 8], Natural Environmental Hazards [8, 9], Climate Change [10-12]
- **Social Issues** – Health [12-15], Community [16], Gender [14, 16], Ownership [16-20], Theft and Vandalism [14, 16]
- **Economic Issues** - Economic Bureaucracy [18, 21-27]
- **Institutional Issues** - Patents, Legislation [28-30], Governance Inadequacies [23]

In many areas of the South water supplies are limited and often contaminated. Such water supplies are often responsible for water related diseases associated with poor environmental health conditions, such as cholera, diarrhoeal diseases, malaria, schistosomiasis and typhoid; represent the single largest cause of human morbidity and mortality. In areas of the South with inhospitable surroundings millions of people do not have an adequate clean water supply consequently 25 000 people die every day due to unsafe water, [14]. For health reasons alone, there is an urgent need to make an improved water supply to the maximum number of people in the minimum period. Short and Oldach state "Good access to a new borehole in Nigeria was found to reduce illness by 50%.", [14].

However, the consequence of not suitably designing and maintaining the water pumps and borehole can still lead to health issues. People build up immunity to certain diseases; should any toxins be removed from the supply immunity may be reduced having potential for increased illness. In case of pump failure, here lies a further problem, as users would revert to the old water source succumbing to what could be a life-threatening illness. In general, sustainable safe water requires good design and a correctly sited borehole, 'clean' borehole surroundings and 'clean' reservoir outlets alongside good maintenance and management of all parts of the system including the borehole.

Humans require a supply of fresh water to sustain life. Water supply systems provide water for irrigation, homes, businesses, industry, and waste removal. Water is also necessary for public needs, such as water hydrants for fire fighting, and street cleaning. Urban water supply systems usually include works for the collection, transmission, purification, storage, and distribution of water. The North may take this for granted however the South does not afford this luxury.

There is a lack of detailed information/knowledge about the long term impacts of domestic water and environmental health initiatives and interventions on local people's hygiene behaviour and physical wellbeing. This makes designing and developing new water and health policies and strategies extremely difficult, since

there is so little realistic and historically informed data on which to base current thinking and future practice.

Both the microstructure and macrostructure of a community need to be considered for any project to be sustainable. Although there is an urgent need to make water readably available to all, without more ado, at present in many areas, this is not possible without major changes to current practices. At current rates of investment, it will take 25 to 40 years to realize this.

Nevertheless, sustainable development is feasible and has already been proven when using VLOM and Appropriate Technology. The case for installing sustainable boreholes as a means of extracting ground water is justified with the case of vastly improved health in Nigeria. Similarly, having set its own guidelines and standards the IFTA has enabled small communities in places such as Malawi to buy boreholes with the extra capital gained from Fairtrade. This investment in domestic water and environmental health systems and services will further contribute to improvements in physical well being and improved prosperity.

Since, 'Water is the keystone of the bridge to Sustainable Development', the axiom remains that people's understanding, participation, and responsibility are indispensable factors for successful projects and programs. The challenge remains how to weave these attributes into the provision of drinkable, reliable safe water supplies to the South in the coming decades.

However, there still remains the problem of a clean water supply for the harsh environment of the remote areas, even some urban areas, of the South. In order to achieve this, full consideration must be given to the principles and practices of Sustainable Development, Appropriate Technology, and Village Level of Operation and Maintenance (VLOM), [16, 31]. For it is a complex matter, where the individual issues overlap and at times are so entwined that they are inseparable. This is important throughout development and implementation of any new system, otherwise, the goal of the project may never be realised.

Bearing in mind that the main aim of the research is to design and develop a linear actuator pumping mechanism for a submersible water pump for use in boreholes; thought must be given to the issues already raised.

1.3 Thesis Structure

This chapter now goes through the layout of the thesis, giving a brief of the contents of each chapter.

Having given the background to and the aim of the thesis in this chapter, the thesis is taken forward in chapter 2 with a literature review. This chapter gives a brief on the principles for lifting and moving water. It then continues with a general description of pumps and wells, providing for the purpose of this thesis a distinction between deep and shallow wells. The chapter continues by listing the most common types of pumps which is supported with a description of some of the pumps that are currently available. This is followed with the reasoning behind the choice of a linear pumping action.

As solar powered water pumps are on the increase, and range considerably in style, listed are some of the solar powered devices, including Photovoltaic Powered Pumps (PVPs) which are potentially the 'end' product for the topic of this thesis, – "Linear Actuator for a Submersible Water Pump for use in Boreholes".

The chapter then probes applied solar energy and gives a brief of the development of solar powered water pumps. It also provides some insight into past failures by outlining the problems and pitfalls of the present day systems that are currently in use. Having explored the problems encountered and the improvements made to PVP systems and their performance; the potential for further improvements is investigated by looking at various ways in which linear motion, actuators, can be achieved. The chapter also provides a comparison of topologies, and concludes with a chapter summary.

Chapter 3 introduces the application for the actuator, the pump system and the individual components of the pump system. The chapter includes a general review of potential power supplies for the linear actuator and pump. Having explored the potential of various power supplies, the chapter examines the characteristics of solar cells (a photovoltaic array, i.e. a constant current source). The chapter continues by discussing the need for a controller for the pumping system. This is followed by a break-down of the pump components, and then explains the principle of operation. The chapter then gives the design requirements, and notes the imposed restrictions, and incorporates an evaluation of the static head and the required frequency to achieve the desired flow rate. This information is then collated in a summary.

Chapter 4 introduces concepts for the realization of linear motion. The chapter then shows the model results and makes a comparison of the generated forces for the different actuator topologies. This is followed with a theoretical evaluation of the stricture of the chosen E-core actuator outlining the requirements and the interlinked issues involved with the design of such a pump. The chapter continues with the initial test results achieved when using a single E-core, giving a brief description of the methods used to determine the generated force, and the inductance, and a summary of the theory.

The chapter then investigates of the use of springs and gives an account of the potential for an increase in the force of the actuator.

The chapter then continues with the design and manufacture, which shows and describes the workings of both diaphragm and piston versions of the linear actuator water pump. This is followed with the results of the pump tests for all the pump variations.

The chapter then continues with a three part discussion, which includes a system analysis, the use of springs, and the performance, problems and potential of the pumps; and then concludes with a brief summary of the chapter.

Chapter 5 considers the results of chapter 3 and chapter 4, and investigates and discusses possible improvements for the design and operation of a solar powered water pump. The first issue under discussion is the thermal quandary of the system and possible solutions are given. It then discusses switching methods for both electrical and mechanical control of the armature movement and provides a solution that utilises a mechanical carbon brush switching system.

Chapter 6 covers areas of preliminary investigations and possible future development. The chapter introduces three possible uses of permanent magnets within the actuator and pump system. The chapter also discusses the 'stacking' of E-core and the relevant inductance changes. This is followed by a section about improving the stroke length of the actuator. Then having given the case for the use of diaphragms, and the factors surrounding the hydraulics of the system, the chapter ends with a method of improving the output flow rate of the present pump.

Chapter 7 gives a general discussion of the findings of the research. Chapter 8 gives recommendations for improving the performance of the D.C. powered linear actuator water pump, the thesis is then brought to a close with the conclusions of the research in chapter 9.

CHAPTER 2

Chapter 2
Literature Review

2 Introduction

This chapter gives a brief on the principles for lifting and moving water. It then continues with a general description of pumps and wells, providing for the purpose of this thesis a distinction between deep and shallow wells. The chapter continues by listing the most common types of pumps which is supported with a description of some of the pumps that are currently available. This is followed with the reasoning behind the choice of a linear pumping action.

As solar powered water pumps are on the increase, and range considerably in style, listed are some of the solar powered devices, including Photovoltaic Powered Pumps (PVPs) which are potentially the 'end' product for the topic of this thesis, – "Linear Actuator for a Submersible Water Pump for use in Boreholes".

The chapter then probes applied solar energy and gives a brief of the development of solar powered water pumps. It also provides some insight into past failures by outlining the problems and pitfalls of the present day systems that are currently in use. Having explored the problems encountered and the improvements made to PVP systems and their performance; the potential for further improvements is investigated by looking at various ways in which linear motion, actuators, can be achieved. The chapter also provides a comparison of topologies, and concludes with a chapter summary.

2.1 Principles for lifting and moving water

To all intents and purposes there are five different mechanical principles in which the way water may be lifted or moved and they are in the main independent of each

other. The most obvious is the downward flow of water under the influence of gravity. The next is the direct lift, the physical lifting water in a container. Since water is incompressible it can therefore be 'pushed' or displaced. Another method is the generation of a velocity head, where water is propelled to a high speed, and the momentum of the water used either to create a flow or to create a pressure. The last, is by using the buoyancy of a gas, such as air, to aerate the water which in turn will lift a proportion of the water.

2.2 Pumps and Wells

Many different types of pumps for water systems are currently available [32], ranging from rural water supply handpumps to fully automated systems. Choosing the wrong one may lead to unsatisfactory water service. At present, firstly the capacity of pump needed is determined, and then an appropriate pump type is chosen. The capabilities of the present systems vary considerably from pump to pump. Some are only suitable for shallow wells and boreholes, with others best suited for deep wells and boreholes. However, this depends on the type of pump in use. Some are only capable of raising water up from depths of 7m (due to losses, 7m is an approximate practical value of a reciprocating suction pump), whilst others such as force pumps can pump water from depths of up to 450m.

Basically there are two categories of pump. Regardless of the pump type, each kind pulls water by suction from the well, and pushes the water by pressure into the distribution system. With this in mind, why then is there a distinction between deep and shallow wells?

Logically, a difference between deep and shallow wells can be defined as a 12m depth being classified as a shallow well, and a deep well as being 12m or greater in depth, for example 450m.

Shallow well pumps placed at surface level, depending on type, can be limited to a delivery head depth of 7m. For a suction pump to be able to lift water from depths

greater than 7m, the pump needs to be lowered until it is within 7m from the water level. It can then raise the water to its own level and then push it to the surface.

Of all the pumps used for deep boreholes, those that are located at the bottom of the borehole are of particular interest, especially the submersible pumps. However, there are several different types of pumps used to achieve this, each differing in performance.

2.3 Pump Types

The complexity of pumps that are used in present day systems, range from the simple mechanical mechanisms of handpumps to the complex electromagnetic pumps of the nuclear industry. Many types of pump are available, which include; Tesla Pump, Clark Pump, Stirling Cycle Pumps, Sonic Water Pumps, Solar Powered Pumps. The most common pump types are listed below,

- Handpumps
- Electromagnetic Pumps
- Centrifugal Pump
    - Impellers
    - Turbine Multistage Pump
    - Submersible Multistage Pump
    - Ejector Pump
- Positive Displacement Pumps
    - Helical Rotor Pump
    - External Gear Rotary Pump
    - Reciprocating (Piston) Pump
    - Reciprocating (Diaphragm) Pump

In general, pumps are either centrifugal or linear; the main types of pumps considered with respect to this thesis are reciprocating linear pumps. In general,

reciprocating pumps operate by suction. Pumps that operate by suction cannot pump air; consequently, the pump must be primed.

In raising water by suction, all the pump is doing is removing air from the inside of the pipe. As this occurs, the pressure inside the pipe drops below its original pressure, i.e. atmospheric pressure. Since the pressure acting on the water outside the well is atmospheric, and the pressure above the water inside the well is less than atmospheric, the water in the well rises because of the difference in pressures. As the pump continues to operate, more and more air is removed from inside the well further lowering the pressure, until the atmospheric pressure finally forces the water in the well to the level of the pump. Assuming the pump in use is 100% efficient, the maximum height to which the atmospheric pressure could push the water is approximately 10m. However, no pump is 100% efficient and in practice, most pumps can only raise the water 5m to 7m.

2.3.1 Handpumps

There are many different handpumps [32] readily available for the use in wells and boreholes. However, the performance, and the many problems associated with these pumps are investigated and presented in 'WORLD BANK TECHNICAL PAPER NUMBER 6 UNDP Project Management Report Number 2', titled Rural Water Supply Handpumps Project - Laboratory Evaluation of Hand-Operated Water Pumps for use in Developing Countries, [33].

In the report there is no clear distinction between deep and shallow wells, however Arlosoroff's [33] report for the United Nations Development Program suggests depths up to 7m for all the pumps tested, with the exception of a shallow force pump (Ethiopia Type BP50 – Manufacturer/Supplier E.W.W.C.A.) having 12m nominal maximum depth, to be classified as shallow wells. Nevertheless, with some of the pumps in the report it is difficult to distinguish at what level the demarcation occurs. For example, the Dragon No.2 (D) manufactured/supplied by Kawamoto of Japan [33] was supplied as a shallow well pump with additional

components for conversion to deep well use, the working range being from 7m to 45m, no demarcation line is drawn between the two levels.

2.3.2 Electromagnetic Pumps

By means of comparison to handpumps, the other extreme is the use of electromagnetic pumps. Electromagnetic pumps are used solely with fluids that are good electrical conductors, such as the liquid metals used to cool nuclear reactors. The pipe carrying the fluid is placed in a magnetic field, and a current is passed transversely through the fluid. This establishes an electromagnetic force in the direction of the flow that drives the fluid forward.

2.3.3 Centrifugal Pumps

The operating principle of the centrifugal pump can be illustrated by considering the effect of swinging a bucket of water around in a circle of water at the end of a rope. The force pushing the water against the bottom of the bucket is centrifugal force. If a hole were cut in the bottom of the bucket, water would flow through the hole. Further, if an intake pipe where connected to an airtight cover over the top of the bucket, the flow of water out the hole would result in the development of a partial vacuum inside the bucket. This vacuum would bring water into the bucket from a source at the other end of the intake. In this way, continuous flow from the source and out through the bucket would be established.

In terms of real centrifugal pumps, bucket and lid correspond the pump casing, the hole and intake pipe correspond to the intake and discharge of the pump, and the rope and arm perform the functions of the impeller, (Re: Figure 2.1).

Centrifugal pumps include radial flow, axial flow, and mixed flow units. Centrifugal pumps consist of a pump casing, an inlet pipe a discharge pipe and an impeller. As the impeller vanes rotate water is drawn in through the central inlet pipe near the axis and the water is then discharged via the outlet pipe located on the circumference of the pump casing. As the impeller rotates, the fluid is forced

outward and passes through the outlet at high speed and therefore at high kinetic energy. The fluid's kinetic energy is then converted into flow energy in a diffusing section, or volute, which increases the cross-sectional flow area before the high-pressure fluid is discharged. Centrifugal pumps can be used for depths up to 4.5m. They are considered very efficient for capacities of over 50gpm and pressures of less than 65psi. Centrifugal pumps rarely exceed 100gpm flow or 100psi discharge pressure [34]. They are considered ideal for use as a booster pump to send water from a well pump to storage or to a distribution system.

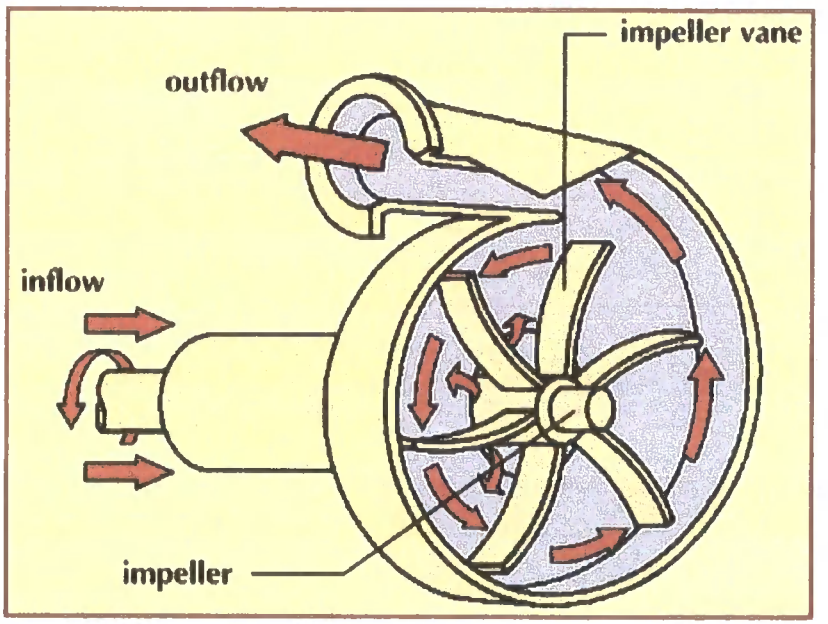

Figure 2.1 – Centrifugal Pump [35]

The advantages: Centrifugal pumps produce a smooth and even flow, and some types pump small amounts of sand. Centrifugal pumps are also usually reliable with a good service life. The disadvantages: Centrifugal pumps lose their prime easily, and their efficiency depends upon operating under design heads and speed.

Axial-flow devices move fluids and gases in the same direction as the rotation of the axis, rather than at right angles to it as in the centrifugal pump. The simplest axial-flow device is the electric fan, whose purpose is to increase the velocity, but not the pressure, of an air stream. If a fan with wide blades 'a propeller' is enclosed in a tightly fitting cylinder, the fan will increase air or fluid pressure without greatly changing the velocity.

2.3.4 Impellers

There are two basic types of impellers, volute, and turbine. Turbine impellers are surrounded by diffuser vanes, which provide gradually enlarging passages in which the velocity of the water is slowly reduced, thus transforming the velocity head into pressure head. Volute impellers are characterized by having no diffusion vanes. Instead, its impeller is housed in a case, which is spiral shaped and in which the velocity of the water is reduced upon leaving the impeller, with resultant increase in pressure. Choice between these two types varies with the conditions of use. The volute type is generally preferred for large capacity, low head use for shallow wells. A volute pump operates best with non-viscous liquids. The turbine type is used in water wells for deep lift installations.

A vane pump consists of a cylindrical casing with a small, internal rotor positioned off centre. Spring-loaded vanes project from the rotor to the casing. As the rotor revolves, the volume of fluid enclosed by successive vanes is decreased, thereby increasing the fluid pressure. Such units can handle small amounts of liquid or gas. For high-speed vane pumps, springs are unnecessary because the vanes are forced against the casing by centrifugal force.

2.3.5 Turbine Multistage

Turbine Multistage pumps operate under the same principle as the turbine-impeller centrifugal pump except there are one or more impellers mounted close together on a vertical shaft. The bowls are positioned below the water level, and the discharge pipe and shaft extend to a motor on the surface. These pumps are usually used for high capacity from deep wells up to 450m deep. The capacity and pressure depends on design, diameter, and number of impellers. The advantages: Produces smooth, even flow and is easy to frost proof. The long drive shaft requires a straight and vertical well casing. The disadvantages: To repair the pump, it must be pulled from the well.

2.3.6 Submersible Multistage Pumps

This type operates like a centrifugal pump except that several impellers are mounted together on a vertical shaft. The impellers and motor are in a housing, which is positioned below the water level. Submersible pumps can lift from up to 300m. The pump capacity and pressure depends on diameter, speed, and number of impellers. The advantages: Submersible pumps produce a smooth and even flow and are easy to frost proof. They also have a short pump shaft to the motor. The disadvantages: This pump type is easily damaged by sand in the water, and repair requires pulling the pump out of the well.

2.3.7 Ejector Pumps

An alternative name for an ejector pump is a jet pump. The basic components of ejectors are a nozzle and venturi tube. The process by which they operate is that, water is delivered, under pressure by the centrifugal pump through the nozzle of the ejector. The sudden increase in water velocity as the water flows through the narrowing nozzle decreases the pressure of the water. As a result, the water speed near the outside of the mouth of the nozzle is very high, and the pressure is very low. The low pressure zone acts as a partial vacuum and water from the well is sucked from the well around the inlet pipe of the nozzle and into a venturi tube. The gradual enlargement of the venturi tube decreases the water velocity and increases the pressure. The centrifugal pump then picks up the flow, sending part of the water through the discharge pipe and the rest back to the injector. If the well is shallow, the pump is on the ground surface and the jet and centrifugal pump are adjacent to each other. Water can be raised from up to 7m. For deep wells, the centrifugal pump is still on the surface, but the jet and venturi are submerged inside the well casing. Water can be raised in this way from up to 26m. The advantages: The only moving part in the pump is the impeller, so repairs are few. For both deep and shallow wells, jets can be offset from the well for easy access. The disadvantages: These pumps are easily damaged by sand, and as the distance the water needs to be lifted increases, the amount of water diverted from the

distribution system to be injected into the jet increases. For instance, to raise water 15m, half of the water pumped is returned to the jet and to raise water 30m, 76% is diverted.

2.4 Rotary Positive Displacement Pumps

In general, in positive-displacement pumps, fluid is displaced, or pushed out of a chamber, as part of the pumping mechanism fills part of the chamber and tends to decrease its volume. This action increases the fluid's pressure. Positive-displacement pumps can have reciprocating or rotary mechanisms.

2.4.1 Gear Pump

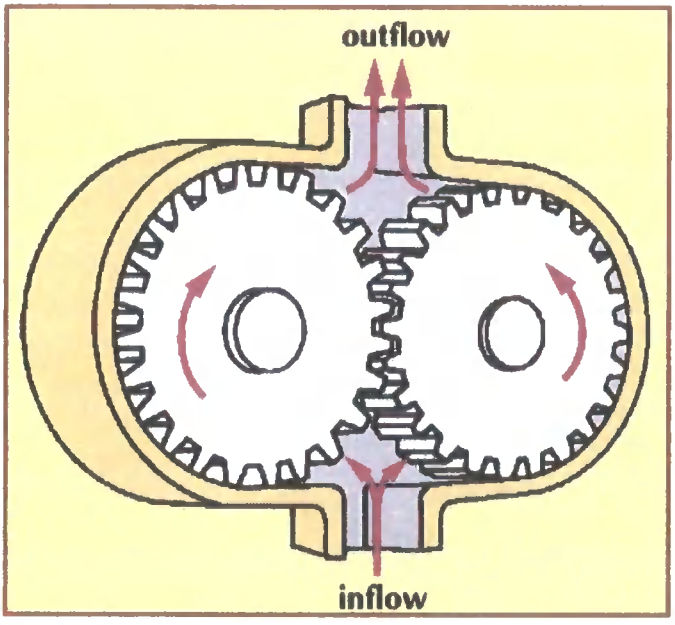

Figure 2.2 – External Gear Rotary Pump [35]

Positive-displacement rotary pumps include gear (Re: figure 2.2), lobe, screw, and vane devices. A common gear pump contains a set of two closely meshed gears enclosed in a tightly fitted casing. Fluid is drawn into the clearance space between the meshing gears, and its pressure is subsequently increased. Lobe pumps resemble gear pumps but have two to four lobes (rounded, projecting parts) in place of gears. They deliver an almost steady flow without pulsations.

2.4.2 Helical Rotor Pumps

The helical rotor pump operates like an auger to force water up through the pump. As the screw rotates, the material is pushed along this moving cavity. If the discharge end is designed to close the cavity, the pressure builds up, forcing the fluid into the outlet line. The motor and auger are in a housing under the water level. The capacity of the pump depends on the design of the rotor. Water can be pumped from depths of up to 300m and well casings can be 100mm or larger in diameter. The advantages: Helical rotors produce a smooth and even flow, and they are easy to frost proof. In addition, there is a short pump shaft to the motor. Sand also damages these pumps less than any other type. The disadvantages: Repair of the pump requires pulling it from the well.

2.5 Reciprocating Positive Displacement Pumps

There are two general types of reciprocating pumps. The piston pump and the diaphragm pump. Both types of pump operate by using a reciprocating piston or diaphragm. The liquid enters a pumping chamber via an inlet valve and is pushed out via an outlet valve by the action of the piston or diaphragm.

2.5.1 Piston Pump

A piston pump can be based on a single piston (figure 2.3) or, more likely, multiple parallel pistons. The pistons are reciprocated using cams or crankshafts, [35]. The stroke length of the positive displacement pump is generally adjustable. This type of pump can deliver heads of up to 1000bar. The largest sizes of piston pumps can deliver flows of $40m^3/hr$ (11.11Litres per second). In practice these pumps are more likely to be used for metering low flow rate fluids at more modest pressures in laboratories and chemical process plants. Piston pumps are not generally suitable for transferring toxic or explosive media.

However, direct linear drive actuators are now more readily available, it may be possible to utilise such actuators to act as the drive mechanism, thus eliminating the need for any rotary driving mechanism, [36].

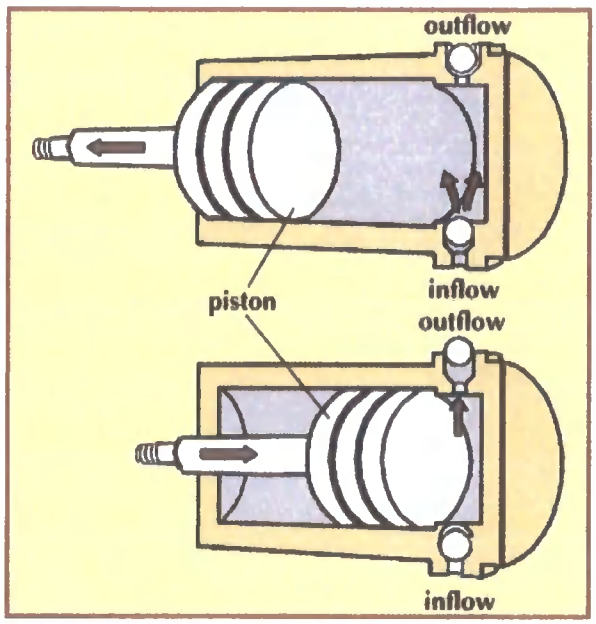

Figure 2.3 – Single Action Positive Displacement Pump [35]

Figure 2.3 shows the cross-section of a single action positive displacement pump. Low pressure fluid enters the pump, usually through a one-way inlet valve, and a tightly fitted piston, or plunger, moves to decrease the cylinder volume. The fluid pressure is increased before the fluid is expelled through an outlet valve. An example of such a reciprocating device is a hand operated bicycle tyre pump. Single action piston cylinder devices can handle only moderate flow rates. Double action units can handle more because the fluid has a point ingress and egress, alternately, on both sides of the piston.

Reciprocating pumps are generally very efficient and are suitable for very high heads at low flows. This type of pump is self priming as it can draw liquid from a level below the suction flange even if the suction pipe is not evacuated. The pump delivers reliable discharge flows and is often used for metering duties delivering accurate quantities of fluid. The reciprocating pump is not tolerant to solid particles and delivers a highly pulsed flow.

If a smooth flow is required then additional the discharge flow system has to include features such as accumulators (figure 2.4) to provide even flows.

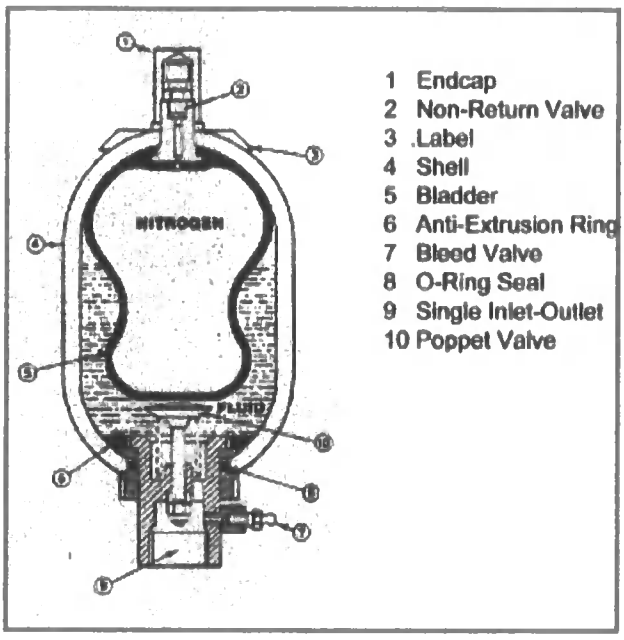

Figure 2.4 – Accumulator [37]

Reciprocating pumps designed for delivering high pressures must include methods or releasing excessive fluid pressures. The pumps should include for built in relief valves or relief valves should be included in the fluid circuit which cannot be isolated from the pump.

Shallow Reciprocating (Piston) Pump: - A piston pump uses the up and down or back and forth movement of a piston to displace water in a cylinder. As a piston is driven in one direction, water fills the chamber behind it. The water is forced into the system when the piston reverses directions. Valves control the Flow of water into and out of the chamber. Shallow Piston pumps can be used up to 7m. Pump capacity depends on cylinder size and the frequency of the stroke. The pressures it can produce are limited by the strength of the pumping equipment and motor horsepower. The advantages: It can pump small amounts of sand. It can also be installed over small diameter wells. It has a constant rate of yield (positive

displacement), and is adaptable to hand operation. The disadvantages: It causes a pulsating discharge, and may cause noise and vibrations.

Deep Reciprocating (Piston) Pump: - This is the same as for shallow except the pump cylinder is attached to the bottom of the drop pipe. As the piston moves up and down, it pumps water up through the drop pipe. Deep-well piston pumps can lift water from 180m. Double acting piston pumps can pump 65% more water with only 15% more horsepower. The advantages and disadvantages for this type are the same as for shallow piston pumps.

2.5.2 Diaphragm Pump

At present there are two types of diaphragm pumps; the hydraulically operated diaphragm pumps and the air actuated type. However, other methods of drives can be implemented, such as the use of electromagnetic linear actuators.

Diaphragm Pumps have many advantages over the traditional piston pumps, particularly because the pump's working parts are never exposed to the liquids being pumped. In comparison, the same liquids being pumped generally lubricate the upper working parts of, piston, plunger, and roller pumps, and the bearings and seals are always in contact with the chemicals or water. Since these devices have no piston rings through which fluid can leak, they are often used to pump toxic fluids or to avoid contamination of biological fluids.

In general, the design of diaphragm pumps is that the diaphragm is pushed not pulled. When they pressurise liquids, they are being thrust by a piston and are correctly seated on the head of the piston for that purpose. Consequently, the diaphragms are fully supported, therefore do not stretch, pull, deform, or suffer any other stress that they were not designed for.

In a diaphragm pump, a pulsating flexible diaphragm replaces the piston. When the piston ends its 'power' stroke; the diaphragm goes back into the lower part of the cylinder, assisted by the piston or under the force of gravity, creating a slight

vacuum in the pressure chamber thus drawing fresh liquid into the head, which will then be pushed out to the non-return output valves by the diaphragm, when it is pushed again by the piston.

Providing that the inlet lines and valves from the source are not clogged, the filter is clean, and the inlet non-return valve in the line feeding the pump is open, there is no problem. The diaphragm pulling the liquid into the chamber is not stressed. However, if there are obstructions in the line of any kind, the diaphragm has to pull hard to fill the chamber, creating a high vacuum. This now causes the diaphragm to be pulled by the piston head, deforming the centre mounting of the diaphragm. If the pulling effect becomes extreme due to a higher degree of clogging, and, of course, a higher inlet vacuum, then the diaphragm will be severely deformed and even be eroded by the edge of the washer holding it to the head of the piston. Inevitably, the washer will cut the diaphragm, subsequently diaphragm failure with possible damage to or failure of the pump and/or a contaminated output the result of mixing of lubricating oil and water.

Maintenance - A common problem encountered when pumping is that of caking-up resulting in blockages and pump failure. Chemicals, especially liquid absorbing powders and coppers have a habit of caking-up in the fittings. However, the function of the proposed pump is to pump water, therefore, the main problems of caking-up are envisaged as those resulting from the minerals present in the water source and those arising from electrolysis, degradation of materials, and rust. Careful choice of materials at the design stage or the provision of a sacrificial earth can overcome/prevent any electrolysis problems.

The best prevention for this problem is to regularly clean the filters, washing the screens out thoroughly. Also, check the inlet non-return valves periodically for blockage. If the output is still reduced to a trickle or little more, and not what is considered normal, then there is some blockage either in the output line or internal plumbing of the pump.

Another common cause of the high vacuum problem is the inlet non-return valves lines that are closed when the pump is started. Diaphragm pumps will pump air when there is no liquid around, so if the inlet non-return valve is closed, they will sit and suck vacuum with the subsequent consequences, probably the easiest solution to this problem is to prime the pump before use.

2.5.3 Hydraulically operated diaphragm pump

The hydraulically operated diaphragm metering pump is used for similar duties as the piston pump. It has some significant advantages compared to the piston pump in that the design does not require glands or piston seals. The diaphragm in the hydraulically operated diaphragm pump [37] (figure 2.5) is actuated using a plunger pump arrangement. This provides full support of the diaphragm allowing high pressure operation. The pump can include for duplex diaphragms with the interface being monitored for failure of the diaphragm in contact with the fluid. This type of pump can be used for pumping toxic and explosive fluids. The pump can deliver heads of up to 700bar and transfer flows of up $20m^3/hr$ (5.56l/s), [34]. These pumps require continuous monitoring as the diaphragm is under high fatigue loading and the inlet and outlet valves are subject to erosion and blocking. Under a high quality maintenance regime these pumps are very reliable, [35]

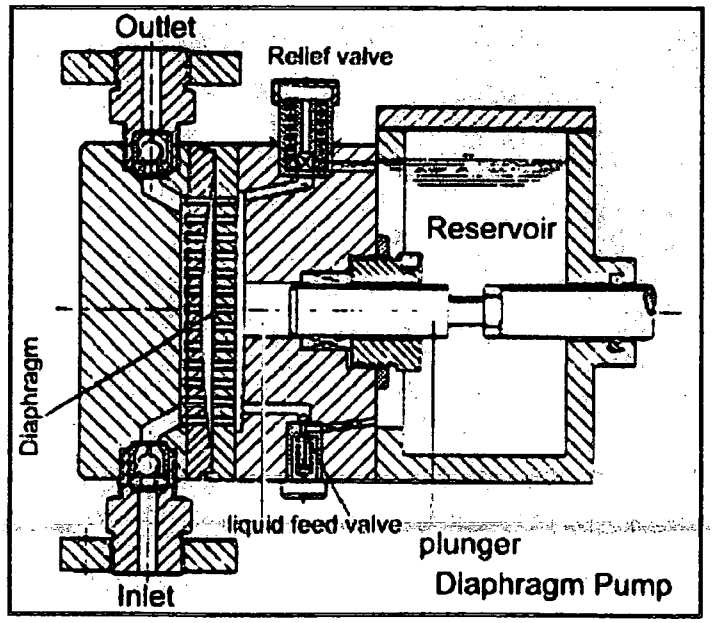

Figure 2.5 - Hydraulic operated diaphragm pump [37]

2.5.4 Air Powered/Operated Diaphragm Pump

The air operated pump is generally a low cost work horse pump used for transferring any type of liquid including sludge. The inlet and outlet valves are often low cost easily replaced flap or ball valves. The pump is comprises two circular chambers each split by a large elastomeric diaphragm. The two diaphragm centres are mechanically coupled together with a shaft, (figure 2.6). An interlocked valve admits air pressure to one side of one of the chambers and exhausts the air from the opposite side of the other chamber. This causes both diaphragms to move; one diaphragm pushing fluid out through a non return valve, the other diaphragm drawing fluid in through a non return valve. On completion of a full stroke the valve reverses the air supply and exhaust directions causing the diaphragms to move back. The diaphragm which was pushing fluid out of the pump now sucks fluid and the diaphragm admitting fluid now pushes fluid out. The system is therefore double acting.

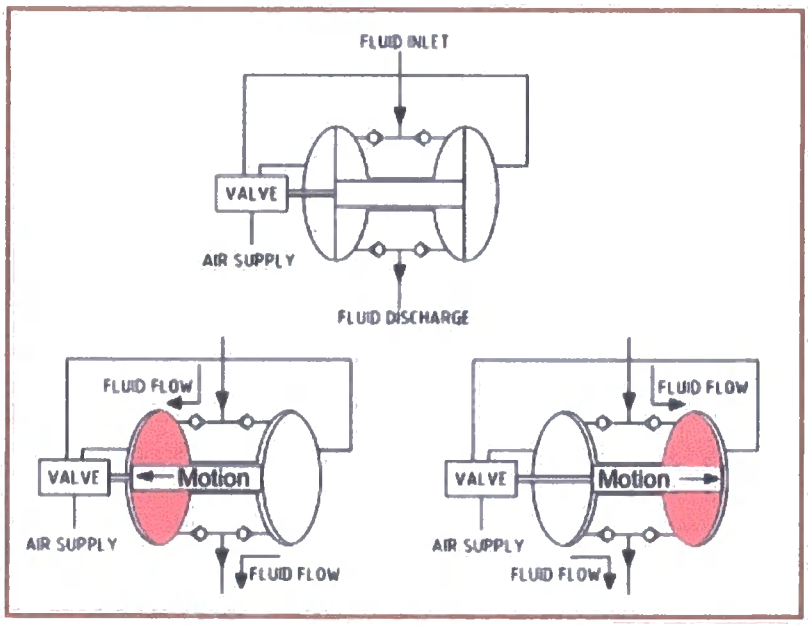

Figure 2.6 – Air Operated Diaphragm Pump Operation Cycle [37]

(Relief valves are not required for safety for the air operated diaphragm valve.)

The pump capacity is limited by the air pressure available, approximately 7bar (100psi), and the design of the diaphragm. An elastomeric diaphragm has a limited life and will only operate for a few million cycles. A flow rate of about 40m^3/hr (11+l/s) is a reasonable maximum achievable flow with a larger pump. For any air operated diaphragm pump the higher the flow the lower the discharge head possible. Air powered diaphragm pumps are self-priming and their flow rate and pressure can be easily controlled.

Figure 2.7 shows a positive displacement reciprocating double diaphragm action pump, with integral inlet and outlet non-return valves and minimum number of components for easy maintenance.

The pump is powered/operated via compressed air, the standard air supply at up to 7Bar (100psi) supply rating. This type of pump can be operated safely in fire hazard zones or areas subject to flooding. Regulating the air supply pressure controls the liquid flow rate and delivery pressure. If operated against closed delivery line, the pump will stall without overloading and restart automatically when the delivery line is reopened.

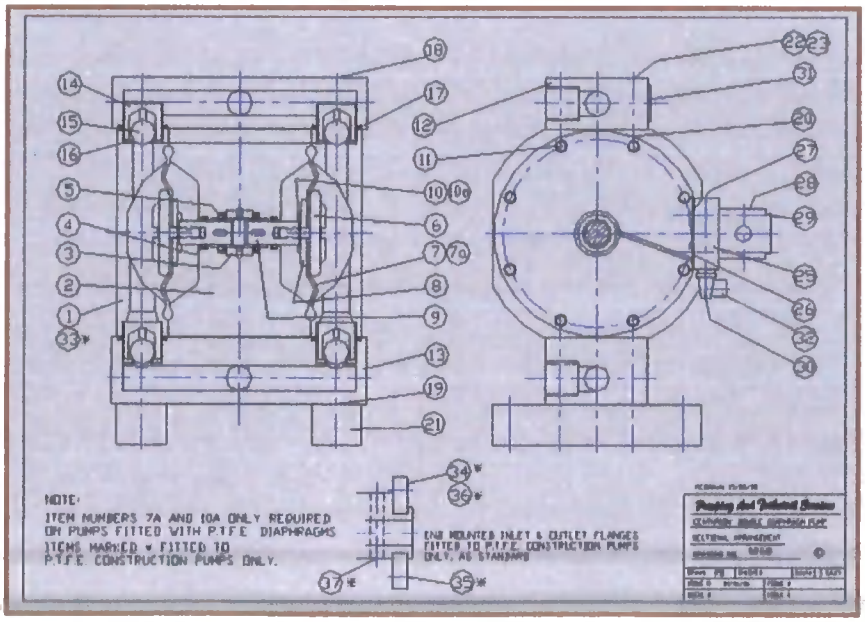

Figure 2.7 - Reciprocating double diaphragm – Air Powered Pump [38]

The pump is designed around a skeleton of stainless steel rods which ensure that hydraulic forces put the plastics components in compression rather than tension. Non-Metallic parts are machined from solid block material for maximum strength and Chemical Resistance. The air shuttle valve is externally mounted.

The sectional drawing, figure 2.7, shows two diaphragms that are connected by a rod. The reciprocating motion is produced and powered via compressed air, and is controlled by the air shuttle valve, which receives a changeover signal at the end of each stroke. Each diaphragm fluid chamber has an inlet and outlet non-return valve, which are connected by manifolds to the respective common inlet and common outlet ports. Depending on the application, the non-return valves can be gravity-seated balls or other types such as flap valves.

The primary control of the pump flow rate and pressure is normally by means of a pressure regulation valve in the air supply line. Because the air acts directly on the fluid via the diaphragms, the maximum fluid pressure which can be generated at zero flow condition is equal to the air pressure being applied. It follows that to make the pump operate at a useful flow rate; the driving air pressure must be higher than the fluid delivery pressure of the pump.

The maintenance intervals for these pumps are normally determined by the life of the diaphragms; the length of diaphragm life is dependant of the total number of operating cycles and degree of stress, which they encounter.

In order to maximise the lifespan of the diaphragm, the following points should be taken into account

- The driving air pressure should be set at the minimum level required to achieve the duty.
- Continuous operation at the maximum flow rate should be avoided - it is best to slow the pump to a steady rate, even if takes longer to finish the task.
- Allowing the pump to run without fluid for long periods should be avoided. Fitting an automatic cut-out device should be considered.

The pump can also be controlled by a valve or similar restriction device but these must be installed in the pump delivery line. If the delivery line is closed completely, the pump will 'stall' and remain stopped. When the delivery line is reopened, the pump should automatically start pumping again.

Due to the reciprocating pumping action, pulsations are generated which can cause vibration in the pump and pipe work; particularly at higher flow rates and pressures. This effect can be reduced or eliminated by utilising one or all of the methods given below.

- Reduce the flow rate and/or operating pressure.
- Use flexible inlet and outlet hose.
- Fit a pulsation damper in the pump discharge line.
- Fit an additional pulsation damper in the pump suction line.

A simple form of pulsation damper may be created by fitting a 'tee' in the line with a vertical/rising branch pipe which is sealed at the top, creating a bubble of air which compresses and expands to absorb the pulsations.

Most diaphragm pumps are capable of self priming even when 'dry', from depths of up to about 8m. However, the practical depth possible depends on several factors, the main ones being: -

- The vapour pressure of the liquid and operating temperature.
- Type and condition of the pump non-return valves.
- Volumetric efficiency of pump.
- Total length and route of the suction pipe work.
- Avoidance of any leaks in suction pipe work.

The pump should be located as close as possible to the liquid source and the suction pipe work should rise steadily from the liquid source to the pump suction. When priming, the pump can only empty air from the suction line into the delivery line at

low pressure. Therefore, there must be a vent for the air arriving in the delivery line.

Diaphragm pumps can be suitable for handling a certain degree of solids and sludge etc. Some pumps are available which, when equipped with flap type non-return valve, will pass any size solid that fits into the suction port. Normal units will be rated for passing solids of a certain size and if necessary, should be fitted with a suction strainer to restrict entry accordingly. Liquids containing abrasive solids may cause wear, particularly in the non-return valves, and may damage the diaphragms. Special materials may be used for the vulnerable parts to achieve a satisfactory life.

2.5.5 Pump Construction Materials

For handling water and other harmless liquids, cast iron or aluminium are the normal materials for diaphragm pump chambers and manifolds. Stainless Steel versions are readily available for handing chemicals, solvents and for ultra clean duties. For the more extreme corrosive chemicals, versions are available in plastics such as polypropylene, polyethylene, P.V.D.F. and P.T.F.E. for ultimate resistance against the properties of the pumped fluids and the working environment. Many of the lower priced polypropylene plastic pumps are of moulded construction and are not as robust as those with solid plastic components.

2.5.6 Materials for Diaphragms

For water and other normal fluids, the common diaphragm materials are Nitrile, Neoprene, and Ethylene Propylene synthetic rubbers. For some chemicals and solvents, Viton synthetic rubber will be suitable although more expensive. For extreme chemicals, P.T.F.E. diaphragms will be specified; often as an over-lay on a synthetic rubber backing. Generally, P.T.F.E. diaphragms, being less flexible, will have a shorter mechanical life and on some makes of pump will require modification to shorten the operating stroke when converting from rubber

diaphragms, [38]. These materials are also suitable for use as valve seats and flap type non-return valves.

2.6 Submersible Pumps

Submersible pumps can have a rotary or a linear driving device, and are either powered by A.C or D.C. The linear device can use either use a piston/s or a diaphragm/s. The type and performance of submersible pumps vary considerably, some examples are given below.

2.6.1 Flygt HX Submersible 5" Water Supply & Irrigation Pumps (50Hz)

(Reference - ITT Flygt - an ITT Industries company - Products, data and performance sheets)

These pumps manufactured by Flygt, are in general used for supplying water; it is claimed that they avoid problems with suction, un-priming and noise. They are radial type impeller pumps for use in 6" boreholes and come in seven sizes.

The pumps operate on a 230±10% voltage supply, and can be either single or 3-phase. Depending on the type/model of pump the power ranges between 0.55kW and 1.1kW. They are approximately 0.5m in length, with a diameter of 128mm; therefore they are suitable for use in a 6" borehole.

On the data sheet provided Flygt state that the 1.1kW pumps that provide a flow rate of 70l/min can achieve dynamic heads of 80m. However, when reading the performance graph it was found that the best dynamic head achievable, with a flow rate of 70l/min, is actually only 38m. Nevertheless, the pump can achieve a dynamic head of 80m, but only with a minimal flow. This ambiguity was found to be true for all the pump data; the highest flow rate for any of the pumps is 120/min, and the greatest obtainable head for any of the pumps is 80m.

2.6.2 Grundfo's Solar Powered Submersible Water Pump

(Reference - Grundfo's - Products, data and performance sheets)

Figure 2.8 gives the performance characteristics of a 'Grundfo's' solar powered submersible water pump for use in boreholes, [39]. The graph shows a rise in current and a reduction in flow rate as the delivery head (vertical lift) increases.

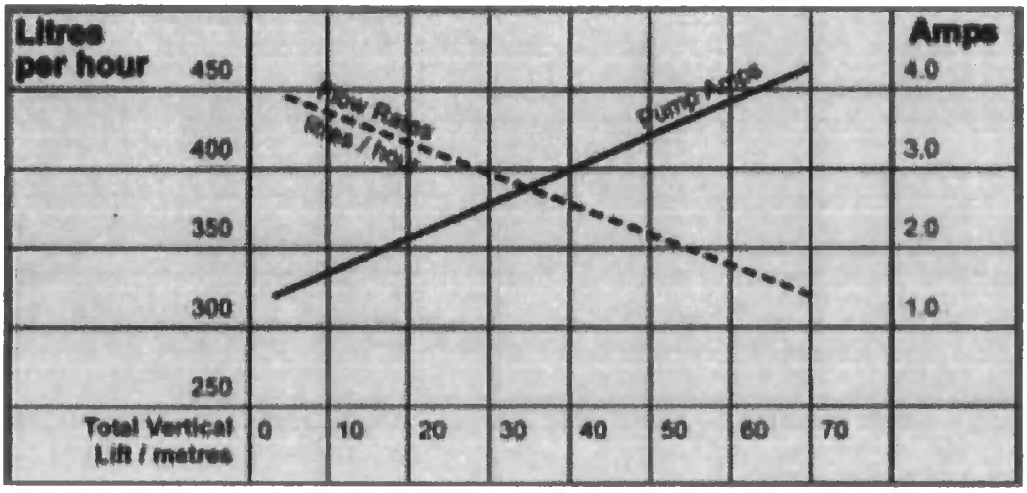

Figure 2.8 – Flow Rate versus Delivery Head
Grundfo's Solar Powered Submersible Water Pump

Figure 2.8 shows that the flow rate ranges from approximately 0.094l/s (5.67l/min or 340l/hr) at a dynamic head of 70m up to approximately 0.0124l/s (7.42l/min or 445l/hr) at a dynamic head of 5m.

This pump provides a steady flow rate, little change, over a wide delivery head range.

2.6.3 'Pedrollo' SK and SR Submersible Pump Ranges

The 'Pedrollo' SK Submersible Borehole Pump Range offers a flow rate up to 1.3l/s (80L/min - 4.8m³/hr) and with a dynamic head up to 77m. Even though the pumps are fitted with a patented anti-seize system, ensuring pump operation, even

after being left idle for long periods, SK pumps should only be used in clean water not containing abrasive substances. These pumps are particularly suitable for domestic use, [40]. This particular range of SK pumps can be installed in wells with a diameter of no less for 4 inches (4SK) and 5 inches (5SK). The 4SKm 100 model has an external diameter 96mm for 4 inch wells. The 5SKm 100, 5SKm 100M, and 5SKm 150 have an external diameter 120 mm for 5 inch wells.

Each pump utilises a bronze impeller with radial peripheral blades. The pump is driven by an induction motor, which is in an oil bath, with a built-in thermal cut-out device, motor protector, which ensures continuous operation at the maximum power required by the pump, the pump is cooled externally by the liquid being pumped. The pump also has a check valve, incorporated in the pump body.

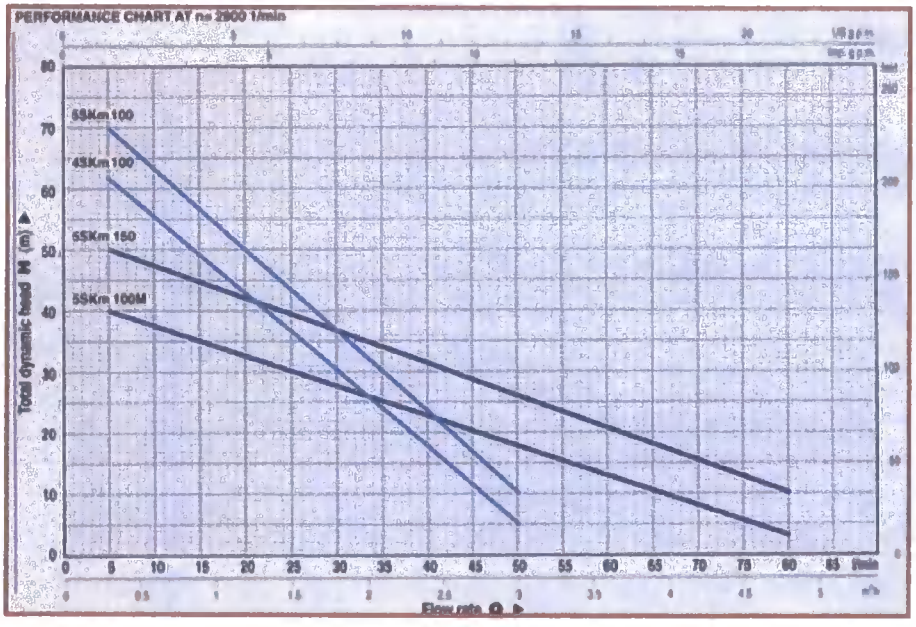

Figure 2.9 - Dynamic Head versus Flow Rate

Performance - The performance of these single phase impeller pumps is shown in figure 2.9; table 2.1 highlights some of the data associated with the performance of the pump.

The performance chart, Figure 2.9, shows long stable characteristic curves, the curve tolerance is in accordance with ISO 2548. The performance characterized by high absolute values over the majority of the curve; flat absorption curves at high

delivery rates, to prevent motor overloading even during prolonged use. The pump also has good suction capacities at both low and high delivery rates.

'Pedrollo' SK Submersible Borehole Pump Range							
Mode No.#	Size (inch)	Power (kW)	Dynamic Head Range (m)	Max. Flow Rate Q at lowest Head			
				l/s	l/min	l/hr	m^3/hr
5SKm100	5	0.75	77m – 10m	0.83	50	3000	3
4SKm100	4	0.75	68m – 5m	0.83	50	3000	3
5SKm150	5	1.1	53m – 10m	1.3	80	4800	4.8
5SKm100M	5	0.75	42m – 3m	1.3	80	4800	4.8

Table 1.1 – The SK Performance Data

The 'Pedrollo' 4SR8 - 4" Multistage Borehole Pump Range offers a flow rate up to 3.3l/s (200 L/min - 12m³/hr), and with a dynamic head up to 280m. As with the SK range the pump are fitted with a patented anti-seize system. However, unlike the SK range the pumps are capable of handling entrained sand, up to a maximum sand content of 150g/m^3. Nevertheless, the pump has some limitations, namely, the maximum temperature of the fluid being pumped is $+30^0$, and the pump is limited to a maximum of 20 starts per hour. These pumps are therefore more versatile in their use, and can be used in both domestic and industrial applications. 4SR pumps can be installed in wells with a diameter of no less than 4"(100m), and by comparison to the SK range five times longer in length, at 1.5m.

The 4SR range has four pumps which can operate with both single and 3-phase and another four more powerful pumps that operate with 3-phase only. The power of these impeller multistage pumps ranges from 0.75kW to 735kW (1HP up to 10HP); the greater the number of impellers the greater the power. The power of the 4SRm/4 and the 4SR8/4 (m indicates single phase: the RHS #4 indicates 4 impellers) is 0.75kW, and both pumps have the same flow rate versus head characteristic; with a 17m output head range from 27m down to 10m, providing a maximum flow rate of 3.3l/s (200 L/min - 12m³/hr). These pumps have minimal output at 27m. Whereas, the 3-phase 4SR8/42 has 42 impellers with a power rating

of 735kW, it is capable of pumping 3.3l/s (200 L/min - 12m³/hr) at a dynamic head of 98m. These pumps have a minimal output at 280m, [40].

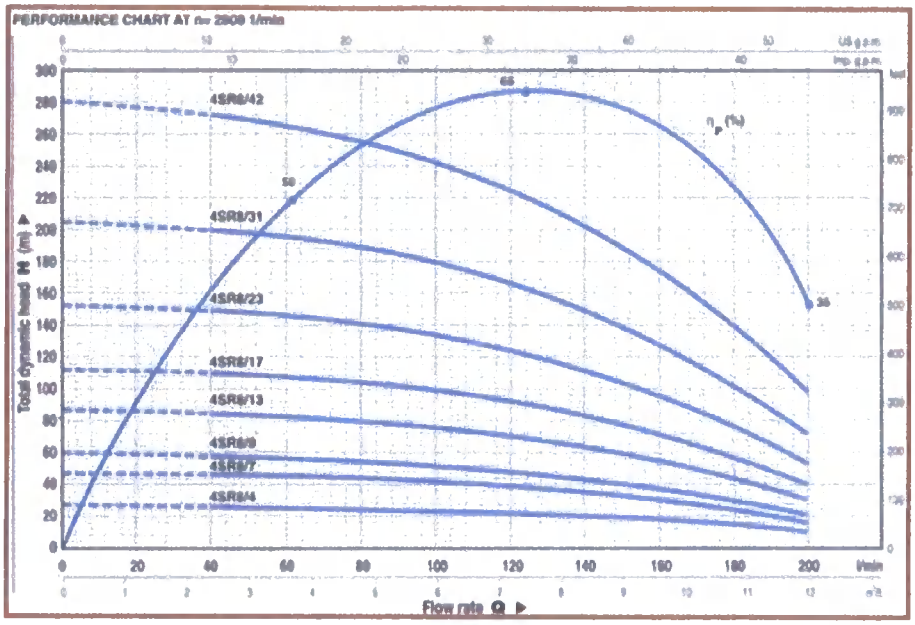

Figure 2.10 – Dynamic Head versus Flow Rate

Performance - The performance of these three phase multistage impeller pumps is shown in figure 2.10. The 4SR range of pumps combines the advantages of a submersible pump with the performance of a centrifugal pump. As submersible pumps, they assure reliable operation even with considerable water depth, up to 280m. The performance chart, figure 2.10, shows the stable performance characteristic curves, the curve tolerance is in accordance with ISO 2548. As multistage pumps they assure high flows at high heads. The check valve enables the weight of the column of water to be dispersed without stress to the impellers and diffusers, thus ensuring long pump life.

2.7 Patents

This section investigates the recent patents with respect to pumps and gives two novel pump examples. The first invention concerns a pump for liquids constructed so as to achieve an oscillating system in which the mass consists of the mass of

liquid itself; and the second invention a submerged pump with coaxial opposing pistons driven by double lobed camshaft.

2.7.1 Patent 1 - Description of Patent number EP0048224 - Liquid pump [41]

This patent states "This patent is based on the creation and maintenance of an oscillatory motion of the liquid in the tubing connecting the original location of the liquid with the point to which it must be transferred. During the various phases of the oscillation the pressure of the liquid in the various points of the tubing varies cyclically, passing alternately from higher to lower pressures than the liquid would have in absence of the oscillations. By designing the oscillating system with suitably rigid elastic organs, so as to achieve oscillations of suitable frequency and amplitude, a pressure cycle is achieved with an amplitude such that the minimum pressure achieved periodically at the starting point of the tubing is lower than that of the liquid to be pumped. However, the maximum pressure achieved at the end point of the tubing is higher than that of the surroundings.

Therefore, by opening and closing certain valves placed between the tubing and the starting and arrival points in correspondence with the phases of the pressure cycle described above, liquid enters the tubing at one end and exits at the other. Obviously, this transfer of liquid through the tubing occurs through the energy of the oscillation. This oscillation in turn must be continually fed through the administration of work by an external energy source, of any type."

This invention concerns a pump for liquids constructed so as to achieve an oscillating system in which the mass consists of the mass of liquid itself. Currently, volumetric pumps, (i.e. piston, membrane, casework pumps), and fluid dynamic pumps, (i.e. centrifuge, axial pumps) are known to be capable of supplying the broadest range of lift and delivery. However all of these pumps have in common the following problem: the pressure at the inlet may not be lower than the vapour pressure of the liquid in question, Torricelli's principle [42]. This limitation places constraints on the position of the pump with respect to the liquid: indeed, in the case of water the pump may never be placed at a theoretical height greater than 10.4m

[43] above the free surface. In practice, the actual limitation is much lower. Therefore by using the above principle may increase the distance between the liquid and the pump.

2.7.2 Patent 2

The patent by Mencarelli et al. [44] is titled "Submerged pump with coaxial opposing pistons driven by double lobed camshaft.", which is shown in figure 2.11. Mencarelli et al. [44] state "It is the aim of the present invention to realise a submerged pump having low power and high efficiency, for high pressures."

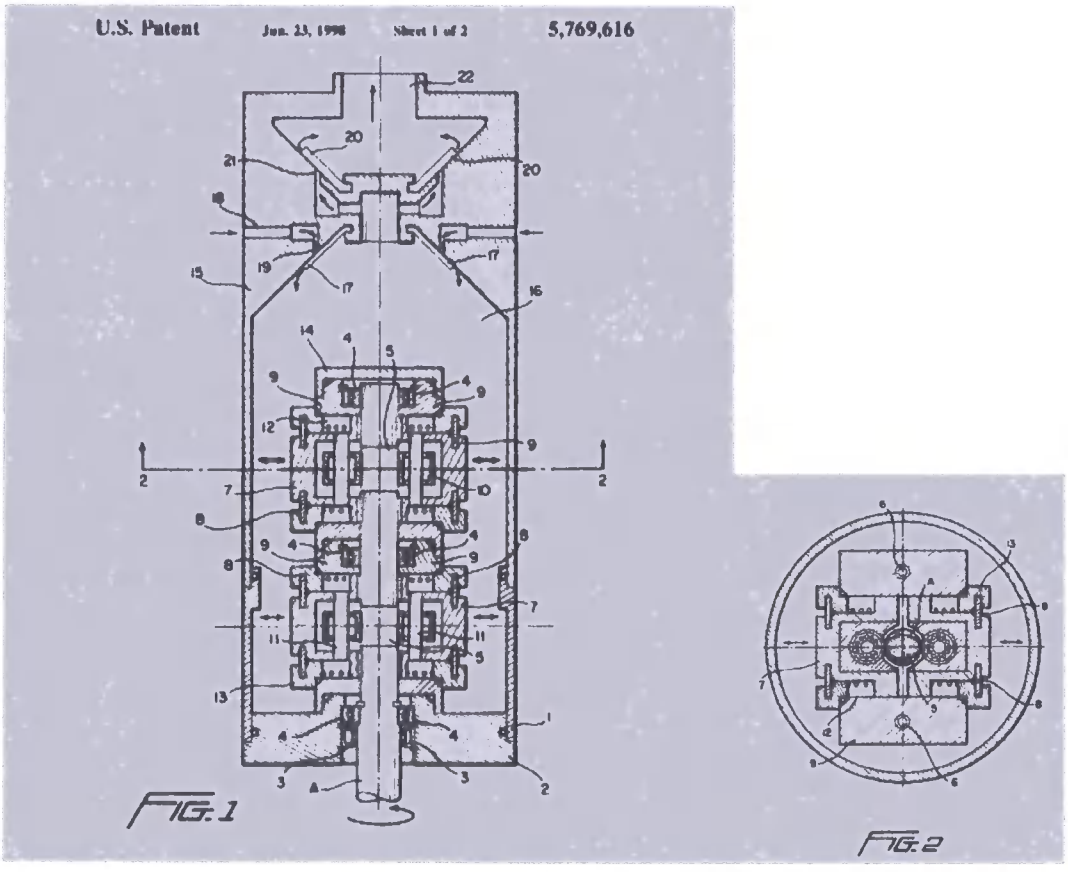

Figure 2.11 - Submerged pump with coaxial opposing pistons driven by double lobed camshaft.

Mencarelli et al. [44] make nine claims and provide two drawing sheets in the patent; however no performance data is given. The abstract states "The submerged pump according to the present invention comprises one or more modular pumping

groups, each consisting of a balanced, coaxial and opposing piston couple 7 on spool 10 and with a spring 12 return."

Apart from the use in boreholes, Mencarelli et al. [44] claim that there is "no practical limit inherent to the pressures" and that the pump has "a particular suitability to applications fed by sun energy or applications with low power".

This is a novel design, although simplistic, it is a rotary pump and consequently it has more than one moving part, as in a linear pump, therefore there is potentially more chance of mechanical failure.

2.8 Solar Energy as Energy Supplies for Pump Applications

Probably the first direct link between water pumping and solar energy occurred in the seventeenth century. "In 1615, Solomon de Caux published a description of a working solar "motor". He used a number of glass lenses mounted in a frame that concentrated the sun's rays on an airtight metal chamber partially filled with water. The sunlight heated the air, which expanded and forced the water out as a small fountain." [45].

The first attempts to convert solar energy into other forms revolved around the generation of low-pressure steam to operate steam engines. The first axicon (conical mirror concentrator, collector) was used to operate steam engines, but proved less efficient than conventional coal-fuelled steam engines. However, the current trend is to move away from coal-fuelled energy supplies, as a consequence, in remote areas there is potential for solar powered engines. Solar collectors of the parabolic type were first used to operate a printing press. The Ericsson-cycle hot-air engine can be used for the conversion of heat into motive power; this therefore provides potential for a solar energy powered pump.

Thermocouples utilising solar energy develop a voltage between a hot junction and a cold junction, each junction consisting of a pair of wires of different materials such as iron and nickel, hence thermoelectricity.

Meinel and Meinel [45] claim that in 1955, some 28 countries were involved in research, covering 15 different categories of solar energy. In 1976, UK-ISES published "Solar Energy, a UK assessment"[46], which was a major review of solar energy and gave particular emphasis to the potential contribution which solar energy might make to the future energy requirements of the UK. Since, then a great deal of new information has emerged, partly because of the increase in national and international research and development programmes. There has also been a marked increase in the number of demonstration projects and in the general level of awareness of renewable technologies.

Solar cells have progressed from the early methods which used the effects of sunlight on semiconductors with transparent gold coatings for electrodes; through a stage of using copper oxide and cadmium sulphide cells; to the use of two new semiconductors, lead sulphide and thallium sulphide. Improvements to solar cells continue and are becoming cheaper as they become more readily available.

All of the above have potential to supply motive power to a pump. As solar powered water pumps range considerably in style and are on the increase, listed are some of the solar powered devices,

- Rubber Belt Elastocaloric Engine (Powered by a Solar Pond)
- Solar Concentrator Stirling Cycle Water Pump
- Solar Powered Belt Turbine Engine
- Solar Powered Spring Engine (Based on Metal Leaf Springs of Shape Memory Metals)
- Solar Powered Wire Engine for Driving Water Pumps
- Stirling Cycle Water Pump Employing Heat from a Solar Concentrator

- Photovoltaic Powered Pumps

2.9 Solar Powered Pumps

In contrast to the pumps previously mentioned, §2.3, solar powered water pumps are on the increase, and range considerably in style. The focus is now Photovoltaic Powered Pumps – PVP's.

In 1981, the use of photovoltaics was still considered as a "future application". However, it was thought that in the near future the provision of pumped water for human and animal consumption and for irrigation, particularly in the South, was feasible. At the time, around 250 million (this figure now exceeds 1.2 billion [47, 48]) of the world's poorest people lived in areas which experience extended dry seasons, during which crop production is impossible without irrigation. It was envisaged that with proper land management and water resources, food production could be at least doubled, and life in many parts of the world could be transformed with pumped water. Jesch [49] gives the example: "a 20m well in the Sahara can provide $20m^3$ of water per day, enough to sustain some hundreds of people and as many head of cattle". Jesch [49] goes on to state, "Water pumping, disinfection, and desalination are very suitable applications for photovoltaics because, with an adequate reservoir, pumping can be restricted to the daylight hours and no electricity storage is required".

Similarly, since solar powered water pumps (PVP's) are localised, they can have additional benefits to merely pumping water, such as the solar panels charging batteries, hence the provision of a lighting system for small communities, so providing for sustainable development. The quantity of solar panels in a PVP's array could be increased so providing additional benefits to the community. Jesch [49] gives a example of "a 3kWp array, extending over an area of $30m^2$ to $40m^2$, could provide basic lighting, refrigeration, educational TV and pumped water for 50 African houses."

Such scenarios would give freedom of human resources within the local community enabling women and children to be educated or being able to help plant and reap crops, leading to self-sufficiency. Other benefits would be improvements in health, which is a major factor for providing safe clean water. Internationally, in excess of 25,000 people die every day due to unsafe water. Vast improvements in health have already been achieved in Nigeria with the use of boreholes to provide clean water thereby reducing illnesses such as dysentery, malaria, and typhoid by around 50% [16]. Further, the provision of a safe clean water supply could be an incentive to prevent the population drift to the towns, even encouraging skilled people to move to the villages, resulting in a boosted economy.

The global health problem arising from the lack of access to clean water is interminable having grave consequences for the future. The UK Meteorological Office predict by 2080 (assuming unmitigated greenhouse gas emissions) an estimated 290 million additional people will be at risk of falciparum malaria, (clinically more dangerous than the more widespread vivax malaria) [15]. The problems of the South can be significantly reduced with the provision of clean water, Short and Oldach [50] state "Solar (photovoltaic) powered water pumps could be a real instrument for the alleviation of water related deaths and illnesses in developing countries through the provision of clean water". However, this is not the sole solution to the problems of the South. Despite the benefits that access to sustainable clean water supplies can bring, the complex, inter-related social and technical issues also need to be addressed. Short and Thompson [16] state "Solar (photovoltaic) powered water pumping has the potential to bring sustainable supplies of potable water to millions of people in developing countries. Unfortunately, in many cases the application of the pump technology ignores the sociological and economic needs of the users, leading to lack of maintenance, inappropriate financing schemes, inadequate system management and ultimately, failure of the pump." To ensure the future sustainability of solar powered water pumps so reaching its full potential the three pillars of sustainable development must be implemented at the design stage to meet the needs of those who could use them. The social and economic aspects of sustainable development and the issues

involved in solar water pumping projects are discussed in the background section of chapter 1.

Short and Mueller [51], state that "For many years, solar (photovoltaic) powered water pumping has been portrayed as being able to revolutionise water provision in rural and developing communities. Mass produced pumps and cheaper PV panels have been promised, with the possibility of bringing safe water to those people who currently lack the basic human right. Although inroads have been made into reaching such an ideal situation, the current reality is somewhat different." Solar powered water pumps have been available since the late 1970s; however, their potential has not yet been accomplished. In 1978, the aim was to install ten million units by the year 2000 [52], however, by the year 1998 only 60,000 units had been sold [53]. In some areas fifty percent of the pumps no longer work. Why? What is the problem? Is it the politics? Is it the design?

2.10 Problems and Improvements to PVP Systems and Performance

Isolating the exact cause of the problem is not easy as there is no singular answer; the political issues are outside the scope of this thesis. Nevertheless, there is a definite link to the take-up rate for installation of systems. However, these complex issues are highlighted and referenced in chapter 1; the references take an extensive look at the issues, encompassing a general synopsis of water and surrounding issues, such as, Sustainable Development, Appropriate Technology, and Village Level of Operation and Maintenance (VLOM).

With respect to the problems pre-1980, system failures were attributed to the solar panels having module encapsulation faults, insect attack on exposed resin surfaces, cleaning problems, 'hot spot' failures, connection faults, and lack of lightning protection, which have now largely been overcome with improved design and protection [49].

However, the physical nature of the site/s where the use of PVP's is envisaged is probably remote often with dusty, arid conditions; consequently cleaning problems will remain. Although Jesch [49] in 1981 claimed that cleaning problems had been resolved evidence suggests otherwise, as in 1999 Hammad [54] quotes "temperature as hot as 40^0C and dust blown from a constant desert wind". Both conditions have the potential for solar panel failure, inverter failure and controller failure. The work of Mosalam Shaltout et al [55], shows that humidity also has an influential bearing on the type of solar panel used. It is evident that climatic variations will always be of significance to the design of a PVP system, however these changes are beyond our control, therefore the system should be designed in such a manner as to minimise the effect.

In 2000, Jafar [56] developed a model that predicts the flow rate of a PV pumping system to an accuracy of 8% and showed that the flow rate is a function of both irradiance and head. The model enables predictions to be made for any combination. The procedure was applied to the Solar Star 1000 pumping system. The reasoning for the model was that the degree of acceptance of PVP's by the people of Fiji was extremely low, the PVP having a history of failures and lower output than that expected by the users. Most of the problems arose because the system had been undersized and did not reach demand levels.

Badescu [57], states "A major advantage of PV pumping systems is that they are naturally matched with solar radiation as usually water demand increases during the summer when solar radiation is a maximum. A directly coupled PV pumping system is composed of a PV array directly connected to a DC motor driving a centrifugal pump. It is certainly the cheapest, simplest, and most reliable of all the different PV pumping systems". The system has been thoroughly investigated [57-60].

It is acknowledged by Badescu [57], that the optimum PVP design would be a PV array directly connected to a DC motor, a point reiterated by Short and Mueller [51].

However, as late as 2001, a 45% failure rate is noted by Kaunmuang [61], who attributes most failures to blockage of pumps and pipes and inverter failure. In 2002, Short and Mueller [51] comment on PVP standard systems, with AC motors driving centrifugal pumps, and highlight an almost 20% inverter failure rate in field tests.

Whether the system is AC or DC, the problem of matching the Maximum Power Point (MPP) curve of an array remains so some kind of controller is required. Inevitably, cost becomes a major issue, particularly in the South. Short and Mueller [51], state "two lessons to be learnt regarding electronics and controller:

1. If any kind of controller is to be used, be it for a DC brushless motor, an inverter for AC provision or a specialised MPP Tracker (MPPT), it must be inherently extremely reliable, or easily repairable/replaceable at local level. This places severe limitations on such a controller;

2. Given these limitations, it must be questioned whether or not a controller should be used at all. Indeed, whilst electronic systems should have increased in dependability since Roger concluded "direct coupling (between motor and array) is the most reliable pumping technique" [62], the evidence points otherwise."

Predictably, cost is always a factor. History demonstrates how dreams and aspirations have been quashed and resulted in a very poor uptake in a concept utilising a new technology, as in the case of solar hot-water heaters and solar house heating systems, 1955–1970, where cost was major factor. The added expense of complex controllers and batteries is immaterial in the more affluent North as spares and repairs are easy to access. However, the expense of complex controllers and batteries adds to the financial burden in the South. Therefore, PVP's must not only be reliable and robust, they must be economically competitive.

The problems associated with pump system failure and downtime for maintenance are:

- If the pump system fails, it may be a considerable time before a competent person is available to inspect the pump, and even longer to source and replace parts.
- Unless planned the same applies to downtime for maintenance.
- The consequences of either being that water users will be forced to resort to the more traditional methods of water collection, with the potential of a recurrence of health and social issues.

Obviously, the key to resolving these problems is reliability.

Another possible reason for the slow uptake of the systems could be that most pumps are designed for a specific application, even custom made, therefore the variations between sites is not provided for, as no single pump is suitable for all sites. As stated previously there are many different types of pumps available, each having their own specifications and performance, none of which have a multipurpose/multi-site use.

In 1999, the performance of different photovoltaic water pumping systems was investigated by Arab et al [59], using Typical Meteorological Year (TMY) data from four distinct Algerian climatic sites: Algiers, Bechar, Oran, and Tamanrasset. Their investigation involved three different profiles, "three tank capacities, two PV modules types, two PV array configurations, and several pumping heads, applied to two centrifugal pumps". Although the study used centrifugal pumps, it takes into account the different parameters of the system and its geographic location.

Arab et al [59], when discussing the performance of PV water pumping systems, state, "Photovoltaic (PV) pumps constitute a potential option whose widespread application is precluded by a lack of information and experience. The system performance is influenced by many parameters like the total manometric pumping head, the motor-pump type, the PV array configuration and the geographical location". Further, they conclude, "the PV generator costs can decrease if the simulation program accounts for the kind of pump, the pumping head and the daily load profile. The system can be optimised by studying individual requirements

with a simulation program." The hard facts of economics have defeated previous solar energy programs [45], consequently any model that encompasses cost is of value. Nevertheless, the study is applied to individual circumstances, which detracts from the idea of an off-the-shelf pump for universal use.

Some sites may require more solar panels or a different type of solar panel [55] to achieve the same output depending upon the geographical location of the site. In order to meet the supply demands of the water pump system the configuration of the array can be adapted as required for each individual installation site. This modular nature of photovoltaic systems greatly reduces cost, when compared to the enormous expense that would be incurred if a grid system were used for the rural districts of the South.

The study by Mosalam Shaltout et al [55], for the determination of suitable types of solar cells for optimal outdoor performance in desert climate investigated the integrated spectral response (ISR) and the electrical power over 32 spectral bands for monocrystalline, polycrystalline, and amorphous solar cells. Deviations were found in the behaviour between the ISR and the electrical output power in the measured bands. The results of ISR are shown in table 1.2.

Solar Cell Type	Spectrum	Maximum sensitivity at wavelength
Amorphous silicon	Visible	$\lambda = 0.522 \mu m$
Polycrystalline silicon	Infrared	$\lambda = 0.922 \mu m$
Monocrystalline silicon	Near Infrared	$\lambda = 0.704 \mu m$

Table 1:2 - Maximum sensitivity wavelengths for different types of solar cells[55]

From the results of their investigation, they conclude that, "the monocrystalline solar cell is more efficient than the other types." Since visible radiation is reduced in the desert climate and the cost of the monocrystalline cell is far greater than that of the polycrystalline solar cell, it is advisable to use polycrystalline cells in PV applications. However, they also recommend that monocrystalline cells be used for areas of increased humidity. Nevertheless, they do not rule out the use of amorphous solar cells suggesting that they could be used in conjunction with an

anti-reflective coating, so increasing the cells efficiency by 1.38%. This is a small improvement in efficiency of the solar cell.

The choice of cell with respect to cost is rarely relevant, as the cost of a cell is evaluated in terms of pounds per peak wattage, £/Wp. The fact that an individual cell costs more is in general outweighed by the improved peak wattage. The advice of choosing one type cell over another due to cost is debatable; perhaps it would be more beneficial if it were the pumps efficiency that was improved.

Muselli et al [63], have developed a methodology to determine the optimal size of PV-hybrid subsystems and to optimise the stand-alone system management. They claim it is a "valuable tool to design and evaluate PV-hybrid power supply systems for remote areas in terms of sizing and system operation". To that end, the installation of a PVP system must be included in such designs, so providing for sustainable development.

In 2001, Joyce, Rodrigues and Manso [64] developed a PV stand-alone system model based on the current–voltage characteristic of the modules and on a linear relation between the battery voltage, the state of charge (SOC), and the internal resistance of the battery. The reason for the model was that Portugal still has approximately 7000 homes isolated from the grid system and the intention was to provide "the same service quality to the end user that a grid system provides". They claim "very good agreement between the calculated yields and the performance indices for both the simulated and measured values". They also conclude "The model can be used to simulate the behaviour of the system during long periods and with different load distributions, using meteorological synthetic data, which will lead to a better understanding of stand alone PV system. An important feature of the model is its modular conception, which permits the model to be used in different types of PV systems like pumping systems". Whether batteries required or not, the model provides a design tool for the development of PVP's.

Badescu [57], claims that the use of batteries in conjunction with solar cells improves the PV pumping system operation by compensating for changes in the irradiance incident on the PV array.

Both Arab et al [59], and Badescu [57] have used a water storage tank to improve the PV pumping system operation. Arab et al [59], discuss the influence of different geographical locations on the PVP system along with the influence of the tank capacity over a number of autonomy days. Self-sufficiency is vital for small communities to survive. Using the total daily supply demand, over 24 hours, and different peak demand times, in order to prevent a water shortage, the tank storage discharge must be able to compensate for the shortfall in the pumps output. Nevertheless, this was found to vary depending on geographical area and time of year, unlike Badescu [57], whose model only included one site, Bucharest, states, "There is no obvious dependence on month and season". However, he agrees that the use of a water storage tank improves the PV pumping system operation. Arab et al [59], conclude "The daily load profile has little influence over the relative deficit if there is a tank with at least one autonomy day." ... "the geographical location influences the system performance." ... "the PV generator costs can decrease if the simulation program accounts for the kind of pump, the pumping head and the daily load profile." From the results it was also determined that the smaller the tank capacity, the greater the number of deficit hours.

In 2000, Kolhe, Kolhe and Joshi [65], when working with a centrifugal pump directly powered by photovoltaic PV array suggest that when designing a DC PM motor the magnetic field constant should be appropriately selected so extracting the maximum power from PV array. They state, "The DC permanent magnet motor coupled with centrifugal pump has the better matching when directly powered by photovoltaic (PV) array. The important parameter of DC permanent magnet (DC PM) motor is magnetic field constant." They conclude, "It has been found that the maximum output is available at the output-energy-weighted average value of magnetic field constant. Their research may well improve the performance of a DC PM motor directly coupled to a PV array by achieving the maximum mechanical output for the pump.

However, the problem remains that this will be only pertinent for a limited number of sites, those that involve the use of (DC PM) motor centrifugal pumps. In the paper it is unclear whether or not the motors are brushless; if not then the maintenance problems associated with brush gear remain. Further, even though the use of PMs improve the efficiency of a DC motor not all centrifugal pumps use permanent magnets, therefore it is still not suitable for all sites.

In 1995 a possible improvement to PVP's was proposed by Perris and Salameh [66], the idea was to replace the rotary motor and gearbox with a linear DC motor drive system positioned at ground level and coupled to the pump via a long connecting rod. Although this is a move towards the desired system, the use of a connecting rod in deep boreholes has potential problems. This idea was not entirely new. Prior to this date, in 1991, when Whitfield et al [67], were researching ways to improve the cost effectiveness of small solar photovoltaic water pumping systems, they moved beyond the assumption of a rotational motor, by suggesting that the drive system should be dc powered, brushless and placed in the borehole directly coupled to a reciprocating piston. Nevertheless, this opens the options of having the drive system based on the brushless permanent magnet principle or the variable reluctance principle. Furthermore, tangential forces from a conventional linear motor topology or normal forces from an electromagnet topology could be used to generate the thrust force.

2.11 Linear Motion Topologies and Actuators

At present, the majority of electrical machines are of a rotary configuration, principally due to their application. Obvious exceptions to this are the development of 'Maglev' levitating high speed trains, projectile launchers, and small biomedical actuators. Historically, long-stroke linear motion has been achieved with the use of motor driven cams and linkages, hydraulic rams, pneumatic rams, and motor driven ball-screws, none of which are appropriate for use in deep narrow boreholes. Therefore, the concept of using a direct drive linear electromagnetic device seems

to be logical. Not only is there the benefit of having a small (in size) actuator that will fit in the reduced envelope of the pumping device, for use in boreholes, the concept allows for efficiency, simplicity, and improved positioning accuracy; however the mechanical advantage of the use of the motor gearbox is lost. Further advantages are reduced maintenance and a far less chance of component and system failure.

For a number of years now the use of linear actuators has been, and continues to be, on the increase, with many advancements being made as the field of linear actuators expands. There are many designs available all serving their own purpose; consequently, this review identifies only some of the innovative concepts of linear actuators. Howe [36] states "many actuator types and topologies are emerging with widely varying operational characteristics, in terms of displacement (rotary or linear), speed of response, positional accuracy and duty cycle. As a consequence, it is difficult to give a general overview of the current status of magnetic actuators." An important point raised by Howe [36], is that most of the work undertaken by himself and his associates on specific actuation systems for a range of applications has only been made possible because of the emergence of high-energy, rare-earth magnets.

Howe [36] states "Of the various motor technologies and topologies, the tubular brushless permanent magnet motor offers significant advantages, in terms of specific thrust force capability and efficiency." There are two designs of tubular brushless motors, slotless, and slotted, both longitudinal flux motors; the latter generates a high thrust force. The work designed for Mueller and undertaken by Baker [68] has developed a linear generator for a direct drive marine renewable energy converter, a tubular machine, which needs to react a shear force of 100 kNm^{-2}.

Similarly, Brooking et al [69], use the principle of a variable reluctance permanent magnet (VRPM) machine for a reciprocating electrical generator claiming a shear stress of $100kNm^{-2}$. The work was based upon the topology developed by Iwabuchi et al [70] and Spooner and Haydock [71]. Weh, Hoffman and Landrath [72], and

the further development of High Torque Machines by Spooner [73] further support this. As with Howe's work on magnetic actuators, Baker also demonstrates the potential advantages of using, Permanent Magnet (PM) based topologies, although it is in the field of generators.

A Linear Induction Motor (LIM) produces a translational motion. Sen [74] compares rotary induction motors with LIM's noting that the thrust-velocity characteristic of the linear induction motor has the same form as the torque-speed characteristic of a rotary induction motor. Sen states "An important application of a LIM is in transportation". Other applications currently implemented include pumping of hot liquid, sliding doors, and curtain pullers, all reciprocating motions, suggesting that LIM's may be suitable for pumping water.

When discussing the linear actuator section of a reciprocating induced flow pump, Short and Mueller [51] state "If an airgap of 1T could be achieved in the electromagnet topology, a normal stress of 400kNm^{-2} would be achieved." When comparing conventional linear motor topologies to that of electromagnet topology, as shown in table 1.3, clearly the final option offers the best choice in terms of desired thrust and the ability to fit inside the physical envelope available in the pumping chamber.

LINEAR TOPOLOGIES		
TYPE	STRESS (Type)	FORCE / Unit Area (kNm^{-2})
Variable Reluctance Machine	Shear	40
Variable reluctance permanent magnet (VRPM)	Shear	100
Electromagnet topology (With an airgap of 1T)	Normal	400

Table 1.3 - Comparison of Linear Topologies[51]

Nevertheless, other means of creating linear motion need to be considered. Solenoids have been used for several years as a means of operating electrical door latches and locks.

Olaru et al [75], embrace a few constructive concepts, e.g. the conceptual idea of utilising the axial force of a solenoid in conjunction with a non-magnetic plate under repulsion. However, this is immersed in a transformer oil-based magnetic fluid which may prove to be impractical unless within a sealed chamber if it were to be used as the driver of a water pumping system. As with Howe's paper and Baker's paper, Olaru et al [75] support the case for the use of permanent magnets stating "Force is greatly increased with use of a permanent magnet placed on [sic 'in'] the core of the solenoid", achieved by applying PM's (sic permanent magnets) to the outside edges of the electromagnet. When discussing displacement, Olaru et al [75] outline two different types of support. The first, an elastic support generating displacements of 0.1mm - 0.4mm although they do state that this is dependent on the elastic constant; they further state that the actuator with elastic support is sturdier and more manoeuvrable than the second type with a support axle. The second, a support axle utilising a pendulum mechanism, produces displacements of several millimetres. They conclude "The actuator proposed in the paper generates low forces and very small displacements controlled rigorously by a dc current." This is the only indication of the generated force, however they do state "The load behaviour is influenced by the value of the resistance force, produced by the actuated piece". A DC current controls the displacements via an electronic tensiometer bridge determining any differential.

A paper by Howe [36], shows the use of an armature placed between two E-cores which produces a tangential force for a reciprocating positive displacement diaphragm air-compressor of the type used in pneumatic medical applications. From the presented model it can be shown that it is possible to achieve a displacement of up to 7.5mm for a given flow rate; however this is dependent on the frequency. The predicted displacement and airflow rate frequency responses are given at 40 and 80 mmHg delivery pressures. No indication is given to the dimensions of the pump; the use is for medical applications, which suggests that the E-core are small and the forces generated are small, however the principle of operation may be of use in the design of a linear actuator for water pumps.

Sedda, Fageon and Yonnet [76] have developed the use of electromagnetic actuator valves with small airgaps, which are robust and easy to control, for use in an internal combustion engine. They have improved on the conventional form of a valve actuator; simple electromagnetic valves are equivalent to two C-core electromagnets attracting a moving part at each end of its stroke. The stroke is relatively high at approximately 8mm. The moving part operates by the use of springs and producing a type of harmonic oscillator. The improvement comes from the fact that they polarize the C-cores by adding the flux of the permanent magnet, in series, to the coil flux. By doing so, it is possible to obtain permanent attraction forces and since the force is now a linear function of current for a given airgap the motion of the moving part is more easily controlled.

Guerin et al [77] have taken this a stage further with the use of parallel polarized actuators, which utilise only one coil and one magnet. They claim, "...the force direction and the force intensity are directly driven by the current in the coil". However, the force intensity is questionable because once again they incorporate springs into the system, so is it the spring force or the electromagnetic force that operates the system? On the other hand, they state, "...main advantages of this configuration are its great compactness", and "...the structure operates as a concentrating flux system", consequently a ferrite magnet can be used. The main disadvantages are the complexity of the shape of the magnetic circuit, and the non-planar flux circulation, which make it difficult to construct with soft iron laminations, but iron powder materials can be used.

2.12 Comparison of Centrifuge and Linear Output Characteristics

With conventional centrifugal pumps and motors the Flow Rate (Q) versus Head (h) characteristic is of a parabolic nature therefore any small change in the x-parameter (due to the quadratic function) will result in large changes in the y-parameter, i.e. a small change in Head will result in a greatly reduced Flow Rate. The point of maximum efficiency for such pumps occurs at the intersection of the apex of the parabola and the axis of symmetry of the parabola, (figure 2.12).

Such pumps are limited to a small change in head, in that the efficiency of the pump is greatly reduced over a small head range. In general pumps of this type are designed for one specific use, because the performance characteristic is individual to that pump, therefore is not suitable for all sites.

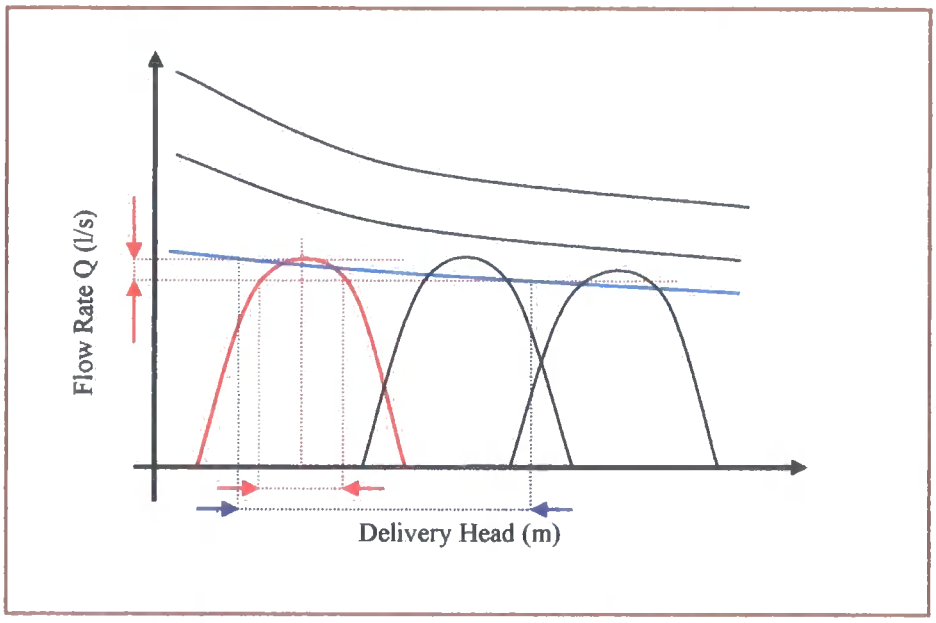

Figure 2.12 – Flow Rate versus Delivery Head - (Comparison of the Centrifuge (Solid Red Line) and the Linear (Solid Blue Line) Output Characteristics)

By comparison a linear pump has an output characteristic where the output flow rate reduces as the output head increases and hence can operate over a larger head range although at a reduced flow rate at higher heads, (figure 2.12). However, the output of a pump utilising a linear motion can be boosted via the use of an induced flow system, although with reduced efficiency, [78, 79].

The reason for the induced flow is that a linear motion system that draws 40W input power and has a hydraulic output power of 30W has an efficiency of 75%. With the introduction of an induced flow system will draw 80W input power; however the hydraulic output power is now only 55W, therefore the efficiency has dropped to 68.75%. Therefore the efficiency reduces, but not sufficiently as to compensate

for the entire power now being drawn and therefore more flow. The 25W increase in hydraulic power means that the flow rate increases by a factor of 1.83.

2.13 Summary

This chapter has introduced the principles of lifting water and distinguished between deep and shallow wells. This chapter has discussed the most common types of pumps and this has been supported with a description of some of the submersible water pumps that are currently available and their performance. The chapter then gave two novel patents on pump design.

The chapter then probed applied solar energy and gives a brief on solar powered water pumps. It also provides some insight into past failures by outlining the problems and pitfalls of the present day systems that are currently in use. Having explored the problems encountered and the improvements made to PVP systems and their performance; the potential for further improvements is investigated by looking at various ways in which linear motion, actuators, can be achieved. The chapter also provides a comparison of topologies.

From the literature gathered, it appears, that improvements made to PVP systems, and the performance of PVP systems have been directed at specific sections opposed to the system in general.

Within the Solar Powered Pumps category Photovoltaic Powered Pumps, PVP's are at present becoming more readily available. Short and Mueller [51] when discussing solar powered water pumps state "Previously designed systems appear to have matched off-the-shelf components, in order to standardise the systems and reduce costs. However, this may not be the optimum solution for the application and the environment in which the system is being used". The aim of the thesis is to provide an actuator for a linear pump which is suitable for all pumping situations.

Within the chapter is the reasoning behind the choice of a linear reciprocating pumping action. Earlier it was concluded that the electromagnet topology, with a normal stress of 400kNm^{-2}, would produce the desired thrust force and hence be able to operate at the greatest depth. Therefore a linear reciprocating pump utilising a normal force has been chosen as the method for driving the PVP. However, the ability to fit an actuator inside the physical envelope available in the pumping chamber may be a limiting factor consequently the tangential topology cannot be ruled out.

The thesis no progresses with chapter 3, which gives the pump and actuator specification, which in turn leads to the design of the linear actuator in chapter 4.

CHAPTER 3

Chapter 3
Pump and Actuator Specification

3 Introduction

This chapter introduces the application for the actuator, the pump system and the individual components of the pump system. The chapter includes a general review of potential power supplies for the linear actuator and pump. Having explored the potential of various power supplies, the chapter examines the characteristics of solar cells (a photovoltaic array, i.e. a constant current source). The chapter continues by discussing the need for a controller for the pumping system. This is followed by a break-down of the pump components, and then explains the principle of operation. The chapter then gives the design requirements, and notes the imposed restrictions, and incorporates an evaluation of the static head and the required frequency to achieve the desired flow rate. This information is then collated in a summary.

3.1 Application

Primarily the actuator is the driving mechanism for a submersible water pump for use in boreholes. Undoubtedly their will be other appropriate applications for the actuator, and other uses for the pump apart from boreholes. However, the focus of the design is for a submersible water pump for use in boreholes.

3.2 Pump System

Figure 3.1 shows the general layout of the water pump system. This system consists predominantly of a photovoltaic array (solar panels), a control system, and the pump system. The reservoir is the point of discharge for the delivered head of water. The importance of the choice of location is mainly for health improvement,

[12-15], further details are given in the background section of the thesis, §1.2 of Chapter 1.

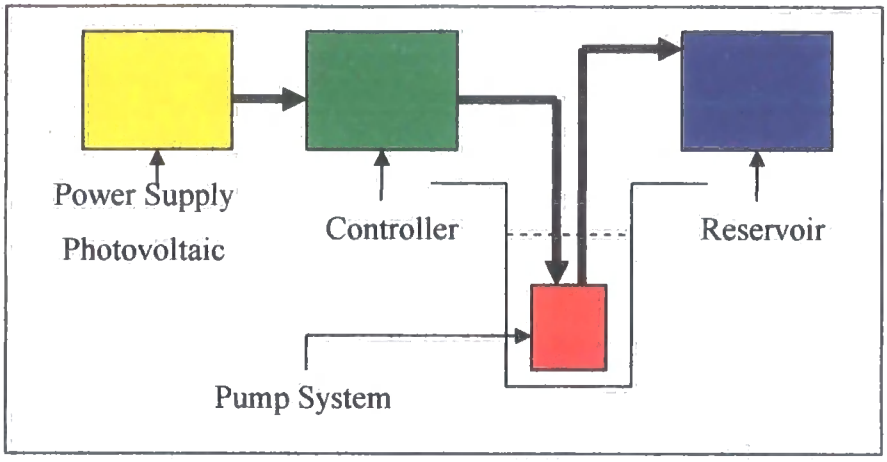

Figure 3.1 - Schematic of Water Pump System

3.3 Power Source – General Review

There are many methods by which a power supply can be produced, the most obvious being man-power and animal power. However, one of the reasons behind the thesis was to provide a clean water supply for the South, and by doing so, free the time of individuals, so that they can develop both themselves and the community, thereby providing prosperity. Therefore, both manual and animal generated power can be ruled out.

Since, the vast majority of the regions of the South are remote it is impractical to supply power via a grid system, this is barred by the cost. This also excludes fission fuels. Therefore, any A.C. supply must be generated locally, that is, on site; consequently this involves the use of fossil fuelled generators, or expensive D.C. invertors. The combustion of fossil fuels emits carbon dioxide into the atmosphere and thus increases the greenhouse effect. Therefore, from the onset of any sustainable development project, and for the benefit of all, renewable energy sources are regarded as environmentally desirable.

Renewable energy sources are sources of energy that do not use up the earth's finite mineral resources. The renewable forms of energy currently being explored and developed are solar energy, solar cells, wind energy, tidal energy, wave energy, geothermal energy, biomass energy, and bio-cell technology. Hydroelectric energy is already widely exploited and has limited scope for further expansion.

In general, geothermal energy can be excluded because in many regions this would involve very deep drilling to reach usable sources, and involves considerable technical problems. Even though many individuals require clean water in coastal areas, at present it is prohibitively expensive to provide either tidal energy or wave energy. Since, any use of such a power supply would not cover all areas this method of power supply can be disregarded. This potentially leaves three categories of power supply for the pump, namely; bio-energy, solar energy, and wind energy.

Wind energy is a pollution free cheap source of energy; however it requires a method of storing electricity for use when the wind drops. Similarly, a method of storing electricity applies to solar energy, for times of poor irradiance, and during the hours of darkness.

Bio-energy falls under two categories, namely, biomass fuels and bio-cells. Biomass energy relies on the combustion of biofuels, such as, methane generated by sewage or by farm, industrial, or household organic waste. Therefore, biofuels could be used for A.C. generation. Biofuels can include specially cultivated organisms or crops, for example, cane sugar, grown for their energy potential. One problem arises from this, in that; the areas in which the pumps are required tend to drought areas, therefore poor crops and no fuel. The other bio-energy method involves the use of bio-cells. This is a comparatively new method in that it uses rotten silage and raw sewage as an electrolyte and has gauze electrodes (i.e. both for the anode and cathode) that are submerged in the sewage. However, this technology is still in its infancy and at present would not produce an adequate power supply. Both these bio-energy methods could also assist in resolving the sanitation problems of the South.

In contrast, the use of the present industrial-sized batteries would supplement the use of either wind energy or solar energy. The main disadvantage of such batteries is the potential pollution problem.

Solar energy, in particular the use of solar cells, has previously been investigated in §2.8, §2.9, and §2.10 of the literature review of chapter 2.

All three energy supplies, that is, solar energy, wind energy, and bio-energy, could be used to power the pump. However, the initial criteria for the project required the development of a solar powered water pump, of the photovoltaic type, a PVP. Since, it was previously decided to use solar cells; the thesis now progresses with the view of using a photovoltaic array, and investigates the potential for using solar cells as a power source.

3.4 Photovoltaic Array

Photovoltaic arrays consist of banks of solar cell devices that convert solar radiation to an electric voltage and provide a DC current. The photovoltaic array provides the power supply; it consists of a number of solar panels connected in series to provide the necessary voltage and a number of these strings connected in parallel to provide the required current rating.

The solar constant $1.35kWm^{-2}$ is a measure of the rate at which solar energy intercepts the earth's atmosphere normal to its edge, when the earth is at its mean distance from the sun. The lower the sun is in the sky the greater is the atmospheric absorption, a consequence of both the time of the day and the latitude. The greatest concentration of solar energy is around the equator; any digression from the equator reduces the intensity. However, because of the earth's tilted axis, the surface of the earth can be divided into different zones, namely the Torrid Zone, the Temperate Zone, and the Frigid Zone.

The Torrid Zone includes all latitudes on the earth's surface where the sun is at the zenith (vertically overhead) at least once a year. The Torrid Zone extends 23.5° on either side of the equator.

The Temperate Zones include all positions on the earth's surface where the sun appears above the horizon but never at the zenith. The Temperate Zones extend from latitudes 23.5° to 66.5° both north and south of the equator.

The Frigid Zones include all locations on the earth's surface where the sun is below the horizon (and above) for at least one full day annually. The Frigid Zones extend 23.5° from the poles.

The geographical effect of reducing the intensity of solar energy is also seasonal, especially in the northern latitudes where the variation from summer to winter can be considerable. Another limiting factor for the intensity of the solar energy is altitude; the greater the height above sea level the less is the absorption by the atmosphere, clouds and pollution.

In the UK, the average solar energy is received at a rate of about $200Wm^{-2}$.

Without delving into the physics of solar cells and how they work it is necessary to have an understanding of their features, the current versus voltage (I-V) characteristic, the power characteristic and maximum power point, along with the polynomial characteristic of the maximum power point (MPP) curve. The effect of these climatic conditions must be considered within the overall pumping system.

Other factors such as the reflection of light, heating of the cell, impurities in crystals and thickness of the cell that contribute to its efficiency, can be more easily controlled and are assumed to be negligible. For example, the heating of a silicon based solar cell will only have $2mVC^{-1}$ drop in voltage (i.e. 2 millivolts per degree centigrade); this small change in voltage has little effect on its overall performance.

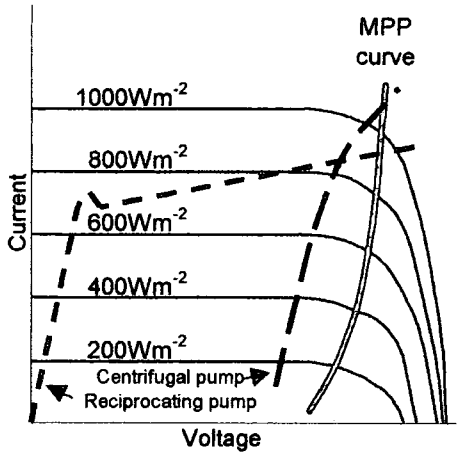

Figure: 3.2 – PV and Pump Characteristics (Ref: [51] Figure 2)

Figure: 3.2 gives a representative comparison of operating points for a centrifugal pump, a reciprocating pump, and the Maximum Power Point Curve.

The I-V characteristic demonstrates the behaviour of the voltage of the solar cell in terms of current. Each plot represents a different light intensity measured in $Js^{-1}m^{-2}$ or Wm^{-2}, or (kWm^{-2}). In general, the cell acts as a constant current source over a given range. However, as resistance increases, figure 3.5, (due to a rise in temperature), a breakdown can occur at the point where the cell can no longer maintain the established level of current and the current drops to zero. At this point, the point of intersection of the I-V characteristic and the abscissa, is the value of the open circuit voltage V_{oc}. Similarly, the short circuit current I_{sc} can be determined from the point of intersection of the I-V characteristic and the y-ordinate. The value of I_{sc} is dependent on the light intensity; I_{sc} reduces as the light intensity reduces, therefore, a reduction in power occurs. However, the I-V characteristics for all levels of light intensity behave in an analogous manner.

To obtain the MPP, the point where the maximum available power is dissipated in the load for any specific light intensity, the product of the current and voltage is calculated over the range 0V–V_{oc} and 0A-I_{sc}. The results superimposed on the I-V characteristic reveal the MPP. By plotting a vertical axis through the peak of the power plot (shown in figure 3.3) the point of intersection with the abscissa determines the maximum operating voltage V_{max}, at point C. By introducing a horizontal axis at the point of intersection of the new vertical axis and the I-V characteristic enables the maximum current I_{max} to be obtained, at point B. The light intensity again plays an important role and the variations in light intensity result in a polynomial track for the MPPs (Figure: 3.4). Consequently, the

maximum current and voltage constantly change along the MPP curve, so the power output is highly dependent on climatic conditions.

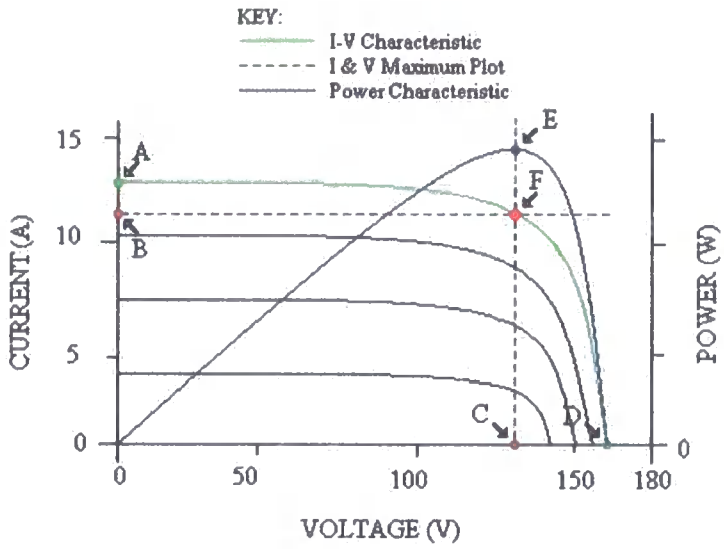

Figure: 3.3 – Maximum Power Point of an I-V Characteristic

Where, A	=	I_{sc}	Short Circuit Current
B	=	I_{max}	Maximum Current at Maximum Power Point
C	=	V_{max}	Maximum Voltage at Maximum Power Point
D	=	V_{oc}	Open Circuit Voltage
E	=	P_{max}	Maximum Power
F	=	MPP	Maximum Power Point

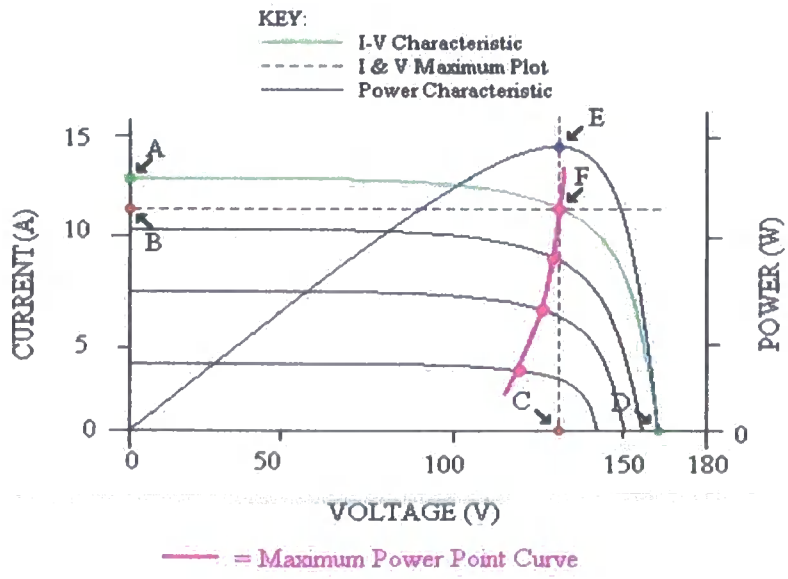

Figure: 3.4 - Polynomial plot of the Maximum Power Point.

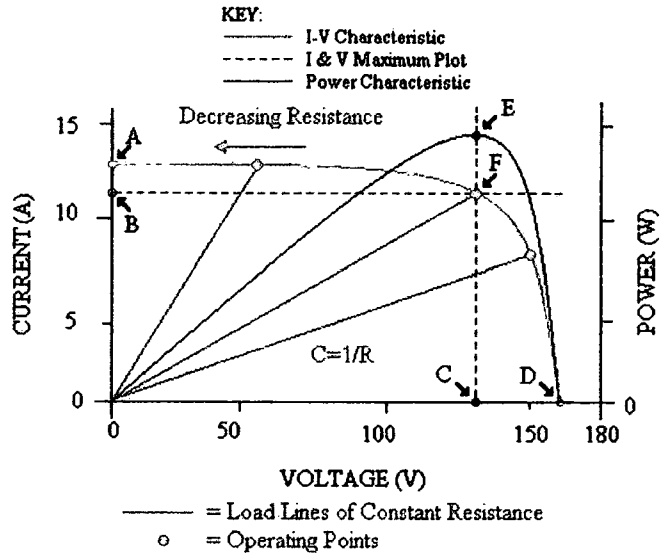

Figure: 3.5 – The effect of load resistance on operating points.

The load resistance determines the operating point that is situated at some point along the I-V characteristic (figure: 3.5); the gradient of the slope of a line connecting the I-V curve to the origin is the conductance.

The ideal scenario would be for the solar cell to act as a 'true' constant current supply, however this is not possible due to climatic changes. The variation in light intensity cannot be prevented. However, increasing the number of solar cells will compensate for low light intensity, thereby catering for geographical variations in individual site conditions. For safety reasons, there are limitations to the number of solar modules that can be connected in series, and this varies according to size, type, and the manufacturer.

3.5 Controller

A controller can be sub-divided into an interface between the PV generator and the pumping system and a switching control mechanism for the driver section of the pump. The alternative is to have a system that is self-oscillating, working at its own natural frequency.

Any variation in the supply current has an effect on the performance of the linear actuator; likewise, any change in the load resistance (figure: 3.5) will affect the performance of the linear actuator. Maintaining the operating point at (or as near as possible to) the maximum power point will achieve maximum efficiency and minimize the amount of solar cells required to produce the required operating power. This is achievable by controlling the load so that it operates at a point where the current and voltage produce maximum power.

The possible need for the use of an interface controller is best explained with reference to figure 3.6.

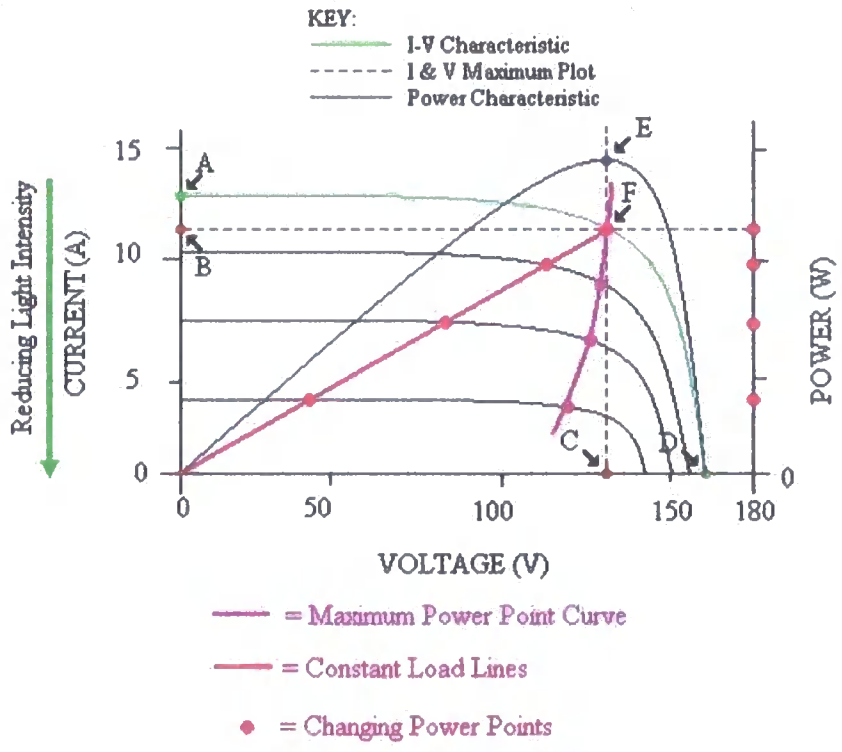

Figure: 3.6 – Power Variations

The problem of matching the Maximum Power Point (MPP) curve of an array is that it requires a tracking system, a Maximum Power Point Tracker (MPPT). The MPPT detects changes in Irradiance and load resistance and maintains the operating point on the MPP curve (figure 3.4 & figure 3.6) so realizing maximum available power at all times.

Should the load resistance remain constant (e.g. the straight line passing through F in figure 3.6) and the irradiance fall, then the available power will reduce. Similarly, as shown in figure 3.5, any change in load resistance (i.e. change in gradient of the straight line) will also affect the available power for the system from the solar cells.

It is acknowledged by Badescu [57], and Roger [62], that the optimum PVP design would be a PV array directly connected to a DC motor. A pumping system that is composed of a PV array directly connected to a DC motor driving a centrifugal pump is certainly the cheapest, simplest, and most reliable of all the different PV pumping systems [57]. This may not be so for the system under consideration, which invokes the use of a DC linear actuator for a reciprocating pump.

The reason that direct coupling may not be appropriate for a DC linear actuator can be seen in Figure: 3.2, which gives a representative comparison of operating points for a centrifugal pump, a reciprocating pump, and the Maximum Power Points Curve, the operating points take completely different tracks.

If any kind of controller is to be used, such as a MPP Tracker (MPPT), it must be intrinsically very reliable; if not, easily repairable/replaceable at a local level. This places severe limitations on such a controller. Despite the fact that electronic systems have increased in reliability, as late as 2001 a 45% failure rate is noted by Kaunmuang [61], attributing many of the faults to the use of electronics itself. Similarly in 2002, Short and Mueller [51] comment on PVP standard systems, highlighting a 20% inverter failure rate in field tests.

Given these limitations and concerns over past problems, it must be questioned whether a controller should be used at all. System failures of the past suggest that the controller electronics will give rise to potential problems and subsequent failures. Inevitably, cost becomes a major issue, particularly in the South; the cost may well outweigh the benefits.

A switching control mechanism for the driver section of the pump can be electrical/electronic, mechanical, or electromechanical. Electrical switches have the advantage of a far greater number of switching actions because mechanical switches have wear and fatigue problems, greatly reducing the number of cycles available. As with the MPPT, the cost of circuitry for electronic switches is a major concern, along with the ease at which they can be maintained, whereas mechanical switches may not be as durable but would more easily comply with the concepts of Village Level Operation and Maintenance (VLOM).

3.6 Pump System

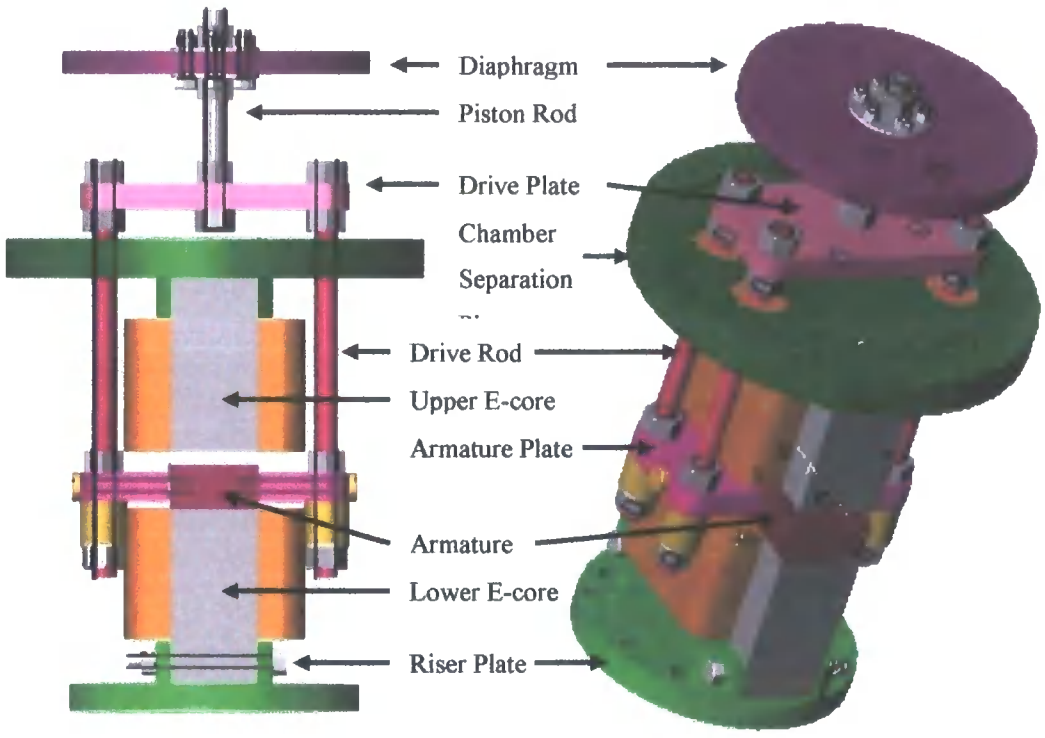

Figure 3.7 – The Actuator

The pump system essentially consists of two parts, a linear actuator, (the driver for the pumping action) providing the output, and the induced flow system, (a form of multiplier for enhanced output). The actuator is the device that causes the process to provide the output, that is, the device that provides the motive power to the process. The actuator (figure 3.7), that is, the driving mechanism for the pump, is not to be confused with the armature, which forms part of the actuator. The

armature is situated between the two E-cores of the system, and is the driver for the piston mechanism. The armature provides the direct link between the electromagnetic force and the mechanical output of the actuator, figure 3.7.

The induced flow section of the system doubles the output of the pump at high heads and increases the output at zero head by a factor of π. However, this is purely theoretical as it is not upheld practically. Burton and Short [79], claim "At low heads a doubling of flow output from existing wind-electric or photovoltaic-driven systems may be achieved".

The induced flow system works on the principle of having a hydraulic equivalent capacitance and inductance incorporated in the output stage of the pump. The capacitance section stores the hydraulic kinetic energy and the hydraulic inductance section causes a restriction in piping; the pulsating output of the pump causes a 'plug' of water to oscillate in the induced flow section, the energy of the 'plug' then draws more water from the pump.

The induced flow is outside of the scope of this thesis, however further details can be obtained from, Burton, J.D. and T.D. Short, *Induced Flow Reciprocating Pumps Part 1 and Part 2.*, [78, 79].

3.6.1 Principle of Operation

The principle of operation is that of a reciprocating pump consisting essentially of a cylinder and a diaphragm/piston, driven by an engine or motor, in this case an electromagnetic linear actuator. As the piston moves down, the inlet non-return valve opens, and simultaneously, the outlet non-return valve closes. Water floods the chamber due to the submerged head. The pressure within the chamber is then at equilibrium with the submerged head. Then as the piston rises, the inlet valve closes, due to the rising water, and the outlet valve opens, likewise due to the rising water, so driving the water from the chamber.

The force exerted by the piston on the chamber of water through a vertical height is known as the delivery head (h), figure 3.8. The delivery head can be considerably greater than that of the submerged head. Figure 3.8 shows a schematic picture of the 'Reciprocating Induced Flow Pump System'.

Since the cylinder is under pressure during the discharge stroke, the worst-case static force acting on the piston is given by equation 3.1.

$$F_{\min} = \rho g h_1 A_{pipe} + \rho g h_2 A_{piston} \quad \text{N} \qquad \ldots \text{Eqn: 3.1}$$

Where;

$F_{\min}$ = Minimum force required to open the outlet valve (N)

ρ = The density of water at $4^{\circ}C$ ($1.0 \times 10^{-3} kgm^{-3}$)

g = Acceleration due to gravity ($9.81 ms^{-1}$)

h_1 = Outlet Head (m)

h_2 = Submerged Head (m)

A_{pipe} = Cross-sectional area of outlet pipe (m^2)

A_{piston} = Cross-sectional area of piston (m^2)

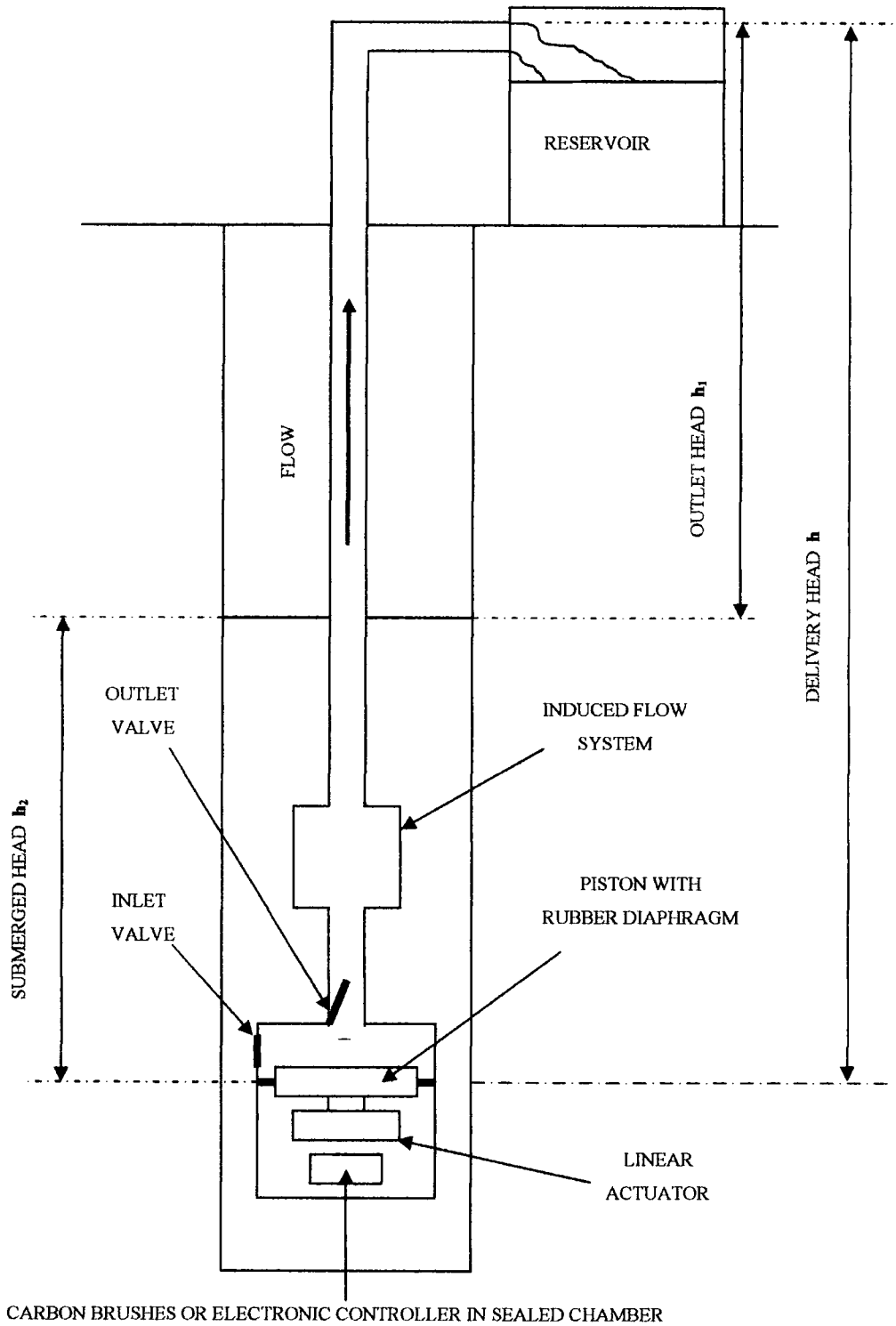

Figure: 3.8 - Schematic diagram of Reciprocating Induced Flow Pump

This expression (equation 3.1) describes the minimum force required to open the outlet valve hence the thrust required from the actuator. The first term represents the force attributed to the outlet head (h_1), the second term, represents the force corresponding to the submerged head (h_2). The cross-sectional area of the outlet pipe is represented by A_{pipe}; likewise, the cross-sectional area of the piston is represented by A_{piston}. Equation 3.1 assumes that the force required within the piston chamber is negligible, because the stroke length is very much smaller in comparison to the borehole depth (100m) and the submerged head (although variable, even at 1m).

3.7 Design Requirements

The focal point of the system for the purpose of this thesis is the design of the linear actuator, (the pumping mechanism). It involves the design of a linear actuator utilising a linear normal force opposed to a tangential shear force by means of electromagnets. In general, the linear actuator forms an integral part of 'An Induced Flow Solar Powered Submersible Water Pump'.

The rationale is to have an off-the-shelf pump for universal use, rather than having to design a pump for each individual circumstance. The aim is to achieve a pump that will pump at least 10 bar pressure with a flow rate of one litre per second. The pump is to be used in conjunction with an induced flow system, which would at least double the output. The main use is envisaged as pumping water from boreholes, this imposes restrictions on the dimensions of such a pump.

In order to investigate an appropriate linear actuator a typical specification of the pumping requirements is necessary. "The swept volume at the piston characteristically varies from $0.1ls^{-1}$ to $0.05ls^{-1}$. This is a consequence of the short stroke length of the actuator. The frequency of operation can be in the range of 10Hz to 20Hz" [51]. Restrictions are imposed to the overall dimensions of the pump by the size of borehole. Borehole diameters are typically either 6" or 4" in

diameter, 152.4mm, and 101.6mm respectively, with typical heads of 100m, (ρgh), which correlates to 10 bar pressure.

3.7.1 Size Restrictions

The housing for the submersible section of the system is restricted to the diameter of the borehole; since the pump is for universal use, the diameter of the smaller borehole is to be used, having a maximum diameter of 101.6mm (4 inch borehole). However, this needs to be reduced in order that the pump can be lowered down the borehole and allow water access to the system. Thus, the suggested value is 90mm or smaller. A cylinder having a 90mm external diameter with a wall thickness of 5mm reduces the available space for the workings of the pump to 80mm internal diameter. The system uses an E-core and an armature as a linear driver, forming the actuator which is the principal moving part for the pumping system. The dimensions of the E-core have a significant influence on the performance of the actuator. This in turn has a direct effect on the force produced, the inductance of the cores [80], and hence the time constant and the frequency of operation.

3.7.2 Determination of the maximum size of the actuator

Consider an E-core with the leg format shown in figure 3.9.

Let, A = x and B = 3x = 3A

Then, $InternalDiameter\phi = \sqrt{x^2 + (3x)^2}$

Giving, $\phi = \sqrt{10x^2}$

So, $x = \sqrt{\frac{\phi^2}{10}}$ m Eqn: 3.2

Let the housing have an internal diameter of 80mm. Using equation 3.2, it can be shown that the maximum dimensions for the cross section of the E-core are 25mm x 75mm, however the depth may vary, depending on the number of turns in the coil.

Nevertheless, further restrictions may be imposed on the dimensions depending on the design of the moving parts.

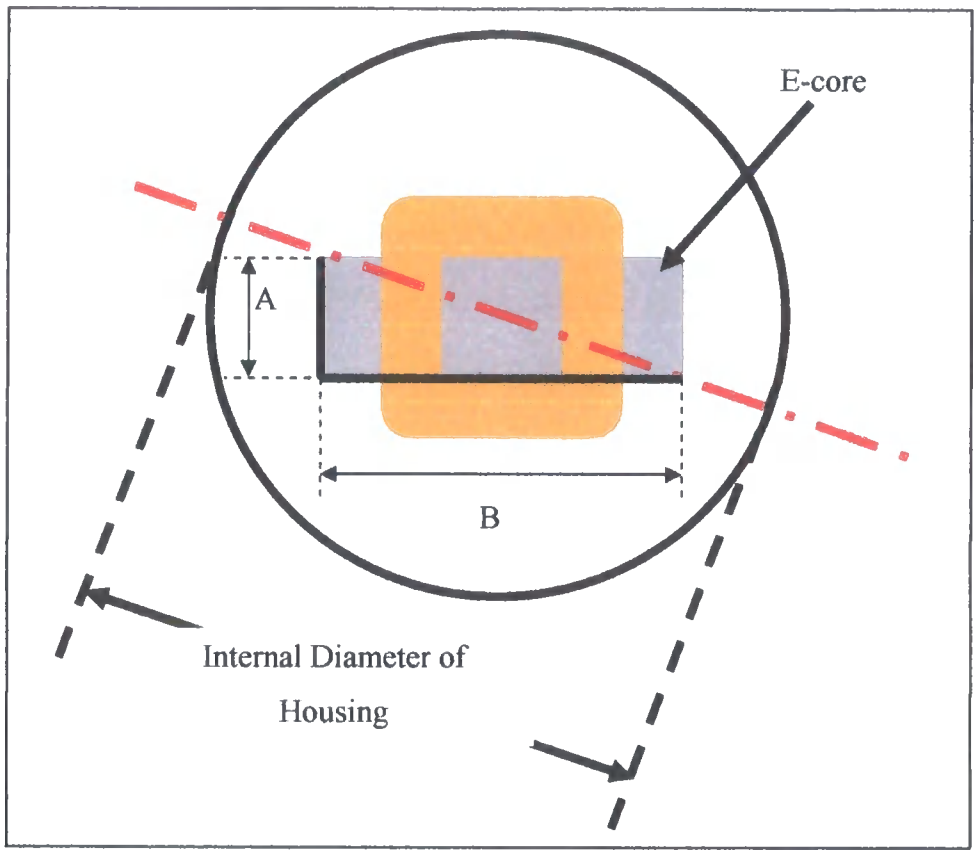

Figure: 3.9 - Limiting Factor for E-core Size

3.7.3 Static Force

From the schematic of figure 3.8 it can be seen that the force, F, required to act on the delivery head (h) ρgh. It follows that the required pressure is this force per unit area. Figure 3.10 shows the direct relationship between pressure and borehole depth, the equation of the graph is $y = 0.0981x$, therefore to achieve a depth of 100m a pressure of 9.81 Bar is exerted on the pump.

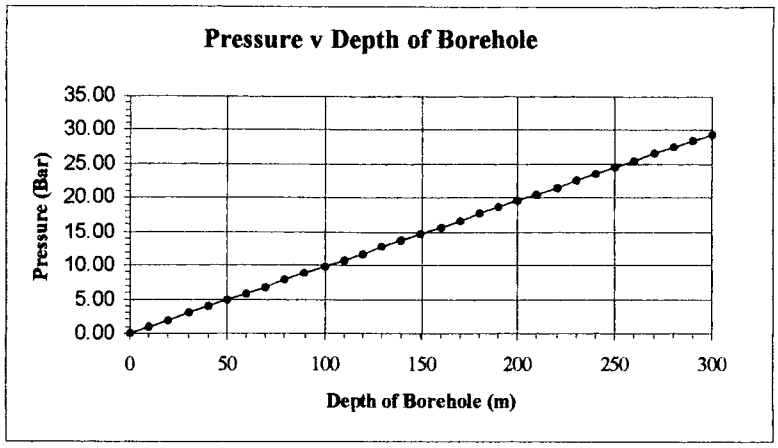

Figure 3.10 - Pressure versus Depth of Borehole

Equation 3.1 gives the worst-case static force acting on the piston. Assuming that a 19mm diameter outlet pipe and a piston of 80mm diameter (value taken from previous section), are used, then it can be determined that for the case of a 1m submerged head and a outlet head of 99m, that is, a total delivery head of 100m, the minimum force required for the system to operate is.

F = Outlet Head (h_1) + Submerged Head (h_2)

$$F = \rho g h_1 A_{pipe} + \rho g h_2 A_{piston}$$

$$F = 1000 \times 9.81 \times 99 \left(\frac{\pi (19 \times 10^{-3})^2}{4} \right) + 1000 \times 9.81 \times 1 \left(\frac{\pi (80 \times 10^{-3})^2}{4} \right)$$

$$F = 2.78141690984 h_1 + 49.3104382907 h_2$$

$$F = 2.7814 h_1 + 49.3104 h_2 \quad \text{N} \qquad \text{Eqn 3.3}$$

For, $h_1 = 99 \,\&\, h_2 = 1$

$$F = 275 + 49$$

$$F = 324 N$$

However, depending upon outlet pipe and piston/diaphragm dimensions this value of force will vary considerably. Equation 3.1 was used to produce figure 3.11, which shows the change in the minimum required force to operate the pump when using an outlet pipe of 48mm diameter, (showing the effect of changing the outlet pump diameter).

The individual plots show the effect of change in the ratio between the pipe (fixed at 48mm) and piston, as the piston diameter is reduced over a range of 96mm to 16mm. The force shown represents the sum of outlet head and the submerged head, thus representing the minimum operating force required for all levels of water within the borehole.

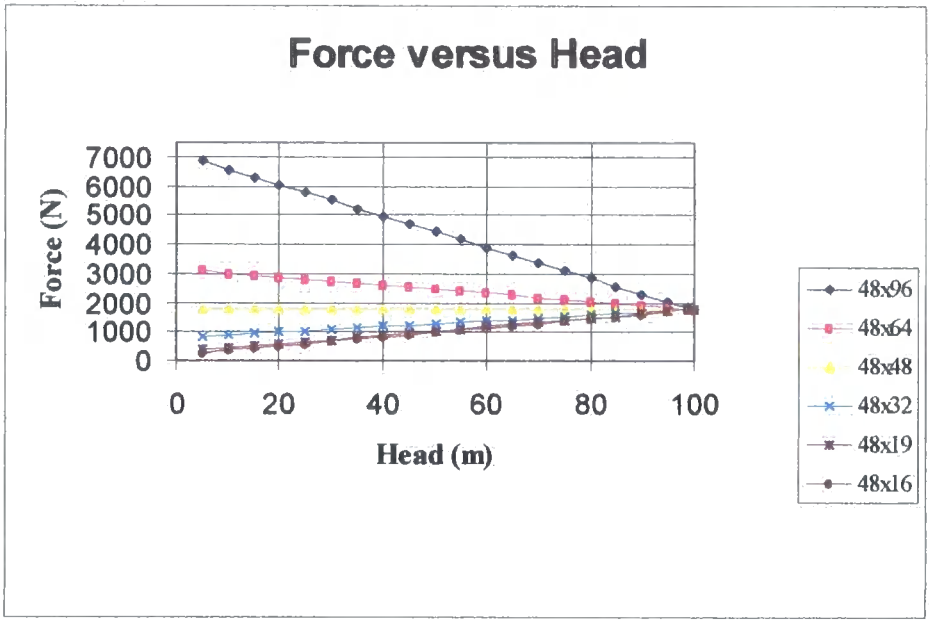

Figure 3.11 – Force versus head for a given outlet pipe diameter with various piston diameters

Figure 3.11 is only applicable for a borehole of depth 100m. From figure 3.11 it can be seen that when the ratio of the outlet pipe diameter to the piston diameter is 1:1 the force required is constant over the whole borehole depth.

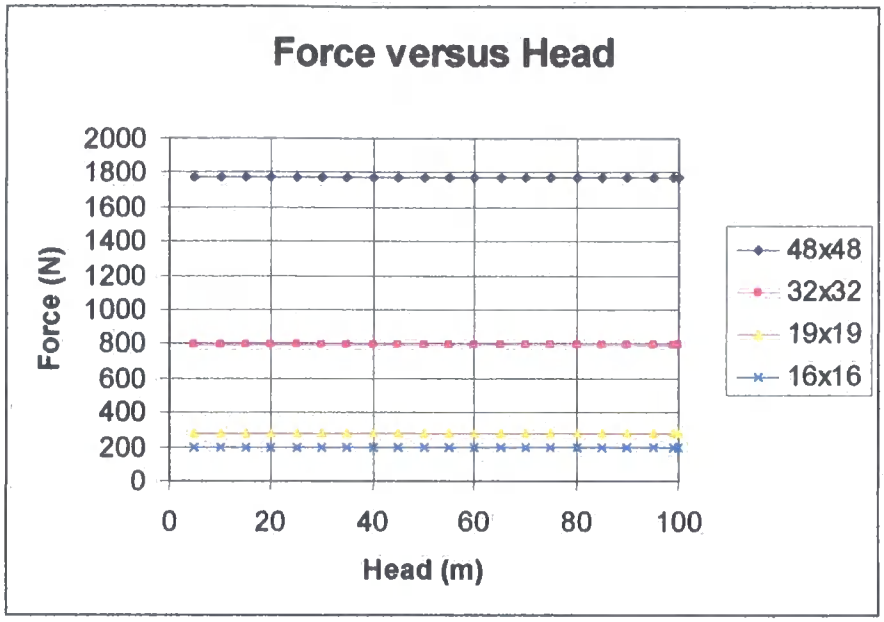

Figure 3.12 – Force versus head for an outlet pipe diameter, piston diameter ratio of 1:1

Figure 3.12 shows the force required for 1:1 ratios for various pipe and piston sizes. The 1:1 ratio is relevant from a design point of view in that the maximum diameter size of piston/diaphragm to produce the minimum force to operate the pump can be determined for any given borehole depth.

A relationship can now be derived from equation 3.1 between the force produced by the actuator and the maximum piston diameter required to produce this force.

$$F = \rho g h_1 A_{pipe} + \rho g h_2 A_{piston}$$

$$A_{pipe} = A_{piston} = \frac{\pi D^2}{4}$$

$$F = \rho g \left[\left(h_1 \times \frac{\pi D^2}{4} \right) + \left(h_2 \times \frac{\pi D^2}{4} \right) \right]$$

$$h_1 + h_2 = h_t = Borehole_{depth}$$

$$F = \rho g \times \frac{\pi D^2}{4} \times h_t \quad \text{N} \qquad \text{Eqn: 3.4}$$

$$D_{max} = \sqrt{\frac{4F}{\rho g \pi h_t}} \quad \text{m} \qquad \text{Eqn: 3.5}$$

All forces shown in figure 3.12 are for a borehole with a depth of 100m. The force (F) required for a pump with a ratio of 19:19 is 278N. Equation 3.4 shows that the borehole depth is directly proportional to the minimum force produced by the actuator, therefore if the pump was to be used at greater depths then the force generated by the actuator (the amount of force generated by the actuator has limitations) would need to be increased proportionally, for a depth of 300m, threefold to 834N. Alternatively, equation 3.5 could be used to determine the new maximum size of piston; for a given maximum force, the present 19mm diameter piston would need to be reduced to a new maximum of 10.97mm.

3.7.4 Flow Rate and Frequency

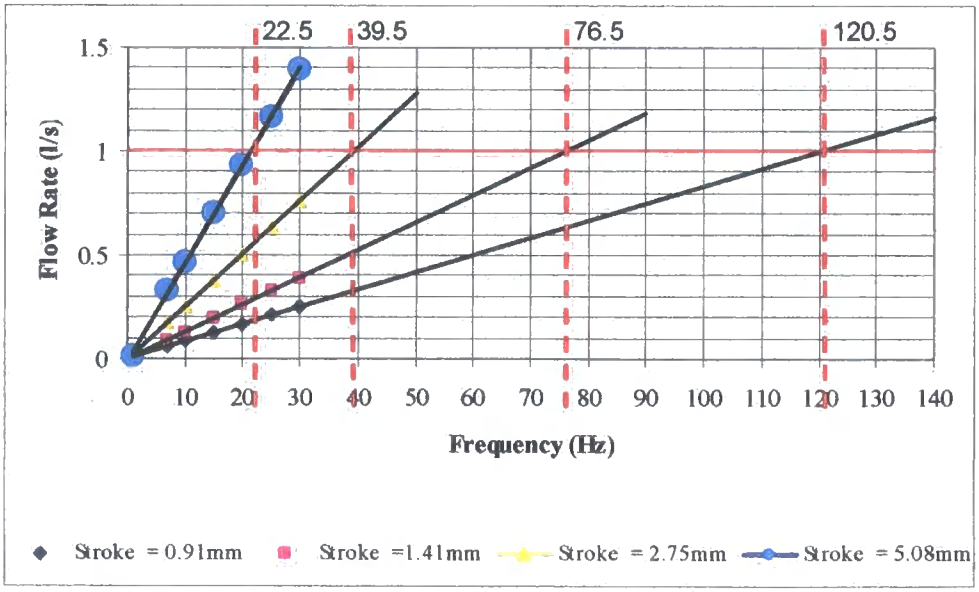

Figure 3.13 – Flow Rate versus Frequency of Operation

The desired flow rate for the pump is one litre per second. This is determined by the swept volume and frequency of operation. The swept volume is determined from the piston diameter and the movement of the armature within the pump, that is, the stroke length of the actuator. "The desired swept volume at the piston for this system characteristically varies from 0.1 to 0.05 litres per second. The required frequency of operation is to be in the range of 10 to 20 Hertz" [51].

Figure 3.13 shows a range of stroke lengths and the frequency of operation required to achieve the desired one litre per second flow rate, [51]. The data for the graph was taken from a pump design model that had a piston with a diameter of 108mm, for use in a 6" borehole. The model calculated the volume of the pump cylinder, hence the amount of litres, and plotted this against a frequency range. The plots were then extruded across the 1l/s y-ordinate to evaluate the frequency that is required to achieve 1l/s, for any given stroke length (airgap size, l_{Ag}, figure 3.14). Flow rate, being the product of the volume of the piston chamber and frequency of operation, also has restrictions imposed. The volume is dictated by the piston size hence the surface area, combined with the stroke length of the actuator.

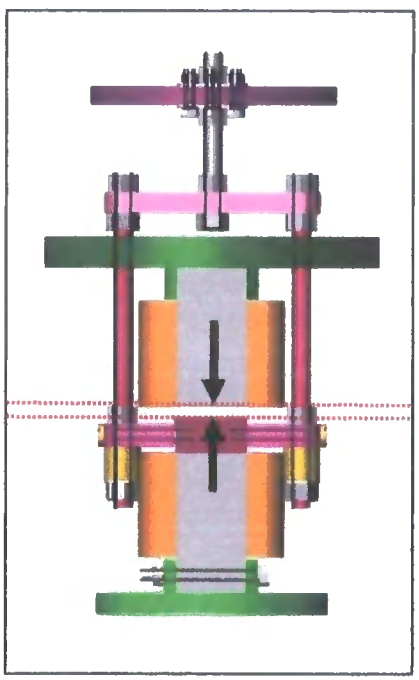

Figure 3.14 – Airgap l_{Ag} (The airgap is indicated with the two black arrows)

The airgap (l_{Ag}) size of the actuator dictates the force generated by the actuator; the stroke length is equal to (or less than) the airgap size. The inductance of the system is also dependent on the airgap size. The frequency restrictions are imposed by the design of the actuator and the associated switching times for the pump. The force generated by the actuator is determined by the current. The rate at which the current is established is determined by the inductance of the system. Hence the

switching time, and the frequency of operation is in part determined by the inductance.

$$FlowRate = Volume \times Frequency \qquad FlowRate = \left(\frac{\pi D_{max}^{\ 2}}{4}\right) A_g f \quad ls^{-1} \qquad \text{Eqn: 3.6}$$

Where; $Volume = \left(\frac{\pi D_{max}^{\ 2}}{4}\right) \times A_g$ and $Frequency = f$

A relationship between the flow rate and force can be derived by substituting equation 3.5 for D_{max} into equation 3.6.

$$FlowRate = \frac{F}{\rho g h_t} A_g f \quad ls^{-1} \qquad \text{Eqn: 3.7}$$

3.8 Summary

This chapter gave a brief system description, which was followed by a brief discussion on potential power supplies. The chapter then by a process of elimination, has established that the actuator would be best powered from any of three renewable energy sources, namely, bio-energy, solar energy, and wind energy; the latter two being supported by a battery storage.

The chapter then investigated the potential of using a photovoltaic array and the requirements for control of the pump system. Having explained the principles of operation, the chapter gave the design requirements, evaluated the size restrictions imposed on the actuator and established a number of design tools.

A prerequisite of the design is to develop a linear actuator that is capable of driving a submersible water pump for use in boreholes, with a flow rate of one litre per second, 1l/s.

The static head, that is, the minimum force required for the pump to operate, of the pumping system has been evaluated, and can be calculated with the use of equation 3.1. Equation 3.2 enables the calculation of the maximum size of the actuator that can be used in the pump. Equation 3.3, when evaluated shows the variation in the force required to overcome the static head, with respect to both the, size of outlet pipe to size of piston ratio, and any change in the outlet head to submerged head ratio.

The 1:1 ratio is relevant from a design point of view in that the maximum diameter size of piston/diaphragm to produce the minimum force to operate the pump can be determined for any given borehole depth. Equation 3.4 enables a calculation of the required force to overcome the static head when this ratio is 1:1. With this in mind, the maximum size of piston or diaphragm, to achieve the force, for any given borehole depth can be calculated from equation 3.5. Once the maximum piston or diaphragm has been established, the flow rate for any given stroke length (airgap size) and frequency of operation can be established, with the use of equation 3.6. Similarly, the relationship between the flow rate and the static force is given in equation 3.7. Manipulation of the equations 3.4 – 3.7 allows for any changes in the given parameters and provides for a useful design tool.

The thesis now moves forward with chapter 4 which gives the design of a linear actuator.

CHAPTER 4

Chapter 4
Design of Linear Actuator

4 Introduction

This chapter introduces concepts for the realization of linear motion. The chapter then shows the model results and makes a comparison of the generated forces for the different actuator topologies. This is followed with a theoretical evaluation of the stricture of the chosen E-core actuator outlining the requirements and the interlinked issues involved with the design of such a pump. The chapter continues with the initial test results achieved when using a single E-core, giving a brief description of the methods used to determine the generated force, and the inductance, and a summary of the theory.

The chapter then investigates of the use of springs and gives an account of the potential for an increase in the force of the actuator. The chapter then continues with the design and manufacture, which shows and describes the workings of both diaphragm and piston versions of the linear actuator water pump. This is followed with the results of the pump tests for all the pump variations.

The chapter then continues with a three part discussion, which includes a system analysis, the use of springs, and the performance, problems and potential of the pumps; and then gives recommendations and concludes with a brief summary of the chapter.

4.1 Concepts for the Realization of Linear Motion

As with all concepts, an understanding of the properties involved for each design is essential, raising the questions of, can they be used, do they need to be suppressed or removed, can they be used for an alternative purpose, or are they irrelevant.

Various methods of achieving linear motion have been considered, including solenoids and their axial forces under attraction or repulsion, toroids with or without slits, C-cores and various combinations of E-core. The use of permanent magnets in conjunction with the electromagnets has also been explored.

4.1.1 Solenoids

Several ideas concerning the use of solenoids were considered and not all of them have been ruled out. The properties of a short solenoid to be considered are that, the strongest field is at the centre, both co-axially and longitudinally. The field external to the solenoid decays rapidly when moving away from the solenoid, in both the direction of the central axis and the direction perpendicular to the central axis. The internal field is greatly enhanced with introduction of a magnetic material, such as mild steel (ferromagnetic) to the core. However, should the core of the solenoid be air, and the internal diameter of the winding is too great then the field will start to decay as it tends toward the central axis.

The flux density B, for a short solenoid, at point 'P' shown in figure.4.1 can be determined as;

$$B = \frac{\mu_0 \mu_r NI}{4L}(\cos\phi_1 - \cos\phi_2) \quad \text{T} \qquad \text{Eq}^{\text{n}}\text{: 4.1.}$$

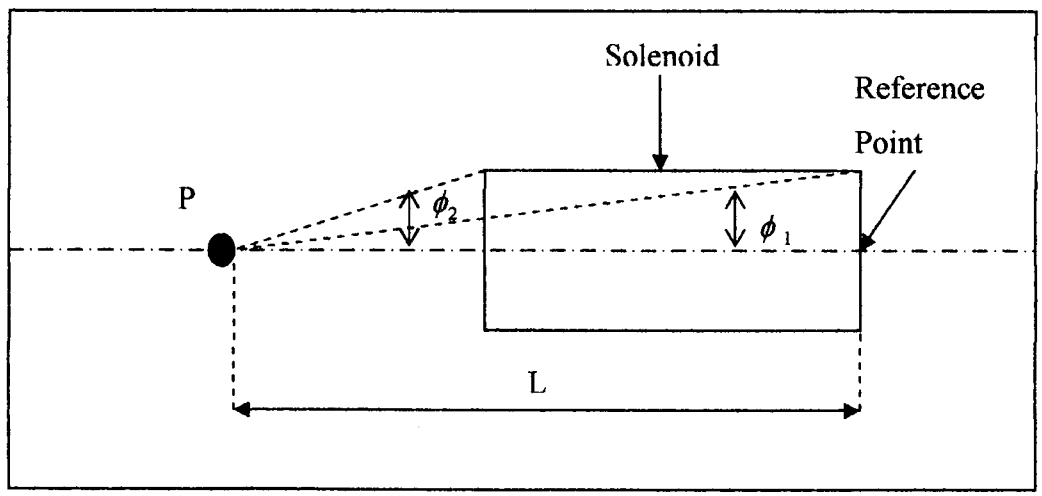

Figure: 4.1 - The external flux density for a solenoid at any point along its central axis.

The first method was to utilize the external magnetic field. Figure.4.2 shows a solenoid with mild steel core and conducting ring, the principle of operation makes use of the eddy currents (Lenz's law) that are induced in the conducting ring when the solenoid is energised. The pumping action, linear motion, is from the repulsion of the conducting ring along the extended core due to the eddy currents induced within the ring.

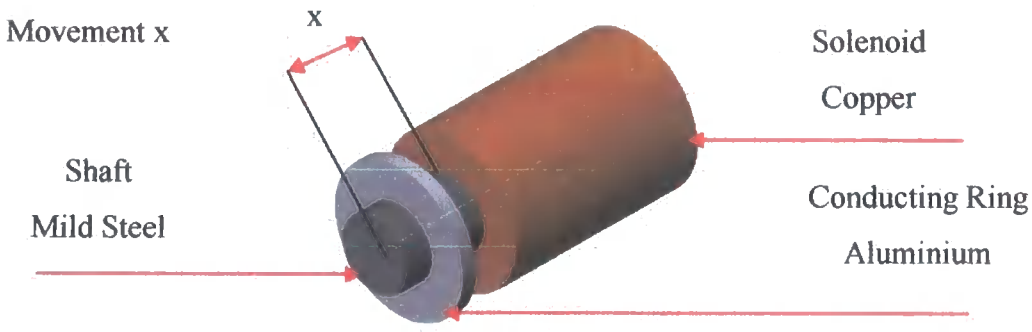

Figure: 4.2 - Solenoid with Mild Steel Core and Conducting Ring

Several variations along this theme were considered, such as, a solenoid with mild steel core and mild steel ring or disc, however this time operating by the attraction force between the ferromagnetic ring (or disc) and the solenoid.

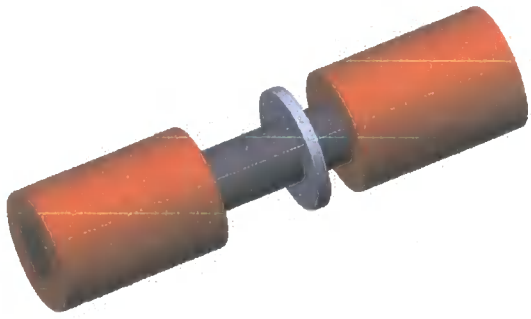

Figure: 4.3 – A ring on a shaft reciprocating between two solenoids

Figure.4.3 shows the design consideration for a double coil system, where, an aluminium (non-ferromagnetic) ring, or mild steel (ferromagnetic) ring, would move between the two solenoids. This would involve the use of a control system so that the solenoids would be energised alternately so causing the ring to reciprocate between the two solenoids.

An alternative to the above would be to have both solenoids energised simultaneously, having a bimetallic ring consisting of mild steel ring coupled to an aluminium ring, placed between them: the resultant force being the sum of the repulsion and attraction forces. However, this would be in the positive upward direction only, and the return stroke would either be by gravity or assisted by means of a spring.

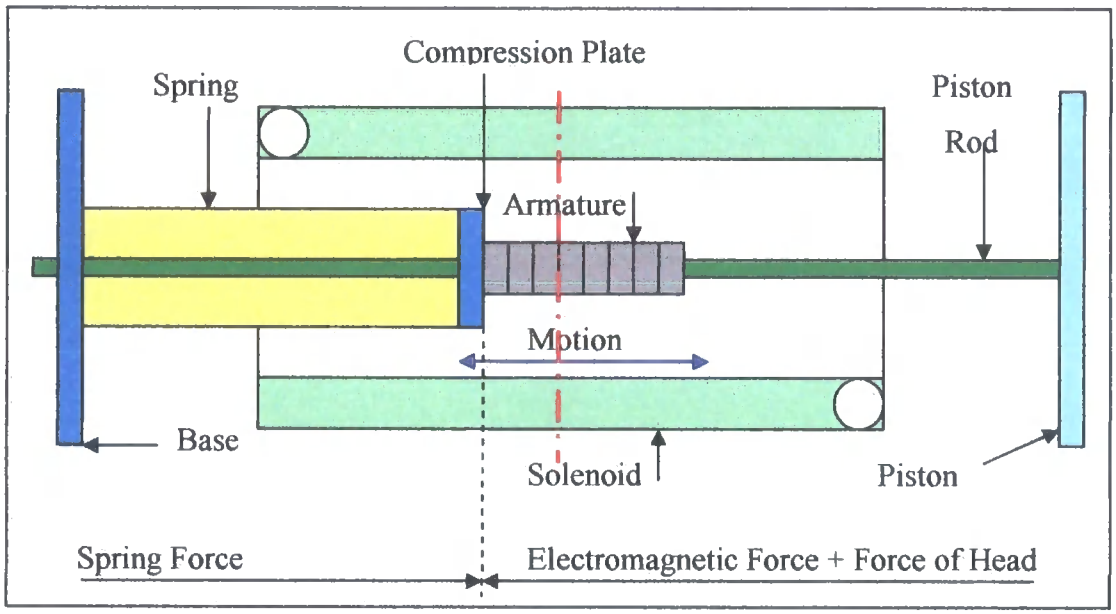

Figure: 4.4 – Schematic diagram of the uses of a solenoids internal field

The second argument was to use the generated internal magnetic field, which circulates around the flux path of the solenoid and armature, shown in figure.4.4. The strongest magnetic field of a short solenoid is at the mid-point within the solenoid along the central axis. When the solenoid is energised the armature, a ferromagnetic material, is pulled toward the centre of the solenoid, compressing a spring. When the solenoid is de-energised, the armature is driven back by the energy stored in the spring, so providing a reciprocating linear motion. It should be noted that the armature only travels to the edge of the solenoid before the cycle is repeated.

A small 20cm solenoid was built which verified that the principle worked. However, as with the other solenoids only very small forces were generated although the stroke length was greatly enhanced.

All these methods for the realization of linear motion were disregarded because the physical size of any such would be too large. In order to achieve sufficient force over the stroke length of the pump, the coil would need to be in excess of three metres in length because the diameter is restricted by the borehole parameters. In addition, the weight of such a coil could cause the coil to collapse under its own weight. Any such pump would not be financially viable due to the cost of the volume of copper required.

4.1.2 Toroids

A toroid is dissimilar to a solenoid in that, in a solenoid the electromagnetic field is confined totally within the core and is concentrated around the coils central axis; this is not the same axis as the toroids central axis, shown in figure.4.5.

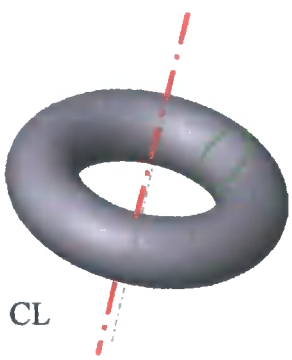

Figure: 4.5 – Toroid

Figure: 4.6 – Toroid with slit

The central axis within the toroid is perpendicular to that of a solenoid central axis the resultant field is $\nabla \bullet \vec{B} = 0$ and no field exists outside of the 'doughnut' structure. However, by creating a transverse slit/airgap in the toroid, shown in figure 4.6 the toroids electromagnetic field can be utilised, the narrower the slit the greater the field strength within the airgap. However, the slit needs to be wide enough to place an armature lever to produce an oscillating linear motion for the

pumping action, but too large an airgap will greatly reduce the magnetic field hence the force produced. Too thin an airgap, and the lever would not be so robust as to withstand the loading force.

An alternative to this was also considered, the use of a conducting ring or disc over a toroid as shown in figure 4.7. Several coils are wound around the toroid. They are equally spaced and have the same number of turns, and have the same size of wire. When each coil in turn is energised then the disc will rotate about the central axis, A-B shown in figure 4.7. Should the disc be attached to a diaphragm at point B and the opposite side of the disc be attached to a threaded bar passing through a hole in the base at point A then a linear motion would be achieved. Circular coils were also considered to produce the same effect.

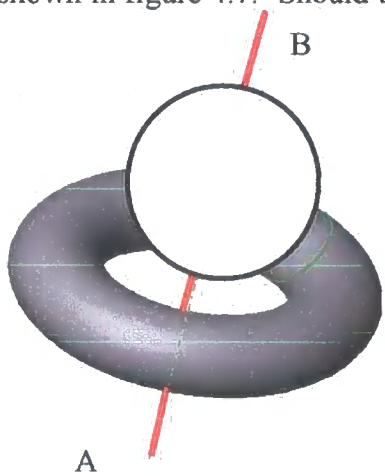

Figure.4.7 - Conducting disc over a toroid

The ideology of the use of toroids was considered but disregarded because the force required would need to be generated with use of high currents. The use of high currents requires a large gauge wire and hence the maximum possible number of turns through the centre of the toroid is restricted, thus limiting the magnetomotive force, m.m.f., (Ni). In addition, the outside diameter of the windings around the toroid is restricted by the diameter of the borehole. The pumping mechanism would be mechanically complex, therefore more moving parts, increasing the chance of breakdown, and ultimately more expensive.

4.1.3 C-core

C-cores were considered for both tangential transitions shown in figure 4.8 and normal transitions, shown in figure 4.13.

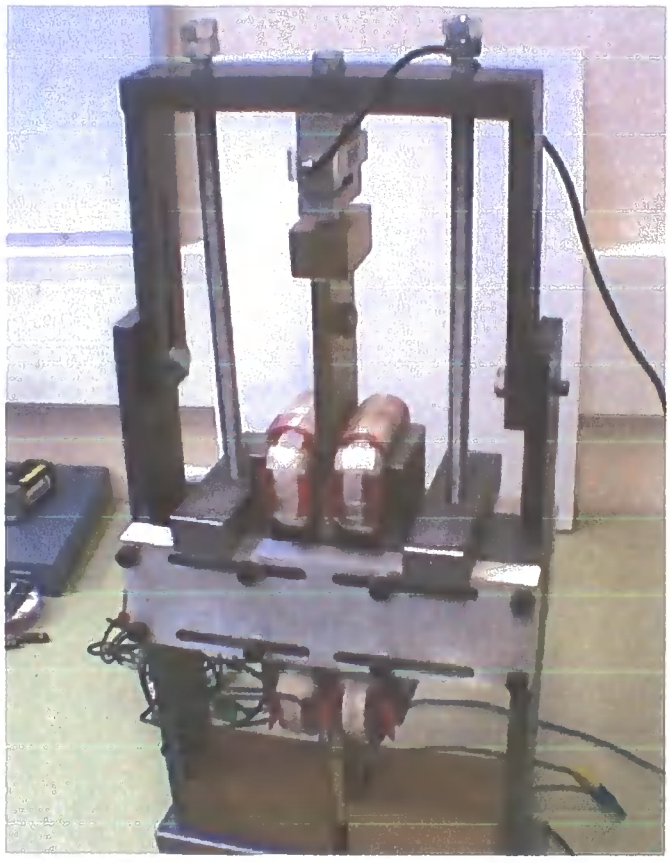

Figure: 4.8 – C-core permanent magnet (PM) tangential transition linear machine installed in a force measurement test rig.

The permanent magnet linear machine shown in figure 4.8 shows the device installed in a test rig attached to an S-type load cell.

The C-core permanent magnet (PM) tangential transition linear machine consists of two C-cores each having two shanks and a back, which were manufactured from solid blocks of mild-steel, (i.e. not laminated), and are shown as green in figure 4.9A.

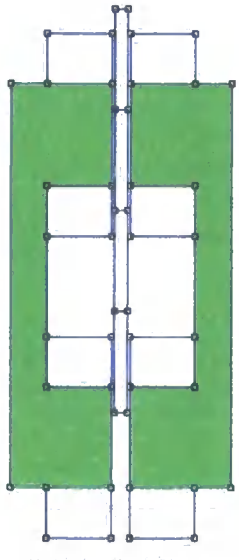

Figure 4.9A

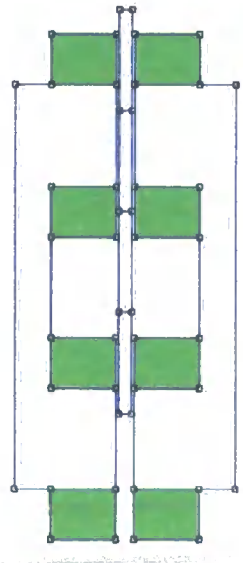

Figure 4.9B

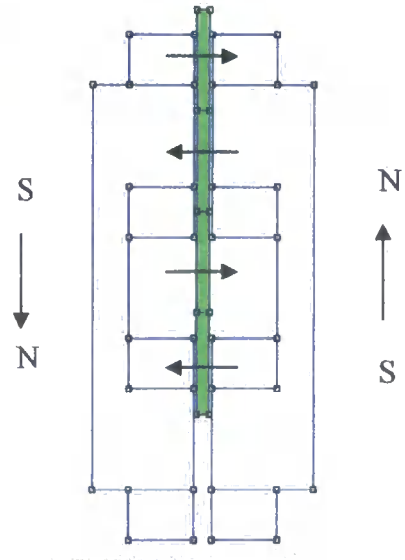

Figure 4.9C

Figure 4.9 - C-core permanent magnet (PM) tangential transition linear machine

Each shank has a coil wrapped around it, which are shown in green in figure 4.9B. The armature consists of a series of permanent magnets which are encased between two brass sheets, and are shown in green in figure 4.9C.

Figure 4.9C shows the direction of the generated electromagnetic field of the two C-cores and the direction of the fields of the four individual permanent magnets; and figure 4.10 shows the direction and magnitude of the flux density of the C-cores.

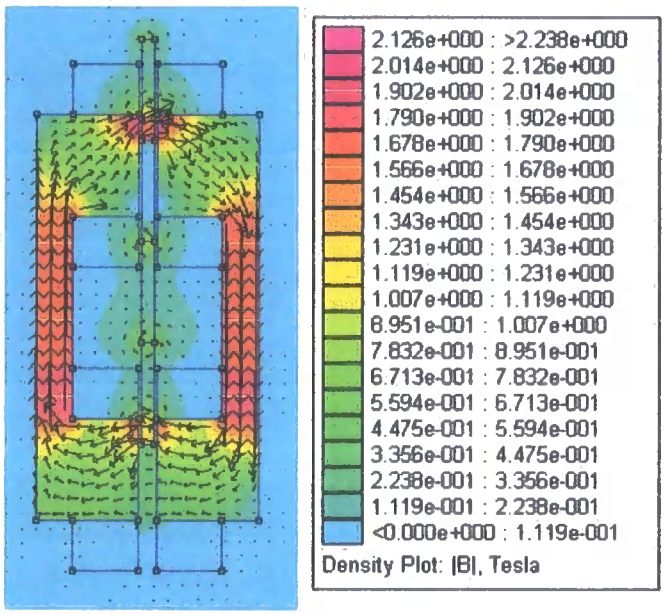

Figure 4.10 – Magnitude and direction of the flux density

Ideally the armature and the two C-cores would be in contact with each other so as to achieve maximum shear force, but in practice, due to the construction of the armature this is not possible. Brass sheets are used to hold and lock the magnets in position, along the length of the armature. This is done to prevent the magnets 'flipping', because the direction of the field of each individual magnet alternates about 180^0, as shown in figure 4.9C, therefore the unlike poles try to align themselves, that is the north and south poles are attracted to each other.

The problem with using the brass sheets is that, the low relative permeability of brass, very close to that of air, causes the brass sheets to act as an airgap; hence the reluctance is increased and consequently a fall in the flux density occurs. Therefore

less shear force is generated. The benefit of using the brass sheets is that, brass has a low coefficient of friction therefore only small friction losses are incurred during operation.

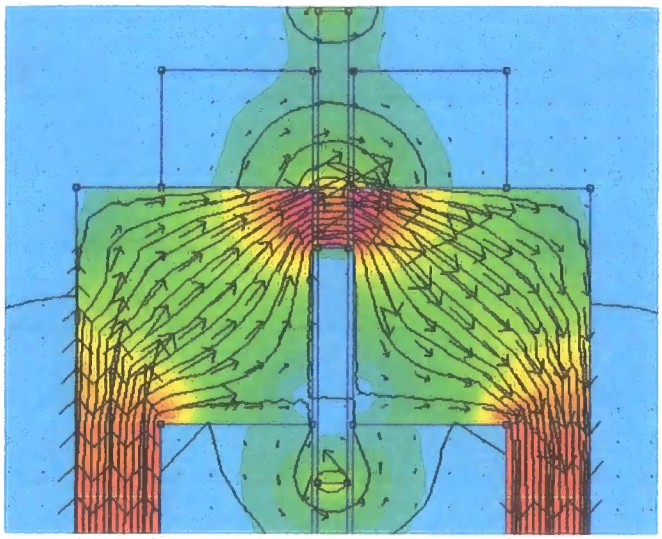

Figure 4.11 – Flux path on downward stroke of the armature

The motion of the central armature is vertical, figure 4.11. When the coils are energised, a magnetic field is induced forming a path around the C-cores so polarising the C-cores. The opposing pole of the armature is then attracted toward the flux path hence moving the armature. By inverting the current in the coils, the polarity is reversed so the motion of the armature is reversed as the other pole is now attracted.

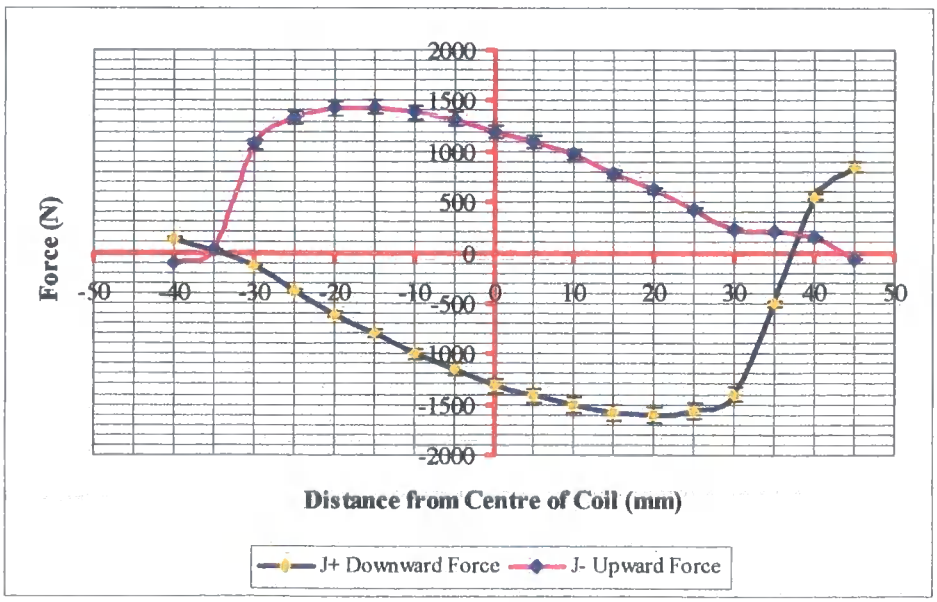

Figure 4.12 – Tangential (shear) force as the armature traverses the C-core face.

The variations in the generated force as the armature traverses across the face of the C-core are shown in figure 4.12. The zero point of the x-axis represents the centre of the C-core face, and the force is calculated at 5mm intervals as the centre of the permanent magnet moves away from the centre of the C-core. The greatest forces are generated when the armature moves towards the inner-side of the C-cores, this is due to the increased field caused by the two centre magnets shown in figure 4.9C. However, when the polarity of the C-cores is reversed the generated force is at a lower value and therefore this is the maximum force available to act against the output head of the pump. Consequently this restricts the stroke length, giving the option of a long stroke with a low force or a shorter stroke with a high force. This model suggests a practical stroke length of about 10mm, which would generate a maximum force of 1kN.

Whilst being involved with the project to design and build a C-core, the tests using the test rig shown in figure 4.8 were undertaken at Durham University by Ludovic Lamberti [81] revealing that the tangential (shear) force generated by such a system are as follows; maximum theoretical force is 377N (supply 4.5A, 10.7V) whilst the practical force was measured at 223N (supply 4.5A, 10.7V) over 40% reduction. Note the dimensions of the actuator used in the Lamberti design were different to those given in the thesis model.

Lamberti [81] states that these losses are attributed to a number of problems namely, the skin effect of the time varying magnetic fields applied to the C-core, resistance changes due to the temperature increase in the core, leakage and fringing flux, friction, and the dimensions of the permanent magnets. Regardless of the type of loss it is dissipated as heat. As the temperature is increased a typical ferrite can suffer a 25% drop in permeability. The consequences of a drop in permeability are that it will cause a rise in reluctance, causing a reduction in magnetic flux and flux density, ultimately reducing the force. This surpasses the losses due to flux leakage and fringing.

Some losses can be attributed to friction; however these have been kept to a minimum with the use of the brass. Whereas any losses that occur due to the dimensions of the permanent magnets are inherent to the design.

In contrast a normal force was modelled for the configuration shown in figure 4.13.

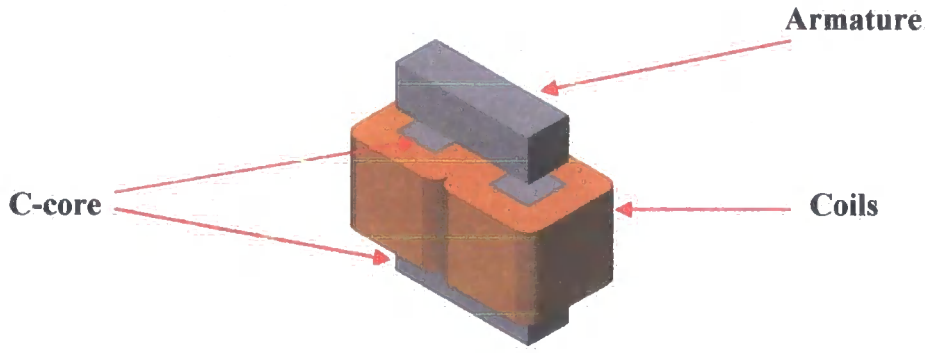

Figure: 4.13 - C-core utilising normal forces, motion of armature is vertical.

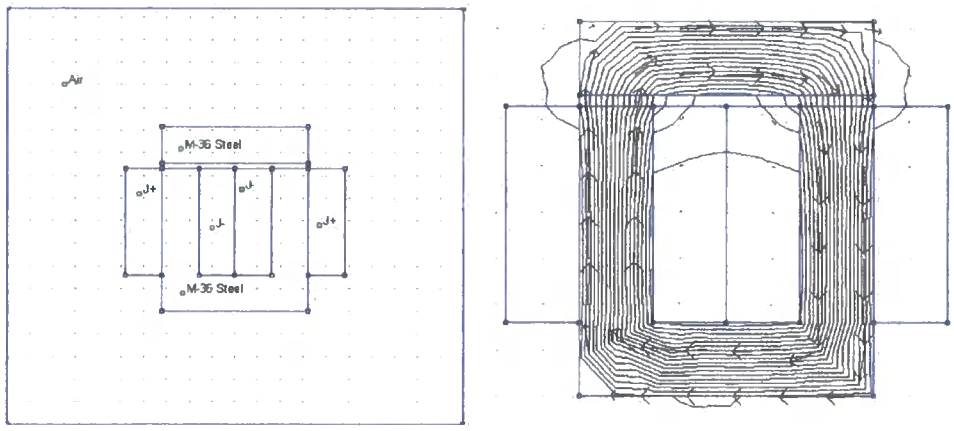

Figure: 4.14 – C-core (type.1) Femme model showing layout (left) and B field and direction of flux path (right)

Although the system shown in figure 4.13 was never built, modelling was used to determine the potential of C-cores for the generation and use of a normal force for the actuator. An evaluation could also be made as to whether the use of a normal force would be more effective than a tangential shear force. Modelling using femme software (a 2-D planar/axisymmetric electromagnetic simulation package)

has shown the potential for such a system. Figure 4.14 shows the C-core (type.1) Femme model layout, the flux density (B) field, and the direction of flux path.

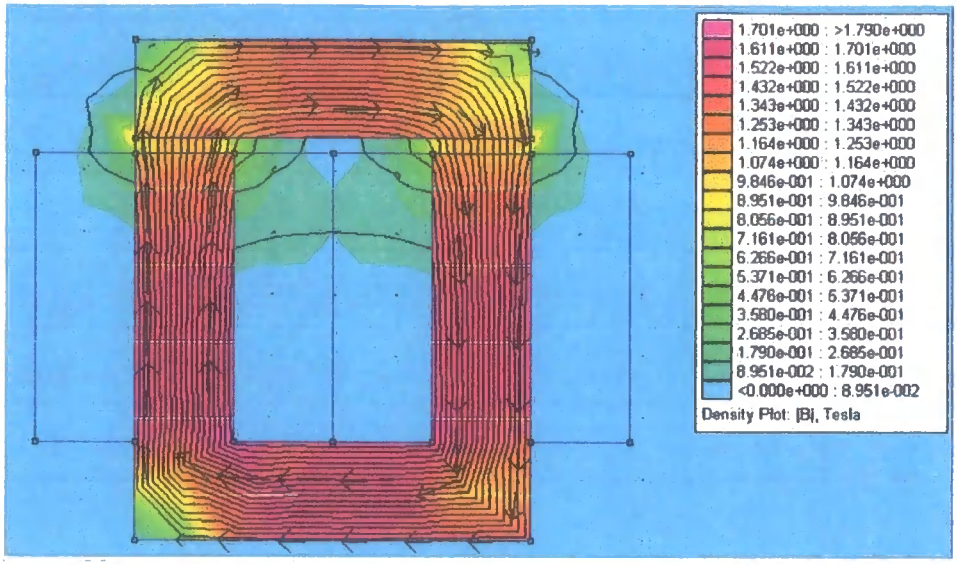

Figure: 4.15 – Density Plot |B|, Tesla & Flux Contours and Path Direction Arrows

Figure 4.15 shows the intensity of the flux density plot for a C-core (type.1) linear actuator producing a normal force. It can be seen that the flux density within the airgap (2.5mm) is between 1.074T and 1.164T, (Re: Key of figure 4.15). The associated forces over a range of 10mm down to 0.5mm are shown later in figure 4.23, (§4.1.5).

Figure 4.16 shows an alternative method; the type 2 C-core having one winding around the back of the core, opposed to the two windings around the legs of the type 1 C-core. The overall envelope dimensions remain, having a maximum width of 96mm and a depth of 32mm, with the height of the C-core and armature at 63mm and 16mm respectively. Whilst permitting the same amount of turns, it also extends the length of the armature by 16mm. However, even though the back of the C-core has also been extended by 16mm, the length of ferromagnetic material within the coil is reduced by 30mm.

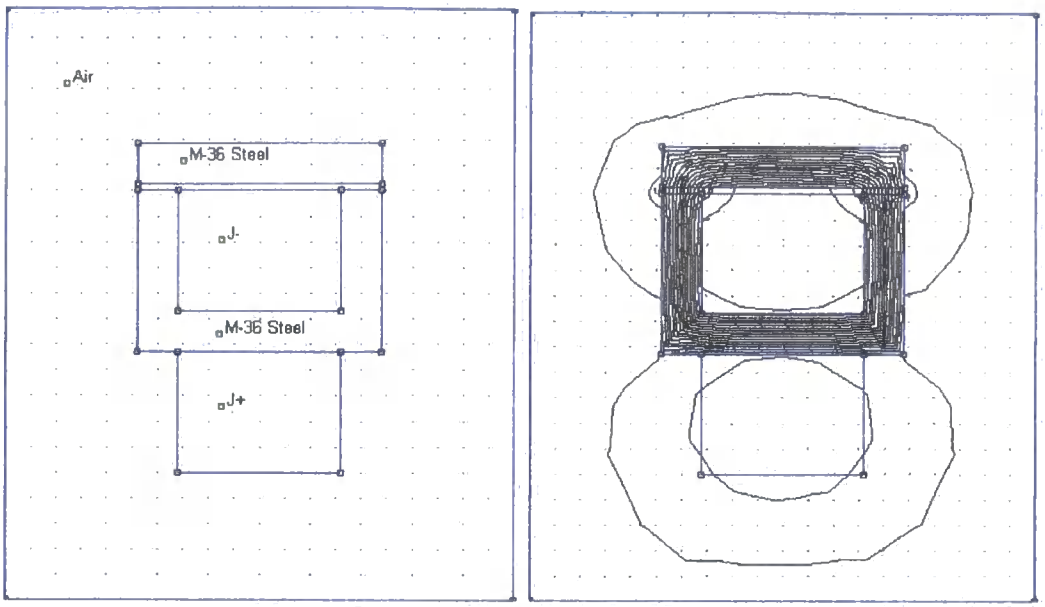

Figure: 4.16 – C-core (type.2) Femme model showing layout (left) and B field and direction of flux path (right)

Figure 4.17 shows the flux density plot for a C-core (type.2) linear actuator producing a normal force. It can be seen that the flux density within the airgap (2.5mm) is now between 1.111T and 1.295T, (Re: Key of figure 4.17) Therefore, the associated forces are not the same as C-core (type.1) over the same range of 10mm down to 0.5mm, shown later in figure 4.23, (§4.1.5).

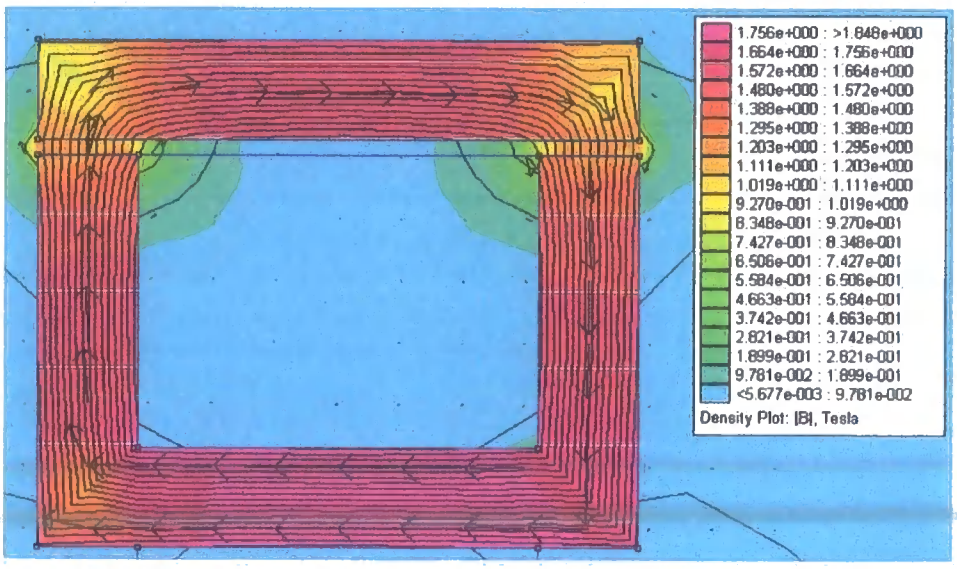

Figure: 4.17 - Density Plot |B|, Tesla & Flux Contours and Path Direction Arrows

4.1.4 E-core

From the modelling of a C-core system followed the modelling and development of the E-core system. Initially this system comprised of one E-core, which was further developed to a double E-core system and then to a multi E-core system.

Figure 4.18 shows a SolidWorks model of the E-core used in the first prototype pump. As with the C-cores modelling using Femm software (a 2-D planar / axisymmetric electromagnetic simulation package) has shown the potential for such a system.

Figure 4.18 - Single E-core System

Figure 4.19 shows the E-core (type.1) Femme model layout, the flux density (B) field, and the direction of flux path.

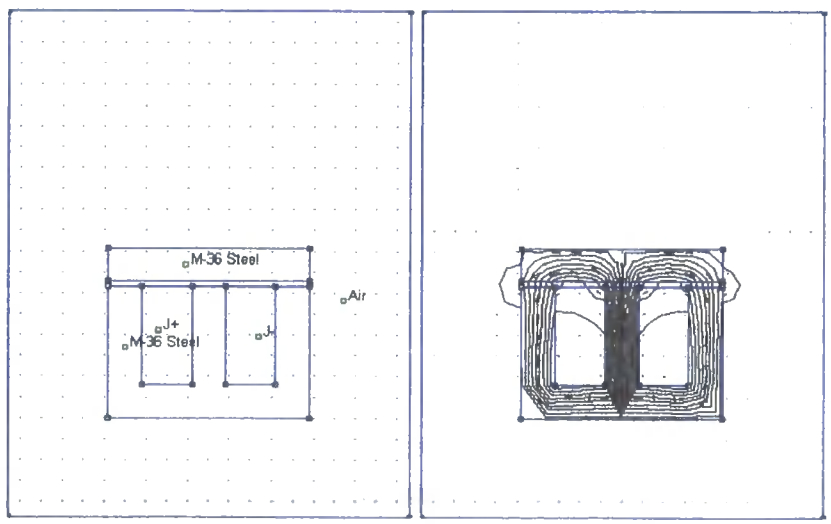

Figure: 4.19 – E-core (type.1) Femme model showing layout (left) and B field and direction of flux path (right)

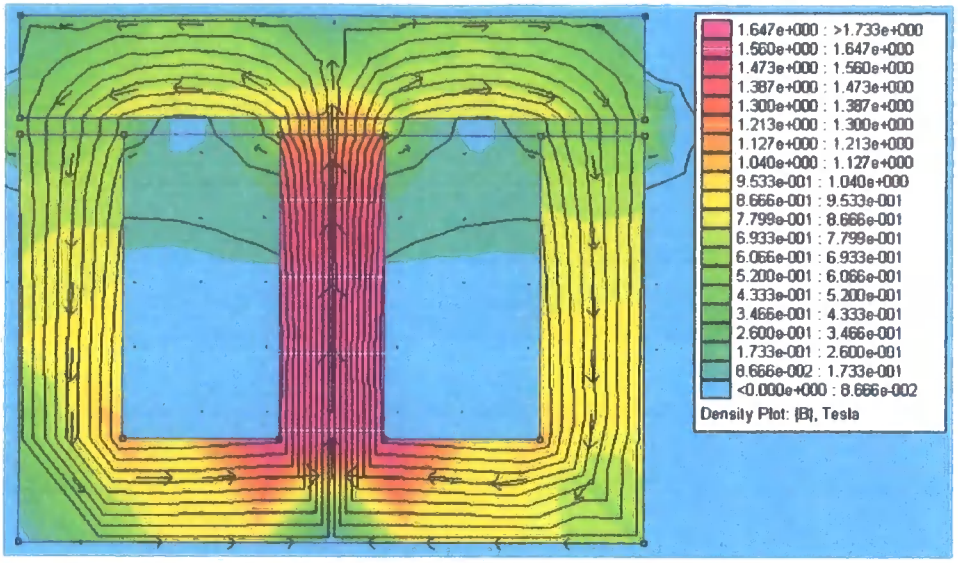

Figure: 4.20 - Density Plot |B| Tesla & Flux Contours and Path Direction Arrows

Figure 4.20 shows the intensity of the flux density plot for an E-core (type.1) linear actuator producing a normal force. It can be seen that the flux density within the airgap (2.5mm) is between 1.127T and 1.213T concentration in the centre leg airgap of the E-core and between 0.4333T and 0.6066T in the two outer legs' airgaps, (Re: Key of figure 4.20). It should be noted that the centre leg of the E-core (type.1) is of the same width as the outer legs'. The associated forces over a range of 10mm down to 0.5mm are shown later in figure 4.23, (§4.1.5).

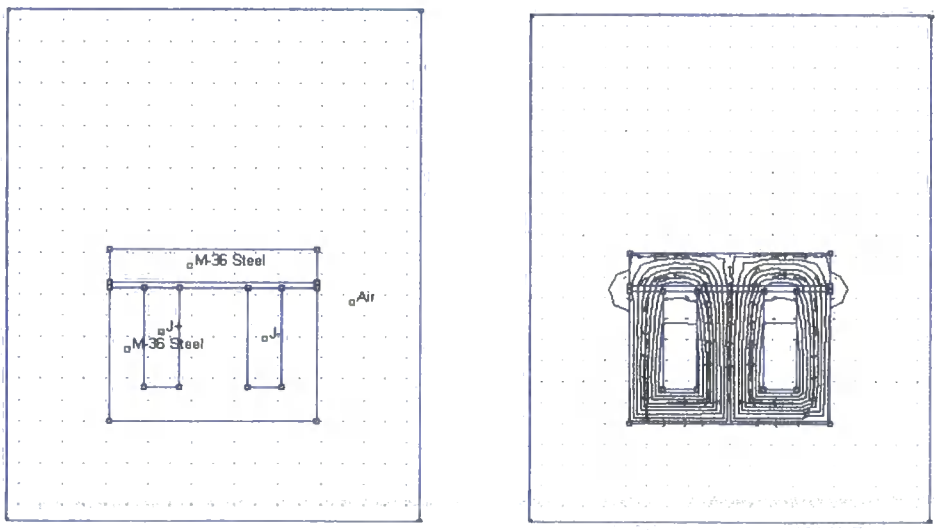

Figure: 4.21 – E-core (type.2) Femme model showing layout (left) and B field and direction of flux path (right)

Figure 4.21 shows E-core type 2; the difference between the two types of E-core is that the width of the central leg of type 2 is twice the width of type 1. Since the window for the coil is now reduced in size assumptions have been made so as a comparison can be made between the different topologies, these are listed in §4.1.5.

Figure 4.22 shows the flux density $|B|$ plot for an E-core (type.2) linear actuator producing a normal force. It can be seen that the flux density within the airgap (2.5mm) is now between 0.8559T and 0.9217T concentration in the centre leg airgap of the E-core and between 0.7242T and 0.79T in the two outer legs' airgaps, (Re: Key of figure 4.22). Again, this changes the value of the associated forces over the same range of 10mm down to 0.5mm, in this case producing almost twice the normal force of E-core (type.1) at an airgap of 0.5mm, shown later in figure 4.23, (§4.1.5).

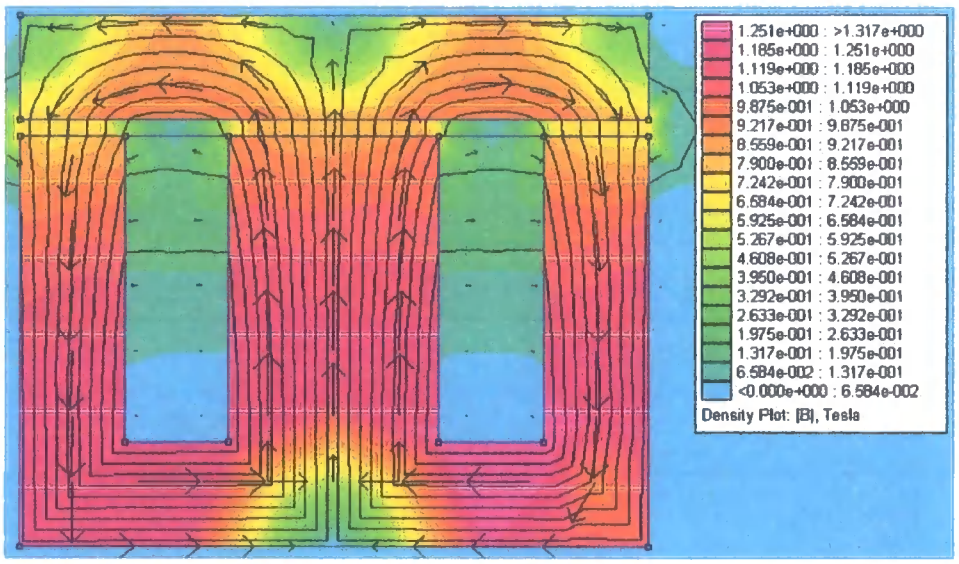

Figure: 4.22 - Density Plot |B|, Tesla & Flux Contours and Path Direction Arrows

Although in this case the flux density is not above the desired 1T as the armature moves towards the E-core the flux density rapidly increases surpassing the previous three core types hence producing double the normal force of the others at very small airgaps.

4.1.5 Comparing the Forces for Different Actuator Topologies

Having previously ruled out the use of solenoids and toroids, deliberation is now given to the tangential force of a C-core system and the normal forces of C-core and E-core systems.

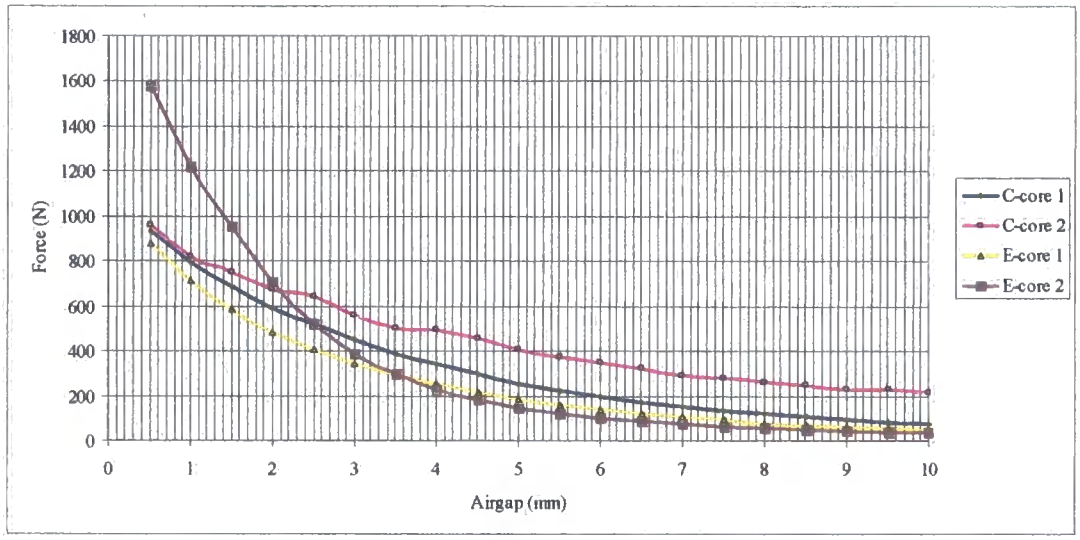

Figure 4.23 – Comparison of force for different Core Types (4.5A)

A comparison of the normal forces is given in figure 4.23 and is possible because of the parameters set for each of the cores, namely,

- The same overall width, 96mm
- The same depth, 32mm
- The same height of core, 63mm
- The same height of armature, 16mm
- The same ferromagnetic core material, M36-Steel
- The same current density (J)
- All operating mediums are in air
- All operate over the same airgap range, 0.5mm to 10mm
- All assume the same number of turns
- The FEA triangulation was set to automatic

For the C-core configuration shown in figure 4.8, the theoretical tangential shear force of 377N is developed with a 4.5A supply and is maintained over a stroke length of 10mm [81]. By comparison, (Re: Figure 4.23) the two C-core (§4.1.3) and the two E-core (§4.1.4) configurations, realize a normal force equivalent to the tangential force of 377N, at shorter stroke lengths, for the same supply current of 4.5A, each are listed,

- C-core type 1 attains 377N at a maximum stroke length of 3.55mm
- C-core type 2 attains 377N at a maximum stroke length of 5.4mm
- E-core type 1 attains 377N at a maximum stroke length of 2.65mm
- E-core type 2 attains 377N at a maximum stroke length of 3.05mm

However, at stroke lengths of less than the above, the forces generated are far greater. Listed are the maximum normal force generated within the airgap when it is reduced to 0.5mm,

- C-core type 1 attains 937.8N
- C-core type 2 attains 961.5N
- E-core type 1 attains 876.9N
- E-core type 2 attains 1579N

Nevertheless, by increasing the supply current the normal forces listed can be increased even further; for example, when the current is increased to 6A E-core type 2 develops a normal force in excess of 1700N within an airgap of 0.5mm. The increase in current also increases the flux density and the desired 1T is achievable over a greater range. Increasing the current also increases the maximum stroke length by approximately 1mm (Re: figure 4.24) for the normal force that is equivalent to the tangential force of 377N.

As stated in the literature review, tangential machines can exert a shear stress in the region of $100kNm^{-2}$. The electromagnet topology, using electromagnets based on variable reluctance principle, requires an airgap with a flux of 1T. This has been

achieved, and exhibits normal forces in excess of 400kNm^{-2}. This has been shown to be possible in the normal force models for all versions of C-core and E-core.

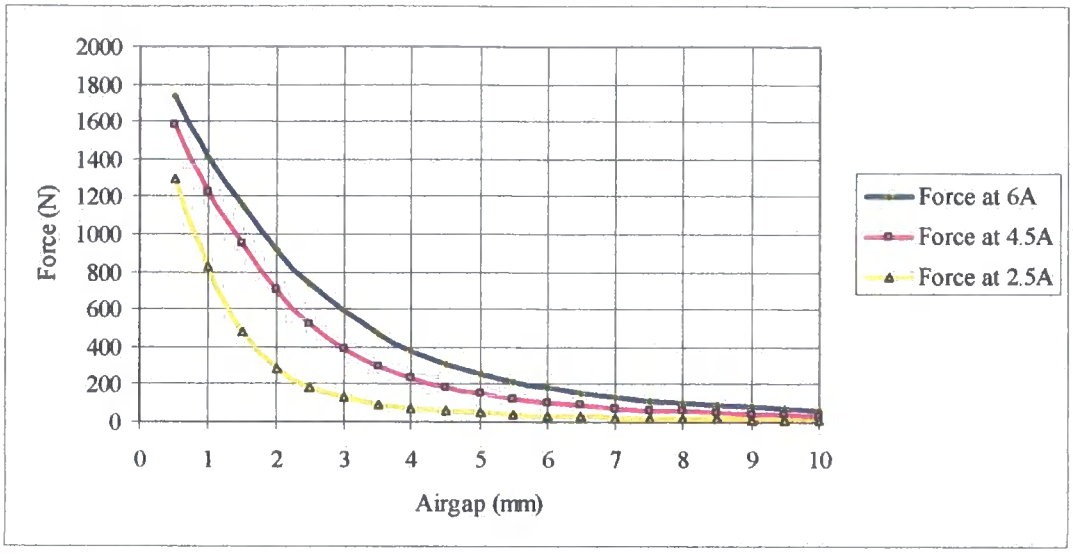

Figure 4.24 – Comparison of Normal Forces for E-core type 2

Current set at 2.5A, 4.5A, and 6A

Comparing the forces for different Actuator Topologies, clearly the E-core type 2 option offers the best choice in terms of desired thrust force hence able to operate at a greater depth. However, the ability to fit inside the physical envelope available in the pumping chamber may be a limiting factor. The advantage of the tangential force is that it can be maintained over a greater distance (stroke length) than that of the normal force devices. Consequently, for these reasons the tangential topology cannot be ruled out. However, at shorter stroke lengths normal forces are greater. C-core (type.2) generates a higher normal force at greater distances compared to the other types of normal core; overall, the response is more linear compared to the other core responses, potentially providing easier control of the armature movement. However, at small distances, E-core (type.2) creates the strongest flux density within the airgap, hence greater forces are achievable. Consequently it was decided pursue this avenue of generating linear motion for the actuator.

4.2 Theoretical Evaluation of E-core System

The electromagnetic modelling of the E-core was done with the use of a Microsoft Excel worksheet and the use of FEA (Femm) software. The spreadsheet incorporated a number of variables enabling an analysis of different sized cores to be compared. Nevertheless, there were some E-core laminations already available so the modelling was developed around these preset dimensions. The E-core dimensions are shown in figure 4.25.

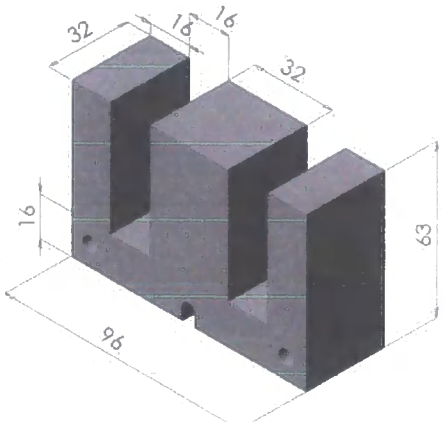

Figure 4.25 – Single E-core with 64mm x 0.5mm Laminations

The E-core laminations had a length to depth ratio 3:1 from which the required tubing dimensions were determined as given by equation 3.2 (§3.7.2). Optimum dimensions for E-core inductors and the effect of changing the dimension on the inductance value are outlined by Mohan, Undeland, and Robbins [82]. The E-core actuator is to all intents and purposes an inductor with a moving armature that acts as a driving mechanism for the reciprocating pumping action.

4.2.1 Force within the Airgap

The armature is supplying the force to displace the water by driving the diaphragm or piston, hence providing the pumping power. The thrust force provided by the force of attraction between the armature and the E-core can be calculated from Maxwell Force, F, shown in equation 4.2.

$$F = \frac{B^2 A}{2\mu_0} N \qquad \text{.... Eq}^{n}\text{. 4.2}$$

Where,

F = force within the airgap (N)

B = airgap flux density (T)

A = cross-sectional area of the airgap between the E-core legs and the armature (m^2)

μ_0 = permeability of free space (Hm^{-1})

Equation 4.2 gives the force; therefore, the flux density (B) in the airgap needs to be calculated. In order to calculate the flux density (B) the length of the mean free path (flux path) needs to be established so enabling an evaluation of the reluctance ($\Re$). The flux path and the direction of the flux path for E-core type 2 are shown in figure 4.26.

As can be seen two loops are formed, loop A in an anticlockwise direction and loop B in a clockwise direction. The assumptions are that loops A and B are symmetrical, and that the flux is contained within the steel structure and the airgaps, i.e. no fringing occurs. For ease of evaluation the E-core, the airgaps, and the armature have been split into eight sections; the equivalent circuits are presented in figure 4.27. The length of the 'mean free path' is taken as the distance along each central axis of each block up to the point of intersection of the next central axis.

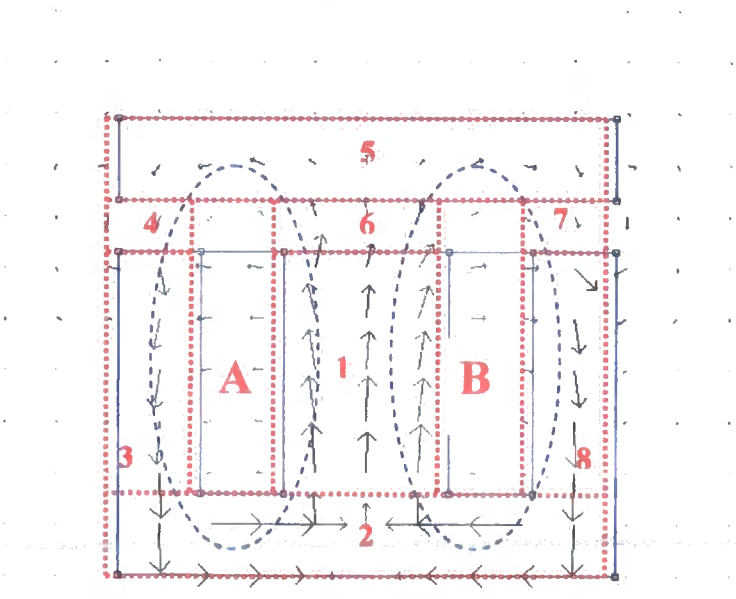

Figure 4.26– Flux Path for E-core type 2

The reluctance ($\Re$), for each section shown in figure.4.26 can be evaluated by using equation 4.3, however by using the equivalent circuits shown in figure.4.27 the total reluctance can be calculated using equation 4.4.

$$\Re = \frac{l}{\mu_0 \times \mu_r \times A} \quad H^{-1} \qquad \text{... Eq}^{n}\text{. 4.3}$$

Where,

$\Re$ = Reluctance (H^{-1})

l = Length of 'Mean Free Path' (m)

μ_0 = the permeability of free space (Hm^{-1})

μ_r = the relative permeability of the material (No units)

A = the cross-sectional area of the section (m^2)

$$\Re_x = \Re_{5/2} + \Re_4 + \Re_3 + \Re_{2/2} \quad H^{-1} \qquad \text{... Eq}^{n}\text{. 4.4}$$

A flow chart of the significance of material choice on the performance of the linear actuator is given in appendix 1.

4.2.2 Reluctance Network

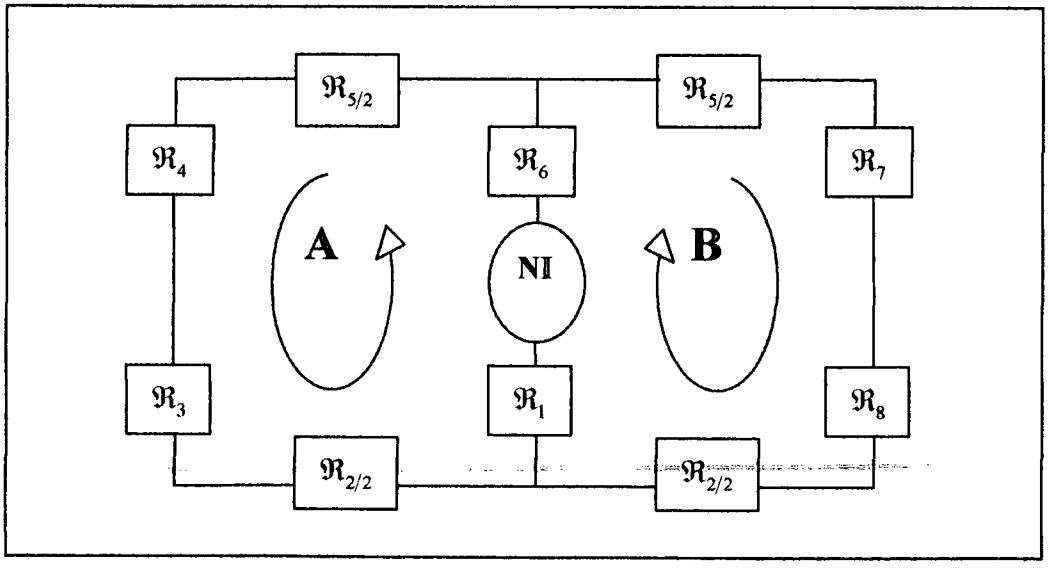

Figure 4.27 - Reluctance network for E-core type 2

Figure 4.27 shows the reluctance equivalent circuit for E-core type 2. It should be noted that reluctances $\Re_4, \Re_6$, and $\Re_7$ vary as the airgap changes. The magnetic flux is reduced when the airgap increases in size because it requires more energy to drive the same flux across the airgap than through an equal volume of the steel (or any other magnetic material) due to the much lower permeability of the air, and thus higher reluctance of the airgaps. All of the other reluctances of this E-core system are a function of the material used, the cross-sectional area, and the mean length. The reluctances $\Re_1, \Re_3$ and $\Re_8$ are directly proportional to the mean lengths of the three legs, (sections 1, 3, and 8 of figures 4.26 and 4.27) of the E-core. The first equivalent circuit (figure 4.28) shows the combined reluctances of both loops A and B can be reduced to a single reluctance for each loop. Equivalent circuit 2 shows how the two new reluctances, $\Re_x$ and $\Re_y$ can be considered to be in parallel. Since the system is symmetrical, $\Re_x$ and $\Re_y$ are of the same value. Circuit 3 shows their combined value of reluctance.

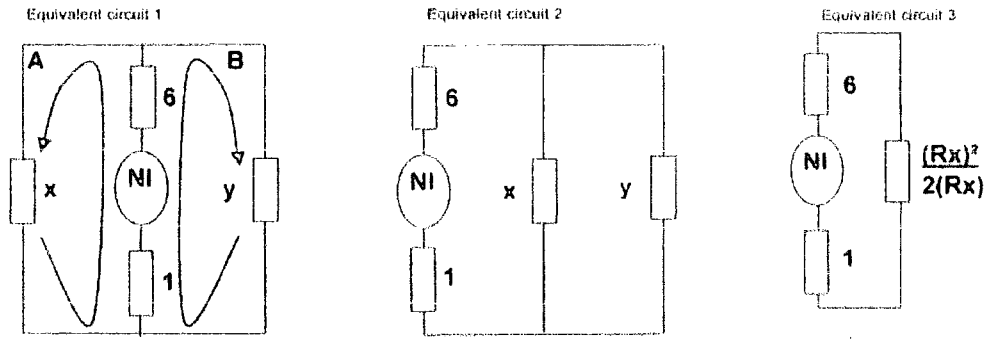

Figure 4.28 – Equivalent Circuits for the E-core type 2 Reluctance Network
(The letters and numbers in this figure relate to the subscripts in equations 4.5–4.8)

The value of reluctance for loop A is,

$$\Re_x = \Re_{5/2} + \Re_4 + \Re_3 + \Re_{2/2}$$

By symmetry,

$$\Re_x = \Re_y \qquad \text{... Eq}^{n}\text{. 4.5}$$

Combined parallel reluctance

$$\frac{\Re_x \Re_y}{\Re_x + \Re_y} = \frac{(\Re_x)^2}{2(\Re_x)} \qquad \text{... Eq}^{n}\text{. 4.6}$$

Since the reluctance network is symmetrical equation 4.6 can be replaced with

$$\frac{(\Re_x)^2}{2(\Re_x)} = \frac{\Re_x}{2} \qquad \text{... Eq}^{n}\text{. 4.7}$$

Giving the total reluctance of the circuit as,

$$\Re_{Total} = \Re_1 + \Re_6 + \frac{\Re_x}{2} \quad H^{-1} \qquad \text{... Eq}^{n}\text{. 4.8}$$

4.2.3 Magnetic Flux

From the reluctance, the magnetic flux (Φ), which is constant throughout the structure, can be determined by using equation 4.9.

$$\Phi = \frac{NI}{\Re_{Total}} \quad Wb \qquad \text{... Eq}^{n}\text{. 4.9}$$

Where, Φ = magnetic flux (Wb)

N = number of turns

I = current (A)

$\Re_{Total}$ = Total reluctance of the system (H^{-1})

Flow charts of the factors affecting the magnetic flux and the effect of current change on the performance of the linear actuator are given in appendix 1.

4.2.4 Flux Density

The flux density (B) can be now be calculated, from equation 4.10, hence the force in the airgap, by using equation 4.2.

$$B = \frac{\Phi}{A} \quad \text{T} \qquad \ldots \text{ Eq}^{\text{n}}. 4.10$$

Where,

B = Flux density (T)

Φ = Magnetic flux (Wb)

A = Cross-sectional area of the airgap (m^2)

4.2.5 Theoretical Force Constant

A flow chart of the effect of change in airgap size on the performance of the linear actuator is given in appendix 1.

The electromagnetic force produced in the airgap between the E-core (type 2) and the armature reduces as the armature moves away from the E-core. The rate of decay is inversely proportional to the square of the distance, and represented by equation 4.11.

$$F = C\frac{1}{l^2} \quad \text{N} \qquad \ldots \text{ Eq}^{\text{n}}. 4.11$$

Where,

F = Generated force of attraction (N)

l = Size of airgap (distance between E-core and Armature) (m)

C = A constant.

4.2.6 Explanation of the inverse square decay of force and the force constant

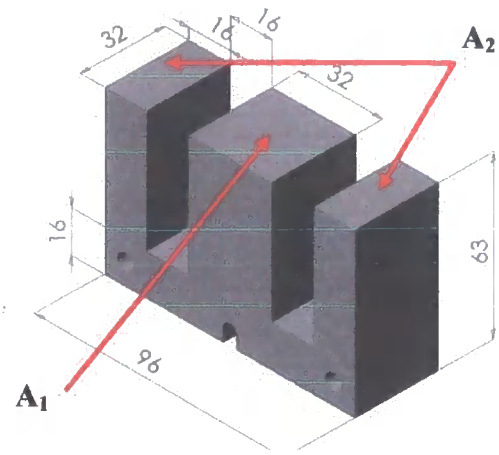

Figure 4.29 – c.s.a of E-core legs

Figure 4.25 shows the E-core system from which the E-core section is shown in figure 4.29 and as can be seen the central leg of the E-core is equivalent in cross-sectional area to the sum of the two outer legs, therefore it can be said that $A_1 = 2A_2$.

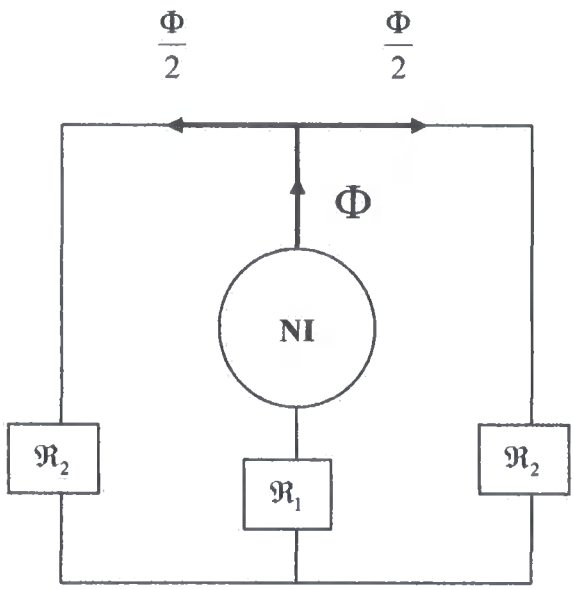

Figure 4.30 – E-core flux path

If an assumption is made that the magnetic flux is contained within the structure then all of the flux will pass through the central leg of the actuator and due to the symmetry of the actuator the flux will split equally in the outer legs, as shown in figure 4.30.

It is known that the force within the airgap per unit area is $F = \frac{B^2}{2\mu_0}$ (N), the flux density is $B = \frac{\Phi}{A}$ (T), the magnetic flux is $\Phi = \frac{NI}{\Re_{Total}}$ (Wb), and that the cross-sectional areas of the airgaps can be represented by $A_1 = 2A_2$ (m^2), it is now possible to evaluate the circuit reluctance.

With an airgap length of l (m), the reluctance, the reciprocal of the permeance, $\Re_1$ can be represented by,

$$\Re_1 = \frac{2l}{2\mu_0 A_1} = \frac{l}{\mu_0 A_1} \quad (\text{AtWb}^{-1})$$

Similarly, $\Re_2$ can be represented by,

$$\Re_2 = \frac{l}{\mu_0 A_2} = \frac{2l}{\mu_0 A_1} \quad (\text{AtWb}^{-1})$$

Therefore, $\Re_2 = 2\Re_1$

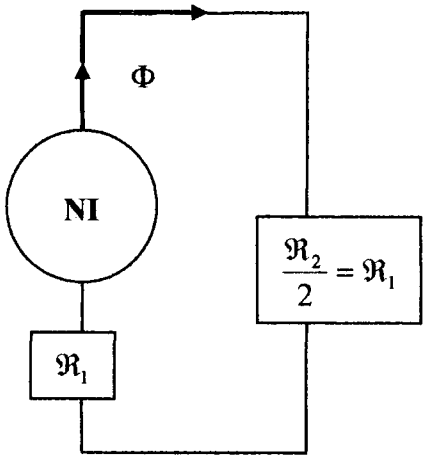

Since, $\Phi = \frac{NI}{\Re_{Total}}$, and $\Re_2 = 2\Re_1$ the equivalent circuit can be redrawn as in figure 4.31, therefore $NI = \Phi 2\Re_1$. Therefore, the magnetic flux can now be represented by $\Phi = \frac{NI}{2\Re_1}$.

Figure 4.31 – Reluctance equivalent circuit

The total force within the airgap can now be evaluated. The force in the central leg airgap can be represented by $F_1 = \frac{B_1^2}{2\mu_0} A_1$, and the force in an outer leg airgap can be represented by $F_2 = \frac{B_2^2}{2\mu_0} A_2$. However, $B_1 = B_2$ (due to symmetry) and $A_1 = 2A_2$, therefore forces can now be rewritten as, $F_1 = \frac{B_1^2}{2\mu_0} A_1$, and

$F_2 = \frac{B_1^2}{2\mu_0}\frac{A_1}{2}$. Therefore, the total force is equal to force$_1$ (F_1) plus twice force$_2$ ($2F_2$), $F_{Total} = F_1 + 2F_2$, shown in equation 4.12, F_1 representing the central leg and $2F_2$ representing the two outer legs.

$$F_{Total} = \frac{B_1^2}{2\mu_0}A_1 + 2\frac{B_1^2}{2\mu_0}\frac{A_1}{2} \quad \text{N} \qquad \ldots \text{ Eq}^{\text{n}}.\ 4.12$$

Giving,

$$F_{Total} = 2\left[\frac{B_1^2}{2\mu_0}A_1\right] = 2F_1 \quad \text{N} \qquad \ldots \text{ Eq}^{\text{n}}.\ 4.13$$

Taking this a stage further, since $B_1 = \frac{\Phi}{A_1}$ and $\Phi = \frac{NI}{2\Re_1} = \frac{NI}{2\frac{l}{\mu_0 A_1}} = \frac{NI}{2l}\mu_0 A_1$, the term for B_1 can now be written as,

$$B_1 = \frac{NI}{2l}\mu_0 \quad \text{T} \qquad \ldots \text{ Eq}^{\text{n}}.\ 4.14$$

Taking equation 4.13 and substituting for the B_1 term (equation 4.14) gives,

$$F_{Total} = 2\left[\frac{NI}{2l}\mu_0\right]^2\frac{1}{2\mu_0}A_1$$

$$F_{Total} = \mu_0 A_1\left[\frac{NI}{2l}\right]^2$$

$$F_{Total} = \mu_0 A_1\left[\frac{NI}{2}\right]^2\frac{1}{l^2}$$

Hence,

$$F_{Total} = \mu_0 A_1 \left[\frac{(NI)^2}{4}\right] l^{-2} \quad \text{N} \qquad \ldots \text{ Eq}^{\text{n}}. 4.15$$

Clearly, it can be seen that the force decay rate is inversely proportional to the square of the airgap length. The constant shown in equation 4.11 is represented by,

$$C = \mu_0 A_1 \left[\frac{(NI)^2}{4}\right] \quad \text{Nm}^2 \qquad \ldots \text{ Eq}^{\text{n}}. 4.16$$

This is a function of the geometry of the E-core, the number of turns in the coil and the current in the coil. Providing that the same type of E-core (i.e. type 2) is used, the use of the constant enables force predictions to be made when the size of the E-core is changed.

For an E-core having the dimensions shown in figure 4.25 and an armature with dimensions of 16mm x 96mm x 32mm, with a coil of 300 turns, and a current in the coil of 6A, the value of the constant is,

$$C = \left(\pi 4 \times 10^{-7}\right)\left(32 \times 10^{-3}\right)^2 \frac{(300 \times 6)^2}{4} = 1.04230504424 \times 10^{-3}$$

$$C \approx 1.0423 \times 10^{-3} \quad \text{Nm}^2 \qquad \ldots \text{ Eq}^{\text{n}}. 4.17$$

Equation 4.17 is the constant for the force evaluation of equation 4.11 for the E-core presented in §4.2 to date. Now, having established the validity of equation 4.11 a graph of force versus airgap can be plotted, as in figure 4.32.

From figure 4.32, it can be seen the regression equation for the power trend line is given as, $y = 1042.3x^{-2}$, with $R^2 = 1$, (R^2 is defined in appendix 2). The power trend line uses the power equation $y = cx^b$. Therefore, it can be concluded that the constant 'c' of the regression equation is the value of force generated at an airgap of 1mm, in this case 1042.3N. This is supported by equations 4.15, 4.16, and 4.17.

This phenomenon can be used as a tool for E-core (type 2) actuator design, providing that the E-core is not saturated, as it enables the force versus airgap characteristic for each specific E-core size to be plotted by only evaluating the force at 1mm.

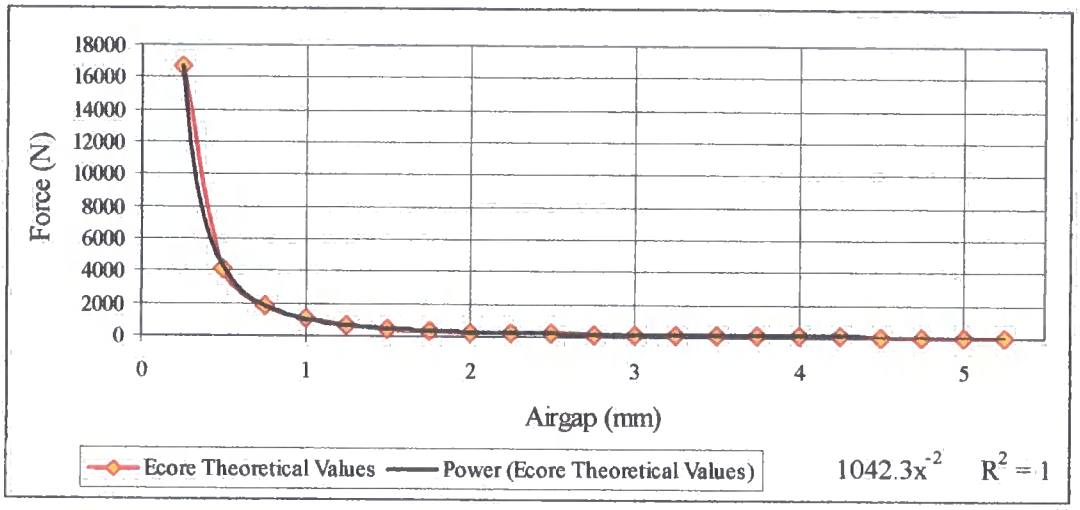

Figure 4.32 – Theoretical Force versus Airgap for E-core (type 2)

For the characteristic shown in figure 4.32, although not shown, the force at 10mm was determined to be approximately 10N; the force remained comparatively low over a distance of 8mm when the increases became more evident. At a 2mm airgap the force is 260N rising to 1042N at 1mm, to 4169N at 0.5mm, and 16676N at 0.25mm. This suggests that any useful generated force is only achievable at small airgaps; say 2mm, hence small stroke lengths.

However, figure 4.32 only provides the total force under given conditions over a given range, and no limits are imposed with respect to magnetic saturation. Consequently, some additional work is required, namely the determination of the minimum airgap size before saturation occurs.

When using a known material the flux density value at the saturation point of the B-H curve, the 'knee' of the B-H characteristic, can be taken as the maximum flux density for that material. The 'knee' of the characteristic is to be used because the

input of any more energy gives little return in magnetisation and the energy is dissipated as heat.

4.2.7 Determination of the minimum airgap size before saturation occurs

The determination of the minimum airgap size before saturation occurs can be achieved by rearranging equation 4.14, making '*l*' the length of the 'mean free path' the subject, giving,

$$l = \mu_0 \frac{NI}{2B} \quad \text{m} \qquad \ldots \text{ Eq}^{\text{n}}. 4.18$$

The assumption in the Microsoft Excel Model is that the relative permeability of mild steel is equal to 2000 at the 'knee' of the B-H characteristic and saturation occurs at 1.4T, [83]. The E-core being considered here has 300 turns and operates at 6A, under these conditions the E-core will saturate when the airgap length is approximately 0.81mm.

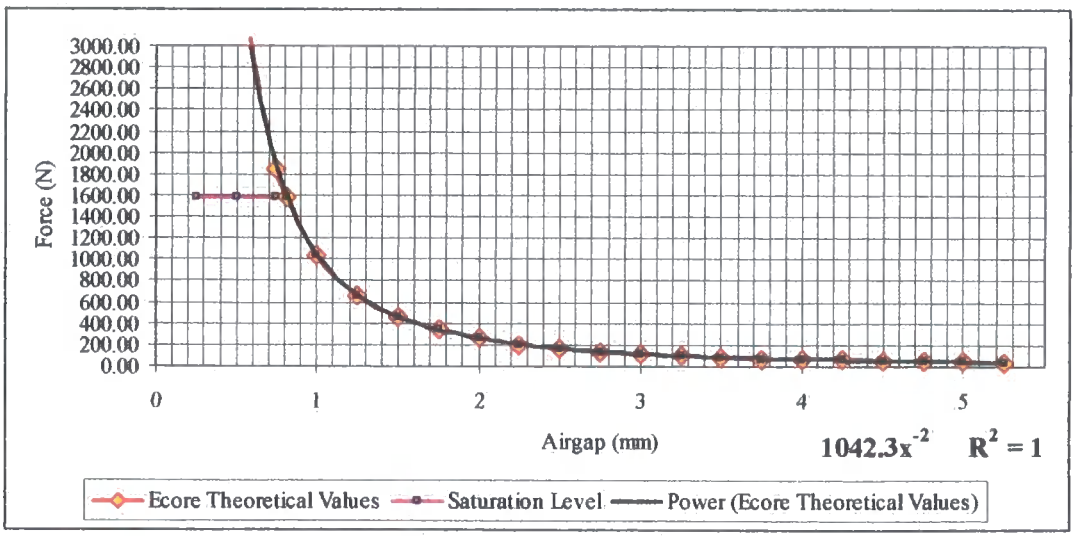

Figure 4.33 – Theoretical Force versus Airgap for E-core type 2
Including Saturation Level at 1588N at an Airgap of 0.81mm

Now, having established the minimum airgap length before saturation occurs, the maximum force that can be generated by the E-core can be determined using

equation 4.15. For the case stated above the maximum force generated is 1597.16N, which complies with the Maxwell's stress, equation 4.2. (Note, due to rounding errors, for the case of two decimal places, the force is reduced to 1588N a reduction of 9.16N). Figure 4.32 can now be modified to include the effect of saturation on the resultant force, as shown in figure 4.33.

Figure 4.33 indicates that various options are available with respect to the force generated over the airgap size, which is the stroke length. In all cases the stroke lengths are short, approximately 2mm or less.

An indication of the requirements is given by way of example. Earlier in §3.7.3, it was stated that when using a system that had a piston to outlet pipe ratio of 19:19 (measured in mm), a minimum force of 278N was required to operate the system. Rearranging equation 4.15 to find maximum stroke length for a known force, gives,

$$l = \sqrt{\frac{\mu_0 A_1 \left[\frac{(NI)^2}{4}\right]}{F_{Total}}} \quad \text{m} \qquad \ldots \text{ Eq}^{\text{n}}. 4.19$$

therefore, the maximum stroke length at which the system can operate with a minimum force of 278N is approximately 1.94mm.

One option is not to drive the actuator into saturation. For an operating force of 260N the operating stroke length would be 1.19mm, that is, from 0.81mm to 2mm. Although the force increases as per the power equation $y = cx^b$ over the range the effective force can only be the minimum force generated at the widest airgap. A second option is the same as the first but on this occasion drive the E-core into saturation. By doing so, the stroke length would be increased from 1.19mm up to 2mm. A third option is to only operate the actuator when it is saturated, by doing so the generated force is increased to 1588N over the entire stroke length, although the stroke length is shortened to 0.81mm

Knowing that the 'knee' of the B-H characteristic is to be used because the input of any more energy gives little return in increased magnetisation and the energy is dissipated as heat, a quandary arises to whether driving the E-core into saturation is beneficial or not.

Despite the fact that once reaching saturation the energy is dissipated as heat; if an adequate heat sink is used, then it may be possible to operate the actuator under saturation conditions. When the actuator is under saturation, it produces a high constant linear force within the airgap, as shown in figure 4.33. However, there are some important points to remember, Jiles [84] states, "If the temperature is increased from say 20 to 80 centigrade then a typical ferrite can suffer a 25% drop in permeability". The consequences of a drop in permeability occurring in this E-core system, is that, it will cause a rise in reluctance, causing a reduction in magnetic flux and hence flux density, ultimately reducing the force. Jiles [84] also states, "Avoid reaching saturation since a drop in inductance accompanies it [...] the rate at which current in the coil increases is inversely proportional to inductance [...]. Any drop in inductance therefore causes the current to rise faster, increasing the field strength and so, the core is driven even further into saturation". However, any drop in inductance for the E-core actuator would be of benefit as the actuator would be capable of operating at a higher frequency. The main concern of the E-core being driven further into saturation is the removal of the heat generated. The effect of hysteresis adds a further complication since the magnetization (M) of the material depends not only on the magnetic field (H), but also on the field history, $B = \mu_0 (H + M)$.

4.2.8 Changing the Flux Density |B|

An alternative to increasing the current in order to increase the flux density, hence the force within the airgap, is to change the material of the structure of the E-core. Changing the type of material used for the construction of the E-core changes the relative permeability leading to a change in force. Previously, when discussing thermal change within the E-core, it was stated that the consequence of a drop in

permeability occurring in this E-core system was to ultimately reduce the force thereby increasing the relative permeability; by changing the material an increase in force will occur. Note: When mentioning relative permeability it means the relative permeability value at the 'knee' of the B-H characteristic, because the relative permeability value is continually changing, as it is the gradient of the curve at any point along the B-H characteristic. However, the increase in relative permeability is not the only factor that affects the point of saturation, it also depends on the physical properties of the material and how the E-core is manufactured.

Nevertheless, even changing the material has limitations and the maximum possible level of saturation is 2.43T. Jiles [84] states, "The highest saturation magnetization available is 2.43T which is achieved in an iron-cobalt alloy containing 35% cobalt". Therefore, the maximum possible force achievable by changing the material of the system operating under the previous conditions, of 300 turns and 6A, can be established. The point of saturation can be calculated by using equation 4.18 and the maximum force at this point can be calculated by using equation 4.15.

Changing the material of the E-core to iron-cobalt, would increase the flux density saturation level and reduce the point of saturation within the airgap to 0.47mm and increase the generated force to 4812N at that point. The increase in force occurs because the force is directly proportional to the square of the flux density, equation 4.2. The change in force also complies with the power regression equation $y = cx^b$ of figure 4.33, because the geometry of the E-core does not change, equation 4.15 and equation 4.21.

4.2.9 Changing the Number of Turns

Having previously established that the generated force within the airgap of the E-core is a function of the geometry of the E-core, the number of turns in the coil, and the current in the coil, the only other method of increasing the generated force is to increase the number of turns in the coil.

Without decreasing the wire gauge in the coil, which would limit the current that could be used, the only option available to increase the number of turns is to change the length of the legs. Since the dimensions of the E-core are restricted by the borehole diameter, the only dimensions that can be changed are the height of sections 1, 3, and 8 of figure 4.26.

Therefore, the number of turns can be represented by the product of the coil width (C_W), the coil height (C_H), and the fill factor (0.4), equation 4.20. A fill factor of 0.4 has been chosen as the initial coil had 300 turns, which fitted a coil slot of 752mm^2 (16mm x 47mm).

$$\frac{300}{752} = 0.399 = 0.4 FillFactor$$

$$N = 0.4(C_W \times C_H) \qquad \text{... Eq}^{\text{n}}\text{. 4.20}$$

Due to the physical nature of the E-core, the resultant value of equation 4.20 can only be taken to the nearest half turn.

Equation 4.15 can now be modified by substituting equation 4.20 for N, which will allow variations in leg length to be taken into account when calculating the force.

$$F_{Total} = \mu_0 A_1 \left[\frac{(NI)^2}{4} \right] l^{-2}$$

$$F_{Total} = \mu_0 A_1 \left[\frac{\left(0.4(C_W \times C_H)\right)^2 I^2}{4} \right] l^{-2} \quad \text{N} \qquad \text{... Eq}^{\text{n}}\text{. 4.21}$$

Changing the length of the legs also changes the length of the mean free path for the evaluation of the reluctance within the E-core. However, the flux density is considered constant throughout; therefore the effect on the force can be considered

negligible. Further, the force within the airgap is evaluated with respect to the geometry, the current, the number of turns, and the size of the airgap.

The force generated within an airgap of 1mm, the constant, now becomes,

$$C = \mu_0 A_1 \left[\frac{\left(0.4\left(C_W \times C_H\right)\right)^2 I^2}{4} \right] \quad \text{... Eq}^{\text{n}}\text{. 4.22}$$

$$C = 0.04\mu_0 A_1 I^2 C_W{}^2 C_H{}^2$$

$$C = \pi 0.16\times 10^{-7} I^2 A_1 C_W{}^2 C_H{}^2 \quad \text{... Eq}^{\text{n}}\text{. 4.23}$$

Note: For C_W and C_H only use the numeric value and **not** the SI metre conversion.

If the height (C_H), equation 4.21, were halved (i.e. 23.5mm, present 47mm) then the generated force within the airgap at 1mm would be approximately 262N, (262 would become the constant of equation 4.11). In this case the constant having a value of approximately 0.262×10^{-3}. Therefore, the power regression equation for the force versus airgap characteristic becomes $y = 261.97x^2$, where 'x' is the numeric value of the airgap in mm.

If the height (C_H), equation 4.21, were doubled (i.e. 94mm, present 47mm) then the generated force within the airgap at 1mm would be approximately 4191N, (4191 would become the value of the constant of equation 4.11). In this case the constant having a value of approximately 4.1915×10^{-3}. Therefore, the power regression equation for the force versus airgap characteristic becomes $y = 4191.49x^2$, where 'x' is the numeric value of the airgap in mm.

Since this is not possible, it has already been established with the use of Maxwell's stress equation that the maximum generated force possible, within the airgap, is

1597.16N. Therefore, the saturation must have occurred at a greater distance than 1mm.

The point of saturation can be established by calculating the number of turns with equation 4.20.

$$N = 0.4(C_W \times C_H) \qquad \text{... Eq}^{n}\text{. 4.24}$$

$$N = 601.6$$

Only half turns can be included therefore N = 601.5.

Now by inserting the N value (601.5), along with the Maxwell stress value (1597.16) for F_{Total} in equation 4.19, the saturation length can be determined.

$$l = \sqrt{\frac{\mu_0 A_1 \left[\frac{(NI)^2}{4}\right]}{F_{Total}}}$$

$$l_{saturation} = 1.6197 \times 10^{-3} m \approx 1.62mm$$

Therefore, the E-core will saturate with a generated force of 1597N within the airgap when the distance between the armature and the E-core is approximately 1.62mm.

Now envisage the scenario that the saturation level, hence force, is to be maintained over an increased stroke length of 10mm. In order to evaluate the number of turns required and the length of the legs of the E-core, N is made the subject of equation 4.19, as in equation 4.25.

$$N = \frac{2l}{I}\sqrt{\frac{F_{Saturation}}{\mu_0 A_1}} \qquad \text{... Eq}^{n}\text{. 4.25}$$

The height of the legs (C_H) of the E-core can now be calculated by inserting the new value of N into equation 4.24, or can be calculated directly from equation 4.26.

$$C_H = \frac{5l}{C_W I}\sqrt{\frac{F_{Saturation}}{\mu_0 A_1}} \quad \text{m} \qquad \ldots \text{Eq}^{\text{n}}.\ 4.26$$

It was determined that in order to maintain a generated force of 1597N within the airgap over a stroke length of 10mm, the length of the legs of the E-core would need to be approximately 580.25mm.

4.2.10 Voltage Equation

For a coil having an applied voltage 'e' with a current 'i' flowing through, so developing a magnetic field of total flux 'Φ', the interrelation is,

$$e = Ri + N\frac{d\Phi}{dt}$$

$$e = Ri + \frac{d\Psi}{dt} \quad \text{V} \qquad \ldots \text{Eq}^{\text{n}}.\ 4.27$$

Where, R = resistance of coil (Ω)

Ψ = NΦ = total flux linkages (Wb)

N = number of turns on coil

t = time (s)

d/dt = time derivative

The flux linkage Ψ is a function of current 'i' and the magnetic properties of the space surrounding the coil. In general, the coil has an inductance, defined by the relation

$$\Psi = L(i).i \quad \text{Wb} \qquad \ldots \text{ Eq}^{n}.\ 4.28$$

where, L(i) is the inductance and can be a constant and independent of 'i' when the coil is in air. When the coil is embedded in mild steel, or any other ferromagnetic material, then non-linear saturation makes the inductance a function of the current.

The voltage equation changes when introducing the inductance, hence substituting for Ψ in equation 4.27 gives,

$$e = Ri + \frac{d}{dt}\left[L(i).i\right] = Ri + L(i)\frac{d}{dt}i + i\frac{d}{dt}L(i) \qquad \text{or}$$

$$e = \left[R + L(i)\frac{d}{dt}\right]i + i\frac{d}{dt}L(i) \quad \text{V} \qquad \ldots \text{ Eq}^{n}.\ 4.29$$

Where, the third term of equation 4.29 represents the back e.m.f, only arising when there is a change in flux due to a change in inductance. For the E-core system employed here, the movement of the armature changes the magnetic properties, because the magnetic field is disturbed, and the flux path changes length and the generated force within the airgap changes.

The voltage equation for the E-core (figure 4.26) can be determined.

In order to establish the inductance of the coil, a lumped parameter is used, defining the relation between the current and the flux linkage.

Since, Φ = m.m.f / reluctance, the flux linkage is given by,

$$\Psi = N\Phi = N\left(\frac{Ni}{\Re}\right) \quad \text{Wb} \qquad \ldots \text{ Eq}^{n}.\ 4.30$$

Where, Φ = flux (Wb)

N = number of turns

$\Re$ = Reluctance of magnetic circuit (H^{-1})

Ni = m.m.f = magnetomotive force (Ampere-turn)

But according to equation 4.28

$$\Psi = Li$$

Thus, from equation 4.30

$$L = \frac{N^2}{\Re} \quad \text{H} \qquad \ldots \text{ Eq}^{\text{n}}. 4.31$$

Neglecting flux fringing at the edges and assuming that $\mu_r \gg \mu_0$, (i.e. $\mu_r \rangle\rangle 1$)

The equivalent circuits of figure 4.30 and figure 4.31 show that the reluctance of the circuit can be represented by $2\Re_1$, where $\Re_1 = \frac{l}{\mu_0 A_1}$.

Therefore $\Re$ can be represented by,

$$\Re = \frac{2l_{Ag}}{\mu_0 A_1} \quad \text{H}^{-1} \qquad \ldots \text{ Eq}^{\text{n}}. 4.32$$

Where l_{Ag} = the length of the airgap

Substituting this value of $\Re$ equation 4.32 into equation 4.31 gives,

$$L = \frac{N^2 \mu_0 A_1}{2l_{Ag}} = L_1 \frac{1}{l_{Ag}} = L\left(l_{Ag}\right) \quad \text{H} \qquad \ldots \text{ Eq}^{\text{n}}. 4.33$$

Where $L_1 = \frac{1}{2} N^2 \mu_0 A_1$

The inductance is therefore a function of airgap length only and independent of current and flux.

Let $x = l_{Ag}$

The voltage equation follows then as

$$e = Ri + \frac{d}{dt}(L.i) = Ri + L\frac{d}{dt}i + i\left(\frac{d}{dx}L\right)\frac{dx}{dt}$$

Where dx/dt is the rate of displacement or speed of the armature along path x.

Substituting for L gives,

$$e = \left(R + \frac{L_1}{x}\frac{d}{dt}\right)i + i\left[\frac{d}{dx}\left(\frac{L_1}{x}\right)\right]\frac{dx}{dt}$$

$$e = \left(R + \frac{L_1}{x}\frac{d}{dt}\right)i - i\frac{L_1}{x^2}\frac{dx}{dt} \quad \text{V} \qquad \ldots \text{ Eq}^{\text{n}}. 4.34$$

The back e.m.f is directly proportional to speed for any value of x; it is also a function of $1/x^2$, therefore more relevant at small airgaps.

4.2.11 Stored Energy

Considering the same coil, having an applied voltage 'e' with a current 'i' flowing through so developing a magnetic field of total flux 'Φ', the aim now is to determine the energy stored in the field produced when a current of 'i' flows through 'N' turns.

The energy U_{in} fed into the coil from the applied electrical source is given by,

$$U_{in} = \int_0^t eidt \quad \text{J} \qquad \text{... Eq}^{\text{n}}\text{. 4.35}$$

Where, e = the applied voltage to the coil terminals

$t = 0$ is the time when the energy input starts

The voltage under the integral can be replaced by the voltage drop across the coil resistance and the rate of change of flux linkages, using equation 4.27, and equation 4.35 becomes,

$$U_{in} = \int_0^t \left(Ri^2 + i\frac{d\Psi}{dt} \right) dt \qquad \text{J} \qquad \text{... Eq}^{\text{n}}\text{. 4.36}$$

However, the heat loss in the coil resistance is

$$U_{res} = \int_0^t Ri^2 dt \quad \text{J} \qquad \text{... Eq}^{\text{n}}\text{. 4.37}$$

Therefore the energy flowing into the field is

$$U = U_{in} - U_{res} = \int_0^t \left(i\frac{d\psi}{dt} \right) dt = \int_{\psi(0)}^{\psi(t)} id\psi \quad \text{J} \qquad \text{... Eq}^{\text{n}}\text{. 4.38}$$

Therefore, the energy is fed into the field at a rate proportional to the induced voltage e_{in}, where $e_{in} = \frac{d\Psi}{dt}$. Even if the coil current and field voltage are present, if no change in flux occurs, no new magnetic energy will be stored. When there is a change in flux the energy changes in proportion to that change.

Therefore, the stored magnetic energy U_f can be determined from equation 4.38

$$U_f - U_f(0) = U = \int_{\Psi(0)}^{\Psi(t)} id\Psi \quad \text{J} \qquad \text{... Eqn. 4.39}$$

Where, $U_f(0) =$ Stored energy in the field for $t = 0$

$\Psi(0) =$ Flux linkage for $t = 0$

If there has been no energy introduced before time $t = 0$ then the initial stored energy $U_f(0)$ must be zero and no field can exist, hence the initial flux linkage must be zero, $\Psi(0) = 0$.

The total energy stored for any flux Ψ is then given by,

$$U_f = \int_{\Psi=0}^{\Psi} id\Psi \quad \text{J} \qquad \text{... Eqn. 4.40}$$

The energy stored in a coil with a constant inductance L, neglecting saturation, has a relation between the flux and the current of $\Psi = Li$, and hence has an energy of,

$$U_f = \int_0^{\Psi} \left(\frac{1}{L}\Psi\right) d\Psi$$

$$U_f = \frac{1}{2}\frac{1}{L}\Psi^2$$

$$U_f = \frac{1}{2}Li^2 \quad \text{J} \qquad \text{... Eq}^{\text{n}}\text{. 4.41}$$

Hence, the stored energy in the coil is proportional to both the inductance and the square of the current. With reference to the geometry of the E-core, the stored energy can now be established as.

Substituting x for l_{Ag} in equation 4.33 gives,

$$L = \frac{N^2 \mu_0 A_1}{2x} \quad \text{H} \qquad \text{... Eq}^{\text{n}}\text{. 4.42}$$

Substituting equation 4.42 for L in equation 4.41 gives,

$$U_f = \frac{\mu_0 A_1 (Ni)^2}{4x} \quad \text{J} \qquad \text{... Eq}^{\text{n}}\text{. 4.43}$$

However, equation 4.41 and equation 4.43 represent the energy stored in the coil for one specific airgap size only. Given that the inductance is directly proportional to the reciprocal of the airgap distance, reducing the airgap size causes an increase in the inductance; this can be represented as follows.

$$U_f = \frac{1}{2} L i^2 \qquad L = \frac{L_1}{x} \qquad L_1 = \frac{1}{2} N^2 \mu_0 A_1$$

$$U_f = i^2 \left[\frac{d}{dx} \left(\frac{L_1}{2x} \right) \right] \frac{dx}{dt}$$

$$U_f = -i^2 \frac{L_1}{2x^2} \frac{dx}{dt}$$

$$U_f = -\frac{\mu_0 A_1 (Ni)^2}{4x^2} \frac{dx}{dt}$$

$$U_f = \frac{\mu_0 A_1 (Ni)^2}{8x^3} \quad \text{Joules} \qquad \text{... Eq}^{\text{n}}\text{. 4.44}$$

If hysteresis is neglected the energy stored in the field when increasing the flux can be regained when reducing the flux to its original value; however hysteresis is inevitable. Therefore, hysteresis must be considered as the amount of energy that

has been added when increasing the flux from $\Psi(0)$ to $\Psi(t)$ will be lost when the flux is reduced as it traverses a different path. The area enclosed by the hysteresis loop represents the amount of energy transformed into heat in the magnetic material.

4.2.12 Inductance

There are many ways in which inductance can be described, however, in this case, inductance may be defined as the property of an E-core and coil to oppose a change in current. The moving magnetic field produced by a change in current causing an induced voltage to oppose the original change.

4.2.13 The Effect of Inductance on the System

This definition of inductance assumes static conditions whereas in practice there is a continuous change in the size of the airgap between the armature and the E-core. Consequently, the inductance is constantly changing due to the movement of the armature, and the inductance is inversely proportional to the size of the airgap, as given in equation 4.33. It has previously been shown that under static conditions the inductance is a function of airgap only and that when the armature is traversing the airgap too becomes a function of current, equation 4.28.

The resultant stored energy is therefore particularly relevant at small airgaps, as the stored energy is inversely proportional to the inverse cube of the airgap size, as given in equation 4.34. The stored energy is also directly proportional to the square of the current, equation 4.41; therefore, particularly at high currents, the stored energy at small airgaps is high.

The third term of equation 4.34 represents the back e.m.f of the coil, from which it can be seen that the back e.m.f is directly proportional to both the current and the inductance. It is also shown that the rate at which the voltage develops is

proportional to the inverse cube of the size of the airgap, therefore large voltages can develop across the coil when switching the supply.

As has been shown the amount of stored energy is directly related to the inductance and the current. When switching the supply on / off or between two sets of E-core the stored energy needs to be dissipated or returned to the supply to minimize losses.

The induced e.m.f, the first two parts of equation 4.34, is also directly proportional to circuit inductance. The magnitude of an induced e.m.f is directly proportional to the rate of change of the current. The frequency of operation of the system is determined by the rate of change of current, and the generated force is directly proportional to current.

When the rate of change of current is too slow, the current cannot achieve the required level and therefore cannot generate sufficient force to pump against the delivery head; also, the system could 'latch out'. Should the rate of change of current be too fast, cavitations could occur.

4.2.14 Changing the Inductance

The reasons for and benefits of changing the value of inductance are as follows.

Inductance of the coil within the system has the ability to store energy and the current flowing through it can generate heat. If the stored energy in the inductor is not returned to the supply then heat is generated which must be removed. Heating of the inductor causes the resistance to rise and consequently the time constant for the rise and decay time of the input signal, and so a change in frequency occurs. Heating of the system also causes a change in the magnetic properties and a change of temperature, $\Delta T=60^0C$ from a baseline of 20^0C, will result in a drop in permeability of approximately 25% [84], and for this reason a reduced generated force.

Although inductance is independent of current and flux (p123) it does change with airgap distance, the inductance increasing, as the airgap tends to zero. The changing inductance also causes a change in frequency. The resistance change due to the thermal effect can be controlled to some degree with the use of thermistors or varistors resulting in negligible change. However, the change in inductance is a function of the nature of the system which can not be controlled; consequently the effect of inductance within the system can only be minimized by reducing its actual value.

4.3 E-Core Test Rig Results and Inductance Test Results

Theoretically, as the airgap tends to zero the force generated within the airgap rises rapidly; that is, large forces at very small airgap settings. Tests were undertaken and the electromagnetic force was evaluated by three different methods, first by the theoretical model, and then by two different measuring techniques, via a Hall Effect probe, and via a Load Cell. The flux density readings from the Hall Effect probe were used to evaluate the inductance of the E-core.

4.3.1 Determination of the Electromagnetic Force

The practical evaluation of the generated force was achieved via the use of the flux density readings and load cell readings, obtained at various airgap settings. Spacers were measured with a micrometer; they were then placed between the E-core and armature. The test rig was then locked into position, and once locked the spacers were removed, thus providing an airgap of known size.

All three were compared and conclusions drawn as to the accuracy of the model and the measurement techniques.

4.3.2 The Model

Several spreadsheets have been developed each serving there own purpose and are all interconnected for at least one parameter. Reluctance Force Inductance models for different cross-sectional areas (c.s.a) of both E-core & C-core electromagnets have been devised and results compared. In addition, the practical results are incorporated within the spreadsheets thus permitting a comparison between the theoretical values and the practical results.

4.3.3 The Hall Effect Probe

The airgap was preset to a known measured distance, the Hall Effect probe inserted into the airgap, and the flux density was taken at stages over the full length of the airgap. The multiple readings were then averaged for each section of the E-core airgap, and the force was then calculated, using Maxwell Force. Using the Hall Effect probe method does have limitations in that the minimum airgap is restricted to the thickness of the probe, (absolute minimum 0.8mm). Consequently, to obtain the force at smaller gaps the data needs to be extrapolated.

4.3.4 The Load Cell

The S-type load cell was calibrated and found to have a hysteresis. Consequently, all results were taken in one direction only, i.e. when the load on the cell was being increased, then used to measure the actual force exerted by the armature, which was attached to the load cell, when the electromagnet was energised; a differential voltage was amplified, and used to calculate the force using the load characteristic of the load cell. This represents the force within the airgap. Load cell measurements were taken at the same time as the Hall probe readings enabling a comparison of results obtained under the same conditions. When taking the readings it was essential to maintain the correct and stable excitation voltage for the load cell. However this was difficult to achieve because the supply to the load cell contained a ripple that caused the readings to fluctuate. Furthermore, when large

forces were exerted on the armature when the airgap was small, the load cell being formed of two cantilevers, would cause a deflection resulting in a change in the preset airgap. This gave rise to doubt as to the accuracy of the readings at small airgaps.

A clock gauge was used to detect any movement of the armature when the coil was energised, thus ensuring a constant airgap; any movement meant that the airgap had changed. Consequently, multiple readings were taken at small airgaps, and an average of the data was taken.

4.3.5 Experimental Set-up

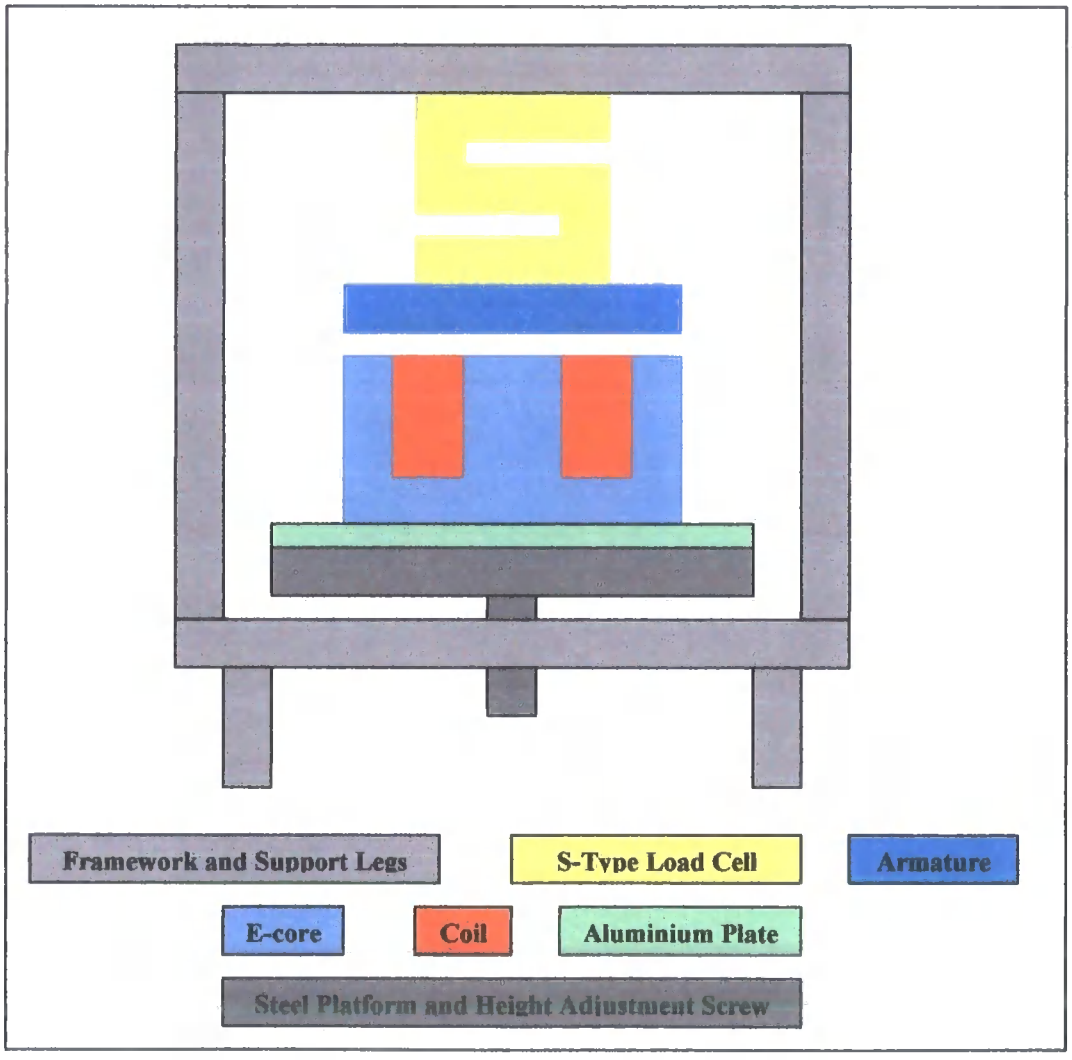

Figure 4.34 – Schematic diagram of the E-core test rig

Figure 4.34 shows a schematic of the E-core test rig. The rigid (mild steel) framework is supported on legs so that the (mild steel) platform can be raised and lowered, via the height adjustment screw, and thereby changing the size of the airgap between the (mild steel) armature and the (mild steel) E-core. The E-core is separated from the platform via an aluminium plate, and both of which are securely clamped to the platform. The aluminium plate is used to reduce the fringing of the magnetic flux. The S-type load cell is bolted to the cross-bar of the framework, and the armature is bolted to the S-type load cell. The airgap is formed between the armature and the E-core.

The airgap is set by inserting sheets of material (the thickness measured with a micrometer) between the armature and E-core, and then raising the platform until all three are in contact. Feeler gauges are used to check the fit of the sheets to ensure a good measurement. The sheets are then removed and the airgap is set. A micro-measuring gauge is placed on the armature before the E-core is energised; this indicates any movement of the armature and by how much at the point of switch on. Movement of the armature was more prominent at smaller airgaps; this gave doubt to the accuracy of the readings at smaller airgaps.

When using the S-type load cell, the load produced a voltage signal which was measured and used to calculate the force from the load cell characteristic. When using the Hall Effect probe; the probe gave a digital reading of the flux density from which the force was then calculated using equation 4.2. However, this method was limited to a minimum airgap size of 0.8mm, which is the thickness of the Hall Effect probe.

4.3.6 Experimental Results

The generated forces for current settings of both 2.5A and 6A were investigated. Forces at 2.5A were measured because this value of current was less than the rated current density (J) for the gauge of wire used within the coil. However, the resultant force produced was far less than that produced using 6A. The 6A test was the maximum supply current available and was undertaken to observe what the

system could actually achieve. Both sets of results were compared to the theoretical values calculated in the spreadsheet.

Knowing that the coil could become excessively hot under the tests, particularly when using 6A, the temperature gradient was measured, along with some temperature contours. The purpose of measuring the temperature gradient was to ascertain the change in temperature to evaluate the change in resistance and the contours to identify any hot spots. The temperature readings were also required for safety because the temperature of the coil rose to approximately 140^0C.

Figure 4.35 shows the results of the single E-core static force tests, which are represented by the Fs characteristic decay rate, which was determined to be $y = 614.28x^{-1.9017}$. The constant term, 614.28, of the equation of the F-s characteristic has previously been shown to be a function of the geometry of the E-core. That is, a function of the number of turns and the coil current, with respect to the square of the airgap size. The theoretical value of $y = 1042.3x^{-2}$ is evaluated from equation 4.15 and is represented in figure 4.32. The constant term in both equations, represent the generated force within an airgap of 1mm. The difference in the power terms is a result of the $y = cx^b$ regression equation having too few points to evaluate an accurate value.

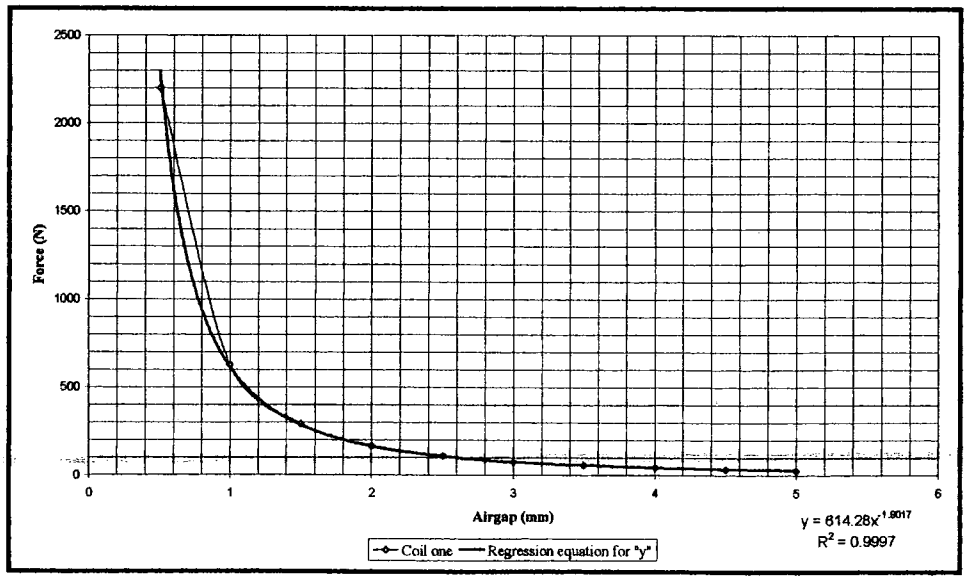

Figure 4.35 – Result of Force versus Airgap

4.3.7 Comparison of Force Results

Figure 4.36, table 4.1 and appendix 3, show a comparison of the Results of Force versus Airgap. An explanation of the differences is now given. The plots for the theoretical values and the Excel model are closely matched. The slight differences are because the model does not account for any losses within the system such as fringing and assumes that saturation occurs at 1.4 Tesla.

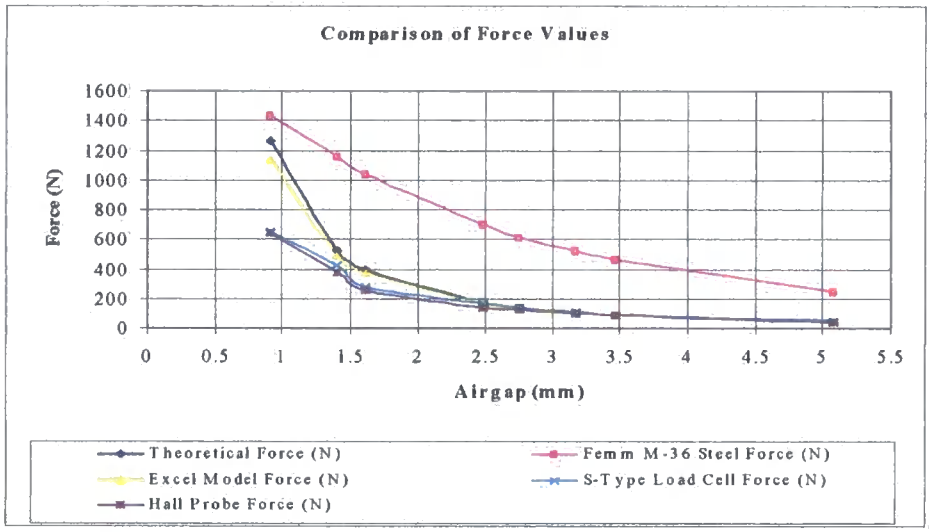

Figure 4.36 – Comparison of Results of Force versus Airgap

RESULTS	Theoretical	Femm M-36 Steel	Excel Model	S-Type Load Cell	Hall Probe
Airgap	Force	Force	Force	Force	Force
(mm)	(N)	(N)	(N)	(N)	(N)
0.90975	1259.33	1434.95	1134.48	652.02	641.23
1.41	524.26	1157.69	489.80	427.83	377.82
1.62	397.15	1035.97	374.28	279.10	255.59
2.48	169.46	701.09	162.99	163.27	139.28
2.75	137.82	611.54	133.06	136.72	128.82
3.175	103.39	525.96	100.29	112.45	95.02
3.46	87.06	461.23	84.66	90.95	86.48
5.08	40.39	248.40	39.62	46.86	39.70

Table 4.1 - Comparison of Results of Force versus Airgap

However, the saturation level can be changed to any required value, for the investigation of different materials. From the results saturation at 1.4 Tesla is high and needs to be reduced to provide a more accurate evaluation. Indications are that it is in the order of 1.1 Tesla to 1.2 Tesla.

Similarly, the force results obtained by the two measuring techniques are closely matched, suggesting that both methods are valid. Since, both of these sets have similar deviations from the theoretical and model values, indicates that there are approximately 50% losses involved. These losses can be attributed to fringing, and thermal energy losses.

4.3.8 Inductance Results

The flux density readings from the Hall Effect probe were used to evaluate the inductance of the E-core.

The current was set at 2.5A, and maintained throughout for all airgap settings. The flux density was measured with a Hall Effect probe. The number of turns, in the coil is known to be 300 and the measured resistance of the coil was 1.46Ω. From the readings of flux density obtained the Inductance was calculated from,

$$L = \frac{NBA_g}{I} \quad \text{H} \qquad \text{Eq}^{\text{n}}.\ 4.45$$

Where, L = Inductance (H)

N = Number of turns within the coil

ϕ = Magnetic Flux (Wb)

I = Current through the coil (A)

$$L = \frac{N\phi}{I} \text{ and } B = \frac{\phi}{A_g} \text{ and } \phi = BA_g$$

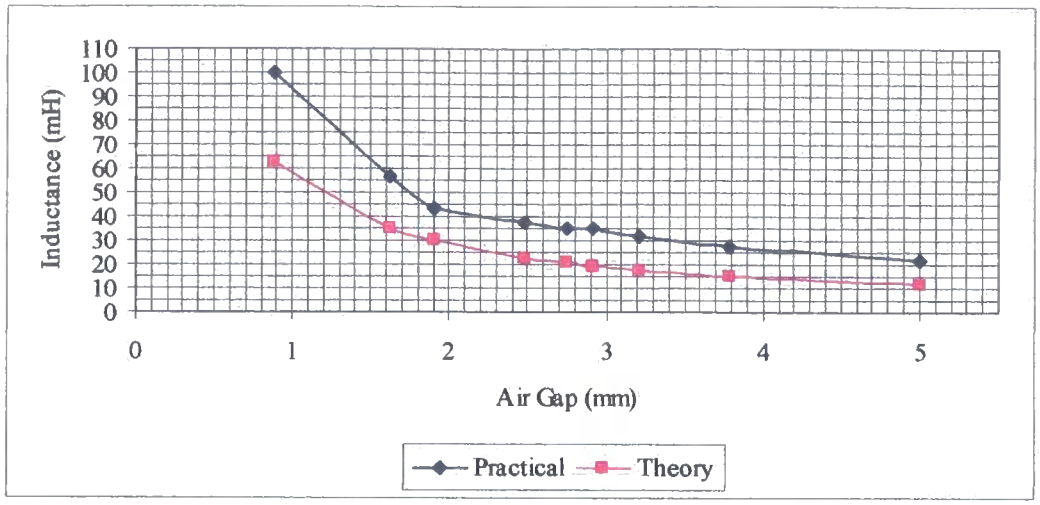

Figure 4.37 - Comparison of the Theoretical and the Practical values of Inductance for the E-core

The results are shown in figure 4.37. By using equation 4.45, the inductance could be calculated directly from the readings obtained. The results were compared to the theoretical values of the spreadsheet; it was found that the theoretical values were only approximately 60% of the practical.

4.4 Summary of Design

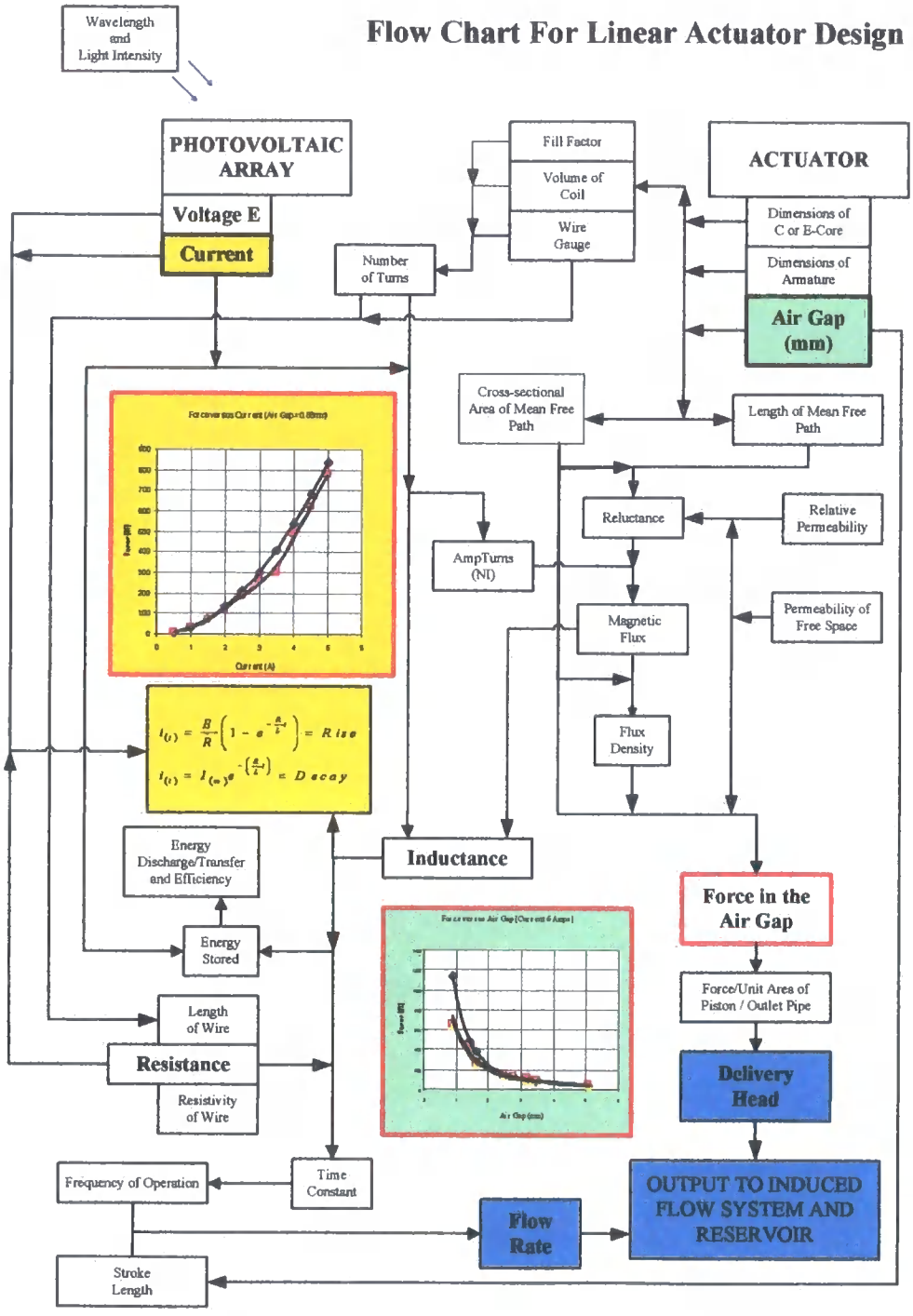

Figure: 4.38 – Flow Chart for Linear Actuator Design

Figure 4.38 is a Flow Chart for the Linear Actuator Design showing the interlinked issues involved with the design of such a pump; (Links: - Rectangles with the same colour boarders likewise with the same colour backgrounds). This section has

investigated all the parameters involved and developed some useful tools for the design of such actuators.

The E-core tests results indicate that the best avenue to take with respect to the type of electromagnet to be used as the driving mechanism for the actuator is the E-core type 2.

The use of a single E-core with longer legs would increase the m.m.f due to the increase in the number of turns in the coil; and consequently the generated electromagnetic force would increase, because the force is directly proportional to the m.m.f. However, this method of pumping only pumps in one direction.

However, this is now taken further by utilising two of the E-cores, one inverted and suspended over the other, with armature placed between the two. The E-cores are to be energised alternately so generating a force in both directions, which provides for a dual pumping action, doubling the output of the pump. The dual pumping action configuration is shown in figure 4.39.

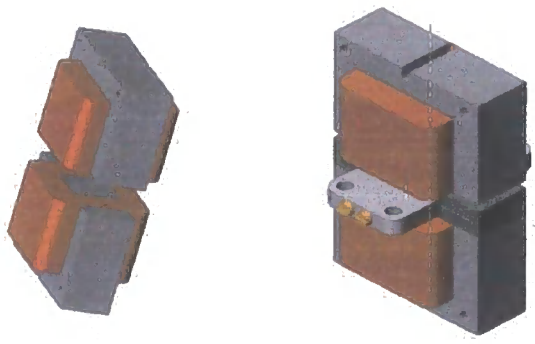

Figure.4.39 – Double E-core with Armature and Driver Plates

Figure 4.39 shows how the armature when assembled locates between the two E-cores. The drive rods, when fitted, are mounted vertically from the armature side plate and clear of the sides of the upper coil. The stroke length is that of the airgap size, that is the distance between the armature and the E-core when the armature is in contact with the other E-core.

4.5 Springs investigation

The electromagnetic force generated by the E-core depreciates rapidly, at a rate of the inverse square of the distance (equation 4.15), with respect to the armature displacement travelling away from the coil. The reduced force imposed by the larger airgap and the potential problems of small airgaps could be rectified by the addition of another source of energy, in this case the use of springs. The idea was to use the energy stored in a spring, and the linear force generated by a spring, (Hooke's Law), as an aid to increasing the stroke length of the pump.

No matter whether the spring is under compression or tension, the relaxation of the spring, releases the stored energy so providing the spring force. The summation of this additional spring force and the electromagnetic force are used to maintain the driving force at a higher level and over a greater distance throughout the actuators pumping cycle. From this, two options could be available; firstly, an increased swept volume/flow rate, or secondly, an increased head over a shorter distance.

By making the stroke longer, the larger airgap reduces the available force; consequently, the springs will also need to compensate for the reduced force until the electromagnets can have any effect.

4.5.1 The Spring System

Various combinations of springs have been considered: under compression, under tension, a mixture, single springs and multiple springs. Both single and double E-core systems utilising different spring scenarios have been considered: free springs, attached springs, and pre-stressed springs acting either under compression or under tension. For all scenarios, the total upward force and the total downward force have been analysed separately, then considered together as an operating system.

The sign convention used throughout the investigation is that all forces acting upwards are positive, forces acting downwards are negative. The reference point is

at the bottom, when the armature is at its lowest point, so the positive 'displacement' is upward (figure 4.40). Three main forces were considered, the weight of the actuator, (mg), the electromagnetic force, (Fm), and the spring force, (Fs). Under the above convention, mg will always be negative, as would be the submerged head, and the others vary.

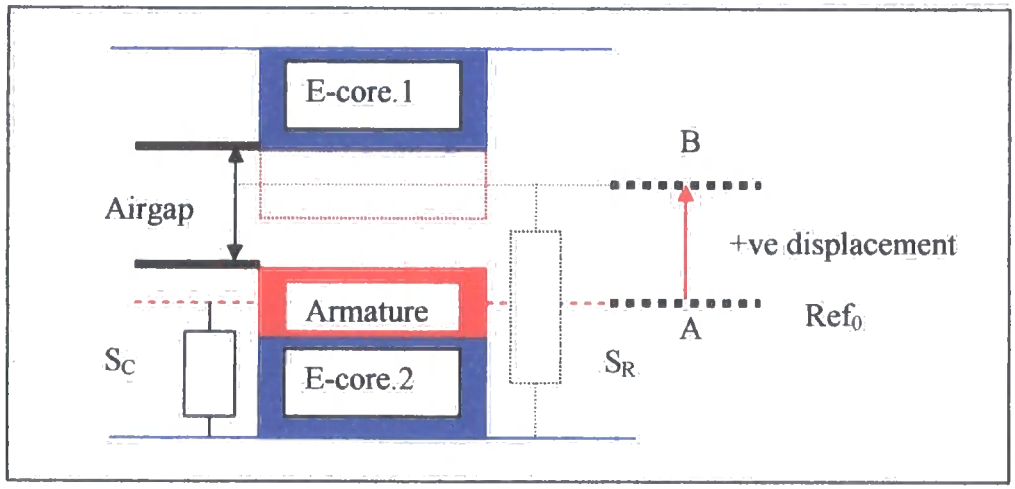

Figure: 4.40 - Schematic diagram of Twin E-core + Compression Spring.

Assumptions and considerations; there is no submerged head, (the submerged head would add to the value of mg) and any excessive submerged head would cancel any benefit gained. However, in the case of the pumping chamber and the outlet pipe being of the ratio of 1:1 (§3.7.3) this matter is irrelevant.

The effect of the spring forces on the upward stroke and the downward stroke were first considered separately, and then over an entire cycle.

The system condition (figure 4.40) at the start of the upward stroke is that the inlet valve is closed, the outlet valve is open, the armature is at zero reference at its lowest point and maximum airgap, the spring network is compressed therefore storing energy, and E-core 1 is energised and E-core 2 is de-energised. The transition from A to B (figure 4.40) is a positive displacement therefore the forces involved are,

- The electromagnetic force of E-core 1, which increases rapidly as the armature attracts toward E-core 1, is positive. (+ve)
- The electromagnetic force of E-core 2 is zero because the E-core is de-energised. (0)
- The force from the relaxation (decompression) of the spring network is positive. (+ve)
- The force attributed to the weight of the drive system, i.e. the armature diaphragm and the connecting pieces, is always negative. (Always –ve)

The summation of these forces is the resultant force available to power the delivery head.

The system condition (figure 4.40) at the start of the downward stroke is that the inlet valve is open, the outlet valve is closed. The armature is its highest point, which is the position of the armature for the minimum airgap for upward stroke. The spring network is relaxed (de-compressed) and therefore has no stored energy, E-core 1 is de-energised and E-core 2 is energised at maximum airgap for downward stroke. The transition from B to A (figure 4.40) is a negative displacement therefore the forces involved are,

- The electromagnetic force of E-core 1 is zero because the E-core is de-energised. (0)
- The electromagnetic force of E-core 2, which increases rapidly as the armature, attracts toward E-core 2 is negative. (-ve).
- The force from the compression of the spring network is positive. (+ve).
- The force attributed to the weight of the drive system, i.e. the armature diaphragm and the connecting pieces is negative. (Always –ve)

The summation of these forces is the resultant force available to draw the submerged head.

It should be noted that the above convention only provides for a single action upward pumping cycle.

4.5.2 Spring Scenarios

Definitions: Free springs have zero force therefore zero effect at some stage during the half-cycle, attached springs have zero force at one end of the half-cycle, and fixed springs are pre-stressed acting either under compression or under tension exerting a force throughout the half-cycle.

The key to the tables 4.2 – 4.3 is as follows,

mg = Weight of armature

Fm = Force due to Electromagnet

Fm1 = Force due to Electromagnet 1 - Top

Fm2 = Force due to Electromagnet 2 - Bottom

Fsh = Force due to submerged head

Fdh = Force due to delivery head

Fs = Force due to spring

Fr = Resultant force

4.5.3 Single E-core

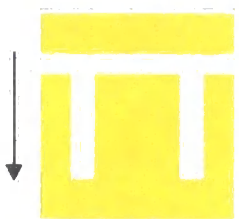

Ordinarily, this system will not work because once the armature has been attracted to the E-core because there is no force available to return the armature to its original position. However, when attached springs or fixed springs are added to the system an additional force (the resultant force (Fr) from table 4.2) is available for the return stroke, half-cycle. The resultant upward force (Fr) is dependent entirely on the stiffness of the springs when the electromagnet is de-energised. The case of the use of free springs becomes obsolete, as it is the equivalent of using attached springs with a shorter stroke length.

Single E-core							
Stoke	Spring Type	Direction of Force					
		mg	Fm	Fsh	Fdh	Fs	Fr
Down	0	↓	↓	↓	0	0	↓
Up		↓	0	0	↓	0	X
Down	Free	↓	↓	↓	0	↑	↕
Up		↓	0	0	↓	↑	↕
Down	Attached	↓	↓	↓	0	↑	↕
Up		↓	0	0	↓	↑	↕
Down	Fixed	↓	↓	↓	0	↑	↕
Up		↓	0	0	↓	↑	↕

Table: 4.2 - Forces of a Single E-core with the use of Springs

4.5.4 Inverted Single E-core

This system will work with or without springs, because once the armature has been attracted to the E-core there is a force available to return the armature to its original position. The direction of the relevant forces of four scenarios, are shown in table 4.3, in each case of the inverted single E-core, having a positive upward force generated by the electromagnet. In the cases of free, attached, and fixed springs, the forces generated vary and can be either positive or negative, depending on the stiffness of the springs. Consequently, the resultant forces act in a similar manner.

Single E-core (Inverted)							
Stoke	Spring Type	Direction of Force					
		mg	Fm	Fsh	Fdh	Fs	Fr
Down	0	↓	0	↓	0	0	↓
Up		↓	↑	0	↓	0	↕
Down	Free	↓	0	↓	0	↑	↕
Up		↓	↑	0	↓	↑	↕
Down	Attached	↓	↓	↓	0	↑	↕
Up		↓	0	0	↓	↑	↕
Down	Fixed	↓	0	↓	0	↑	↕
Up		↓	↑	0	↓	↑	↕

Table: 4.3 - Forces of an Inverted Single E-core with the use of Springs

4.5.5 Double E-core

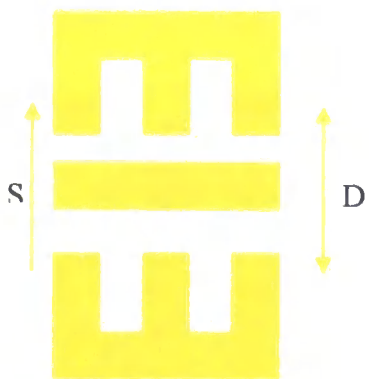

S = single stroke action

D = dual stroke action

The four spring scenarios are as with the single E-core systems, but consideration is now given to both a single stroke action and a dual stroke action. In conjunction with this is how each type of stroke is achieved. The single downward stroke can be due to various combinations of positive forces, gravity, the attraction force of the bottom E-core, the repulsion force of the top E-core. The two E-cores can be energised either individually as in the cases of purely attractive forces or purely repulsive forces, or together, as in the case of attraction to one E-core and repulsion forces from the other E-core being generated simultaneously. The same applies to the single upward stroke and can be due to various combinations of positive forces. However in this case, the attraction and repulsion of the two cores are reversed, and the force due gravity is negative. The

forces are represented in table 4.4. The positive pumping stroke could also be inverted.

In the case of the dual pumping stroke action (pumping in both directions), the downward stroke becomes a positive displacement consequently the convention previously set out in this chapter changes. Not only do the downward strokes become a positive action, the springs acting under these conditions can be either positive or negative. The forces are represented in table 4.4.

Double E-core - Single Pumping Stroke and Double E-core - Dual Pumping Stroke								
Stoke	Spring Type	Direction of Force						
		mg	Fm1	Fm2	Fsh	Fdh	Fs	Fr
Down	0	↓	↕	↕	↓	↓	↕	↕
Up		↓	↕	↕	↓	↓	↕	↕
Down	Free	↓	↕	↕	↓	↓	↕	↕
Up		↓	↕	↕	↓	↓	↕	↕
Down	Attached	↓	↕	↕	↓	↓	↕	↕
Up		↓	↕	↕	↓	↓	↕	↕
Down	Fixed	↓	↕	↕	↓	↓	↕	↕
Up		↓	↕	↕	↓	↓	↕	↕

Table: 4.4 - Forces of a Double E-core Single Stroke with the use of Springs

4.5.6 The Results of the Effect of the Use of Springs Model

The following scenarios do not take into account the effects of saturation or submerged head. However, the graphs show the summation of the generated electromagnetic force and the spring force, which enables a prediction of the effect of the use of springs on the total force. Different scenarios were considered, 14 in total, some of which are now shown and discussed.

Scenario 2 involved a single E-core with the legs pointing upwards; the spring is fixed (pre-stressed). The resultant upward (Ftu) and downward (Ftd) forces are shown in figures 4.41 and 4.42, respectively.

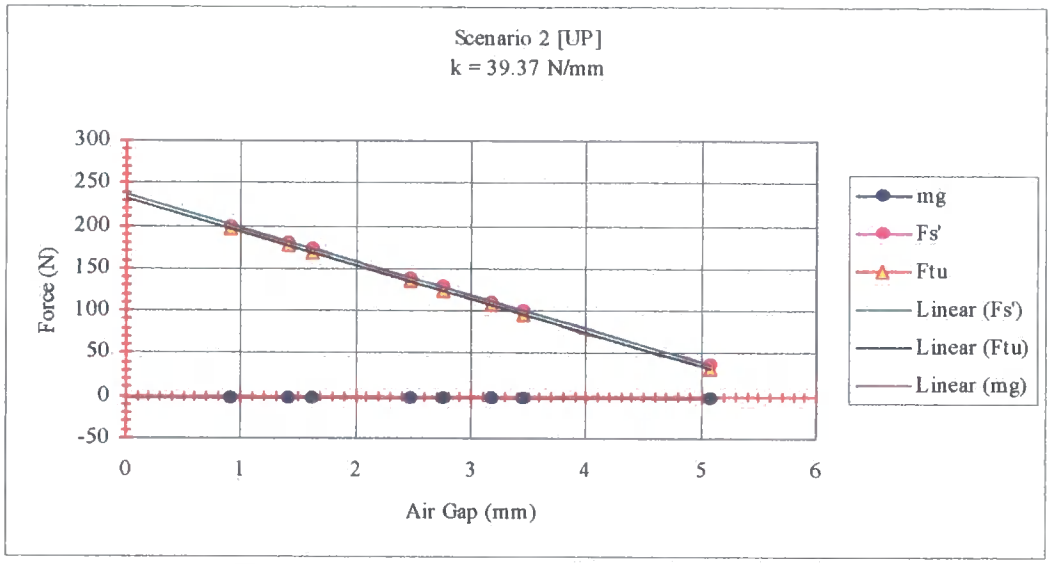

Figure 4.41 – The resultant upward force of scenario 2

Scenario 2 [UP] – k = 39.37N/mm

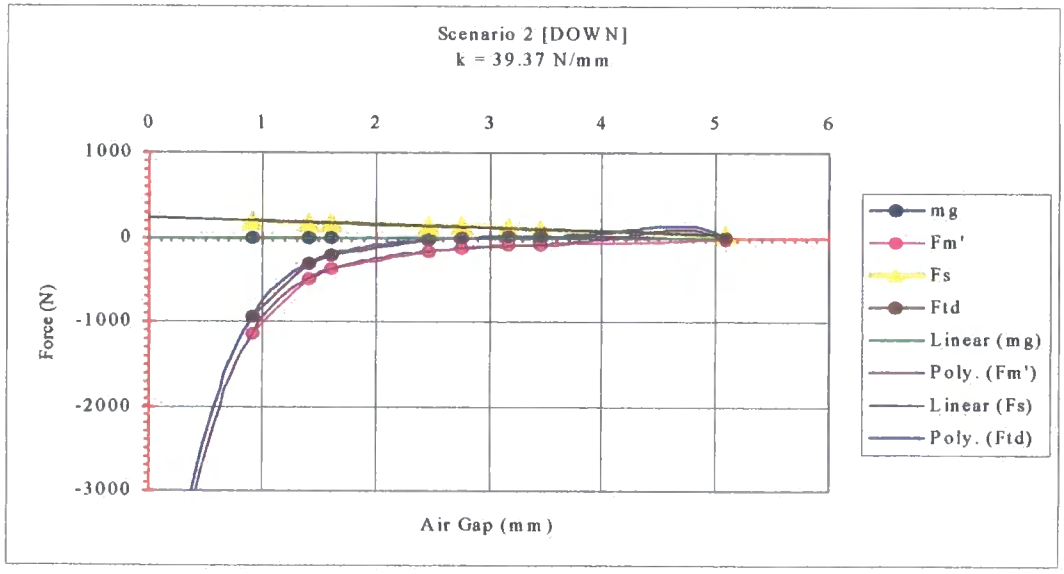

Figure 4.42 – The resultant downward force of scenario 2

Scenario 2 [DOWN] – k = 39.37N/mm

Figure 4.41 shows that the maximum force available on the upward stroke (Ftu) is approximately 230N, which occurs at the point of contact between the armature and the E-core. The graph also shows that the upward force is entirely due to the force

generated by the spring. Since, the upward stroke for this scenario is the delivery stroke, which is pumping against the delivery head, the resultant force is too small, and the pump would not be able to overcome the worst-case static force.

Figure 4.42 shows that the maximum force available on the downward stroke (Ftd) is far greater by comparison, especially at small airgaps. However, the resultant downward force (Ftd) is zero at an airgap of approximately 2.5mm; therefore at that point the pump would stall.

The best that can be achieved under these operating conditions is to make the downward stroke the positive action, that is, pumping against the delivery head, and shorten the stroke length to 1mm, thereby increasing the available pumping force to approximately 900N. The springs would then be used for the return stroke and 200N would be available to pump against the submerged head.

Scenarios 8 and 8c – Both scenarios involved a double E-core system as shown in §4.5.5, with the upper and lower E-core labelled as Fm1 and Fm2, respectively. Both scenarios use attached springs where the springs are entirely relaxed when the armature is in contact with the upper E-core (Fm2), the difference between the two scenarios is that, scenario 8 compresses the springs, and in scenario 8c the springs act under tension. The resultant upward (Ftu) and downward (Ftd) forces are shown in figures 4.43 and 4.44, respectively.

Figure 4.43 shows the change in the resultant force as the armature moves from the lower E-core (Fm1) towards the upper E-core (Fm2). The resultant upward force (Ftu) is shown to have increased when the airgap is at its maximum, and the resultant force is still comparatively low compared to that of the electromagnetic force at small airgaps. In general, there is an overall improvement in the system performance for the upward stroke.

However, figure 4.44 shows that resultant force (Ftd) is reduced as the armature moves in the opposite direction. At airgaps greater than 1.8mm, the resultant

downward force is zero. Consequently, the pump would stall; therefore, this system is only suitable for short stroke lengths of less than 1mm.

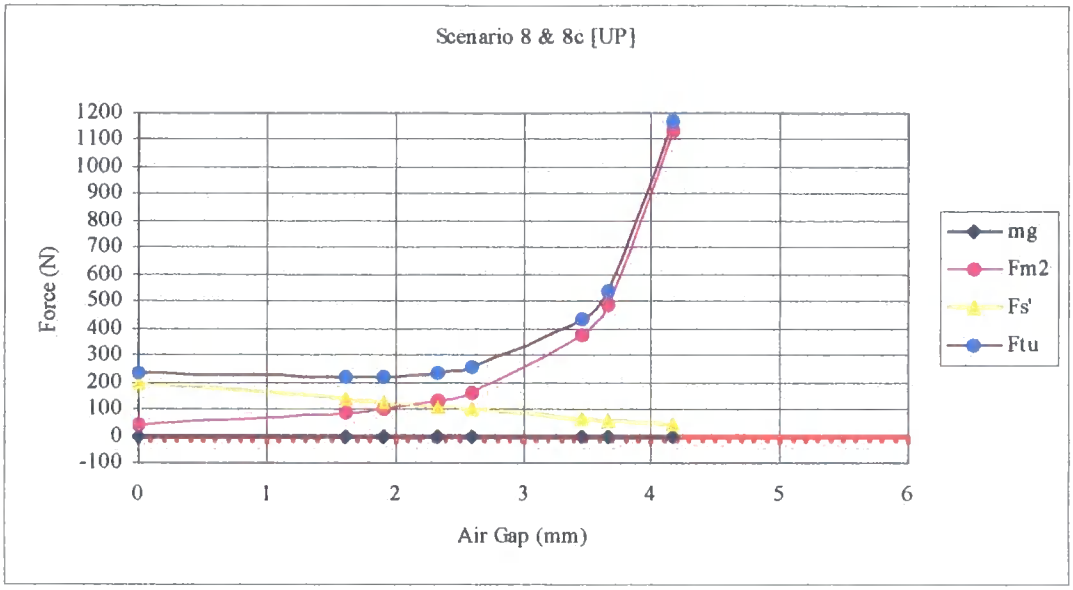

Figure 4.43 - The resultant upward force of scenarios 8 and 8c

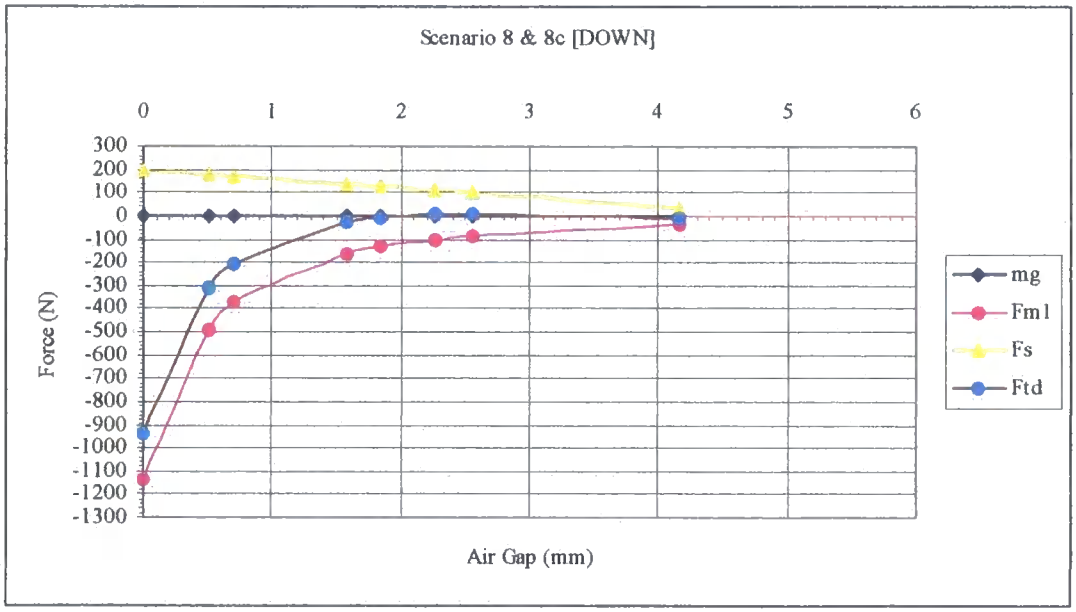

Figure 4.44 - The resultant downward force of scenario 8 and 8c

The best that can be achieved under these operating conditions is to shorten the stroke length to 1mm, using the upward stroke as the positive action against the delivery head. However, the available force on the return stroke to pump against the submerged head is reduced because of the springs. The maximum available

force is taken as the lowest force at the point of maximum displacement of the armature from the E-core.

Scenario 9 involved a double E-core system as shown in §4.5.5, with the upper and lower E-core labelled as Fm1 and Fm2, respectively.

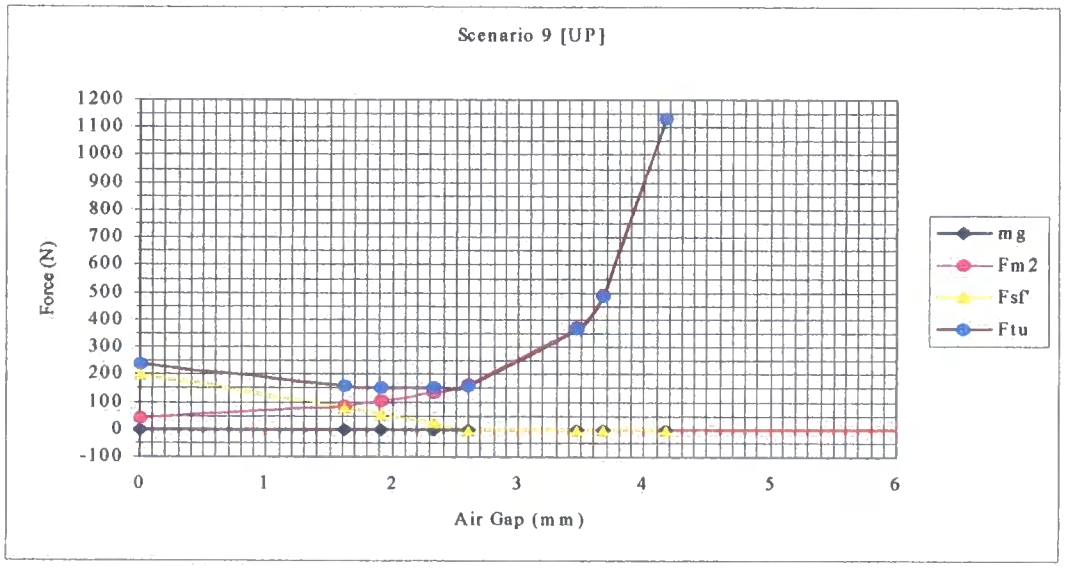

Figure 4.45 - The resultant upward force of scenario 9

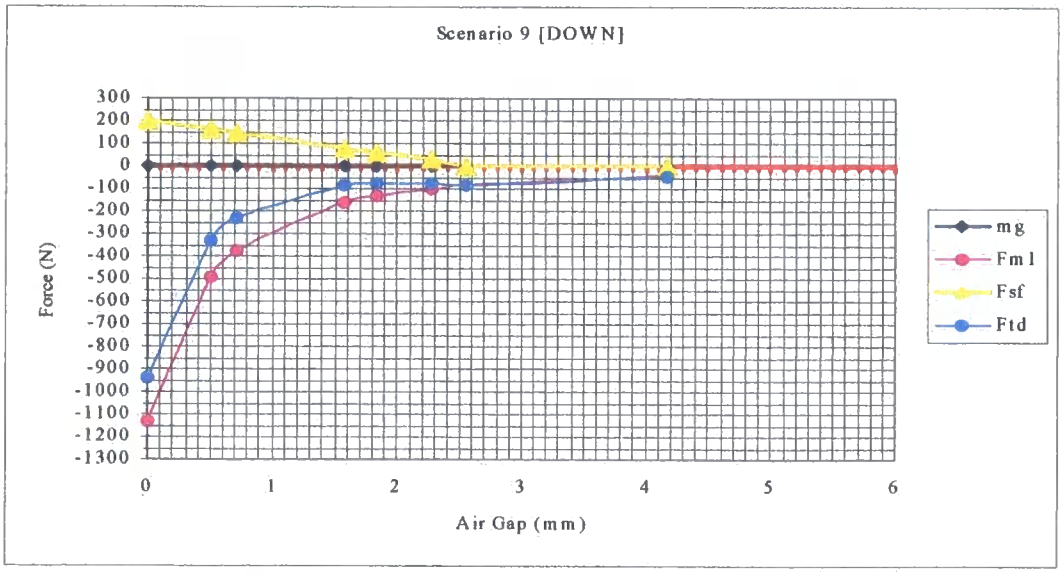

Figure 4.46 - The resultant downward force of scenario 9

Scenario 9 used a free spring where the spring is entirely relaxed at a preset distance between the two E-cores, in this case 2.6mm. As the armature moves away from the upper E-core (Fm2) it is free space and engages the spring at 2.6mm

from the lower E-core (Fm1), at which point the spring begins to compress. The resultant upward (Ftu) and downward (Ftd) forces are shown in figures 4.45 and 4.46, respectively.

The results for scenario 9 are similar to those of scenarios 8 and 8c, but with two important differences. Figure 4.45 shows a small decrease in the resultant force at the point where the armature encounters the spring. Figure 4.46 shows that the introduction of the spring force enables the resultant force, although small in comparison to the electromagnetic force Fm1, to be maintained over the entire stroke length.

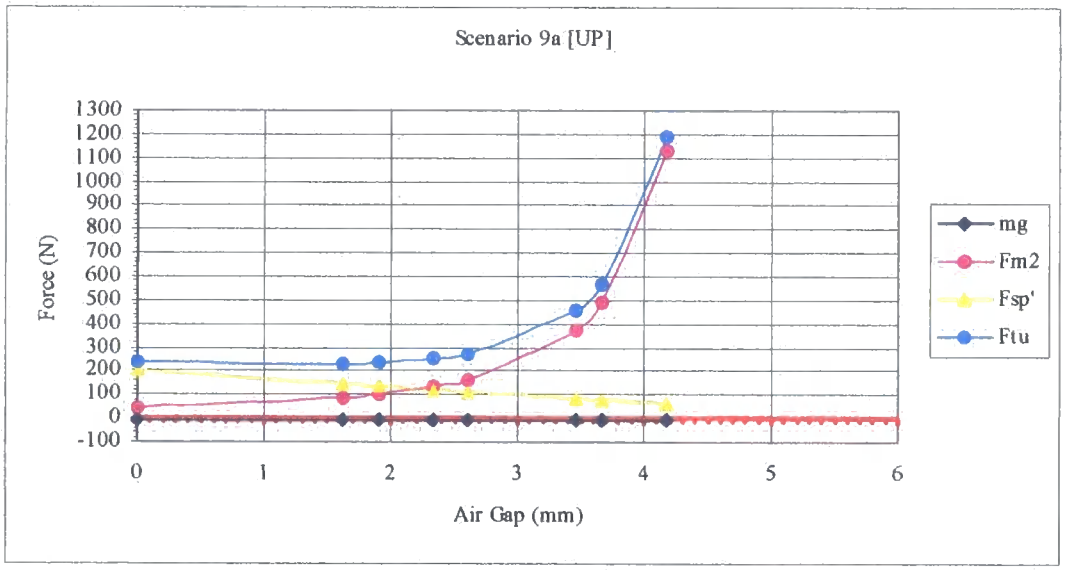

Figure 4.47 - The resultant upward force of scenario 9a

Scenario 9a used a pre-stressed spring where the spring is partially compressed prior to the activation of the E-core. The resultant upward (Ftu) and downward (Ftd) forces are shown in figures 4.47 and 4.48, respectively. As the armature moves away from the upper E-core (Fm2) towards the lower E-core (Fm1), the electromagnetic force must also overcome the pre-stress of the spring and continue to compress the spring until the end of the stroke. From figure 4.47 it can seen that the pre-stressed spring improves the resultant upward force (Ftu) and maintains the force at a constant level over a larger airgap range. However, figure 4.48 again shows a zero force occurring at a small airgap.

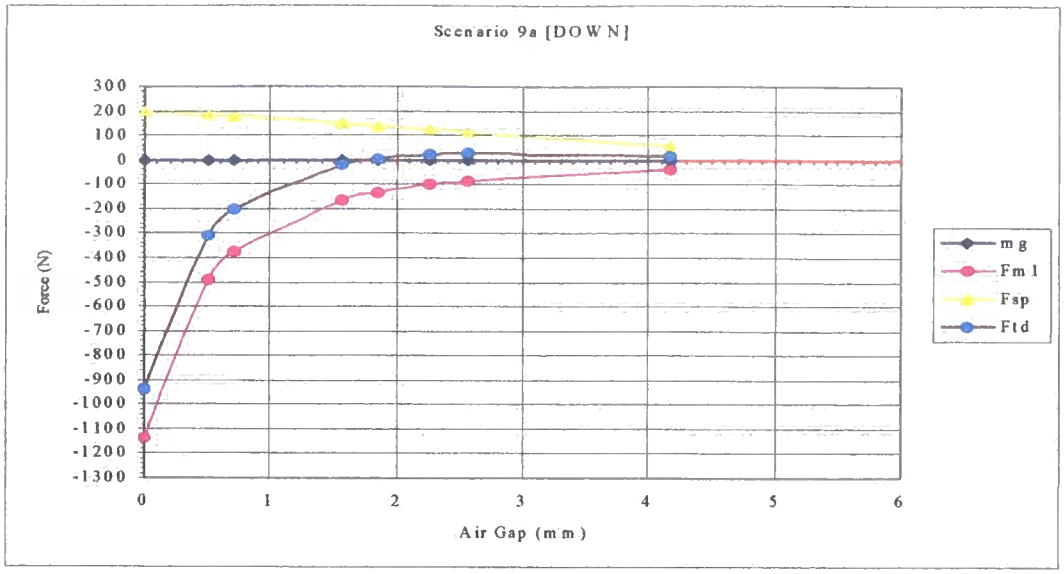

Figure 4.48 - The resultant downward force of scenario 9a

4.6 Design and Manufacture

The design and manufacture of the prototype pump involved the modelling and testing of the linear motion concepts, the design and building of test rigs and the testing of materials and components with unknown properties because they had been cannibalised from old equipment, or obtained from obsolete stores. Further, the testing involved the calibration of sensors and recalibration after the sensor had been impacted. Once a design concept was agreed, the pump was developed with the aid of conventional engineering drawings, the use of a 3D drawing package ('SolidWorks'), and dialogue with the technicians.

Having tested both single and double E-core systems in force test rigs it was decided to use the double E-core system, as it was capable of pumping regardless of the force exerted on the actuator within the pumping chamber by the submerged head. However, when testing the pump in the laboratory the submerged head was kept to a minimum, 0.1m – 0.2m. Although the double E-core system was chosen the pump only pumps in one direction that is on the upward stroke. Incorporated into the design is the provision for two different types of switching control systems, i.e. electrical/electronic control, and mechanical switching control.

This section now shows and describes the workings of the completed pumps.

4.7 The Diaphragm Version of the Linear Actuator Water Pump

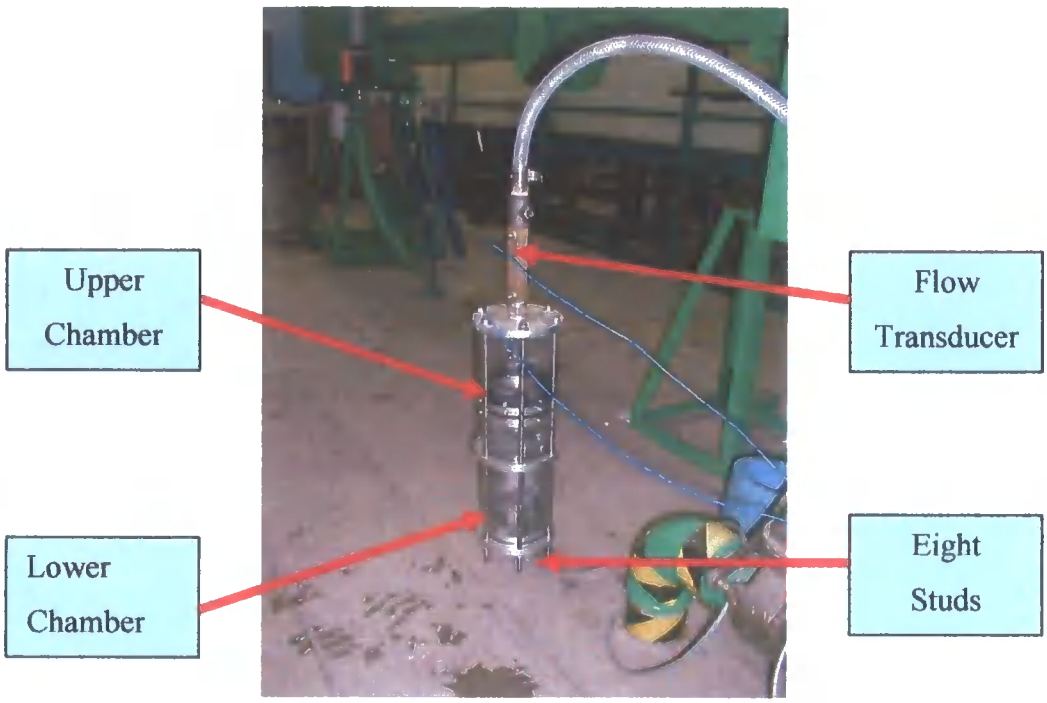

Figure 4.49 - Prototype Linear Actuator Water Pump

The prototype linear actuator water pump comprises of two chambers, encased in a transparent plastic tube/casing; the two chambers are separated by the chamber separation plate, with the lower chamber capped with the base plate and the upper chamber capped with the top plate.

The lower impermeable chamber contains the electromagnets, and the carbon brushes if electro-mechanical control is used, or the connections to the driver circuit for external electronic control. The electromagnets are located in the lower chamber because their weight acts as an anchor to retain the pump in a vertical position.

The upper chamber contains the diaphragm pumping mechanism and both the inlet and the outlet valves. The inlet valve is located in the upper chamber, as would be

the case in a well or borehole installation, to avoid sucking up mud from the bottom of the well. Having the inlet valve near to the outlet valve also reduces internal losses of the pump. Connected to the upper chamber is a flow measuring transducer which in turn is connected the head control. The system is shown in figure 4.49.

Note: that the chambers are of clear plastic to enable visual inspection of the pump operation during testing. This removes conjecture and aids analysis of any problems. Since the properties of the material used for the chambers were unknown, for safety reasons, the tube was pressure tested up to 18 Bar prior to use.

4.7.1 The Lower Chamber of the Linear Actuator Water Pump

The lower chamber (Figure 4.50) contains the lower half of the actuator (i.e. the drive mechanism), including the electromagnets and the armature, along with the airgap adjustment studs and riser plate, and in this case, the supply wires direct to the electronic control system. However, in the case of carbon brushes being adopted it would also contain, the carbon brushes, the contact slider strips of copper, the energy dispersing resistors and diodes. (Re: §4.10.3 and figure 5.1 §5.3.1 for description of energy dispersing resistors)

Figure.4.50 - The Lower Chamber of the Linear Actuator Water Pump

Located at the base of the pump is a four core electrical cable, the four cores providing two wires for each coil of the two electromagnets. The opposite ends are connected to the external electronic control system. The control system comprised of a Twin 2 Transistor Forward Converter, (the circuit diagram is shown in figure 5.11), with the input signal being provided via a square-wave generator. The current/voltage supply was via a constant current source, providing a constant 6A.

The springs, shown in figure 4.50, are situated underneath the armature shown in figure 4.51, and act as an assembly aid. However, the use of the springs that have a low stiffness, also acts as a preset positioning device for the armature at start-up of the pump. The springs dictate the direction of the first stroke, downward; therefore, the first stroke draws water into the chamber. The preset positioning of the armature also facilitates the setting of the airgap size, as described in §4.7.4.

4.7.2 The Actuator - The Pump Drive Mechanism

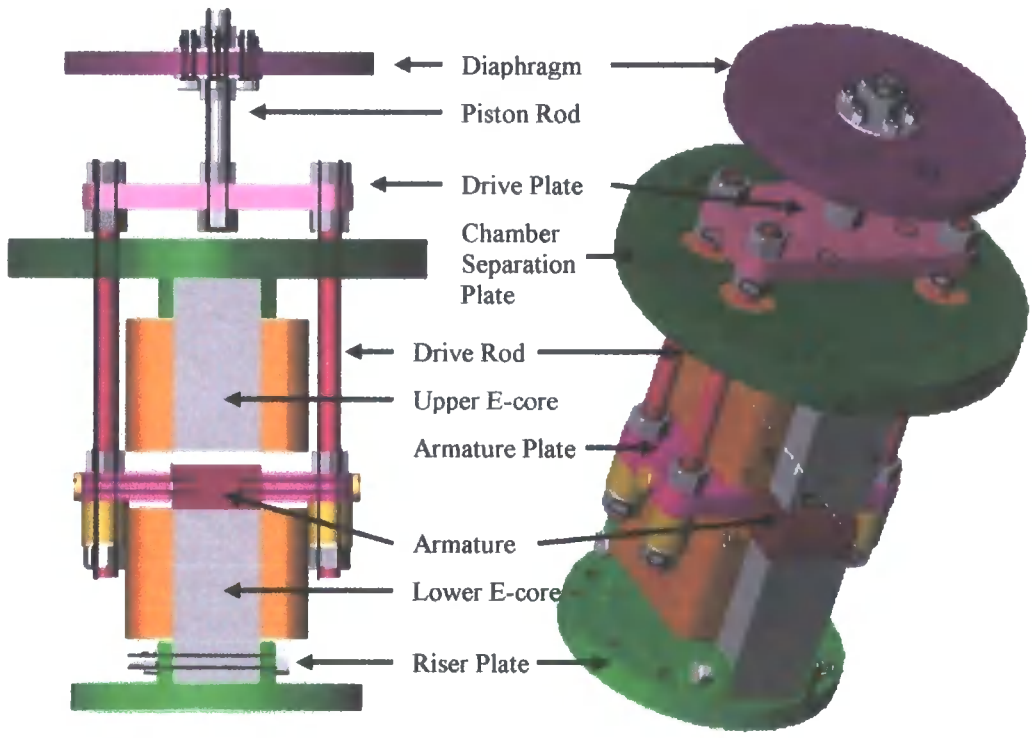

Figure 4.51 – Actuator System

The system controlled either electrically or mechanically, incorporates two E-cores, an armature, two armature plates, four drive rods, a drive plate, a piston rod, and a diaphragm, as shown in figure 4.51. Attached to the sides of the mild steel armature, which is located between the two E-cores, are two aluminium plates, the plates support four drive rods, two on each side. The drive rods pass through the four brass bushes which are located in the central chamber separation disc to the

drive plate. From the centre of the drive plate a single piston rod connects to the diaphragm.

The principle by which the system operates is that the E-cores are energised in turn; when an E-core is energised, the armature is attracted to the energised E-core. When that particular E-core is de-energised, the other E-core is simultaneously energised reversing the direction of the armature motion due to the attraction of the second E-core. The two aluminium plates enable the transfer of the energy from the movement of the armature situated between the two electromagnets to the diaphragm. The diaphragm, which is attached to the armature via the components mentioned above moves in the same direction thus providing a pumping action. Since the armature and the diaphragm are rigidly attached, the airgap between the armature and the E-core determines the stroke length.

4.7.3 The Armature

Incorporated into the design is the provision for Mechanical Switching Control by means of Carbon Brushes. The lower chamber (figure 4.50) contains the electromagnets part of the lower half of the actuator, (the drive mechanism), which includes the armature. The armature design is shown in figure 4.52.

In the case of carbon brushes being adopted, each armature plate is held in place by a bolt and a grub screw. A plastic bush is used to electrically isolate the spring-loaded carbon brush and the copper contacts of the switch from the armature. The carbon brush is spring loaded so ensuring that a constant pressure is applied to the copper strips of the switches.

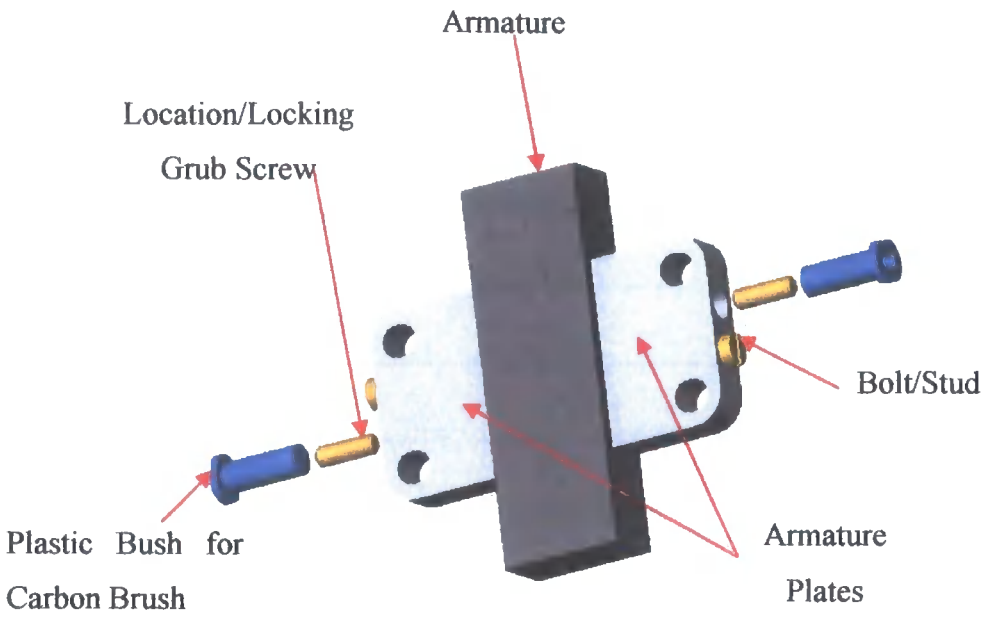

Figure.4.52 – Adaptation to Armature for Carbon Bushes

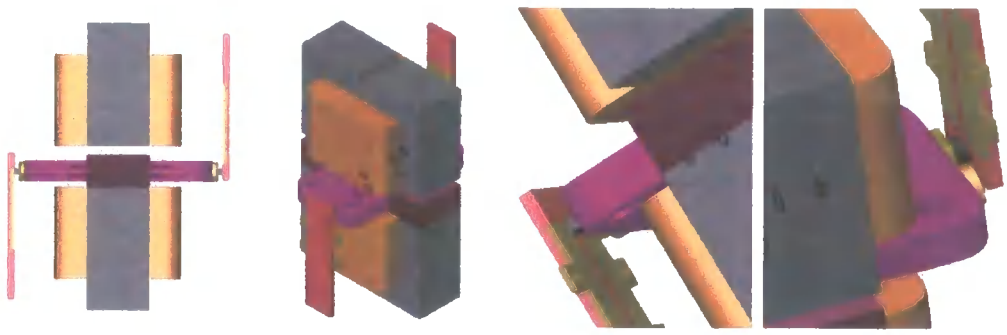

Figure 4.53 – Part of the Carbon Brush Set-up

The system can be adjusted for different armature airgap settings as the upper pair of copper contacts on either side of the armature is fixed, whilst the lower pair is attached to the riser plate of the pump. Behind the rounded copper contacts is a hard insulating board to ensure a smooth transition for the carbon brushes between the opposite pairs of contacts. In order to convert to an electronic control system, the carbon brushes and copper strips were simply removed, and the grub screws were replaced with bolts. The two wires of each coil of the two electromagnets were fed direct to the external electronic control circuit board.

When the carbon brush system is used, the armature hence the armature plates dictate the position for the switches, figure 4.51.

4.7.4 The Airgap Adjustment and Control of the Linear Actuator Water Pump

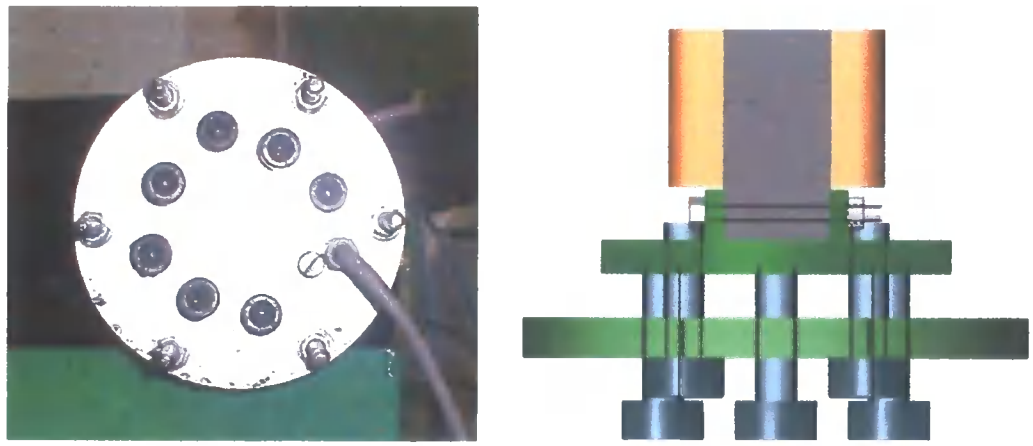

Figure.4.54 The Airgap Control of the Linear Actuator Water Pump

Figure.4.54 shows the under-side of the pump. The six outer studs, which travel the full length of the pump, act as both a stand and a clearance for the adjuster studs and the electric cable. Figure.4.54 also shows the inlet for the electric cable, along with the eight-adjuster studs. The adjuster studs are in two sets of four; starting at the 'headless' stud next to the cable inlet alternating clockwise form the locking mechanism, hereafter called 'lock', the others form the adjusting mechanism, hereafter referred to as 'adjuster'. The lock, for the system moves the riser plate in an upward direction, closing the airgap. The adjuster pulls the riser plate downward which enables the airgap to be adjusted to a required setting. The two acting together locate and lock the riser plate in position.

The studs need to be robust, and be able to withstand the forces generated by the electromagnets, to ensure the riser plate remains rigid. The fact that the riser plate can be locked into position ensures that the airgap is equal along the total length of the armature, ensuring a balanced magnetic flux path. They also give control to the size of airgap, since the studs are M12 x 1.75, one complete revolution of the studs

gives a change in airgap of 1.75mm, and so by marking increments around each stud a gauge can be implemented, the accuracy determined by the tolerance of the thread. The gauge is marked around the four adjuster studs.

The technique, by which the airgap is set, is to completely close the airgap so that the armature is in contact with both E-cores. The tightness of the stubs can vary; however, by using a ratchet-tightening device some equality control is established. For symmetry of movement, the system is locked in this position. Then the locks are slackened, permitting the adjusters to set the required airgap, and then the locks are once again locked, figure 4.55.

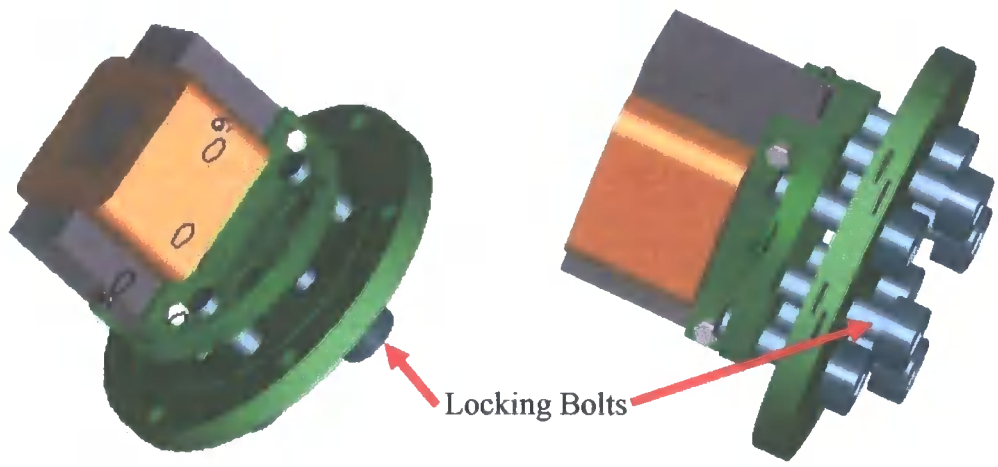

Figure 4.55- E-core airgap control – locking bolts

4.7.5 The Upper Chamber of the Linear Actuator Water Pump

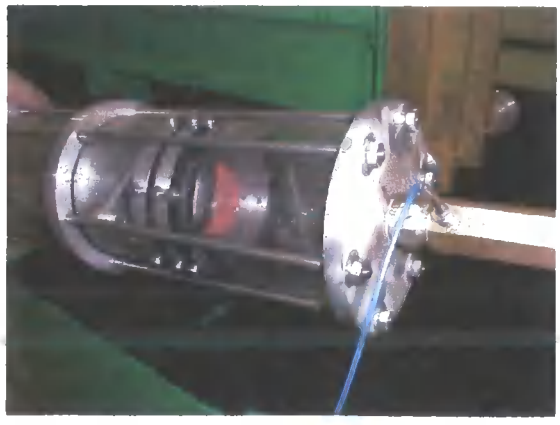

Figure 4.56 - The Upper Chamber of the Linear Actuator Water Pump

The Upper Chamber, shown in figure 4.56, incorporates the upper section of the drive mechanism, the diaphragm (actuator), and the diaphragm seal located between the two locking rings. In order to establish a seal the diaphragm is

made oversize, so when the locking rings compress the rim it pushes toward the inside of the chamber. The diaphragm is bevelled at the centre due to being oversized. The bevel deforms twice each complete stroke/cycle; as the transition occurs, it exerts an outward force and so enhances the seal.

The Upper Chamber also houses both the inlet and outlet valves. The inlet valve comprises of six slits equally dimensioned and spaced. The rubber inlet valve covers the inlet slots internally and an aluminium ring holds it in position. The outlet valve is a simple standard non-return valve, requiring 10mBar (negligible effect on the system) to open it.

The principle of operation starting with the diaphragm in its upper position and bevelled upward is as follows: the starting position is predetermined with the use of the springs in the lower chamber. A partial vacuum is created as the actuator begins to move downward, the pressure within the chamber being slightly lower than that of the external pressure; this causes the inlet valves to open. (The outlet non-return valve is closed.) Water then floods the chamber, due to the submerged head. The pressure within the chamber is then at equilibrium with the submerged head. Then on the return stroke the inlet valve closes due to the rising water, simultaneously the non-return outlet valve opens, likewise due to the rising water, so driving the water from the chamber.

4.7.6 Flow Transducer

Figure 4.57 -Signal Conditioner - The pump outlet pressure transducer control

Two-matched pressure transducers are placed at the exit from the outlet valve of the pump chamber; these are located in the brass hexagonal tube, from which the two blue wires extrude. The blue wires are connected to a PCB Constant-Current Power/Signal Conditioner (which ensures correct power to the sensor), figure 4.57, which gives an electrical

output signal corresponding to the pressure. This is input to a connection card, which in turn is connected to an A/D card, internal to a computer, for signal processing. This data gives an instantaneous flow reading. The other end of the transducer tubing is connected directly to the outlet pipe. However, due to problems with the software no satisfactory results were obtained.

4.7.7 Head Control

Figure 4.58 - Head Control

The outlet section of the pump comprises of a 25m length of hosing-pipe, attached to a pressure gauge, an output pressure transducer, and a hand operated valve. The purpose of the 25m length of hosing-pipe is to act as a damper to the output valve flow. The inlet end of the housing-pipe is connected to the output pressure transducer, which is connected to the ADC card of the computer and a gate-valve to simulate the delivery head. The pressure gauge is attached to the other end of the hosing-pipe enabling immediate visual recognition that the system is under pressure (and for safety reasons), shown in figure 4.58. The output pressure transducer measures the dampened flow, sending a 0-5V signal to the ADC of the computer for processing. The output transducer is located between the pressure gauge and the control valve, shown in figure 4.58. The hand operated valve is for control of the output flow rate.

As verification of this data, water can be collected, timed, and weighed. The weight of the water relates directly to the quantity of water in litres, hence the flow can be determined by comparison of the weight and time taken. A further comparison could be made by comparing the output of the output transducer with the output of the two matched pressure transducers readings.

The gate-valve when fully open permits continuous flow, hence by closing the valve the flow is restricted thus causing the pressure to increase, simulating a greater delivery head.

4.8 The Piston Version of the Linear Actuator Water Pump

The pump was dismantled, and rebuilt with some improvements and adaptations to the original diaphragm pump. With the aim of seeing whether the actuator could pump against delivery heads in excess of 100m that is, in excess of 10Bar, and after the failures of the diaphragm pumps it was decided to use a piston instead of a diaphragm.

The pump drive mechanism shown in figure 4.51 was changed by removing both the diaphragm and the drive rod, and was replaced with an extended drive rod with a ptfe piston positioned on its end. Figure 4.59 (left), shows the piston protruding the original pump casing. The brass piston chamber with the inlet valve is located in side of the chamber, and the outlet valve is situated in the top of the piston chamber. Both the materials, that is, the brass and ptfe were chosen because of the low coefficient of friction.

Figure 4.59 – Piston and Chamber (left) and Stroke Length Measuring (right)

The mild steel mounting rods/bolts that held the bottom E-core to the base were replaced with larger diameter silver steel rods/studs; this resolved the collapsed airgap problem. In addition, 'loctite' was used to fix both the adjusting and locking

studs, on the base of the pump. This greatly improved the clamping down of the riser plate, which holds and positions the lower E-core. Consequently, the problems of the vibrations caused by the impact of the armature against the E-core were partially removed, and the E-core movement was prevented, so providing a better airgap control. This was verified with the use of a measuring gauge as shown in figure 4.59 (right).

In an attempt to resolve the malfunction of the inlet valves, the rubber of the valve flaps was trimmed, making them less rigid, which resulted in an improved performance.

The water seals for both the upper and lower pump chambers were modified; rectangular cross-section (flat) O-ring seals were used as opposed to cylindrical cross-section O-ring seals. Although, this initially improved the seal for the lower chamber the pump did eventually flood.

It was apparent that the pumping chamber would not be watertight and this would have an effect on the results, however the pump was rebuilt with some adaptations/improvements, as previously mentioned, and some results were obtained.

4.9 Results

This section presents the test results from both the diaphragm pump and the piston pump.

4.9.1 Results Relating to the Diaphragm Pump

Theoretically, for a borehole with a depth of 100m, the minimum start-up force required for the system to operate is approximately 346N, when using a 19mm outlet pipe and a 96mm piston/diaphragm, Eqn 3.1, §3.7. However, the E-core will generate a force 1597N, within an airgap of 0.81mm, before it saturates, §4.2.7.

This gives an available force for pumping against the delivery head of approximately 1251N, which when using a 96mm piston/diaphragm equates to a pressure of 172832Nm^{-2}, the equivalent of 1.73Bar, which in turn equates to an approximate delivery head or depth of 16.96m. Since the minimum start-up force is 364N therefore at any force value lower than this will cause the pump to stall, figure 4.60 shows that this would occur at a stroke length of approximately 1.7mm.

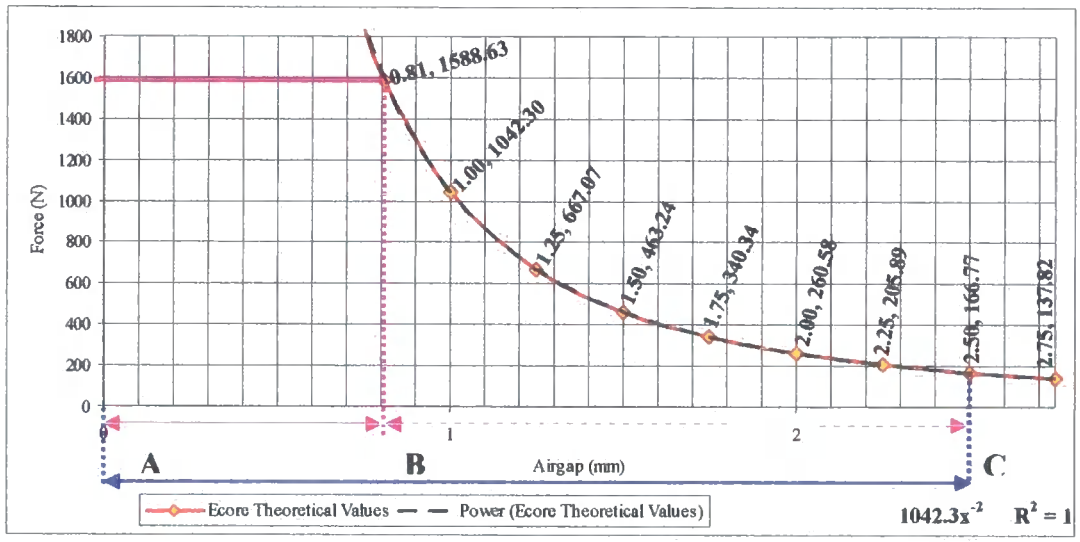

Figure 4.60 – Theoretical Force versus Airgap - (Zoom of figure 4.33)

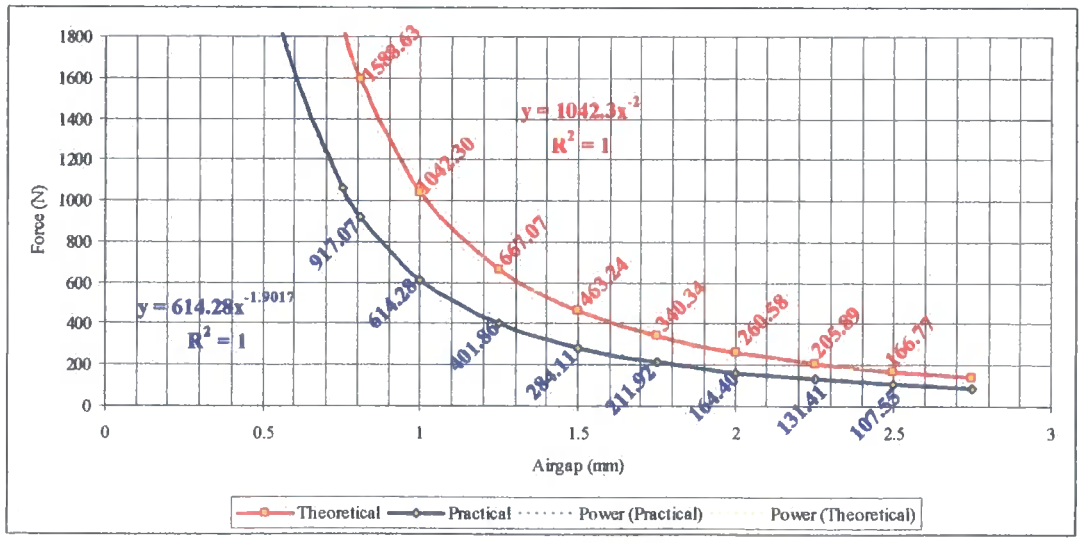

Figure 4.61 – Comparison of Theory and Practical Force versus Airgap

Figure 4.61 gives both the theoretical force values and the practical force values up to an airgap of 2.5mm. Assuming that the flux density of the E-core saturates at

when the airgap is 0.81mm then difference between the theoretical and practical force shown in figure 4.61 can be attributed to flux fringing and heating losses in the coil and E-core. The value of saturation is 1.4T. The figure 4.61 shows a practical force value of 917.07N at 0.81mm, the actual measured value at 0.81mm was 936N; the difference is due to the 2.05% error in the power value of the regression equation, (i.e. a standard value from equation 4.11 $y = 614.28x^{-2} = 936.26N$ and a practical value $y = 614.28x^{-1.9017} = 917.07N$). The difference is a result of taking too few readings for the F-s characteristic.

If the E-core saturates at the theoretical airgap size of 0.81mm, the practical saturation force level will be 917.07N, this is evaluated from the power regression equation of figure 4.61. The force required to act against the submerged head of 0.1m, from equation 3.1, is approximately 7.1N, therefore, the available pumping force is approximately 910N, which equates to a pressure of 125703Nm^{-2}, the equivalent of 1.26Bar, which in turn equates to an approximate maximum delivery head or depth of 12.3m. This is 27.3% less than the maximum theoretical value.

Figure 4.61 shows the maximum force that is available over a stroke length 0.81mm is 917.07N, from A to B in figure 4.60, thereafter the force reduces as the stroke length increases from B to C; the overall stroke length A to C is 2.5mm. The maximum available force at a stroke length of 2.5mm is 107.55N. Therefore when the pump has a stroke length of 2.5mm, the maximum generated force available is 107.55N. Since, a submerged head of 0.1m requires an approximate force of 7.1N; the maximum pumping force available is 100.45N, which equates to 13877Nm^{-2}, the equivalent of 0.14Bar, which in turn equates to an approximate maximum delivery head of 1.36m. The measured delivery head was 1.22m; this is a reduction in delivery head of 10.3%.

Practical results summary for 96mm diameter diaphragm pump;

- Force 100.45N
- Airgap 2.5mm
- Delivery head (h_1) 1.22m

- Submerged head (h_2) 0.1m
- Pipe : Piston ratio 19:96
- Pressure 0.14Bar
- Pumping frequency 7Hz
- Flow rate 0.127ls^{-1}

4.9.2 Results Relating to the Piston Pump

During the tests for the results shown in figures 4.62-4.64 the stroke length for the 19mm diameter piston was 2.625mm. The results were taken over a frequency range of 10-20Hz.

Figure 4.62 shows that at 10Hz the practical flow rate is 2.85 times greater than the theoretical valve and converges toward the theoretical value at 20Hz where the practical value is 1.33 times greater than the theoretical value. This decay in flow rate approximates the fall in input power as the frequency increases, as shown in figure 4.63.

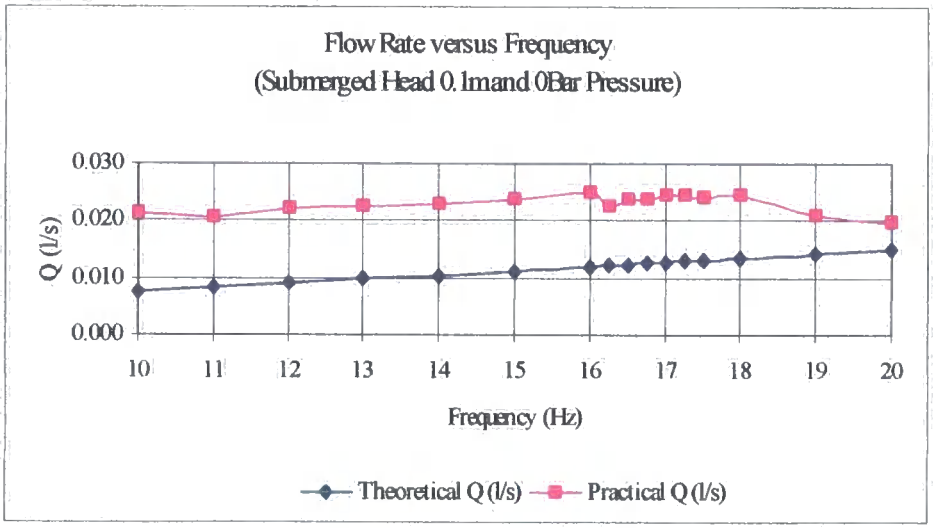

Figure 4.62 – Flow Rate versus Frequency at 0Bar Pressure

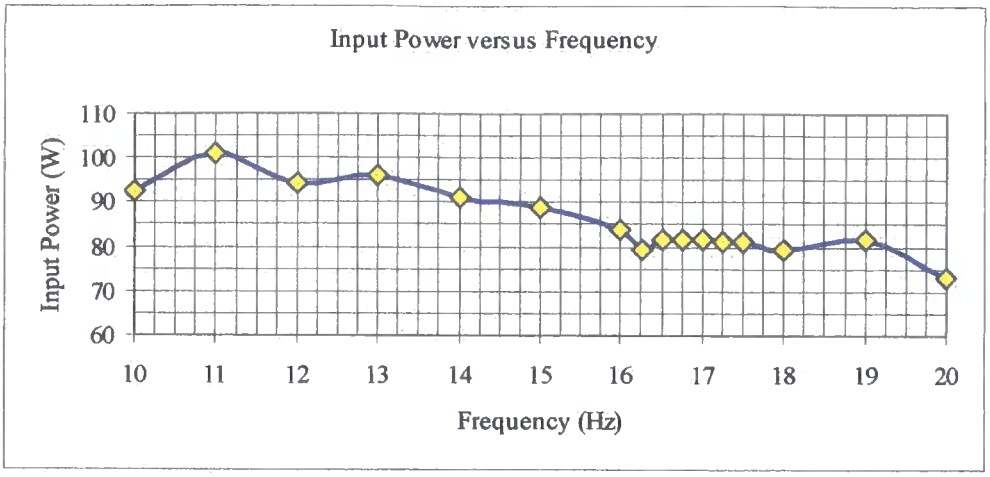

Figure 4.63 – Input Power versus Frequency

During the tests the input voltage was maintained at 24V, therefore the fall in input power was due to a fall in current. The reduction in current and power was evaluated to be approximately 23.75%. Given that the current reduced as the frequency increased, it indicates that the E-core did not have sufficient time to fully energise before switching. Consequently, a reduction in generated electromagnetic force occurred and hence a decrease in the flow rate.

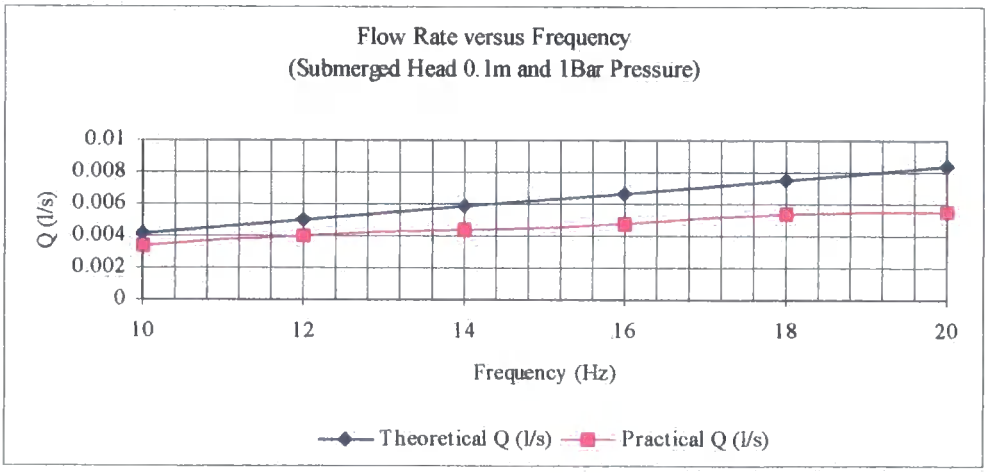

Figure 4.64 – Flow Rate versus Frequency at 1Bar Pressure

Figure 4.64 shows the results for the tests carried out under 1Bar pressure; here both the theoretical and practical flow rates have a linear response. The practical results show, as expected, a reduction in the flow rate compared to the theoretical values. The divergence of the practical results from the theoretical values is a

consequence of the reduction in the supply current. This implies that the current/voltage supply used in the tests was not capable of meeting the demands of the actuator, when operating under a constant voltage condition, therefore future tests must employ a constant current supply.

During the tests for the results shown in figure 4.65, the stroke length for the 19mm diameter piston was 1.47mm. The results were taken over a frequency range of 3Hz-7Hz.

Again, at a submerged head pressure of 0Bar (figure 4.65) the practical flow rate is greater than the theoretical value, albeit over a lower frequency range. It is difficult to justify the variations in flow rate for the Q-f characteristic (0Bar), further tests are required to confirm or disprove the results. However, the spikes can be explained; neither the current nor the voltage were constant, therefore the spikes can be attributed to the fluctuations in the power.

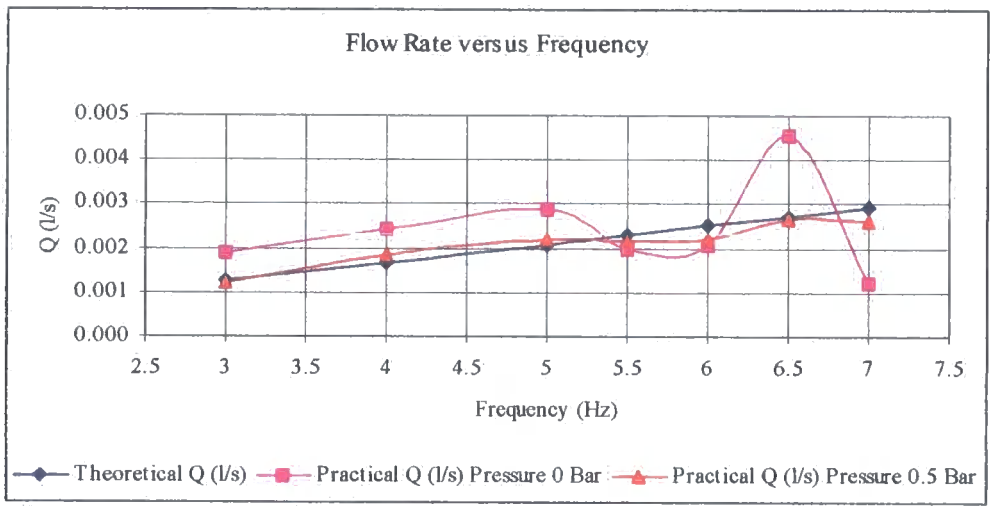

Figure 4.65 – Initial Flow Rate versus Frequency Results

With respect to the results for the Q-f characteristic (0.5Bar) (figure 4.65), a near linear response was achieved. On this occasion, the actuator was supplied with a constant current of 5A, and the power supply increased the voltage to compensate for the increased power demand as the frequency increased. The Q-f characteristic variations, for 0.5Bar pressure, are within +/-12.5% of the theoretical values. The

reasons for the variations are that the frequency control switch of the square wave generator can only be set to within 5% of the true value, and any losses were due to the backpressure water leakage between the piston and the sleeve.

Further results obtained during the tests are now presented in figure 4.66 and 4.67. Figure 4.66 shows that the practical flow rate does not achieve the theoretical values, however the flow rate does increase slightly with an increase in frequency, regardless of the pressure, as expected. Ideally, the rise in the practical flow rate should match that of the theoretical values. The increase in flow rate is restricted because the power supply (the largest available) used in the tests can not meet the power demands of the actuator. Figure 4.66 shows the input power changes over the same range of pressure changes shown in figure 4.66. Both figures 4.66 and 4.67 show that the practical flow rate remains approximately the same over the entire pressure, suggesting that other losses need to be considered, such as backpressure losses, flow losses, and cavitation.

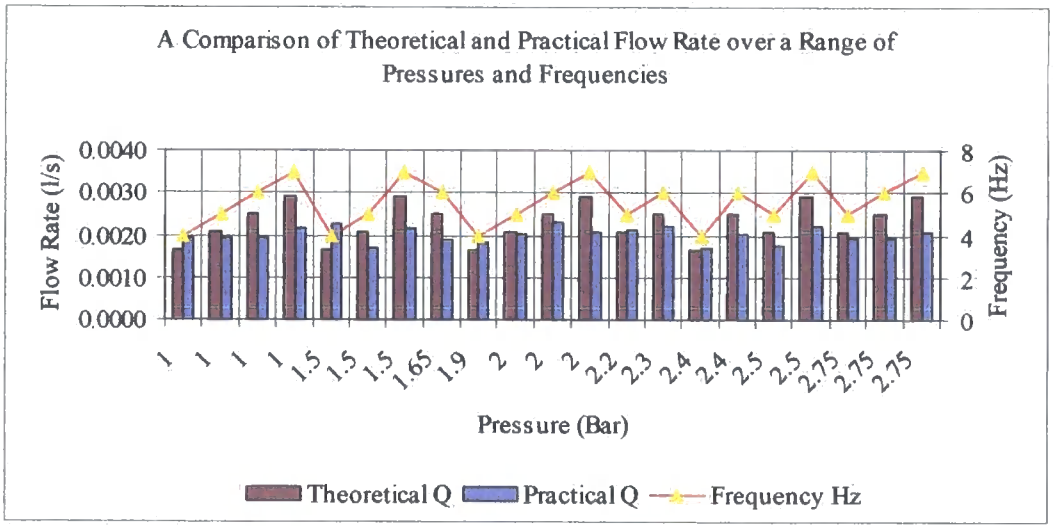

Figure 4.66 – A Comparison of Theoretical and Practical Flow Rate over a Range of Pressures and Frequencies

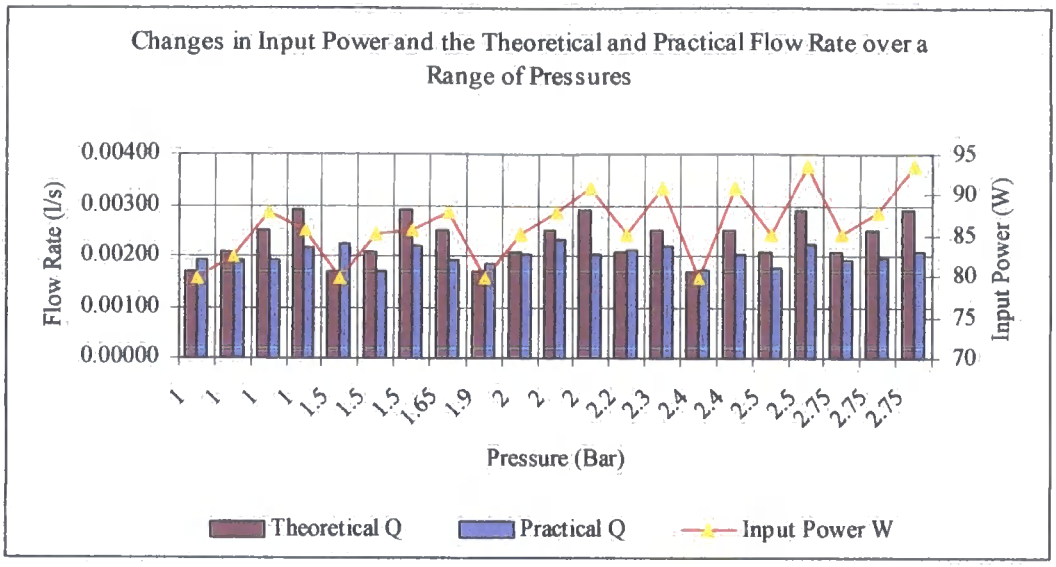

Figure 4.67 – Changes in Input Power and the Theoretical and Practical Flow Rate over a Range of Pressures

The backpressure losses can increase by a factor of 2.5 [34] when the piston is pushed by pressure to one side or the other, thus allowing a large increase in flow, which is inevitable. "The laminar flow rate is proportional to the cube of the clearance" [34]. However, this was reduced with the placing of an O-ring on the piston and inside the sleeve. The above results were only obtained after the addition of the O-ring to the piston.

The tests showed that the flow rate was maintained over a range of pressures up to 3-4Bar. However at higher pressures (10Bar) the flow rate was so diminished that no flow rates were taken. Further tests are therefore required. Cavitation may have occurred if the water flow did not keep up with the movement of the piston; prevention is by the correct choice of size and type of valves, and the control of the piston speed. Any flow losses can be improved by design.

4.10 Discussion

This section first gives a discussion on both the electrical and mechanical aspects of the actuator system; it then discusses the springs' investigation. The section then evaluates the performance, problems and the potential for the actuator.

4.10.1 System Discussion

The initial current flow results in a back-e.m.f of self-inductance. This is greatest when the rate of change of current is greatest, that is at switch on. When the coil is de-energised, at switch off, the collapsing flux induces an e.m.f such as to prolong the current and decays to zero exponentially.

At small airgaps, the time taken by the coil to reach the required level of current to produce the necessary force may not be of long enough duration. Consequently, the rate of change of current plays an important part in the design, for if the current rise-time is too slow then the electromagnetic force generated will be smaller. That is, the rate of change of current must be as fast as possible, the longer the time constant the slower the current rise.

The coil is an inductor; therefore the induced e.m.f opposes the original current. This is of great importance when pulsating dc voltages are applied, the inductor offering a strong opposition to the current changes. The behaviour of an inductor may be linked to a mechanical flywheel the function of both being to oppose energy fluctuations. Since the coil is wound around a ferromagnetic yoke the high permeability of the core increases the flux, hence the inductance.

Inductance relates the magnetic flux to the current flowing in the circuit. The inductance is at a minimum when there is a large airgap and increases as the airgap is reduced.

At switch on the voltage drives the current around the circuit. The current through the inductor builds up a magnetic field and the current rises exponentially. However, in dc circuits containing an inductor, there is a delay in current build-up that depends on the time constant of the circuit.

This electromagnet topology, based on the electromagnet's variable reluctance principle, presents another problem, because the high attraction forces require high currents and the coils are inductive loads. Therefore they involve a time constant

$$\tau = \frac{L}{R}.$$

Since the resistance changes very little as it is controlled via a thermistor, the governing factor of the time constant is the inductance; if the inductance decreases, the effect of the time constant is to produce a higher operating frequency.

Energy Loss - The factors that give rise to an energy loss are both mechanical and electrical. The mechanical factors to be considered are frictional losses, the diaphragm, inertia, potential energy, kinetic energy and the impact of the armature against the E-core. The electrical factors are the current density (J), the copper losses i.e. I^2R losses in windings of the coil, and eddy currents.

Electrical Factors - The effect of the current density is to limit the current that can be supplied to the coil without heating the coil. The maximum J is approximately $4.5Amm^{-2}$. Should the current density increase to a level above this then cooling is required to maintain the ambient temperature of the coil. For a system to use larger current densities then a larger gauge wire is required. This in turn changes the geometry of the coil/E-core giving less turns for the same space. There is a fine balance for NI ratio restricted by the available standard gauge wires. Reducing the number of turns by using larger standard gauge wire and increasing the current will not produce the same force. (NI = m.m.f)

The power loss due to the flow of current in the windings, i.e. the copper losses, is probably one of the two main factors for the heating effect of the system. When an electrical device is loaded, the temperature rise of the device is largely due to the I^2R loss in the conductors; and the greater the load, the greater the loss, and therefore the higher the temperature rise. That is the greater the increase in temperature, the greater the increase in resistance.

Eddy currents are another factor that can produce a heating effect. The induced e.m.f of the windings induce an e.m.f in any nearby conducting material, such as the yoke of the E-core, by the flux changes; thus giving circulating currents in an

infinite number of parallel paths. They are a serious disadvantage because they represent an energy loss and generate a superfluous temperature rise. It is not possible to prevent the induction of the eddy currents but they can be greatly reduced by providing a high resistivity path for them. This can be achieved with the use of laminations; the eddy currents and the resistivity paths meet in series, and consequently are greatly reduced. When the pump is operating at low frequencies, i.e. less than 50Hz, the problem of eddy currents is minimal.

Mechanical Factors - Frictional losses are attributed to the force involved to overcome the normal force between two surfaces and vary depending upon the materials that are in contact. These forces are minimal within the system and can be alleviated with use of a lubricant.

The diaphragm geometry, weight, and stiffness, all affect the amount of energy required to overcome force to operate the system.
Force is required simply to overcome the inertia of the drive mechanism, which incorporates the armature. However, this will be very small in comparison to the electromagnetic force produced.

In the case of a collision, when the armature 'impacts' the E-core, the kinetic energy is 'lost', because the steel is non-elastic. This 'lost' energy in fact reappears as heat, sound, and mechanical vibration, none of which is recoverable. The force of the impact causes deformation, and the work done remains as free energy, which is dissipated as above, with a small amount stored elastically. The magnitude of the forces that are allowable and the capability for energy intake are both time and temperature dependent. To avoid structural failure the breaking stress is not to be exceeded and this is best achieved by preventing the armature from impacting on the E-core.

4.10.2 Use of Springs Discussion

For some time now, electromagnetic actuators that incorporate springs have been used for valve control. However, the springs do the work and not the

electromagnets. The armature stays in a static position in either the high or low point, and is held in place by the electromagnet. When the electromagnet is switched off the armature then travels to the other position, and again is held in position by another electromagnet. The valve opening time is obtained by adjusting the interval between the up and down motions. The neutral position of the actuator is in the middle, and the two electromagnets mainly operate by holding the moving part at the ends of the stroke. The landing noise of the armature is a major issue for this type of actuator. To reduce it and to maintain a longer lifetime, a soft-landing must be achieved.

In the tests carried out on the pump springs were used, but were too weak, they had too low a 'k' value to be of any benefit to the pumping action. Nevertheless, they did prove useful, as an assembly device, and for the locating of the armature at start up. Springs with the required stiffness would be far larger geometrically and would not fit within the chamber of the present pump configuration. Therefore, if springs were to be used, the pump will have to be redesigned to incorporate the spring mechanism.

The solar powered water pump system requires a minimum force of 278N to operate (§3.7.3 Static Force). The force resulting from the weight of the armature and connection parts to the drive piston of the actuator, mg was approximately 11N therefore the minimum force before the electromagnets have any useful effect is approximately 289N. Had this force been achievable with the use of springs then an additional 289N would have been available to pump the delivery head.

For all scenarios, the total upward force and the total downward force were analysed separately, then considered together as an operating system. Further, after assessing the resultant force a comparison is required to ascertain whether or not the use of springs cancels the effect of using them. Throughout the assumptions were that there is no submerged head and any excessive submerged head could cancel any benefit gained.

In order to determine the effect of the springs on the system various spring combinations with different stiffness (k) were considered.

Use of Springs Conclusion - With respect to the use of springs in conjunction with single E-core systems, it can be concluded that the resultant force is dependent on the pole orientation of the E-core. (The pole orientation, the direction in which the three legs of the E-core are pointing) When the orientation of the E-core poles is upward, irrespective of the type (compression or tension) of springs used, the resultant total upward force is solely due to the force contribution from the springs. The stiffness of the spring dictates the resultant force. The stiffer the spring the shorter the effective stroke length. The resultant downward force is diminished when springs are introduced. For any preset distance, the linear force from the spring is limited to the tangent to the initial rate of change of force of the electromagnet force curve. The maximum value of spring force occurs at the intercept with the y-axis, which is at the point of contact between the armature and the E-core. However, depending on the control of the armature movement, which in turn determines the turning point for the armature, this force may not be realised.

With respect to the use of springs in conjunction with double E-core systems, it can be concluded that the benefits and restrictions of single E-core systems also apply to a double E-core system. Here the orientations of the E-core poles are opposing one another, therefore the benefits and restrictions apply for both half cycles. Even though the spring force is small in comparison to the electromagnetic force, it is possible under certain conditions to maintain the minimum operating force available over longer stroke lengths. It may be possible, practically, for a finally tuned system to utilise the spring force to compensate for the start up force. Another, possible use is in a free oscillating system where the springs could prevent the impact of the armature against the E-cores, and by doing so provide a smoother output.

Use of Springs Summary - Had the use of springs proven useful then the use of springs would have eliminated start-up losses due to mg and removed or at least reduced the effect of the worst-case start up static head. However, the results have

shown that, the increased force could be used to enhance the generated force of the electromagnets over a shorter stroke and the springs can be used as a braking mechanism preventing the armature impacting against the E-cores. At the very least, provide a softer landing.

4.10.3 Performance, Problems, and Potential

The supply voltage was set at 30V and provided a constant current of 6A. This first version of the pump actuator utilised a carbon brush switching system. However, during the electrical safety tests (dry run tests) two main problems were encountered, namely, the springs used to ensure the electrical contact evaporated as the current increased, and the other was that the support brackets that held the copper tracks for the mechanical switches snapped after only a few pumping cycles.

The circuit for the mechanical switch is the same as figure 5.1 §5.3.1, but with the addition of a low value resistance, high wattage, (i.e. 1Ω, 30W), resistor placed in series with the positive end of diode D2. It was decided that the return path for current of this circuit was of a poor design losing excessive energy in the form of heat, on switching, in the energy dispersing resistor and diodes, and for that reason an improved system was required.

In addition, the make and break time for the switch was of a very short duration, because the switch contacts were only applied at the terminus of the half cycles. Consequently, the E-core did not have sufficient time to fully energise and hence the generated force could not achieve the necessary force level.

The use of carbon brushes seems to be the ideal mechanical control. However, the use of the carbon brushes for switching has an inherent problem, namely the wear on the brushes and the associated accumulation of carbon dust within a confined space, which presents the potential hazard of a short circuit.

The layout design of the contacts posed the problem of finite control due to the close proximity of the contacts, particularly at small airgaps where the carbon brush

could energise the coils simultaneously. This could generate equal forces in opposing coils and the forces would cancel each other, resulting in no motion, and therefore no pumping action. In order to prevent the above, the brush system needs to be redesigned.

The outcome of the accumulation of problems encountered with the carbon switching system was that no satisfactory results were obtained when wet testing; the pump did not pump.

After the carbon brush failures, the first electronic switching device used was the Electronic Switch Circuit Board in Figure 5.5, the circuit for the IGBT with a Zener Diode. The Diode Feedback Loop Electronic Switch is shown in figure 5.4. This switch was used both in the single E-core dry tests and as a switch for the two E-core pumping system. The switch was used to switch the supply between the two E-cores during the pump trials instead of the carbon brush setup.

However, overheating problems were encountered and therefore the first electronic switch was replaced with a Twin 2 Transistor Forward Converter, as shown in figure 5.10 and figure 5.11.

The electronic control switching system consisted of a 'Twin 2 Transistor Forward Converter' (the inverter board) by means of the square-wave mode of a signal generator controlling the frequency. The inverter board was connected directly to the E-core of the actuator of the pump. The driver for the input signal for all the electronic circuits was a square wave signal generator. This provided frequency control. However, the scale on the signal generator was not accurate, therefore for any future testing an oscilloscope should be used to obtain an accurate reading.

Other problems encountered were that the seals were not watertight, poor diaphragm design, the impact of the armature against the E-core, and the pump failed because the actuator locked.

Water penetrated at many points; the O-ring seals of the two chambers of the pump, the centre of the diaphragm via the through-hole of the piston connection, and at the points where the locating studs passed through the pump housing. An attempt to rectify the problem was made by using a silicon-based sealant in these areas; however this did not resolve the problem, therefore the seals needed to be redesigned.

It was observed (visual inspection) whilst the pump was operating that the diaphragm was distorting. The distortion was attributed to the diaphragm being unevenly cut, being too large, and too rigid. The diaphragm was to act as a seal; this also failed. However, in this case the silicon-based sealant did resolve the problem.

It was also observed that the inlet valves system did not open in all sections, suggesting that they were too rigid.

Although the chambers flooded, the system still worked, because the electrical circuit had been previously sealed with a waterproof spray, enabling some results to be taken, shown in §4.9. It was observed (visual inspection) whilst the pump was operating that as the lower chamber flooded the output flow rate decreased, therefore, although the pump operated the water within the chamber effected the results. The assumption was that the force was reduced because the armature was no longer moving in air. Since the chamber always flooded no evidence for the assumption could be gathered.

It was noted that the repeated impact of the armature upon the E-core was a potential problem for the lifespan of the pump. Although the impact of the armature against the E-core could demagnetise the armature before the return half cycle any possible benefit was far outweighed by the deformation of the E-core, which would ultimately destroy the actuator.

The repeated vibration generated by the impact of the armature against the E-core also slackened the locking studs on the base of the pump. Therefore because the

lower E-core was free to move there was a change in the airgap size. Consequently, a reduction in force occurred.

Since, the pump output flow rate and delivery head was poor, virtually nil, the airgap of 2.5mm was reduced to approximately 1.0mm, in an attempt to increase the force and hence the delivery head. It can only be approximated because the stud locks were unreliable.

The results shown in §4.9, are for an airgap setting of 2.5mm. No further results were possible because the pump failed. The failure occurred because the actuator locked. That is, the airgap closed because of the holding rods in the E-core mounting, bending. This was due to the high generated electromagnetic force and the continuous vibrations due to the impact of the armature against the E-cores.

4.10.4 Recommendations

From the work to date, the following recommendations for improving the performance of the present D.C. Powered Linear Actuator Water Pump are:

- Design a self-oscillating system.
- Prevent the armature from impacting against the E-cores either by an electrical or mechanical means. Electrically, by bringing forward the switching time thus permitting one coil to be energised before the other has de-energised, therefore prior to the start of the return stroke a high force is achieved. Mechanically, with the use of freestanding (unattached) springs that engage the armature to reduce the force prior to the impact, so providing a soft landing for the armature. Alternatively, use a combination of the above methods.
- Redesign the carbon brush switching system, using a more robust material for the support brackets, or use a new design, such as a cam to control the switching time. In addition, change the type of springs in the spring-loaded contacts that maintain the contact to a flat spring instead of the present helix

spring.

- Improve the robustness and anchorage of the E-core/s mountings by replacing the mild steel studding E-core mounting bolts with silver steel, plus increase the diameter of the shafts, and harden and temper the shafts if necessary.
- Redesign the upper and lower pump chamber water seals of the chamber separation plate, ensuring that the lower pump chamber is watertight.
- Redesign the inlet valves making them less stiff by trimming the rubber. In addition, enlarge the inlet valve holes and experiment with different materials for the valve flaps. Alternatively, change the design of the valves or use standard valves.
- For the diaphragm pump, use a thinner and smaller diameter diaphragm making it less stiff. Also, ensure that the seal around the diaphragm is watertight. As with the inlet valves experiment with different materials.
- For the piston pump, use an O-ring on the piston this has been shown to improve the performance of the pump by decreasing the backpressure losses.
- Investigate methods for the prevention of overheating of the actuator, particularly the use of the borehole water and surrounding earth as a heat sink.

4.11 Summary

The chapter has investigated concepts for the realization of linear motion and demonstrates the feasibility of an electromagnetic driver topology with models and a series of tests. The results did demonstrate the principle of operation for the use of the E-core electromagnets and the potential of the linear actuator as a driver for a water pump. The E-core electromagnet driver can generate a normal force in excess of $400kNm^{-2}$ when there is a flux density of 1T in the airgap.

However, when the E-core electromagnet linear actuator driver is used within the pumps and the results highlight both actual and potential problems. Although, the

results from the testing of the piston pump were an improvement on those of the diaphragm pump, the desired product is still to use a diaphragm. From the results obtained during the testing, it is evident that the diaphragm pump is not viable under the present set-up, as demonstrated by the results of §4.9, as it not possible to achieve the desired output. Nevertheless, with some of the recommendations set out in §4.10.4 there is potential for the system to work efficiently. However, due to the multiple problems associated with the pumps during testing, it was decided that the eventual prototype pump would not be of the same design. Further investigations are therefore required.

The chapter also investigated the use of springs to improve the force over the length of larger airgaps. Had the use of springs proven useful then the use of springs would have eliminated start-up losses due to mg and removed or at least reduced the effect of the worst-case start up static head. However, the results have shown that the increased force could be used to enhance the generated force of the electromagnets over a shorter stroke and the springs can be used as a braking mechanism preventing the armature impacting against the E-cores. At the very least, provide a softer landing.

The chapter also gave a three part discussion, which includes a system analysis, the use of springs, and the performance, problems and potential of the pumps. The thesis now moves forward with chapter 5 which investigates the actuator control and the associated design considerations, and chapter 6 which investigates possible future development.

CHAPTER 5

Chapter 5
Actuator Control and Design Considerations

5 Introduction

This chapter considers the results of chapter 3 and chapter 4, and investigates and discusses possible improvements for the design and operation of a solar powered water pump. The first issue under discussion is the thermal quandary of the system and possible solutions are given. It then discusses switching methods for both electrical and mechanical control of the armature movement and provides a solution that utilises a mechanical carbon brush switching system.

5.1 Thermal Quandary

It is inherent that the coil temperature will rise when the pump is in operation. Consequently, variations in the operating point will occur, and therefore the subsequent rise in resistance will affect the operating point. When an increase in load resistance occurs, (the probable cause being the heating of the actuator), the operating point moves to the right, this is shown on the solar cell I-V characteristic of figure 3.5. By moving beyond the MPP, a large current drop and hence a power drop transpires, so reducing the force generated by the actuator. Similarly, if a large decrease in load resistance occurs, although unlikely, the consequence would be for a large voltage drop to occur, (Re: §3.4, Figure: 3.5).

Several options are available to deal with the thermal quandary owing to the heating of the coils and actuator.

- The size restrictions limit the number of turns for the coil; too small a diameter of wire reduces the available current density, without overheating, so reducing the current and the available force. Too large a diameter of wire

will reduce the number of turns also reducing the magnetomotive force (m.m.f), the product of the current and number of turns.

- Redesign the E-core; by incorporating a larger wire gauge so improving the current density (J) capacity, or by reducing the current. Both will affect the force produced. Therefore to increase the force the E-core would need to be 'stacked' so that there is an analogous resultant force. Stacked E-cores are explained §6.2.

- Design an electronic controller, a method of tracking the maximum power point and comparing this to the operating point and making any necessary adjustments.

- The resistance is kept to a minimum by providing a heat sink. However, this could impinge on the operation of the system. Any substance introduced to the electromagnetic driver chamber, other than air (or vacuum), will reduce the available force due to the viscosity of that material. Further, it provides for the potential of contamination through leakages to the water supply.

- Alternatively the pump operates in a freestanding mode where the water within the well combined with the surrounding earth acts as a natural heat sink; the dissipation of the thermal energy being aided by the materials of the internal parts and the pump chamber.

5.2 Switching

If a pump were to run continuously for a minimum of eight hours per day and to be operational for one year without needing maintenance, then a pump operating at 20Hz would require in excess of 210 million switching movements within a year.

A number of switching concepts have been considered namely, Mechanical Switches, Reed Switches, and Relays. To date none of these methods have been found to be suitable, the problem arises because of the lifespan of such manufactured devices, (typical switching specification of 50K – 200K cycles), far short of the required 210 million cycles. However, this does not necessarily rule out such devices. The maintenance schedule for the pump could be revised, so, reducing the number of cycles required.

However, one concept, although not investigated, was to use the flow of the water under pressure (pressure switch), or the flow of the water (flow switch), to activate a mechanical stop switch. The principle of operation being that at the end of a stroke the switch is tripped causing the return section of the actuator to energise.

Obviously, the longer the time the pump is operational the greater the number of cycles, and the typical switching specification of 50K – 200K cycles would be exceeded, therefore the advantages of using electronics, in that there are no mechanical fatigue constraints, would be more apt.

Nevertheless, one avenue that has potential is the use of carbon brushes. Carbon brushes have typical life spans of 1000 – 1500 hours, this equates, at 20Hz, to 72 – 108 million cycles. However, in order to prevent switch arcing and the possibility of the welding of the switch, the use of some electronics is still necessary to dissipate the energy generated by the inductor coil of the actuator.

Until now only switching for a single coil system has been considered, further consideration must now be given to a push-pull system, which incorporates two actuator coils being activated alternately, so generating a force in both directions of the stroke. As with the single coil system the individual coils may be controlled in the same manner, however, the switching between the two coils requires additional circuitry. Apart from the obvious electronic control, other methods for the control of the push-pull system have been considered; in general, methods involving a position detector for the movement of the armature.

5.3 Prevention of Switch Arcing

In order to prevent switch arcing and the possibility of the welding of the switches, it is necessary to dissipate the energy generated by the inductor coil of the actuator. The first method that was considered was to use a resistor connected in series with a capacitor, in turn connected across each of the switches, however this would result in an energy loss, as heat, in the resistor/s. The second method considered was to use Metal Oxide Varistors (MOVs) connected in parallel with the switch/s. The third method considered was to use capacitors enabling the energy to return to the supply.

5.3.1 Dissipation of Energy with MOVs

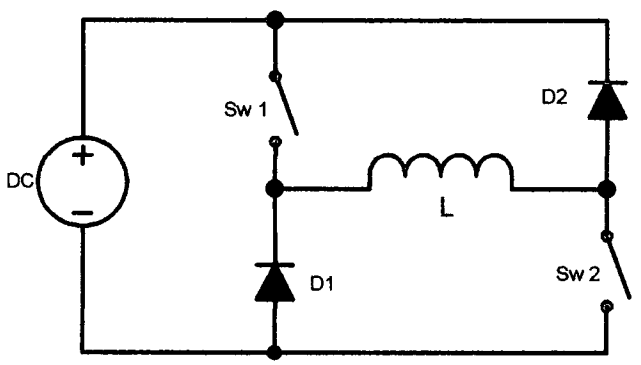

Figure: 5.1 – Actuator inductance coil for a single E-core System

Figure 5.1 is a circuit diagram for switch activation of the coil current. Sw1 and Sw2 can be either mechanical or electronic switches. When the switches Sw1 and Sw2 are simultaneously closed, the current flows through switch Sw1, the inductor (L) and switch Sw2. The return path for the current when the switches Sw1 and Sw2 are simultaneously opened the current flows through diode D1, the inductor (L) and diode D2.

The energy in the coil shown in the circuit diagram figure 5.1 is represented by equation 4.41.

$$U_f = \frac{1}{2}Li^2 \quad \text{J} \qquad \text{Eq}^{\text{n}}\ 4.41$$

Where, U_f = the energy in the coil

MOVs connected in parallel with Sw1 and Sw2 – Although their use has been illustrated by a manufacturer, (Harris Semiconductor – MOV Application Handbook), they would have to be used at much reduced energy rating for continuous operation, and therefore their large number would be uneconomic. This is shown below.

By example: the inductance (L) shown in figure 5.1 represents three identical coils connected in parallel, which would reduce the 102mH inductance of the single coil used in the force tests of the actuator to a value of 34mH. The circuit now requires a current of 18A to pass through the switch that is 6A for each coil; therefore, the energy in the coils is 5.508J.

$$U_{Coil} = \frac{1}{2} \times \left(34 \times 10^{-3}\right) \times \left(18\right)^2 = 5.508 Joules$$

It is also necessary to consider the power, equation 5.1, which is the product of the energy in the coil and the operating pumping frequency.

$$P_{Coil} = \frac{1}{2}L\left(i\right)^2 f \quad \text{W} \qquad \text{Eq}^{\text{n}}.5.1$$

At a pumping frequency of 6Hz, the power would be 33.048W, however if the pumping frequency were 20Hz the power would be substantially higher, at 110.16W.

The largest 38Vdc MOV (a 21.5mm diameter disc by 7mm thick) rated at 28J for the maximum energy is capable of absorbing the 5.508J, but the maximum power

rating is only 3W. Hence, even two MOVs (max 6W) connected in parallel across the switch, cannot absorb the power.

Since MOVs reduce arcing (voltage) across the switch by absorbing the energy in the coil, and with the system operating at 30V and 6A, MOVs are not suitable for this application.

5.3.2 Dissipation of Energy with Capacitors

A better way is to return the energy to the supply with the use of two switches, two diodes, and a decoupling capacitor, as shown in the circuit diagram of figure 5.2.

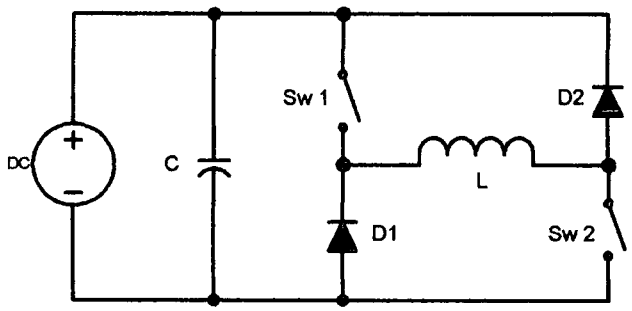

Figure: 5.2 - Actuator inductance coil for a single E-core System with a Decoupling Capacitor

The energy of the decoupling capacitor (C) when the switches are closed can be represented by equation 5.2.

$$U_{Cap} = \frac{1}{2}CV^2 \quad \text{J} \qquad \text{Eq}^{\text{n}}.\ 5.2$$

For a $30V_{dc}$ supply, and a 4700μF - 63V Capacitor the energy is 2.115J.

$$U = \frac{1}{2}\left(4.7\times10^{-3}\right)(30)^2 = 2.115 Joules$$

Therefore, the energy returned to the supply was 5.508J (from §5.3.1) and the energy due to the capacitor is 2.115J, the total energy in the capacitor is therefore 7.623J, with a terminal voltage of approximately 57V.

Since, 7.623 joules of energy is large enough to cause arcing across the switches therefore further improvements are required. One method of preventing switch arcing is to connect 'snubber' capacitors C1 and C2 across the switches, as shown in the circuit diagram of figure 5.3.

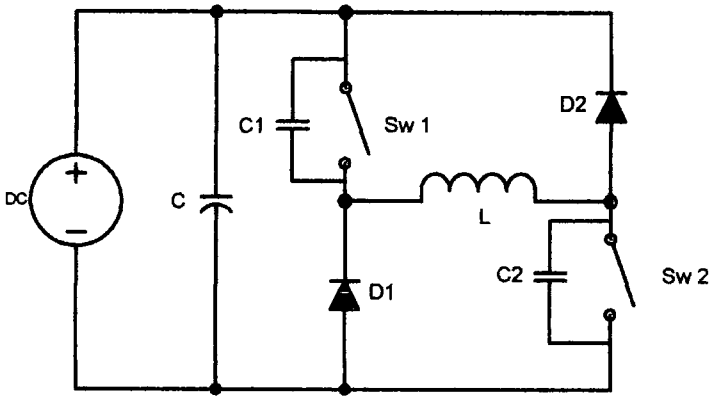

Figure: 5.3- Actuator inductance coil for a single E-core System with a Decoupling Capacitor and Switching Capacitors C1 and C2

The principle is that there is zero voltage across C1 and C2 when the switch opens, so no arcing occurs. When the switches open, both C1 and C2 must charge to $30V_{dc}$ before D1 and D2 conduct. For this to happen in less than 10μs (slower than the turn-on time of D1 and D2) then the quarter resonant cycle, formed by $\frac{C1+C2}{2}$ and L, must by approximately 10μs for design, i.e. $f = 25kHz$.

The resonant frequency can be represented by equation 5.3.

$$f_{res} = \frac{1}{2\pi\sqrt{\frac{L(C_1+C_2)}{2}}} \quad \text{Hz} \qquad \text{Eq}^{n}.\ 5.3$$

Since the values of C1 and C2 are identical, the value of the two capacitors can be evaluated from equation 5.4.

$$C = \frac{1}{2\pi^2 f^2 L} \quad \text{F} \qquad \text{Eq}^{\text{n}}.\ 5.4$$

Therefore for the case of L=34mH and f=25kHz the values of C1 and C2 are 2.38nF; therefore a small polyester capacitor can be used.

The energy can now be evaluated from equation 5.2.

$$U = CV^2 = \left(2.38\times10^{-9}\right)(30)^2 = 2.142\mu J \qquad \text{Eq}^{\text{n}}.\ 5.5$$

Therefore, each capacitor will have a terminal voltage of 30Vdc and when the energy is discharged into each switch at switch closure the energy dissipated is only 2.142μJ, which is negligible, and will not cause arcing. Now the only loss within the system is the conduction through the diodes D1 and D2.

5.3.3 Comparison of Power Loss between MOVs and Capacitors Circuits

The supply voltage is $30V_{dc}$ and the input current is 18A, therefore the input power of the system is 540W. The power loss in the MOV system was determined to be 33.048W at a pumping frequency of 6Hz, and 110.16W at a pumping frequency of 20Hz. In the capacitor system the current ramps down from 18A to 0A, therefore the current through each diode is 4.5A. Each power diode has a voltage drop of approximately 0.7V, therefore a total voltage drop of 1.4V. The corresponding power loss is therefore 6.3W, or 3.15W per diode. However, the use of Schottky diodes, having an approximate 0.3V voltage drop at turn-on will reduce this still further to 2.7W, or 1.35W per diode.

From equation 5.1, it can be seen that the power of the system is directly proportional to both the energy and the frequency of operation; therefore, the

greatly reduced energy/power losses (0.5%) of the capacitor system also provides for a far greater operating frequency for the pumping action.

5.4 Electronic control

An alternative to mechanical switching is the use of electronics. Figures 5.1 – 5.3 all use two mechanical switches, these can be replaced with a single transistor switch, and the circuit diagram is shown in figure 5.4.

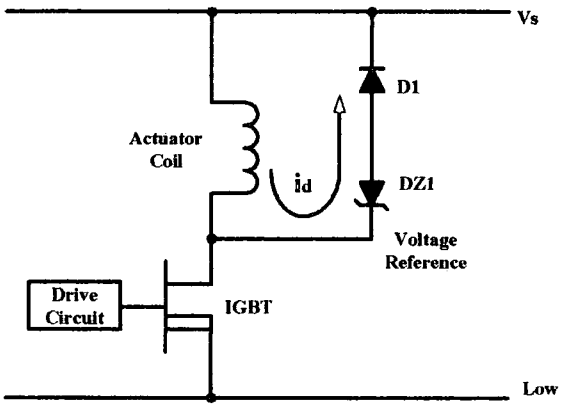

Figure: 5.4 – Electronic Switch - IGBT with Diode Feedback Loop

When the IGBT switch is activated, the coil current increases to its limiting value dependent on the supply voltage and coil resistance. When the switch is turned off, the coil has a negative voltage across it of $V_{D1}+V_{DZ1}$ as the coil current circulates through the diodes. Hence the diodes act as the discharge path (*shown in red*) for the current when the coil is de-energised and clamp the maximum switch voltage to Vs - V_{D1} - V_{DZ1}, which protects it against large transients at switching. The zener diode gives a faster 'rampdown' of the current than just using the diode D1, and hence the removal of the pumping force, but the energy in the coil is dissipated in the zener diode, reducing efficiency.

The drive circuit used when testing was a square-wave generator, model – TTi, (Thurlby Thander Instruments) TG120 – 20MHz Function Generator – Serial No. 098671.

The circuit board shown in figure.5.5 utilises a BUP603D - IGBT, which is rated at 600V, 42A. The circuit board also shows a number of diodes connected in series; this is merely a cheap version of a higher power zener diode. Each of the fifteen diodes has a voltage drop of 0.7V, providing a 10.5V negative voltage across the coil for current ramp-down.

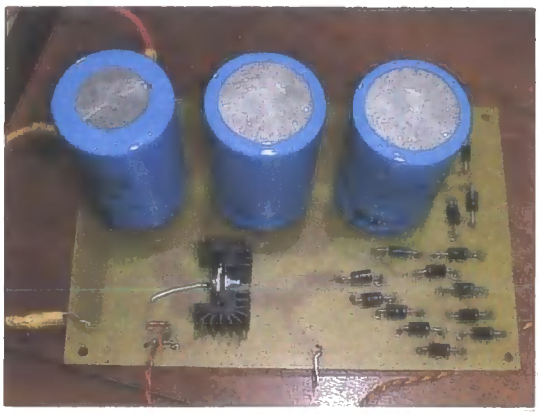

Figure: 5.5 – Electronic Switch Circuit Board

The circuit of figure.5.5 is suitable for a single coil to run at 10 – 20 Hertz. The IGBT requires a minimum operating voltage for operation of approximately 4V. The disadvantage of the circuit shown in figure.5.4 – 5.5 is that the coil energy dissipates in the diodes at turn-off.

The power dissipation of the diodes is crucial and is directly related to the inductance, coil current, and frequency of operation. In this case, the inductance of the coil was determined as 107mH; the system operated at 20Hz and the peak coil current was 5A. Hence, the energy dissipated was 26.75W, or 1.8W per diode.

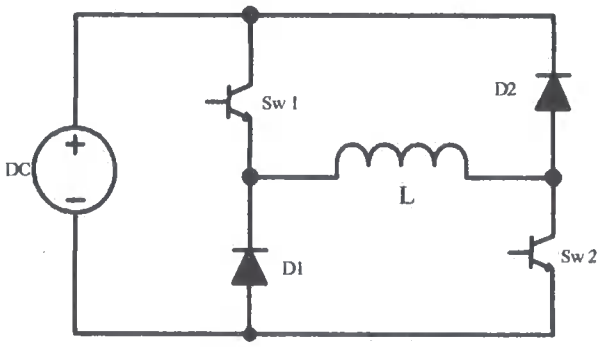

This high power loss can be avoided by the electronic version of figure.5.1, shown in figure.5.6, where the coil energy is returned to the supply via D1 and D2 when S1 and S2 are turned off.

Figure: 5.6 – Electronic version of figure.5.1

A further addition for improvement is to place a reservoir capacitor C across the DC supply, so as the coil de-energises the capacitor charges. Capacitor C is normally required to supply the current pulses of inductor L, however, the value of

capacitance can be reduced if the two E-core push pull pump system is used. When one is de-energised, the other is immediately energised, that is the current ramp-down in one is the current rise in the other, hence reducing the pulse currents through the capacitor.

Another method of switching is to use a tertiary winding (secondary winding) as shown in figure 5.7. The argument for the use of a secondary winding is that it avoids the power loss across the diodes of figure 5.4 by returning the energy back to the supply, when switching.

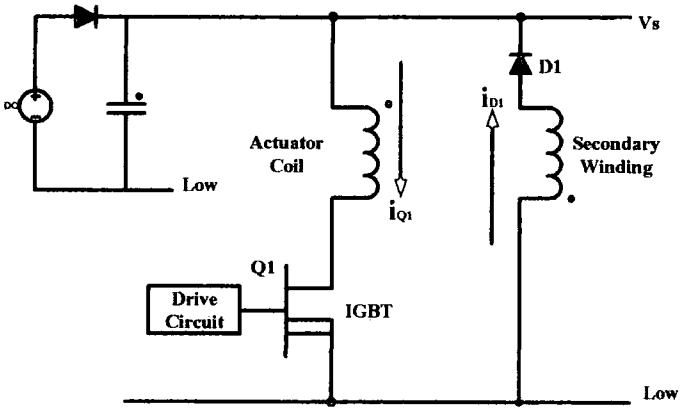

Figure: 5.7 – Tertiary Winding on a Single Switch Forward Converter

The tertiary winding is counter-wound because of the reversed polarity. The tertiary winding is of a smaller gauge wire because the average current at ramp-down is far less than the average current during the energizing of the coil of the actuator, that is $i_{D1} \langle i_{Q1}$.

When connecting two coils the use of a tertiary winding is also viable, that is for a push-pull system, which incorporates two actuator coils being activated alternatively. The reservoir capacitor shown in figure 5.7 – 5.8 can be removed providing that the input signal for switch Q2 is brought forward; by doing so the demagnetisation energy on ramp-down of L1 is fed directly into L2 on excitation instead of going into the capacitor. However, the switching between the two coils requires additional circuitry.

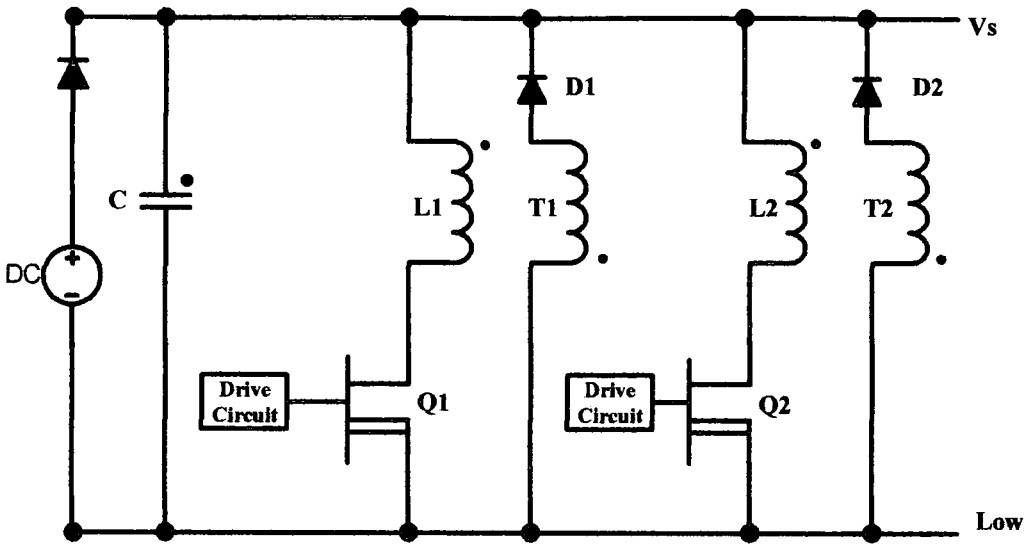

Figure: 5.8 – Tertiary Windings of a Push-Pull System

Four-transistor switch forward converter as shown in figure 5.9 could also be utilised however they have the potential problem of 'shoot through', a short-circuiting of the supply via switch Q1, and switch Q2. The problem arises because the current through the inductor can be both negative and positive therefore, Q1 and Q2 can be on at the same time. Consequently, protection circuitry is required for the power transistors, i.e. a dead time generator or blanking generator where in switching from Q1 to Q2, there is a dead time during which neither transistor is driven.

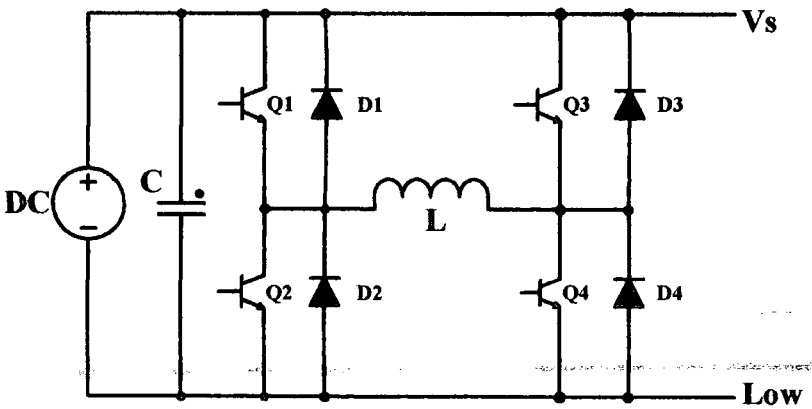

Figure: 5.9 - Four-transistor Switch Forward Converter

5.5 Twin 2 Transistor Forward Converter

Figure 5.10 shows the completed circuit board for the 'two E-core system', which controlled the prototype pump during testing. Again, the input signal was provided via the square-wave generator.

Figure: 5.10 – Twin 2 Transistor Forward Converter

Acknowledgement

Dr. P.R.M. Brooking provided the development and building of this circuit.

The circuit diagram for the 'Twin 2 Transistor Forward Converter' is shown in figure 5.11, which is followed by the principle of operation of the circuit.

Mosfets were used for the switches, and the upper switch S1 was a p-channel mosfet to permit a drive signal referenced to the same common (0V) point for both switches, thereby simplifying the circuit. A single high level at BR1 will turn S2 (Q2) on and is inverted by Q3 to turn on S1 (Q1) at the same time, thereby allowing current to build up in the coil through one of the bridges.

A built-in signal level inverter formed by Q5 enables driving of both coils through both bridges alternately from a single drive signal.

The drive circuit producing the 'command to energise' signals for both coils could be an Astable multivibrator instead of the signal generator used for testing. An alternative would be the use of a 555-timer circuit. However, the circuit would require both a buffer, for example an emitter follower, and an ex-or gate to ensure that both coils could not be 'live' simultaneously.

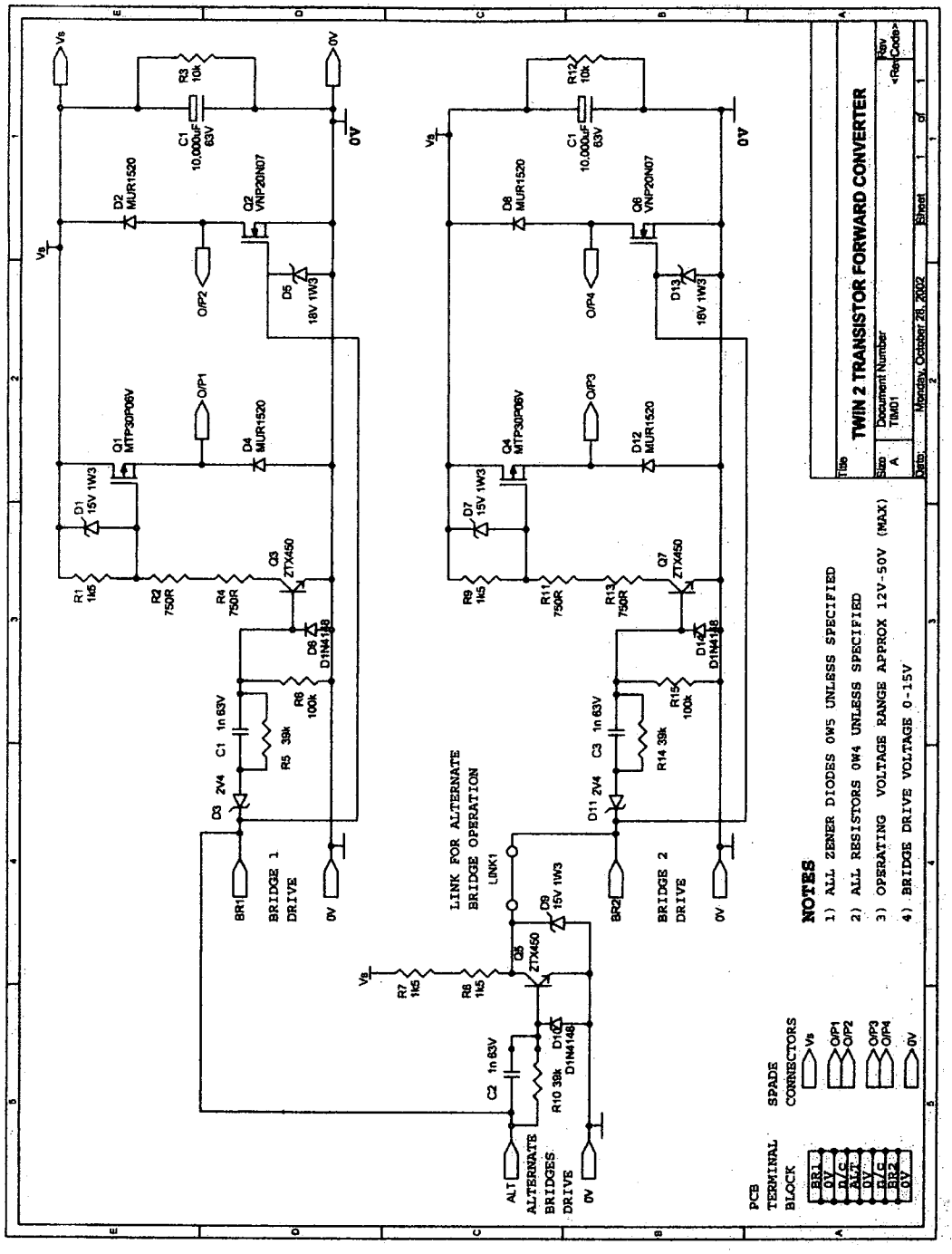

Figure: 5.11 - Twin 2 Transistor Forward Converter Circuit Diagram

The circuit is protected by the lower n-channel mosfet, VNP20N07, which has an internal over-current shutdown. The mosfet was chosen primarily for its low resistance, but its over-current shutdown level of 17A can result in the p-channel mosfet overheating. A lower current rating n-channel mosfet, VNP10N07, could be

used with a 10A shutdown current, but this would increase the resistive losses in the mosfet.

The 'Twin 2 Transistor Forward Converter', compared to a four switch single phase full bridge previously designed, does not have the potential problem of 'shoot through' of the switches via Q1 and D4, i.e. short circuit of the supply, in figure 5.11. Hence, the 'Twin 2 Transistor Forward Converter' is intrinsically more reliable and able to withstand environmental hazards such as bridging due to insect nests, etc.

5.6 Switching Control

When connecting two coils for a push-pull system, which incorporates two actuator coils being activated alternatively, a method of determining the armature position is required. The control system for movement of the armature can range from a simple switching device to a predetermined driving mechanism. There are several methods of achieving such control, such as the use of a signal level inverter, being control driven, or by a position detector, each method with their own advantages and disadvantages. Ideally, any control device should be simplistic and inexpensive.

Several concepts have been explored and some possible solutions are now discussed.

The use of a microphone to detect the impact of the armature against the E-core was considered. Although tests demonstrated the possibility of utilising such a method by producing a signal with an amplitude in excess of 0.7V from the shockwave, which activated a transistor switch, the method proved to be unreliable. The duration of the signal was only a few microseconds. The signal varied to such a degree that the repeatability of the signal form was not possible without additional circuitry. The signal would need to be isolated from such things as harmonics,

rebound vibrations, and resonance. In addition, the impact of the armature against the E-core is detrimental to the system. Therefore, acoustic control was ruled out.

An optical solution was also sought. However the concept of using fibre optics where the movement of the armature would cause the breaking of a light beam, combined with the associated electronics, was considered not to be financially viable, and therefore disregarded.

Some of the magnetic solutions were not realized, such as a magnetic make/break switch, and utilising the fringing of the magnetic field of the E-core in conjunction with Hall effect probes, enabling the changing field to act as a trigger for the control of a switch. However, a magnet passing through two coils was investigated. The principle of operation is that a magnet plunger (which could be a magnetic ring placed around the drive shaft) is passed through two separate coils, which switch the supply to the opposing coils in turn. That is, when the plunger is inserted into the upper coil the lower coil is energised, and vice-versa. The laboratory tests were successful in changing the supply direction signifying that this option may be viable. However the device was never attached to the test pumps.

Electrically, reed switches and relays have previously been ruled out. Even so several options are available such as, a simple oscillator control, and the use of the back e.m.f as a trigger for a switch, and the use of a signal level inverter.

A large back e.m.f is generated when the armature impacts against the E-core, due to the rate of change of the flux. The quandary is what to do about this, remove it, dampen it, or use it. The back e.m.f could be used to activate a gate on a thyristor for control purposes; alternatively, it could be used for a timing circuit, however these options have been ruled out because of the problems incurred due to the impact of the armature on the E-cores.

The 'Twin 2 Transistor Forward Converter' (§5.5) has a form of position detector by means of the built in signal level inverter (located in area 4C of figure 5.11) which is capable of driving both coils through both bridges alternately from a single

drive signal. Possible drive circuits are shown in figures 5.12 and 5.13. The buffer on/off for drive circuit B, less than 1μs, is faster than that of circuit A.

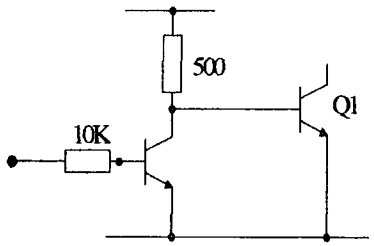

Figure 5.12 – Drive Circuit A

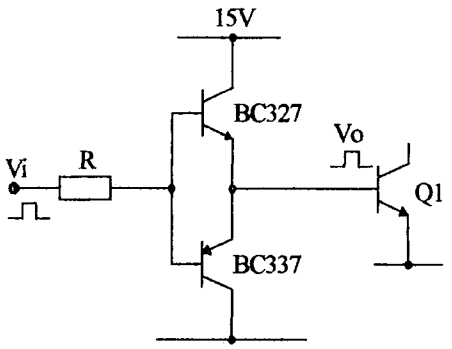

Figure 5.13 – Drive Circuit B

5.7 Use of Carbon Brushes

Previously it was stated that mechanical switching is limited due to the number of switching actions and the switches usually fail due to fatigue. However, an electromechanical system is possible, similar to that shown in figure 5.3, for a single E-core System, which incorporates an inductance actuator coil with a decoupling capacitor and switching capacitors. A carbon brush system can therefore be used; the circuit for the two-E-core system is shown in figure: 5.14.

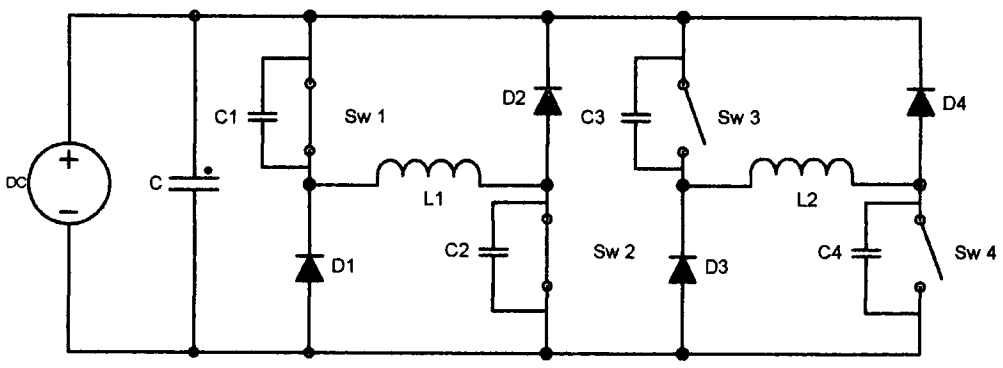

Figure: 5.14 – Carbon Brush Mechanical Switching Circuit for use in a Two E-core System

The use of the capacitors in the mechanical system shown in figure 5.14, removes the need for energy dispersing low ohm, high wattage, resistors, which would be placed in series with diodes D2 and D4 after the inductors L1 and L2, respectively. The circuit conserves energy in the same way as previously described for figure 5.3 of §5.3.2. In addition, the larger the reservoir capacitor, C, the smaller the ripples on the DC supply.

The principle of operation is that as the armature moves between the two E-cores, the individual circuits are 'made' and 'cut' in an alternating mode. Both the switches, for each individual coil, are 'made' simultaneously, thus completing the circuit, hence energising the respective coil.

When the armature reverses direction, the circuit for the energised coil is 'cut'. The discharge paths for the current are from low to high via D1, L1, and D2, and for the return half of the cycle, from low to high via D3, L2, and D4. The energy in the de-energising coil in both halves of the cycle is $\frac{1}{2}Li^2$, that is, at the moment of the diode conduction, at which point the energy is returned to the supply.

Previously, one of the problems was the retention time of the switch, in that the required current level had not been reached and therefore the maximum force had not been achieved before the supply was switched to the other coil. In order to overcome this problem, spring loaded brushes can be used. The springs hold the carbon brushes until sufficient time has elapsed such that the coil has fully energised. In addition, a further improvement can be made by ensuring that the retention time of the switch results in an overlap of the duty cycles thereby bringing the duty cycle of the second E-core forward. The benefit of bringing forward the duty cycle is that it ensures that the second E-core has developed a large force at the beginning of the return half of the cycle, thereby achieving a higher force throughout the complete cycle. This in turn increases the available pressure and the pump can be used at greater depths.

CHAPTER 6

Chapter 6
Possible Future Development

6 Introduction

This chapter covers areas of preliminary investigations and possible future development. The chapter introduces three possible uses of permanent magnets within the actuator and pump system. The chapter also discusses the 'stacking' of E-core and the relevant inductance changes. This is followed a section about improving the stroke length of the actuator. Then having given the case for the use of diaphragms, and the factors surrounding the hydraulics of the system, the chapter ends with a method of improving the output flow rate of the present pump.

6.1 Permanent Magnets

Until now only the force of attraction has been considered, the alternative to this is to use a repulsion force. Preliminary investigations into methods of achieving repulsion have been undertaken. The obvious one is to use permanent magnets (PMs). However permanent magnets tend to be brittle and the physical properties of permanent magnets will have to be investigated to determine the practicalities of using them.

Three possible uses for PMs are,

- PM Armature – where a PM is attached to the armature,
- Magnetic Brakes – where PMs are used as a braking system to prevent the impact of the armature against the E-core, or at least provide a softer landing,
- PM Cores – where PMs either are placed in series or parallel with the flux path of the E-core in order to strengthen the magnetic field.

6.1.1 PM Armature

Initial investigations into the use of PMs where a PM is attached to the armature have been undertaken. The indications from tests undertaken were that the magnetic fields of the PMs were too great, because the electromagnets used in the tests could not generate an equivalent magnetic field. Even though a repulsion force was generated during the tests, if the armature was in close proximity the repulsion force would flip to an attraction force and consequently the actuator locked-out. The problem of the magnetic field flip may be rectified if alternative materials are used for the construction of the E-core, for example, iron-cobalt alloy, containing 35% cobalt, with a saturation point of 2.34T, could be used. However, this may not be fiscally viable, as further investigations would be required.

6.1.2 Magnetic Brakes

When using PMs a repulsion force is generated when two like poles are facing each other; this could act as a breaking mechanism for the pump, so preventing the impacting of the armature against the E-core. Preliminary investigations show that high repulsion forces can be generated at small airgaps. However, the repulsion force is dependent on the material and geometry of the PMs.

No results are available because the models are still in the development stage.

As the repulsion force within the airgap may well be of a different magnitude to the attraction force of the electromagnets for the equivalent airgap between the armature and E-core, the two parts of the actuator system will need to be matched.

A further consideration is that the magnetic field of any PMs used within the system must be placed at such a distance that it has no effect on the electromagnet field of the E-core.

In addition, the PMs would need to be placed within a chamber to prevent side flip of the PMs as they came into close proximity. Further investigations would also be required for the use of the chamber, as it would effectively form a piston that compresses air, which potentially could reduce the resultant available force. However, it may also aid the braking and so prove to be of benefit.

Tests are required to determine whether the repulsion force, when switching the supply from one E-core to the other, could be of any benefit by adding to the initial force generated by the E-core.

Since the pump must be robust, cheap, and reliable, the possibility arises that a self-oscillating, impact free system, could be developed; which satisfies the requirement to develop and build a pump that works and has met the conditions for sustainable development.

6.1.3 PM Cores and the Advantages of Polarized Structures

In 2003, Guerin et al. [85], presented a paper that demonstrated the use of a linear actuator with parallel polarization and in the same conference Sedda, Fageon, and Yonnet [76, 86], presented a paper that demonstrated the use of PM actuators for electromagnetic valves in automotive applications. The Guerin et al paper involved a complex configuration that gave good control of the movement of the actuator. However, the construction of the actuator for practical applications may be difficult to achieve when applied to the confined space of a borehole. Nevertheless, the paper by Sedda, Fageon, and Yonnet [86], shows that placing PMs in series with the electromagnets' magnetic field can enhance the resultant force and provide a linear response. The experimental results of the force and current measurements show a linear response. The Sedda, Fageon, and Yonnet [86], paper states "The moving part stays in a static position in the high and low point, then goes to the other position in less than 3ms, 1kHz. The valve opening time is obtained by adjusting the interval between the up and down motions. The landing noise of the moving part is a key issue for this type of actuator. To reduce it and to maintain a longer lifetime, a soft-landing must be achieved." The system benefits from the

fact that the neutral position for the armature is in the middle, and the two electromagnets mainly operate by holding the moving part at the ends of the stroke.

The potential benefits of using these methods need to be investigated, because they provide for a rapid response time, so potentially enabling the pump to operate at higher frequencies, whilst also controlling the landing relatively easily.

In general, other considerations will be to determine the availability of such magnets, along with shape, size, and material.

6.2 Stacking E-core

The size of the present E-core will fit into a chamber small enough to fit into a four-inch borehole and therefore needs to be reduced in size.

The advantages of stacking the E-core is that, even though the geometry of the E-core is reduced and they can fit into a smaller envelope, the equivalent resultant force of larger E-core can be obtained, because the generated forces of each individual E-core accumulate. Further, the total inductance is reduced, and consequently the frequency will increase at the same ratio as the change in force. The system will work providing that the armatures between the E-core are connected mechanically, this rules out any problems caused by an imbalance in the inductance and the generated forces of the individual E-core.

6.3 Changing the Inductance

The changes in inductance are outlined in §4.2.14

Not only is inductance a function of the airgap size, for the case of E-core type 2, the inductance is a function of the cross-sectional area of the central leg, the number of turns of coil, the length of coil. Previously it has been shown that problems are incurred due to the inductance, for that reason a reduction in inductance is

necessary. Since the inductance is a function of the geometry of the E-core, then by varying the geometry, the inductance can be changed, so reducing the problems and improving the operation of the system. The effect of changing the geometry is now shown by examples.

A reduction of 50% in the width of the central leg of the E-core will reduce the cross-sectional area (c.s.a) of the central leg by 25%. The effect of reducing the c.s.a of the central leg, whilst maintaining the leg width ratio, is to reduce the generated force by 25%. Since the current can be maintained at the same level, then the m.m.f needs to be maintained by keeping the same number of turns. Therefore, the generated force will be maintained. In order to keep the number of turns the same the length of the leg must be doubled, having the effect of quadrupling the inductance. The increases in inductance are directly proportional to the square of the number of turns.

In order to maintain the generated force, four E-cores, connected in parallel, could be stacked, with the sum of the forces matching the original generated force. This method will also maintain the present value of inductance. Therefore, by reducing the size of the E-core, there is no change in generated force. However, the inductance remains the same.

If stacked E-core are used in conjunction with the extended leg length then not only is the force maintained, but it is quadrupled, and the inductance is also reduced to a quarter of its original value.

It was found, by observation, whilst working on the models, that the frequency, at an airgap, at the point where saturation has occurred, can be evaluated from equation 6.1.

$$Frequency_{Opertion} = \frac{R_{Coil}}{2\pi L_{Total}} \quad \text{Hz} \qquad \text{Eq}^{n}.\ 6.1$$

6.4 Increased Stroke Length

Small airgaps are required to produce large forces of attraction; however, they also create problems. Firstly, they vastly reduce the stroke length and which in turn reduces the flow rate. However, this can be overcome by increasing the frequency. A limit to the maximum frequency at which the pump can operate effectively is imposed. If the pump were operating at too high a frequency then there could be a risk of cavitation occurring. Secondly, the high attraction forces require high currents; if the airgap is too small then the time taken for the coil to reach the required level of current to produce the necessary force may not be of along enough duration. This is a consequence of the inductive load; and the effect the changing inductance on the time constant. Thirdly, if there was not sufficient time for one coil to de-energise before the other energises there could be an imbalance causing the system to stall. To overcome such a problem, changing the duty cycle of an electronic control system could be utilised. The preferred method, to cause the same effect, can be achieved changing the position of the terminals on a mechanical switching device.

The length of the stroke can be increased electrically, by increasing the length of the central leg of the E-core, whilst maintaining the overall geometry ratio. The effect of this is to generate a force over a larger airgap, as shown in §4.2.7 - §4.2.9.

The mechanical option is to use a lever system; however the result will be a loss in generated force within the lever system. The other disadvantage of using levers is that, the more moving parts there are the greater the risk of failure due to fatigue and breakages.

The final option is to increase the output flow rate within the hydraulic section of the pump, as shown §6.6.

6.5 The Case for the Use of Diaphragms

Diaphragm Pumps have many advantages over the traditional piston pumps, particularly because the pump's working parts are never exposed to the liquids being pumped. In comparison, the same liquids being pumped generally lubricate the upper working parts of piston, plunger, and roller pumps, and the bearings and seals are always in contact with the chemicals or water.

In general, the design of diaphragm pumps is that the diaphragm is pushed, not pulled. When they pressurise liquids, they are being thrust by a piston and are correctly seated on the head of the piston for that purpose. Consequently, the diaphragms are fully supported, therefore do not stretch, pull, deform, or suffer any other stress for which they were not designed.

When the piston ends its stroke, it pulls the diaphragm as it goes back into the lower part of the cylinder, creating a slight vacuum in the pressure chamber thus drawing fresh liquid into the head. This will then be pushed out to the non-return output valves by the diaphragm, when it is pushed again by the piston.

Providing that the inlet lines and valves from the source are not clogged, the filter is clean, and the inlet non-return valve in the line feeding the pump is open, there is no problem. The diaphragm pulling the liquid into the chamber is not stressed.

However, if there are obstructions in the line of any kind, the diaphragm has to pull hard to fill the chamber, creating a high vacuum. This now causes the diaphragm to be pulled by the piston head, deforming the centre mounting of the diaphragm. If the pulling effect becomes extreme due to a higher degree of clogging, and, of course, a higher inlet vacuum, then the diaphragm will be severely deformed and even eroded by the edge of the washer holding it to the head of the piston. Inevitably, the washer will cut the diaphragm, subsequently damaging it or causing the pump to fail and/or contaminating the output as a result of mixing of lubricating oil and water.

Fraenkel [87] states, "In general, the advantages of a diaphragm pump are:

- The sealing is perfect, except for any inadequacies of the check valves.
- They have high mechanical efficiency, since flexing a diaphragm involves much less friction than sliding a piston with seals up and down a cylinder.
- No seal is needed at the pump rod, which also reduces friction losses still further compared with piston pumps.
- They are self-priming, hold their prime very well, and can often handle a higher then average suction head.
- They often function well with gritty or muddy water, which could damage a piston pump.

However, diaphragms also have disadvantages:

- Diaphragms need to be high-quality rubber if they are to last, and are therefore expensive.
- Diaphragm pumps are often dependent on specialized spare parts that cannot easily be improvised in the field.
- A diaphragm pump is similar to a large-diameter piston pump with a short stroke, so the pump rod forces are high in relation to the head and swept volume. This imposes a high load on transmission components and on the point of attachment of the pump rod to the diaphragm.
- Diaphragm pumps are generally less capable of handling high pressures than piston pumps and they also do not readily fit down narrow boreholes, so they tend to be used for low-head application (usually of less than 10m) and especially those involving suction lift from an open water source."

A common problem encountered when pumping is that of caking-up, resulting in blockages and pump failure. Chemicals, especially liquid absorbing powders and coppers have a habit of caking-up in the fittings. However, the function of this pump is to pump water, therefore, the main problems of caking-up are envisaged as those resulting from the minerals present in the water source and those arising from electrolysis, degradation of materials, and rust. Careful choice of materials at the design stage, and the provision for a sacrificial earth can overcome/prevent the electrolysis problem.

The best prevention for this problem is to regularly clean the filters, washing the screens out thoroughly. Also, check the inlet non-return valves periodically for blockage. If the output is still reduced to a trickle or little more, and not what is considered normal, then there is some blockage either in the output line or internal plumbing of the pump.

Another common cause of the high vacuum problem is the inlet non-return valves lines that are closed when the pump is started. Diaphragm pumps will pump air when there is no liquid around, so if the inlet non-return valve is closed they will sit and suck vacuum with the subsequent consequences. Probably the easiest solution to this problem is to prime the pump before use.

6.6 Method to improve output flow rate

With respect to the last disadvantage stated above by Fraenkel [32], it may be more appropriate to use a piston system when pumping high heads. The use of pistons can improve the output flow rate if the pistons are connected mechanically in series and hydraulically in parallel, as shown in figures 6.1 and 6.2.

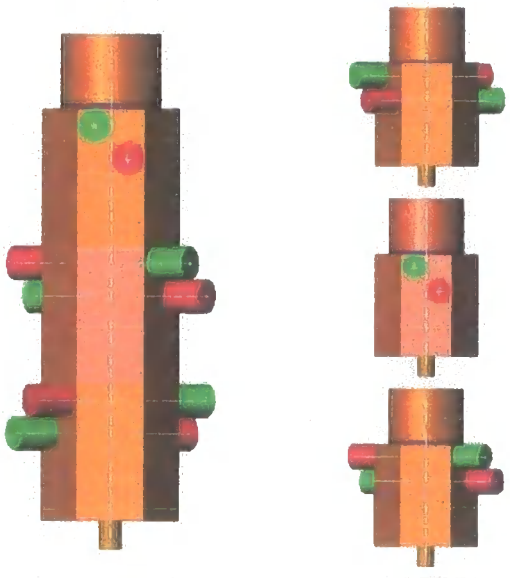

Figure 6.1 – 3x Piston Chambers

Figure 6.1 shows a set of three piston chambers for a short stroke, high volume reciprocating water pump that takes advantage of the high force low displacement armature of an E-core actuator system. Three reciprocating water pump piston chambers are connected mechanically in series on the same drive shaft, but they are connected hydraulically in parallel. Thereby, the volumes of the three piston chambers are additive to provide a larger output volume from a relatively short stroke. The bi-directional pumping action provides for double the output of a single pumping action. In addition, the individual sections multiply the output by the number of sections. In this case providing for a six-fold output compared with that of the single pumping action.

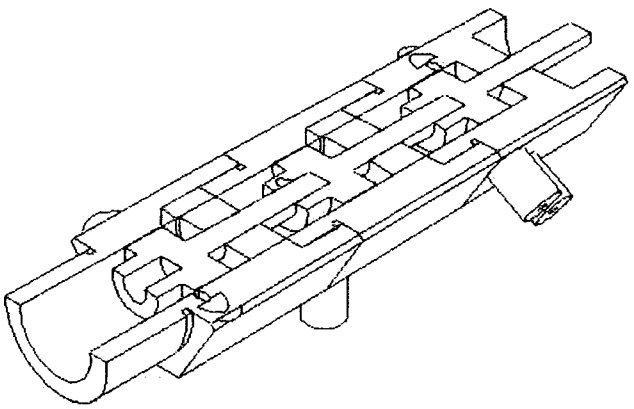

Figure 6.2 – Cross- section of Piston Chamber

There is also the added bonus of being able to increase the number of sections according to demand. This provides for advantageous use of a solar powered water pump system.

This method of improving the output flow rate has been incorporated in the design shown in figure 6.3. The brown section is the piston chamber; the yellow section is the permanent magnet braking system, which prevents impact of the armature against the E-core, and the blue hexagonal chamber is the 6:1 ratio manifold for the discharge of the six outlet valves. The section is encased within a filter mesh to prevent blockage of the inlet valves.

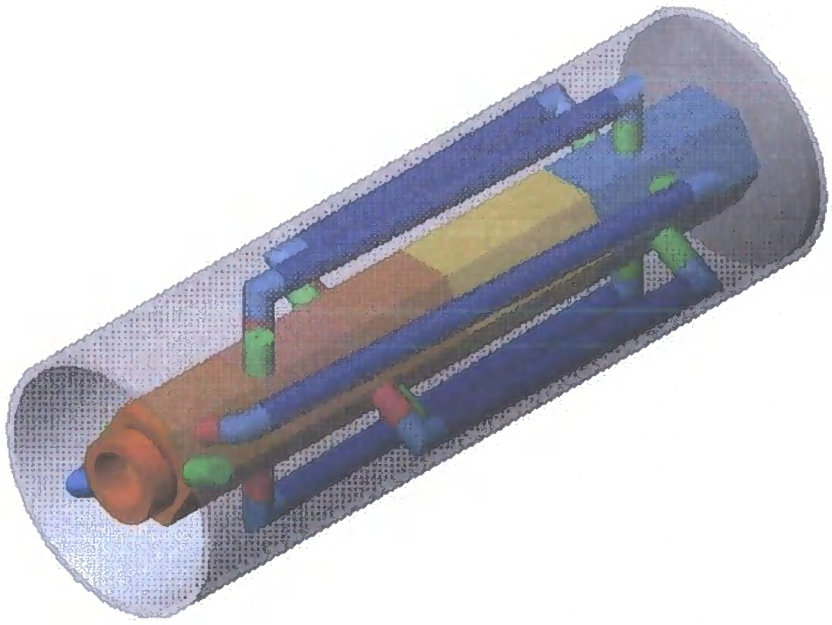

Figure: 6.3 – Multi-section piston chamber with inlet valves, PM braking system chamber, and 6:1 ratio outlet valve manifold chamber.

CHAPTER 7

Chapter 7
Discussion

7 Introduction

This chapter gives a general discussion of the findings of the research.

7.1 Discussion

Previously designed systems appear to have matched off-the-shelf components, in order to standardise the systems and system parts, and reduce costs. However, this may not be the most favourable solution for the application and the environment in which the system is being used. Drive systems for PVPs operating in a rural community in the South ought to be cheap, robust, exhibit high performance, is reliable, and maintainable by an untrained user. The literature review and background investigations indicate that reductions in cost and gains in reliability can be achieved by minimising the complexity of power electronics and reducing the number of electro-mechanical stages in the drive system.

Consequently, to have an 'off the shelf' pump for universal use, rather than having to design a pump for each individual circumstance, would be of great benefit in improving the number of installations for photovoltaic powered water supplies. At present, this is not possible without a new design of pump. Consequently, a relatively new technology has been chosen, a linear actuator. The principle of this kind of Driver is understood, and is now implemented as an integral part of 'An Induced-Flow Solar Powered Water Pump'.

The aim was to achieve a pump that would pump at least 10 bar pressure and a flow rate of one litre per second. The pump is to be used in conjunction with an induced flow system, which will at least double the output.

Measurements show that Linear Actuators as Drivers for Submersible Water Pumps in Boreholes are feasible. From the theory shown in §4.2 and the results of the initial force tests §4.3 it can be seen that the E-core linear actuator can generate a normal force in excess of $400kNm^{-2}$ when there is a flux density of 1T within the airgap. However, this force collapses rapidly once the E-core is no longer in saturation which in turn limits the stroke length of the actuator. Nevertheless, the pump tests results in §4.9 show that it is possible to achieve approximately 90% of the desired delivery head at larger stroke lengths, although at a greatly reduced head. Therefore, the pump design needs to be modified, so as to achieve the required specifications.

The whole system has been investigated from photovoltaic array to controllers, pumping system through to the reservoir. The main focus is to be the design of the actuator for the pumping system. Starting at the PVP, it was discussed that MPPT would be required to control the system. However, after investigation, the control was far better achieved within the actuator section of the pumping system.

The variations in light intensity can be catered for by increasing the number of solar panels in the solar array; any excess supply could be diverted to other systems within the community, such as batteries. Seasonal variations in light intensity are also catered for with the increased number of solar cells. Earlier in the literature review, it was discussed about the batteries compensating for the deficiency in light intensity. However, this is a negative approach and it would be far better to use excess energy.

One aspect of the actuator, which could potentially be a problem, is the heat generated within the system, in particular the E-core due to the large energy exchanges. In order to compensate for this, thermistors or varistors can be used to control the core temperature by limiting the current through the windings. Therefore, the load line of the IV characteristic of the solar cells will deviate little, providing a constant supply, thus removing the need for an MPPT.

As previously mentioned the pump system consists of two parts – the linear actuator and induced flow system. Even though the induced flow system is outside the scope of this work, it needs to be considered because the overall flow rates needs to be one litre/sec. The induced flow section of the system doubles the output at high heads and increases the output at low heads by a factor of π. Consequently, the output from actuator pumping section, ideally one litre/sec, only needs be half of this flow rate.

Due to the nature of the application size restrictions of space and diameter are imposed on the actuator because the design is to achieve a pump that will fit down a four inch borehole. Therefore, the actuator must fit within the internal dimensions of the pump chamber, which is smaller than the diameter of the borehole. Additionally, there is an overall length limitation of the complete pump and induced flow system due to the straightness of the borehole. The actuator system has been designed within these physical restrictions of space and diameter.

The actuator must be capable of pumping a delivery head of up to 100m. 100m equates to approximately 10 bar pressure. However, the actuator must first overcome the static force, which is the minimum amount of force required before the pump begins to pump. By example, the worst-case static force for a pump with a diaphragm size of 96mm and a 19mm outlet pipe, to pump against a dynamic head of 100m is 346N. This is the static force that the pump must overcome before it does any useful work.

The pumping force requirements vary seasonally and as the force due to the submerged head rises and falls. However, should the ratio of the diaphragm or piston and the outlet pipe be 1:1, then a constant force can be utilised over the entire depth. Useful equations have been developed which enable calculation of the piston size and pipe diameter from a known force developed by the actuator for a specific depth of borehole.

The flow rate is dependent on the frequency of operation and the stroke length. Obviously the smaller the stroke length, the greater the frequency, therefore, work has been focused on increasing the stroke length of the actuator.

Concepts for achieving the linear motion have been discussed. The decision to use linear motion is to try to reduce the losses in a circular motion being converted to linear motion.

Forces of attraction and repulsion are both considered. Solenoids were investigated, along with toroids, C-cores and E-core. Solenoids have been used for many years for door latches and locks. However, to generate the required forces the physical envelope was considered to be too large, and therefore disregarded, and similarly for toroids.

Both C-cores and E-core were found to be able to produce both tangential and normal forces, which created a linear motion. C-cores §4.1.3, in conjunction with permanent magnets as shown in Fig. 4.8 – Fig. 4.11, were found to be capable of producing sufficient force with a long stroke length. The permanent magnets within the system were encompassed in the translator. However, this method is considered dangerous because of the tendency of the like poles of the magnet to dislodge, as discovered during construction. It also proved to be difficult to build the system due to the powerful magnets that were used.

Consideration was therefore given to C-cores and E-core using a normal force. Two types of C-cores and two types of E-core were examined, for which the resulting forces for different styles of cores are shown in figure 4.23 and are covered in §4.1.3 and §4.1.4. As can be seen from figure 4.23, E-core type 2 generates by far the greatest force. Therefore, this type of core was chosen to be taken further. However, C-core type 2 cannot be ruled out because of its more linear response over a longer stroke.

The development of the E-core 2 type system proved that the forces generated by such an E-core have an inverse square relationship for the distance force

relationship and the constant of the characteristic equation is a function of the dimensions of the E-core, §4.2.6, Eq^{n}. 4.15.

As with all magnetic materials, at some stage it will reach saturation point, this has been taken to be at the knee of the BH curve. Equation 4.18 was developed with the aim of determining what the minimum stroke length before saturation occurred, at which point the generated force would become constant. From that point the armature of the actuator would traverse the remaining airgap distance due to momentum and the magnetisation attraction force of the armature. The results of §4.3.6 and §4.9 show that the actuator achieves a high constant force within the saturation region.

However, the current used to maintain the magnetism would increase and would dissipate as heat, further adding to the existing thermal problems. Consequently, some form of cooling is required, either by a heatsink or by cooling it with borehole water. This has yet to be tried. Should the borehole run dry, a safety thermal trip could be installed.

There are further considerations, in that a temperature change of 60°C from a base of 20°C in a typical ferrite core leads to a 25% drop in permeability, hence a rise in reluctance, and reduction in magnetic flux and flux density, and ultimately a reduction in the force. On a positive note, saturation causes a drop in inductance, which results in an increase in the rate at which the current in the coil increases. This enables a higher operating frequency of the actuator.

With respect to the material of the core, and the saturation point, at present the material that can generate the highest level of magnetisation is iron-cobalt alloy, containing 35% cobalt, with a saturation point of 2.34T, so the maximum possible force possible within the airgap can be evaluated using Maxwell's stress equation inserting this value. However, this material is expensive. Consequently, a cheaper material such as mild steel, which saturates between 1.1 & 1.4T depending on the alloy content, has been chosen. The material in the tests was unknown, because the E-core were cannibalized from old equipment, but was assumed to be mild steel.

The modelling was done with mild steel, and the material used, not being mild steel, could attribute to some of the differences between the theoretical and practical results.

The practical results have proven that an airgap flux of 1T can generate forces in excess of $400kNm^{-2}$. This force is dependent on core material and the core dimensions.

Theoretically the E-core shown in Fig. 4.29 can generate a force of 1259N within an airgap of 0.90975mm; the model value was 1134.5N, the difference was attributed to the fact that the relative permeability in the model was fixed at 2000. The Load Cell calculated generated force was 652N, and the flux density Hall probe method was in close agreement at 641N. The difference/losses are in the region of 48-49%. Some of the losses could be attributed to the unknown material of the E-core and the relative permeability of that material being greater than that of mild steel, because the greater the relative permeability the greater the force, as shown previously. The remainder of the losses were attributed to fringing, which accounts for approximately 25%, and the remainder attributed to mechanical, head, and thermal energy losses.

A method of increasing the force is to increase the number of turns, obviously. Physically, this can only be done by extending the length of the E-core because of the restrictions imposed by the overall diameter. This also has the benefit of changing the point of saturation to a point where saturation occurs at a larger airgap. Therefore, a constant force can be generated over a larger airgap, making the landing of the armature on the E-core softer. Although the impact of the armature against the E-core would have the benefit of demagnetising the armature before the return stroke, so reducing residual magnetism on the second half of the cycle, avoidance of impact is essential because the mild steel work-hardens and deform and the pump will eventually self destruct. To avoid the impact of the armature against the E-core, various methods can be considered: -

1. A magnetic means of preventing the impact is to install a braking system that utilises two permanent magnets, with like poles facing each other, therefore acting under repulsion. When the permanent magnets are in close proximity the repulsion force prevents the impact of the armature on the E-core. However, the PM braking system must be installed at such a distance that it will not affect the electromagnetic field of the E-core. The permanent magnets could be used in conjunction with a pneumatic piston airbrake, with the moving permanent magnet acting as a piston, which compresses air. The use of the PMs has the additional benefit of aiding the electromagnetic force at the start of the return stroke due to the repulsion force of the PMs.

2. Two mechanical means of preventing impact both involving the use of springs, are the use of freestanding (unattached) springs that engage the armature, to reduce the force, prior to impact, so providing a soft landing for the armature, and the use of springs where the neutral point is central to the distance between the two E-cores. The energy stored in the springs opposes the magnetising force and stops the armature from impacting onto the E-core.

3. Achieving the same result by an electrical means is via the supply switch timing. The switching mechanism of the pump can be used to de-energise one coil prior to completion of the full half-cycle, whilst the other E-core energises, thus reversing the direction before impact occurs. Alternatively, bring forward the switching time thus permitting one coil to be energised before the other has de-energised, therefore prior to the start of the return stroke a high force is generated.

The E-cores used in the tests are oversize and will not fit into a four-inch borehole; therefore, the size of these E-cores must be reduced. Consequently, if the same dimensional ratios are kept, the force will be reduced. In order to compensate for this, the length of the E-core legs can be increased, thereby increasing the number of turns and maintaining the m.m.f. In addition, the force can be maintained, if two or more E-cores are connected in parallel electrically and operate in series mechanically, providing there is equal current in each winding. The force is

increased directly in proportion to the number of E-cores within the stack. This term is now referred to as 'stacked' E-core. With respect to stacked E-cores, the inductance increases when the length of the E-core legs are increased due to the number of turns, but this is compensated for by connecting the windings in parallel, which reduces the inductance.

The inductance of the 'two E-core system' under static conditions is inversely proportional to the airgap distance. However, once the armature begins to move, the inductance also becomes a function of the current. The back e.m.f of the coils is directly proportional to speed for any value of airgap distance. It is also a function of the inverse square of the distance, and therefore more relevant at small airgaps. Consequently, the control of the system becomes more difficult due to the non-linearity of the system.

Irrespective of the type of control, whether mechanical, electronic, or electromagnetic, the stored energy in the inductor must be dealt with on switching. Several methods have been shown, of which the cheapest and most practical is the use of a reservoir capacitor connected across the circuit supply, and decoupling capacitor across the main switch, to which the inductor electrical energy is returned. Therefore, there is a minimal energy loss. Even though there are electronic circuits, such as PWM, that remove the need for this, this is by far the cheapest method.

The first pump that was built only achieved a delivery head of 1.2m. This was due to the contact time of the switches being of insufficient length. Consequently the opposite E-core did not have time to energise fully, so did not generate any sizeable force. In addition, the inlet valve system was poor in design, and the seals failed, flooding the chamber with water. Therefore, the armature of the actuator was not in free air, and agitated the water, losing pumping effort in the process. There was a problem with the carbon brushes in that the support leg snapped after only a few minutes of cycles. In addition, the loading springs for the carbon brushes were vaporised due to the large energy discharge, and high current density. There were also no capacitors in the system to return energy to the system, which resulted in large voltages on interruption of inductively driven current.

However, this system was then connected directly to a twin two-transistor forward converter, at which point the pump would operate indefinitely. Therefore, the aforementioned electrical problems only account for some of the failure.

In order to obtain a greater force and increase the delivery head the airgap was then reduced to 1mm and the reduced flow rate would be compensated for by increasing the frequency. However, at 7Hz the pump output became intermittent, the actuator started to latch-out, and after a short period the pump stopped working. On inspection, it was noted that the two bolts holding the bottom E-core in place had deformed to such a degree that the airgap had collapsed. The forces generated by the electromagnets had caused the two E-cores and the armature to lock together.

This gave cause to doubt the previous results because throughout the bottom E-core could have, and probably did move, and by doing so, the airgap varied. Therefore, the force would have been reduced, resulting in less pressure for the delivery head, and the flow rate being reduced due to a reduced volume of water being pumped.

The above pressure values produced were when using a diaphragm of 96mm diameter. In order to increase the pressure a smaller diaphragm is required, because the pressure is inversely proportional to the cross-sectional area of the diaphragm. Therefore, having the same available force with a smaller denominator (cross-sectional area) provides greater pressure and depth. However, the consequence of doing so is that the volume of water for pumping is reduced giving a reduced flow rate. In order to compensate the stroke length needs to be increased, thus reinstating the original flow rate. This also has a negative attribute because the field strength, hence the available force, reduces inversely by the square of the airgap distance.

The flow rate is a function of pumped volume (i.e. the product of the diaphragm/piston size and the stroke length), and the frequency of operation. An improved flow rate can be achieved by increasing any, or all, of the above.

The diaphragm system needed further investigation. Due to design and technical problems, it was decided to change to a piston type pump.

A 19mm bore brass piston chamber with a ptfe piston was used because of the low coefficient of friction. As with the previous pump, this was connected to the twin two transistor forward converter drive circuit, and achieved pressures in excess of 10 bar, so proving that the actuator is capable of achieving the required borehole depths. However, the flow rate was poor, at best, 0.126litres/sec, which was approximately an eighth of the required flow rate. It was also found that this flow rate changed with the frequency of operation of the pump, as expected. Nevertheless, some losses were noted, and this was attributed to the frictional losses of the piston. Although the piston was unidirectional in that it only pumps one way, this could be improved or doubled if it pumped in both directions.

Having achieved the desired pumping pressure, it was necessary now to improve the flow rate, by changing the length of the stroke, either mechanically or electrically.

The electrical option would have required new E-core to be built and ideally with a stack system to minimize the overall size of the pump. As previously mentioned, another method of increasing the stroke length would be to install mechanical lever arrangements. However, this had to be ruled out due to the number of cycles required, some 210 million per year, on the operating basis of eight hours per day at a frequency of 10Hz. The more moving parts, the greater the risk of mechanical and fatigue failure. The best option is to use a piston multiplier system where three pistons or more are connected in series and pumping hydraulically in parallel. Any more than three becomes practically difficult to assemble. If the pump is pumping bi-directionally, this will give a six-fold improvement in the output. Therefore, it is recommended that any future pump should use this in conjunction with the electrical improvement of stroke length.

Permanent magnets were attached to the armature with the intention of opposing the electromagnetic field of the coils, thereby creating a null and a repulsion force.

This was envisaged to act at the same time as the other core was under an attraction force, thereby creating a greater force in one direction. However, practically this was not possible because during tests, initially there was a repulsion but when the airgap was reduced, the field flipped, attracted to the E-core, and the system locked. Although this system failed when using mild-steel E-core, it may be possible if another material was used such as iron-cobalt alloy, containing 35% cobalt, which generates a field of 2.34T. The permanent magnets field of 1.2T would then be weaker by comparison, and would repel. This has an additional benefit, which would need to be proven, in that it could alternatively act as a brake to stop the impact of the armature against the E-core.

Modelling has shown that two opposing permanent magnets external to the armature, and therefore acting under repulsion, can act as a brake when confined within a chamber.

Other future work could be to consider C-core type 2, which generated a more linear force over a larger stroke length. Even though the force was not as high as the E-core, stacked C-cores could make them viable.

Further considerations for improvement of the actuator could be to insert a permanent magnet with the field in series with the core field. This enhances the attraction force and provides easier control. Polarised actuators give a linear I-F characteristic, therefore making them easier to control, (Re: Chapter 2). If this is used in conjunction with the permanent magnet braking system, a contact free oscillating system can be achieved because there is no impact of the armature. The system would operate by the armature moving towards the E-core, which is prevented from impacting by the permanent magnets. Whilst that E-core is energised, the armature would be held in that position until the coil is switched off. During this time the other E-core is energising and is then switched, at which point there is no force holding the armature in place, and a small repulsion force initialises the motion in the opposing direction in conjunction with the activated coil having the attraction force.

The spring investigation revealed that springs did little to enhance the electromagnetic force, and would be best used for the braking mechanism to prevent impact. Alternatively, springs could be used to do the pumping and the electromagnets of the actuator only did the switching of the direction of the spring force. The only gain found with the use of springs was the initial rate of change of the linear spring force, which was minimal in comparison to the electromagnetic force generated.

For security reasons any controller, in whole or by part, may be submersed along side the pump system.

Ideally, to complete the system, a reservoir large enough to store enough water to cover maintenance or breakdown, should be installed so that there is a constant supply of water.

The main use is envisaged as pumping water from boreholes; however, alternative uses for the pumps can be envisaged, such as a surface pump, pumping water from a river to a village some distance away. As the demand for 'clean water' increases, it provides for sustainable development.

CHAPTER 8

Chapter 8
Recommendations

8 Recommendations

In addition to the recommendations of §4.10.4 for improving the performance of the present D.C. powered linear actuator water pump other recommendations are as follows:-

1. Design a self-oscillating system.

2. Prevention of the impact of the armature against the E-core/s - In order to develop a robust and reliable pump which utilises an E-core electromagnet actuator as the driver for the pump, the prevention of the impact of the armature against the E-core/s is paramount. To prevent the inevitable damage and loss of energy this can be achieved by any or a combination of three methods.
    - Electrically, by bringing forward the switching time thus permitting one coil to be energised before the other has de-energised, therefore prior to the start of the return stroke a high force is achieved.
    - Mechanically, with the use of springs, where the springs engage the armature to reduce the force prior to the impact of the armature against the E-core, so providing a soft landing for the armature.
    - Magnetically, with the use of permanent magnet braking system that utilises two permanent magnets attached to the drive shaft of the pump, with like poles facing each other, therefore acting under repulsion.

3. Carbon Brushes - Redesign the carbon brush switching system, using a more robust material for the support brackets, or use a new design, such as a cam

to control the switching time. Use spring-loaded contacts to maintain contact for a longer duration to ensure that the return coil has energised completely. In addition, change the type of springs in the spring-loaded contacts that maintain the contact to a bevelled spring instead of the present helical spring.

4. Anchorage - Improve the robustness and anchorage of the E-core/s mountings by replacing the mild steel studding E-core mounting bolts with silver steel, plus increase the diameter of the shafts, and harden and temper the shafts if necessary.

5. Seals - Redesign the upper and lower pump chamber water seals of the chamber separation plate, and the seal of the base plate, ensuring that the lower pump chamber is watertight.

6. Valves - Redesign the inlet valves making them less stiff by trimming the rubber. In addition, enlarge the inlet valve holes and experiment with different materials for the valve flaps. Alternatively, change the design of the valves or use standard valves.

7. Diaphragm Pump - For the diaphragm pump, use a thinner and smaller diameter diaphragm making it less stiff. Also, ensure that the seal around the diaphragm is watertight. As with the inlet valves experiment with different materials.

8. Piston Pump - For the piston pump, use an O-ring on the piston this has been shown to improve the performance of the pump by decreasing the backpressure losses.

9. Thermal Solution - Investigate methods for the prevention of overheating of the actuator, particularly the use of the borehole water and surrounding earth as a heat sink.

10. Investigate direct contact of the water with a waterproof electrical circuit as a means of cooling the E-core.

11. Stacks - Investigate a stacked E-core system, where the E-cores are connected electrically in parallel, with the armatures connected mechanically in parallel.

12. Multiplier - Investigate multistage piston (or diaphragm) chambers, where the pistons are mechanically connected in series and the water is pumped hydraulically in parallel, to improve the output flow rate.

13. Diaphragm Pump - The theoretical flow rate is as expected a linear response; however figure 4.62 shows that the practical flow rate is greater than the theoretical flow rate. Why is this anomaly happening? Both the theoretical evaluation and the practical calculations have been checked and crosschecked and no error could be found. Therefore, the actual measurements from the tests are questionable. Nevertheless, the anomaly only occurs when the pressure is at 0Bar, irrespective of the frequency and airgap setting. Therefore, to resolve the issue, and determine whether something else is happening, more tests are required.

14. Piston Pump - Again, the anomaly occurs, where the practical flow rate is greater than the theoretical value, albeit over a lower frequency range. It is difficult to justify the variations in flow rate for the Q-f characteristic (0Bar), and as stated previously, further tests are required to confirm or disprove the results. However, the spikes can be explained; neither the current nor the voltage were constant, therefore the spikes can be attributed to the fluctuations in the power.

15. Investigate Two E-core push pull system
    - With permanent magnets built into the armature
    - With permanent magnets in series with the flux path of the E-core
    - With permanent magnets in parallel with the flux path of the E-core

- With dual action, pumping in both directions

16. Develop the tangential linear actuator permanent magnet linear machine. This has a dual purpose, to determine the practicality of such pumps and to act as a comparison for the normal stress linear actuator.

17. Design a test rig to approximate field conditions. Test all pumps under these conditions and evaluate their potential.

18. Investigate the suggested possible future development issues raised in chapter 6.

CHAPTER 9

Chapter 9
Conclusions

9 Conclusions

1. The normal force for the E-core electromagnetic topology based on the variable reluctance principle is in the excess of 400kNm^{-2}. From the theory shown in §4.2 and the results of the initial force tests §4.3 it can be seen that the E-core linear actuator can generate a normal force in excess of 400kNm^{-2} when there is a flux density of 1T within the airgap.

2. The E-core electromagnetic linear actuator is restricted to short stroke lengths by the collapsing electromagnetic field, hence force, beyond the saturation point, (Re: §4.9.1, figures 4.60 & 4.61), it is possible to achieve the required flow rate of one litre per second. Providing the E-core remains in saturation a high force will be generated, thus maintaining both the force to overcome the static head and the pressure. Therefore minimal modifications are required for the pump actuator. However, the control system then becomes the governing factor.

3. In the case of the use of solar panels for the D.C. power supply, there is no need for a Maximum Power Point Tracker (MPPT) or complex electronics to control the system providing that the energy is returned to the system via capacitors, and the mechanical switching device maintains contact and holds the current for sufficient time as to energise the second E-core before switching.

4. An electromechanical switching system, such as carbon brushes can be used, §5.7, figure 5.14.

5. Variations in climate conditions and demand rates can be catered for, §3.4. There is a natural match between the availability of UV (and other wavelengths of light associated with solar cells) and the need for water. The system pumps more water during summer months – longer-hotter days, typically when more water is needed.

6. With the use of solar panels as the D.C. power supply variations in geographical location and borehole depths can be catered for, §3.4.

7. The actuator utilises a renewable energy source giving potential for global use and provides for sustainable development.

8. It is possible to build a self-oscillating, impact free system. This can be achieved with the use of points 2 and 3 above, in conjunction with the use of springs §4.5 and/or the use of permanent magnets §6.1, in particular the use of magnetic brakes §6.1.2.

9. The principle of operation of the Linear Actuator Water Pump is valid. The electromagnetic force collapses rapidly once the E-core is no longer in saturation which in turn limits the stroke length of the actuator. Nevertheless, the pump tests results in §4.9 show that it is possible to achieve approximately 90% of the desired delivery head at larger stroke lengths, although at a greatly reduced head. Therefore the pump design needs to be modified, so as to achieve the required specifications.

10. An E-core linear actuator that utilises a normal force when incorporated within a pump can achieve the desired 10 bar pressure and one litre per second flow rate. In the case of the piston pump; prior to the use of an induced flow system the output flow rate of the pump can be increased with use of the multiplier shown in §6.6. In the case of the diaphragm pump; the output flow rate can be improved by making the pump dual action that is pumping in both directions.

11. The least amount of force is required for a diaphragm pump when the flow rate ratio of the diaphragm to outlet pipe size is 1:1.

12. The linear actuator pump has the capacity to be used at a far greater number of sites than a centrifuge pump because it covers a larger range of delivery heads. Therefore it may be possible to design an 'off the shelf' submersible water pump that is suitable for all sites.

APPENDICES

Appendix 1

Flow Charts

The Significance of Material Choice on the Performance of the Linear Actuator

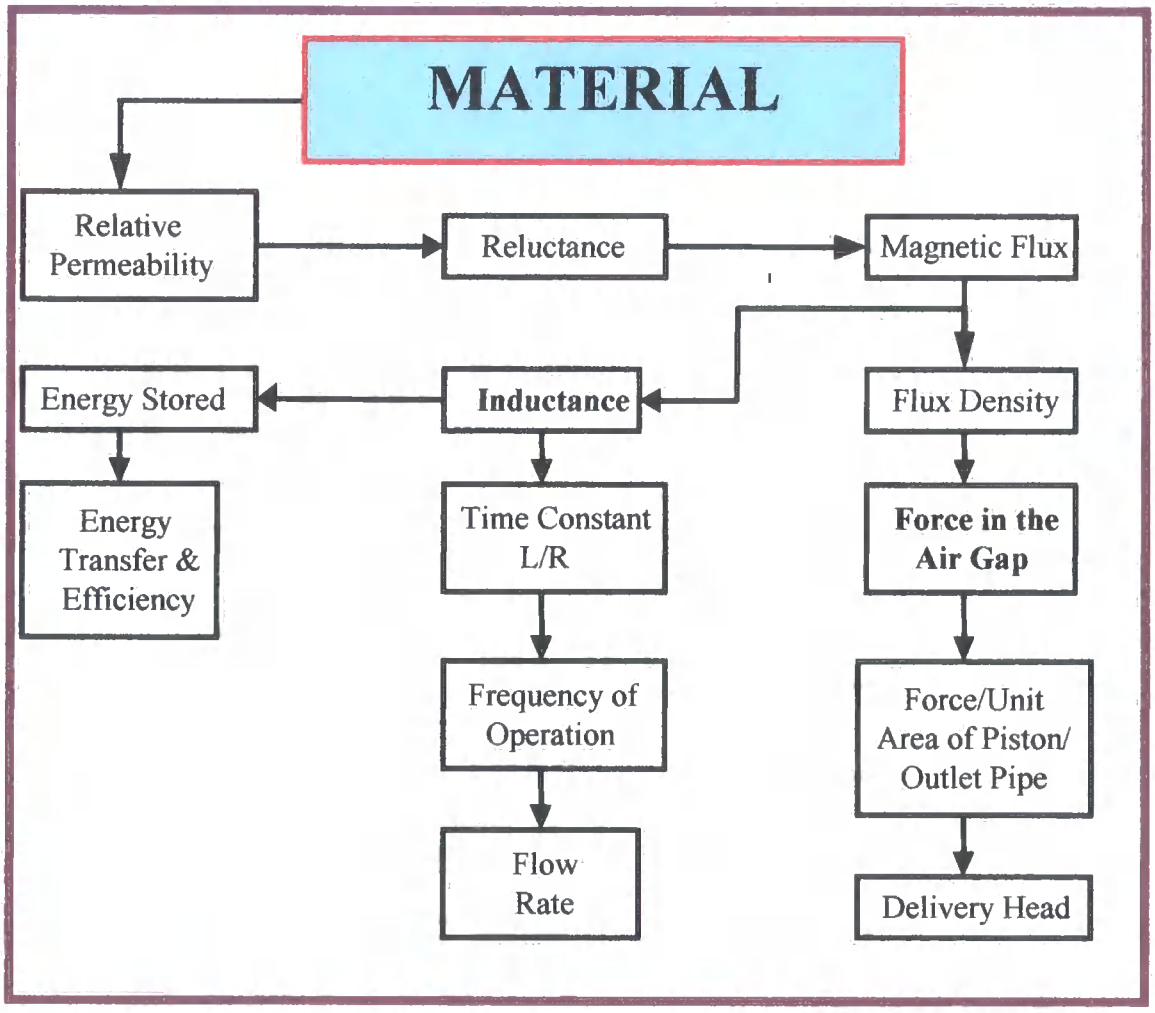

Factors Affecting the Magnetic Flux

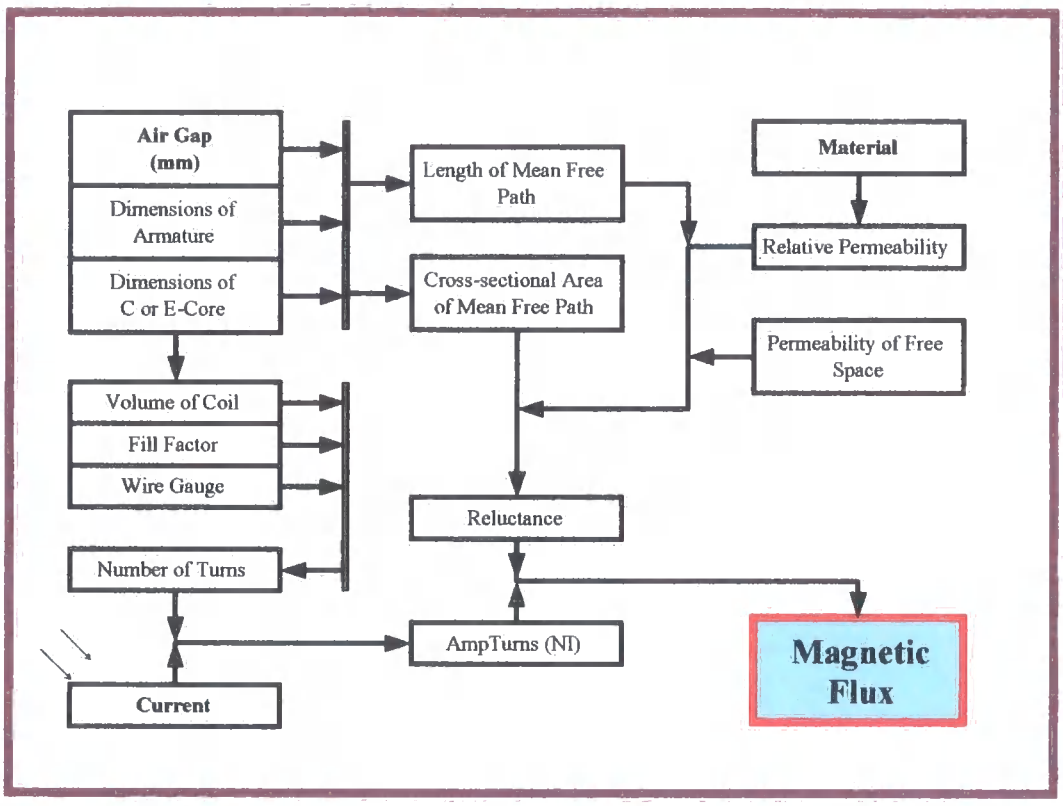

The Effect of Current Change on the Performance of the Linear Actuator

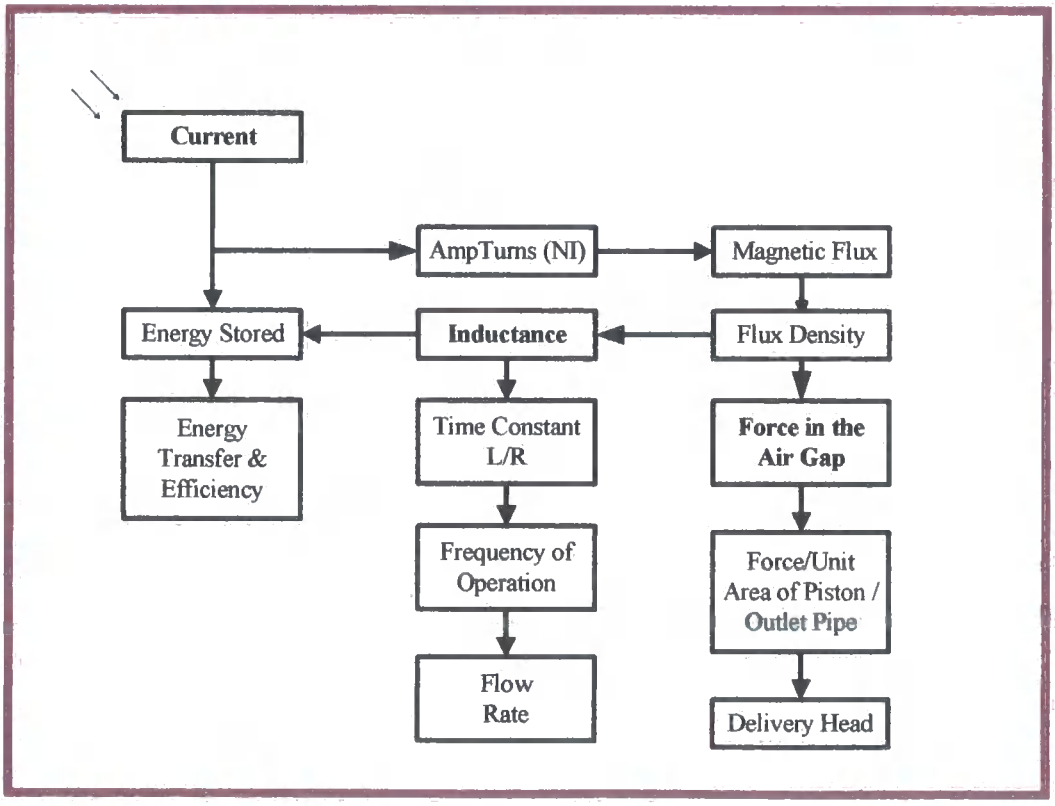

The Effect of Change in Air Gap Size on the Performance of the Linear Actuator

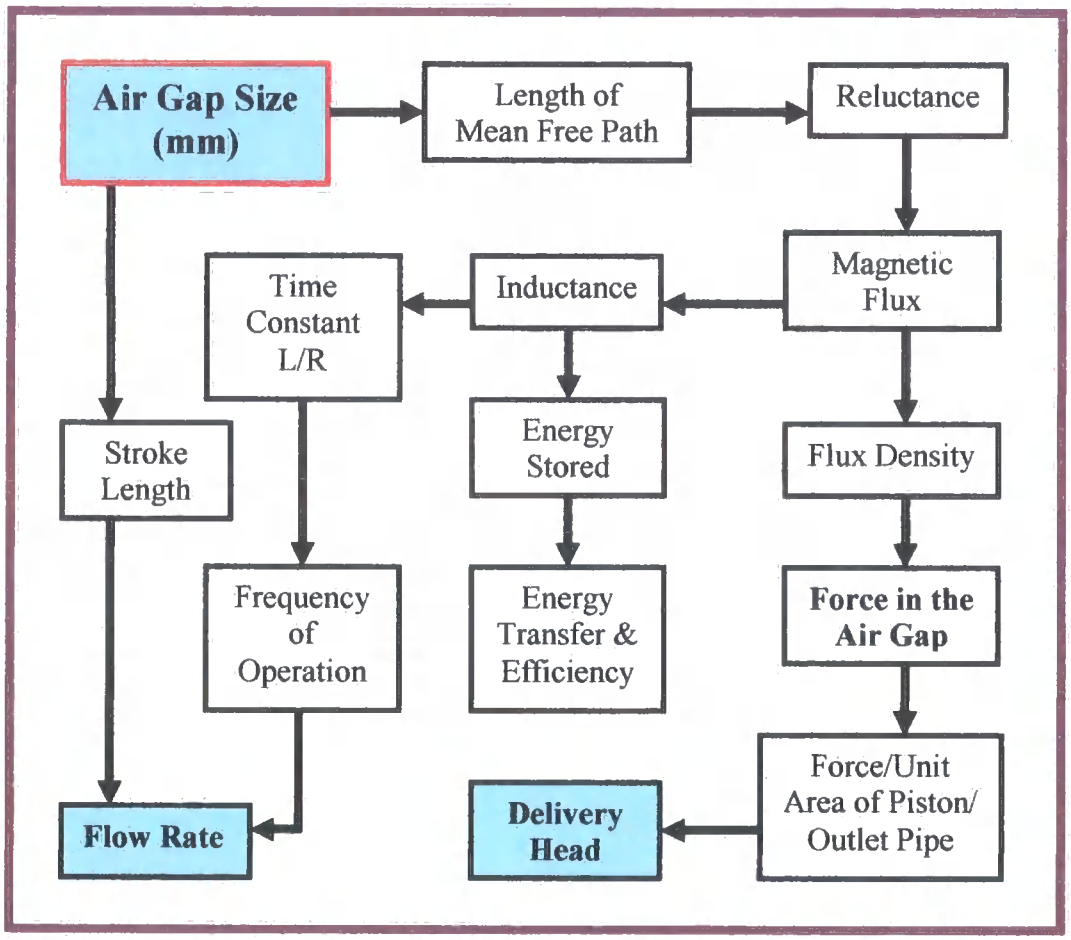

Appendix 2
R^2 Definition

An explanation of the term R^2

(As stated in Microsoft Excel Help Directory)

The equation for the Pearson product moment correlation coefficient, r, is:

$$r = \frac{\sum(x-\bar{x})(y-\bar{y})}{\sqrt{\sum(x-\bar{x})^2\sum(y-\bar{y})^2}}$$

Where x and y are the sample means AVERAGE (known_x's) and AVERAGE (knowns_y's).

RSQ returns r^2, which is the square of this correlation coefficient.

PEARSON – Returns the Pearson product moment correlation coefficient r, a dimensionless index that ranges from -1.0 to 1.0 inclusive and reflects the extent of a linear relationship between two data sets.

The square of the correlation coefficient (r) is R^2 which is the coefficient of determination for trend line regression analysis. A trend line is most reliable when its R-squared value is at or near 1, i.e. unity.

The CORREL and PEARSON worksheet functions both calculate the correlation coefficient between two measurement variables when measurements on each variable are observed for each of N subjects. (Any missing observation for any subject causes that subject to be ignored in the analysis.) The Correlation analysis tool is particularly useful when there are more than two measurement variables for each of N subjects. It provides an output table, a correlation matrix, showing the

value of CORREL (or PEARSON) applied to each possible pair of measurement variables.

The correlation coefficient, like the covariance, is a measure of the extent to which two measurement variables "vary together." Unlike the covariance, the correlation coefficient is scaled so that its value is independent of the units in which the two measurement variables are expressed. (For example, if the two measurement variables are weight and height, the value of the correlation coefficient is unchanged if weight is converted from pounds to kilograms.) The value of any correlation coefficient must be between -1 and +1 inclusive.

You can use the correlation analysis tool to examine each pair of measurement variables to determine whether the two measurement variables tend to move together that is, whether large values of one variable tend to be associated with large values of the other (positive correlation), whether small values of one variable tend to be associated with large values of the other (negative correlation), or whether values of both variables tend to be unrelated (correlation near zero).

The r-squared value can be interpreted as the proportion of the variance in y attributable to the variance in x.

Appendix 3

Errors in Results

RESULTS Airgap (mm)	Theoretical Force (N)	Excel Model Force (N)	% Error – when compared to theory
0.90975	1259.33	1134.48	9.9%
1.41	524.26	489.80	6.6%
1.62	397.15	374.28	5.8%
2.48	169.46	162.99	3.8%
2.75	137.82	133.06	3.5%
3.175	103.39	100.29	3.0%
3.46	87.06	84.66	2.8%
5.08	40.39	39.62	1.9%

RESULTS Airgap (mm)	Theoretical Force (N)	S-Type Load Cell Force (N)	% Error – when compared to theory	Hall Probe Force (N)	% Error – when compared to theory
0.90975	1259.33	652.02	48.2%	641.23	49.1%
1.41	524.26	427.83	18.4%	377.82	27.9%
1.62	397.15	279.10	29.7%	255.59	35.6%
2.48	169.46	163.27	3.65%	139.28	17.8%
2.75	137.82	136.72	0.8%	128.82	6.5%
3.175	103.39	112.45	-8.8%	95.02	8.1%
3.46	87.06	90.95	-4.7%	86.48	0.7%
5.08	40.39	46.86	-16%	39.70	1.7%

References

1. O'Neill. P., *Environmental Chemistry.* 1991 ed. 1991: Chapman & Hall. 232.
2. Andrews. J.E., et al., *An Introduction to Environmental Chemistry.* 1996: Blackwell Science Ltd. 209.
3. Merritts. D., D.W.A., Menking K., *ENVIRONMENTAL GEOLOGY - An Earth System Science Approach.* 1997: W. H .Freeman and Company. 452.
4. Pipkin. B.W. and Trent. D.D., *Geology and the Environment.* Second Edition ed. 1994. 522.
5. Howard. G. and Bartram. J., *Domestic water quantity, service level and health.* 2003, WHO: WSH.
6. Gallon. G., *6.2 Billion World Population put Pressure on Human Life-Support Systems.* The Gallon Environment Letter, 2001. **5**(29).
7. ENS, *Growing Population Stamps Heavy Ecological Footprint*, in *Environment News Service (ENS).* 2001: New York.
8. McGuire. B., Mason. I. and Kilburn. C., *Key issues in environmental change - Natural Hazards and Environmental Change.* 2002: (Co. Pub.) Arnold, London / Oxford University Press Inc., New York.
9. Blaike. P., et al., *At Risk.* 1994: Routledge, London.
10. Jones. P.D., Briffa. K.R. and Tett. S.F.B., *High resolution palaeoclimatic records for the last millennium,* in *The Holocene.* 1998. p. 455-471.
11. Tett. S.F.B., et al., *Causes of twentieth-century temperature change near the Earth's surface*, in *Nature.* 1999. p. 569-572.
12. Roaf. S., *Designing for Climate Change.* in *Architectural Education Exchange 2001.* 2001. Cardiff University: AEE2001.
13. FWR, *The Development of Effective Community Water Supply Systems Using Deep and Shallow Well Handpumps Report No TT 132/00.* 2000.
14. Short. T.D. and Oldach. R., *Solar Powered Water Pumps: The Past, the Present - and the Future?* in *ASME International Solar Energy Conference - SOLAR 2002: Sunrise on the Reliable Energy Economy.* 2002. Reno, Nevada, USA.

15. UK/Meteorological/Office, *Observations, Predictions, and Climate Change.* 1999, Metoffice.
16. Short. T.D. and Thompson. P., *Breaking the Mould: Solar Water Pumping - the Challenges and the Reality.* Solar Energy, 2003. **75**(1): p. 1-9.
17. Gleick., (2000), *Potential Conflict Zones*, in *Vital Water Graphics, United Nations Environment Programme.* 2004, UNEP.
18. UN, *Sources and nature of water quality problems in Asia and the Pacific.* 1998: United Nations Publication. 164.
19. WDM, *Corporate pirates up close and ugly.* 2004, World Development Movement - Justice for the world's poor.
20. Villars, (1999), *Potential Conflict Zones*, in *Vital Water Graphics, United Nations Environment Programme.* 2004, UNEP.
21. WDM, *WDM's response to the UN conference on Financing for Development- Monterrey, 18-22 March 2001.* 2001, World Development Movement: London. p. 6 para.17.
22. UNCTAD, *Economic Development in Africa: Performance, Prospects and Policy Issues.* 2001, Geneva.
23. WDM, *THE MISSING LINK - Debt and Trade.* 2000, World Development Movement - Justice for the world's poor: London.
24. WDM, *GATS The forgotten battle over WTO investment rules.* 2004, World Development Movement: London.
25. UN, *Resolution adopted by the General Assembly [without reference to a Main Committee (A/55/L.2)] - 55/2. United Nations Millennium Declaration.* 2000, United Nations. p. 5, Section III, para.19.
26. UN-CESCR, *The right to the highest attainable standard of health: E/C.12/2000/4. (General Comments).* 2000, United Nations - Economic and Social Council. p. Section II.33, and footnote 23 of General Comment No. 14.
27. UN-CESCR, *The right to water (arts. 11 and 12 of the International Covenant on Economic, Social and Cultural Rights) E/C.12/2002/11.* 2002, UN. p. General Comment No. 15 (2002).
28. IFTA, *The key principles of fairtrade.* 2004.
29. IFTA, *The International Fair Trade Association, What is IFAT - What is fair trade?* 2004.

30. IFTA, *2003 Report on Fair Trade Trends in US, Canada & the Pacific Rim.* 2003.

31. Dunn. P.D., *Appropriate Technology.* 1978: THE MACMILLAN PRESS LTD.

32. Fraenkel,. P., *WATER-PUMPING DEVICES - A handbook for users and choosers.* Second ed. 1997, Southampton: Intermediate Technology Publications. 254.

33. Arlosoroff. S., *Rural Water Supply Handpumps Project - Laboratory Evaluation of Hand-Operated Water Pumps for use in Developing Countries.* 1983, Consumer's Association Testing and Research Laboratory: Washington, D.C., U.S.A. p. 89.

34. Yeaple. F., *Fluid Power Design Handbook.* 1984, New York and Basel: Marcel Dekker, Inc. 614.

35. The Learning Company, *Compton's Encyclopedia 2000 - Pumps.* 1999, Broderbund: Crawley. p. Electronic Encyclopedia.

36. Howe. D., *Magnetic actuators.* Elsevier Science S.A., 2000. **81**: p. 268-274.

37. Author Unknown, *Diaphragm Pumps*, M. Cain, Editor. 2005, Publisher Unknown,. p. Email form Dr P Brooking.

38. Centurion Pumping and Technical Services, *Diaphragm Pumps.*

39. Grundfo, *Solar Powered Water Pumps*, Grundfo's.

40. Pedrollo, *SK Submersible Borehole Pump Range.*

41. CEFIS GIOVANNI, *Liquid Pump.* 1982: United States Patent.

42. Eastop. T.D. and McConkey. A., *Applied Thermodynamics for Engineering Technologists.* Third edition ed. 1982, London and New York: Longman. 813.

43. Hillier. J.H.M.J., *Mechanical Engineering Science.* First metric edition ed. 1970, London, Victoria, New York, Toronto: Pitman. 447.

44. MENCARELLI ENZO (IT) and CEFIS GIOVANNI (IT), *Submerged pump with coaxial opposing pistons, driven by double lobed camshaft.* 1998: United States Patent.

45. Meinel. A.B. and Meinel. M.P., *Applied Solar Energy.* First ed. Addison-Wesley Series In Physics. 1976, London.: Addison-Wesley Publishing Company. 651.

46. UK-ISES, *Solar Energy: a UK assessment: report of the panel convened by UK-ISES to analyse all aspects of solar energy systems and to assess the potential for solar energy utilisation and research and development needs in the United Kingdom and for export.* 1976, UK-ISES: London.

47. WHO, *Water Sanitation and Health (WSH) - Water-related Diseases - Malaria.* 2001.

48. WHO, *25 Questions and answers on health and human rights.* 2002, World Health Organisation: Geneva.

49. Jesch. L.F., *Solar Energy Today.* 1981: UK-ISES. 223.

50. Short. T.D. and Oldach. R., *Solar Powered Water Pumps: The Past, the Present - and the Future?* in *ASME International Solar Energy Conference - SOLAR 2002: Sunrise on the Reliable Energy Economy.* 2002. Reno, Nevada, USA.

51. Short. T.D. and Mueller. M.A., *Solar Powered Water Pumps: Problems, Pitfalls and Potential.* in *IEE International Conference on Power Electronics Machines and Drives.* 2002. University of Bath, UK.

52. Barlow. R., McNelis. B., and Derrick. A., *Solar Pumping: An Introduction and Update on the Technology, Performance, Costs and Economics.* World Bank Technical Paper Number 168. 1993, London: Intermediate Technology Publications Ltd.

53. Derrick. A., *20 years of PV powered water pumping - successes and problems.* International Workshop on PV Water Supply Issues. 1998: Marrakech.

54. Hammad. M.A., *Characteristics of solar water pumping in Jordan.* Energy, 1999. **24**(2): p. 85-92.

55. Mosalam Shaltout. M.A., et al., *Determination of suitable types of solar cells for optimal outdoor performance in desert climate.* Renewable Energy, 2000. **19**(1-2): p. 71-74.

56. Jafar. M., *A model for small-scale photovoltaic solar water pumping.* Renewable Energy, 2000. **19**(1-2): p. 85-90.

57. Badescu. V., *Time dependent model of a complex PV water pumping system.* Renewable Energy, 2003. **28**(4): p. 543-560.

58. Akbaba. M., Qamber. I., and Kamal. A., *Matching of Separately Excited DC Motors to Photovoltaic Generators for Maximum Power Output.* Solar Energy, 1998. **63**(6): p. 375-385.

59. Arab. A.H., et al., *Performance of PV water pumping systems.* Renewable Energy, 1999. **18**(2): p. 191-204.

60. Narvarte. L., Lorenzo. E., and Caamano. E., *PV pumping analytical design and characteristics of boreholes.* Solar Energy, 2000. **68**(1): p. 49-56.

61. Kaunmuang. P., et al.,, *Assessment of photovoltaic systems in Thailand - one decade of experience.* Solar Energy Materials and Solar Cells, 2001. **67**(1-4): p. 529-534.

62. Roger. J.A., *Water and Photovoltaics in developing-countries.* Solar Cells, 1982. **6**(3): p. 295-308.

63. Muselli. M., et al., *PV-hybrid power systems sizing incorporating battery storage: an analysis via simulation calculations.* Renewable Energy, 2000. **20**(1): p. 1-7.

64. Joyce. A., Rodrigues. C., and Manso. R., *Modelling a PV system.* Renewable Energy, 2001. **22**(1-3): p. 275-280.

65. Kolhe. M., Kolhe. S., and Joshi. J.C., *Determination of magnetic field constant of DC permanent magnet motor powered by photovoltaic for maximum mechanical energy output.* Renewable Energy, 2000. **21**(3-4): p. 563-571.

66. Perris. C. and Salameh. Z., *Photovoltaic-powered Piston-type Water Pump Controlled by a Linear Motor.* Progress in Photovoltaics: Research and Applications, 1995. **3**: p. 265-271.

67. Whitfield. G.R., Bentley. R.W., and Mogotsi. B., *Improving the cost effectiveness of small solar photovoltaic water pumping systems.* Renewable Energy Sources '91. 1991: Prentice. 51-56.

68. Baker. N.J., *Linear Generators for Direct Drive Marine Renewable Energy Converters*, in *School of Engineering.* 2003, University of Durham: Durham. p. 265.

69. Brooking. P.R.M., et al. *Power conversion in a low speed reciprocating electrical generator.* in *15th International Conference on Electrical Machines.* 2002. Brugge - Belgium: Technologisch Instituut vzw.

70. Iwabuchi. N., et al., *A Novel High-Torque Reluctance Motor with Rare-Earth Magnet.* IEEE Transactions on Industry Applications, 1994. **30**(3).

71. Spooner. E. and Haydock. L.. *Vernier Hybrid Machines.* in *IEE Proceedings Part B Electric Power Applications.* 2002.

72. Weh. H., Hoffman. H., and Landrath. J.. *New Permanent Magnet Excited Synchronous Machine with High Efficiency at Lower Speeds.* in *International Conference on Electrical Machines.* 1988. Pisa, Italy.

73. Spooner. E., *High Torque Machines.* in *Manchester Machines Seminars.* 1999. UMIST, UK.

74. Sen. P.C., *Principles of Electric Machines and Power Electronics.* Second Edition ed. 1997: John Wiley & Sons.

75. Olaru, R., et al., *Magnetic fluid actuator.* Elsevier Sciences S.A., 2000. **81**: p. 290-293.

76. Sedda. E., Fageon. C., and Yonnet. J., *Permanent Magnet Actuators for Electromagnetic Valve in Automotive Applications.* in *4th International Symposium on Linear Drives for Industry Applications.* 2003. Birmingham, UK: LDIA2003.

77. Guerin. S., et al. *An original configuration of linear actuator with parallel polarization.* in *4th International Symposium on Linear Drives for Industry Applications, LDIA2003.* 2003. Birmingham, UK.

78. Burton. J.D. and Short. T.D., *Induced Flow Reciprocating Pumps Part 1.* Journal of Power and Energy, 1999. **213 Part A**(A5): p. 363-373.

79. Burton. J.D. and Short. T.D., *Induced Flow Reciprocating Pumps Part 2.* Journal of Power and Energy, 1999. **213 Part A**(A5): p. 375-389.

80. Mohan, Undeland, and Robbins, *Power Electronics: Converters, Applications and Design.* First ed. 1989: Wiley (1989) 1st Edition.

81. Lamberti. L., *PV Water Pumping System.* 2002, Durham University. p. 77.

82. Mohan, Undeland, and Robbins, *Passive Components and Practical Design Considerations, of Power Electronics, Converters, Applications, and Design.* 2nd Ed. ed. 1995.: Wiley.

83. Mogami-wire.co, *Physical Constants.* 2002, Mogami-wire.co.

84. Jiles. D., *Introduction to MAGNETISM and MAGNETIC MATERIALS.* 1996, London, Weinheim, New York,Tokyo,Melbourne, Madras: Chapman & Hall. 440.

85. Guerin. S., et al. *An original configuration of linear actuator with parallel polarization.* in *4th International Symposium on Linear Drives for Industry Applications, LDIA2003.* 2003. Birmingham, UK.

86. Sedda. E., Fageon. C., and Yonnet. J. *Permanent Magnet Actuators for Electromagnetic Valve in Automotive Applications.* in *4th International Symposium on Linear Drives for Industry Applications.* 2003. Birmingham, UK: LDIA2003.

87. Fraenkel. Peter, *WATER-PUMPING DEVICES - A handbook for users and choosers.* Second ed. 1997, Southampton: Intermediate Technology Publications. 254.